VOLUME 75 MARCH 18, 1971 NUMBER 6

JPCHAx

THE JOURNAL OF PHYSICAL CHEMISTRY

PUBLISHED BIWEEKLY BY THE AMERICAN CHEMICAL SOCIETY

The ADVANCES IN CHEMISTRY Series...

Excellent Reviews in Book Form of Specialized Chemical Topics

For comprehensive reviews of all the important aspects of a chemical subject... read the books in the ADVANCES IN CHEMISTRY Series.

Ranging up to 750 pages in length, ADVANCES volumes include...

- Authoritative, thought-provoking articles by as many as several dozen scientists per volume.
- Carefully compiled collections of data.
- Groups of related papers presented at important national and international symposia.
- Invited reviews of current work written by researchers eminent in the field discussed.

With the ADVANCES you learn about brand-new chemical subjects... and bring yourself up to date on familiar chemical topics. The numerous scientists contributing to each volume provide you with stimulating reading enriched by a variety of viewpoints. And the ADVANCES bring material together under one cover which would otherwise be scattered among many journals... *or not available at all.*

... Put chemical topics of interest to you in proper perspective. Read the ADVANCES IN CHEMISTRY Series.

The order form lists the 20 most recent titles in the ADVANCES IN CHEMISTRY Series. Use it to order your ADVANCES *now.*

No.	Title	Price	Number of copies ordered	Cost
96	Engineering Plastics and Their Commercial Development 128 pp (1969)	$7.50	___	_____
95	Cellulases and Their Applications 460 pp (1969)	$14.50	___	_____
93	Radionuclides in the Environment 522 pp (1970)	$15.00	___	_____
92	Epoxy Resins 224 pp (1970)	$10.50	___	_____
91	Addition and Condensation Polymerization Processes 767 pp (1969)	$19.50	___	_____
90	Fuel Cell Systems—II 446 pp (1969)	$17.50	___	_____
89	Isotopes Effects in Chemical Processes 278 pp (1969)	$13.00	___	_____
88	Propellants Manufacture, Hazards, and Testing 395 pp (1969)	$12.00	___	_____
87	Interaction of Liquids at Solid Substrates 212 pp (1968)	$9.50	___	_____
86	Pesticidal Formulations Research. Physical and Colloidal Chemical Aspects 212 pp (1969)	$9.50	___	_____
85	Stabilization of Polymers and Stabilizer Processes 332 pp (1968)	$12.00	___	_____
84	Molecular Association in Biological and Related Systems 308 pp (1968)	$10.50	___	_____
83	Chemical Marketing: The Challenges of the Seventies 199 pp (1968)	$9.50	___	_____
82	Radiation Chemistry—II 558 pp (1968)	$16.00	___	_____
81	Radiation Chemistry—I 616 pp (1968)	$16.00	___	_____
81	and 82 ordered together	$30.00	___	_____
80	Chemical Reactions in Electrical Discharges 514 pp (1969)	$15.00	___	_____
79	Adsorption from Aqueous Solution 212 pp (1968)	$10.00	___	_____

TOTAL COST _____

Postpaid U.S. and Canada; all others please add $0.20 for each volume ordered.

Payment must be in U.S. funds, by international money order, UNESCO coupon, or U.S. bank draft; or order through your book dealer.

Please ship my ADVANCES to:

Name _____

Address _____

City _____ State/Country _____ Zip _____

☐ Bill me. ☐ Payment enclosed.

Return this order form to AMERICAN CHEMICAL SOCIETY, Special Issues Sales, Dept. GG-68, 1155 16th Street, N.W., Washington, D.C. 20036.

... There are over 50 other volumes in the ADVANCES Series. To receive your pricelist for all the ADVANCES, just send us your request... or write it on your order. You'll receive the list by return mail.

THE JOURNAL OF

PHYSICAL CHEMISTRY

AMERICAN CHEMICAL SOCIETY, BOOKS AND JOURNALS DIVISION,
1155 Sixteenth St., N.W., Washington, D. C. 20036
JOHN K. CRUM, *Director, ad interim*
JOSEPH H. KUNEY, *Head, Business and Production Department*
RUTH REYNARD, *Assistant to the Director*

 Published biweekly by the American Chemical Society at 20th and Northampton Sts., Easton, Pa. 18042. Second-class postage paid at Easton, Pa.

All manuscripts should be sent to *The Journal of Physical Chemistry*, Department of Chemistry, University of Minnesota, Minneapolis, Minn. 55455.

Additions and Corrections are published once yearly in the final issue. See Volume 74, Number 26 for the proper form.

Extensive or unusual alterations in an article after it has been set in type are made at the author's expense, and it is understood that by requesting such alterations the author agrees to defray the cost thereof.

The American Chemical Society and the Editor of *The Journal of Physical Chemistry* assume no responsibility for the statements and opinions advanced by contributors.

Correspondence regarding accepted copy, proofs, and reprints should be directed to Editorial Production Office, American Chemical Society, 20th and Northampton Sts., Easton, Pa. 18042. Manager: CHARLES R. BERTSCH. Assistant Editor: EDWARD A. BORGER. Editorial Assistant: EVELYN J. UHLER.

Advertising Office: Century Communications Corporation, 142 East Avenue, Norwalk, Conn. 06851.

Business and Subscription Information

Remittances and orders for subscriptions and for single copies, notices of changes of address and new professional connections, and claims for missing numbers should be sent to the Subscription Service Department, American Chemical Society, 1155 Sixteenth St., N.W., Washington, D. C. 20036. Allow 4 weeks for changes of address. Please include an old address label with the notification.

Claims for missing numbers will not be allowed (1) if received more than sixty days from date of issue, (2) if loss was due to failure of notice of change of address to be received before the date specified in the preceding paragraph, or (3) if the reason for the claim is "missing from files."

Subscription rates (1971): members of the American Chemical Society, $20.00 for 1 year; to nonmembers, $40.00 for 1 year. Those interested in becoming members should write to the Admissions Department, American Chemical Society, 1155 Sixteenth St., N.W., Washington, D. C. 20036. Postage to Canada and countries in the Pan-American Union, $4.00; all other countries, $5.00. Single copies for current year: $2.00. Rates for back issues from Volume 56 to date are available from the Special Issues Sales Department, 1155 Sixteenth St., N.W., Washington, D. C. 20036.

This publication and the other ACS periodical publications are now available on microfilm. For information write to: MICROFILM, Special Issues Sales Department, 1155 Sixteenth St., N.W., Washington, D. C. 20036.

Notice to Authors last printed in the issue of December 24, 1970

Cleaning Our Environment The Chemical Basis For Action

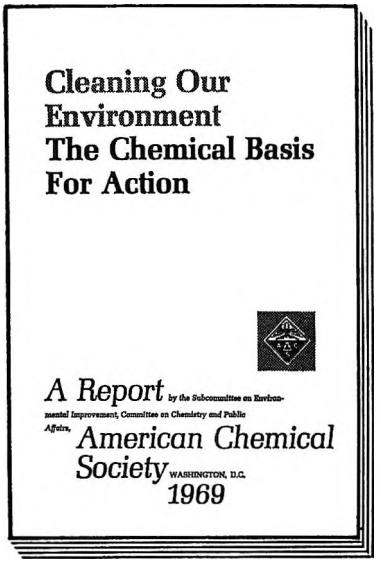

Cleaning Our Environment—The Chemical Basis for Action is the highly acclaimed 249-page report based on a three-year study by the Subcommittee on Environmental Improvement of the ACS Committee on Chemistry and Public Affairs. Leading experts from the fields of chemistry, biochemistry, chemical engineering, biology, entomology, and other disciplines comprised the Task Force on Environmental Improvement which conducted the study, one of the most comprehensive of its kind.

The report divides the problem of environmental improvement into four parts: air environment, water environment, solid wastes, and pesticides. It clearly shows where extensive fundamental research is required to provide a better working understanding of the environmental system. Focusing strongly on chemistry, chemical engineering, and related disciplines, the report concludes that the U.S. possesses enough technical know-how to take enormous strides now toward a cleaner environment.

Included in the report are 73 recommendations for action on such topics as:

- *flow, dispersion, and degradation of water and air pollutants*
- *short- and long-range effects of water and air pollutants*
- *municipal and industrial waste water treatment*
- *advanced treatment processes*
- *eutrophication*
- *air quality criteria*
- *air monitoring systems*
- *emission control on motor vehicles*
- *abatement of pollutants from power plants*
- *municipal and industrial solid wastes*
- *mining and processing wastes*
- *pesticides and human health*
- *pesticides and wildlife*
- *methods of pest control*

Although the ACS report is directed primarily at technical and nontechnical administrators in the environmental field, research managers, legislators and others working in this area, the nature of the subject makes it required reading for all scientists interested in environmental problems and their solutions.

The report is available from the ACS Special Issues Sales. Price: $2.75.

American Chemical Society
Special Issues Sales
1155 Sixteenth Street, N.W.
Washington, D.C. 20036

Please send me the ACS Report "Cleaning Our Environment—The Chemical Basis for Action."

*Name*_____

*Address*_____

*City*_____ *State*_____ *Zip*_____

Number of copies _____

I enclose _____. *(Payable to the American Chemical Society.)*

Please bill me _____. *$2.75 a copy.*

THE JOURNAL OF
PHYSICAL CHEMISTRY

Volume 75, Number 6 March 18, 1971

AUTHOR INDEX

THE JOURNAL OF
PHYSICAL CHEMISTRY

VOLUME 75, NUMBER 6 MARCH 18, 1971

Some Relative Total Scattering Cross Sections for Homologous Series of Polar and Nonpolar Molecules[1a]

by W. H. Duewer,[1b] G. J. Williams, C. F. Aten,[1c] and B. S. Rabinovitch*

Department of Chemistry, University of Washington, Seattle, Washington 98105 *(Received September 10, 1970)*

Publication costs assisted by the U. S. Air Force Office of Scientific Research

Relative total scattering cross sections were measured for several homologous series of gases using low-resolution thermal crossed molecular beams. The experimental cross sections were compared with cross sections calculated on various models and with energy-transfer cross sections obtained by other workers from the study of unimolecular methyl isocyanide isomerization. The experimental values for polar gases were well reproduced by calculations using a treatment developed by Cross and Gordon. Those for other gases were in reasonable agreement with conventionally calculated scattering cross sections.

Introduction

The low-pressure thermal unimolecular isomerization of methyl isocyanide (A) has provided activation–deactivation (energy transfer) cross sections for a large number of inert bath gases (M).[2] These cross sections may be interpreted as the product of a collisional efficiency, β_c, and a gas kinetic cross section, πs_{AM}^2. The gas kinetic cross sections for nonpolar bath molecules were calculated with the use of Lennard-Jones potential constants derived from viscosity measurements of the pure gases; standard mixing rules were used.[3] Estimates of potential parameters were employed when experimental values were not available. Among the bath molecules studied were homologous series of similar gases,[4,5] *n*-alkanes, 1-alkenes, 1-alkynes, terminal nitriles, and *n*-fluoroalkanes. The potential constants used for the larger gases in each series were usually based on estimates from the known constants of the smaller members.

For the series of strongly dipolar terminal nitriles, a dipole orientation effect was suggested[5] as the explanation for an apparent near-equivalence of kinetic cross sections measured for acetonitrile and propionitrile; the method of Monchick and Mason[6] was used to treat the dipolar interactions. This involves approximations, pointed out by the original authors, which may introduce a systematic error into the cross sections; this treatment used the Stockmayer potential and simple geometrical weighting of dipole orientations; as a result, the cross sections are independent of molecular rotations. A more recent treatment[7] of the interactions of dipoles based on the Born approximation shows a strong dependence of calculated collision cross sections

(1) (a) This work was supported by the U. S. Air Force Office of Scientific Research (SRC), Contract No. F44620-70-C-0012; (b) NSF predoctoral fellow 1967–1970; (c) Sabbatical visitor.

(2) S. C. Chan, B. S. Rabinovitch, J. T. Bryant, L. D. Spicer, T. Fujimoto, Y. N. Lin, and S. P. Pavlou, *J. Phys. Chem.*, **74**, 3160 (1970).

(3) J. O. Hirschfelder, C. F. Curtiss, and R. B. Bird, "Molecular Theory of Gases and Liquids," Wiley, New York, N. Y., 1954, Chapter 8.

(4) Y. N. Lin, S. C. Chan, and B. S. Rabinovitch, *J. Phys. Chem.* **72**, 1932 (1968).

(5) S. C. Chan, J. T. Bryant, L. D. Spicer, and B. S. Rabinovitch *ibid.*, **74**, 2058 (1970).

(6) (a) L. Monchick and E. A. Mason, *J. Chem. Phys.*, **35**, 1676 (1961); (b) E. A. Mason and L. Monchick, *ibid.*, **36**, 2746 (1962).

(7) (a) R. J. Cross and R. G. Gordon, *ibid.*, **45**, 3571 (1966); (b) since this paper was written, a recent treatment by H. Rabbitz and R. G. Gordon [*J. Chem. Phys.*, **53**, 1815, 1831 (1970)] gives the magnitude of some additional terms. Inclusion of their terms may improve the agreement between calculation and experiment for most of the gases in this study.

on the rotational periods of colliding dipolar molecules. This treatment has been moderately successful in predicting total scattering cross sections in high-resolution beam experiments.[8]

In order to investigate further the cross-sectional behavior of the nitrile series, we have made total scattering molecular beam measurements on acetonitrile–nitrile collision pairs. The beam apparatus which was available was not originally designed for total scattering measurements. Its chief failings were low resolution and lack of velocity-selection. All of the measured cross sections are thermal average values. Because of the difficulties introduced into the interpretation of the data by the low resolution, measurements were made on acetonitrile–alkyne collision pairs which, by comparison with the acetonitrile–nitrile scattering, specifically isolates the contributions of dipole–dipole interactions in the latter pair. Other suitable comparison series were also studied.

Experimental Section

A diagram of the apparatus is given in Figure 1. The slit dimensions, pressure measuring devices, and typical operating conditions are collected in Table I.

Table I: Apparatus Parameters

	Dimensions, cm	Pumping	Pressure, Torr — Beams off	Pressure, Torr — Beams on
S_1	0.010 × 0.5			
S_2	0.032 × 0.5			
P_1[a,b]		2-in. oil diffusion	$<10^{-6}$	10^{-6}
S_3	0.015 × 0.5			
S_4	0.15 × 0.5			
P_2[b]		6-in. oil diffusion	$<10^{-7}$	$\sim10^{-5}$
S_5	0.10 × 0.5			
P_3[b]		2-in. oil diffusion	$<10^{-6}$	5×10^{-6}
S_6	0.22 × 0.5			
P_4		500 l. sec^{-1} sputter-ion	$<10^{-8}$	5×10^{-8}
S_7	0.62 diameter			

[a] A liquid nitrogen cold finger extended into the chamber. [b] All oil diffusion pumps were trapped by a liquid nitrogen cryobaffle adjacent to the apparatus.

The detector was an EAI Quad 200 mass filter equipped with an axial beam ionizor. The ionization efficiency was estimated to be $\lesssim 10^{-4}$.

The parent beam was modulated at 200 Hz by an American Time Products tuning fork chopper, C_1. The secondary beam could be similarly modulated at 223 Hz, C_2.

The primary beam intensity was measured by detecting the 200-Hz component of a suitable peak in the mass spectrum of the parent beam molecule with a PAR 121C lock-in amplifier. The scattered intensity was taken as the 223-Hz component of the same peak. A peak was suitable if it was prominent in the spectrum of the primary beam molecule, absent from the spectrum of the scattering gas, and weak in the general background spectrum. It is obvious that there were no suitable peaks available for the study of the scattering of a gas by itself.

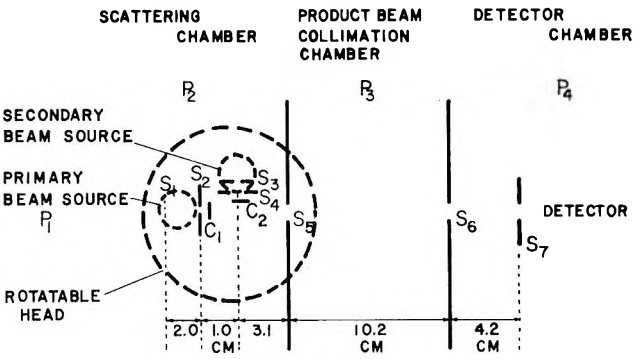

Figure 1. Schematic of the apparatus.

Experimental Measurements and Treatment of the Data

The observed total scattering cross section, Q_{obsd}, is defined by the relation

$$Q_{obsd} = \ln (I_0/I)/n_j L \qquad (1)$$

where I_0 is the intensity of the primary beam in the absence of scattering, I is the intensity of the primary beam after scattering, n_j is the density of scattering particles in the secondary beam, and L is the length of the scattering zone. Since, for effusive flow from a long slit collimated at a distance from the zone of interaction, n_j and L are inversely related, they were evaluated together. Assuming Knudsen flow

$$n_j L = N_0 L_0 F/4$$

where N_0 is the density of particles behind the source slit, L_0 is the width of the source slit (0.015 cm), and the collimation factor F is given by[9]

$$F = \int_{-a}^{+a} \cos\theta \, d\theta \Big/ \int_{-\pi/2}^{+\pi/2} \cos\theta \, d\theta = 0.20 \pm 0.08$$

where $2a$ is the angular width of the secondary beam collimator; the rather crude error limits for F were estimated from experimental measurements and apparatus features. All of the above factors were constants of the apparatus except for N_0 which was made a constant of the experiment; thus $n_j L = KN_0$, where $K = 7.5 (\pm 3.0) \times 10^{-4}$ cm and N_0 is calculated from P_0, the pressure behind the secondary beam slit. P_0 was mea-

(8) R. J. Cross, E. A. Gislason, and D. R. Herschbach, *J. Chem. Phys.*, **45**, 3582 (1966).

(9) For a more complete discussion of these matters see W. H. Duewer, Ph.D. Thesis, University of Washington (1970).

sured on a thermocouple gauge that had been calibrated by expansion of the gases involved between standard volumes; actually, absolute calibration was not required for the present relative measurements. I, the intensity after scattering, was proportional to the maximum amplitude of the 200 cycle-chopped primary beam, measured with the secondary beam on; the intensity before scattering, I_0, was taken to be equal to the sum of I and I_{sc}, the total intensity of molecules scattered out of the beam. For the purpose of calculating Q_{obsd}, I_{sc} was taken to be proportional to the amplitude of the 223-cycle signal at its maximum; this signal was 180° out of phase with respect to the chopper. In the calculation, the ratio of true molecule density to signal intensity was assumed to be the same for both frequencies. This should introduce only minor errors into the absolute cross section, already uncertain by ~40% due to uncertainty in F. Also, since I_{sc} was always less than 4.5% of I, then $I_0/I \simeq 1$, and since for small x, $\ln(1 + x) \simeq x$, the relative cross sections should be virtually unaffected by a failure of this assumption. The chopper characteristics were not altered during the course of the investigation.

The observed collision diameter is defined by $\sigma_{obsd} = (Q_{obsd}/\pi)^{1/2}$. The experimental quantity Q_{obsd} (eq 1) may be equated simply to calculated values based on the intermolecular potential only if the scattering beam particles are stationary and if the primary beam is velocity selected, say at some reference velocity, v_0. Since the scattering molecules are not stationary, the relative velocity, g, differs from the primary beam velocity and the calculated collision rate is too small if based on the primary beam velocity. The cross section calculated from the attenuation is too large by a factor of (g/v_0), for a velocity-independent (*i.e.*, hard sphere) cross section; also, the true cross section is velocity dependent for potentials other than hard sphere. For thermal beams, it is necessary to average over the distribution of velocities.

Berkling, *et al.*,[10] have given functions which correct for these effects. Since our experiments were carried out at low resolution, it was necessary[8] to use the classical relation for the dependence of total cross section on the relative velocity,[9] $Q_c \propto g^{-2/3}$. In Berkling's notation, we used a $G_{b'o}(4, y)$ correction for thermal crossed beams, a density-sensitive detector, and spherical molecules. The argument y is the ratio of the most probable velocity in the primary beam to that of the secondary beam. The velocity-corrected cross sections are given by

$$Q(v) = Q_{obsd}/G_{b'o}(4, y) \qquad (2)$$

This correction refers the experimental cross sections to the most probable velocity of the primary beam. The velocity-corrected collision diameters are designated as $\sigma_{obsd}(v)$.

Calculated Collision Properties. The energy transfer collision diameters obtained from isomerization studies have been compared with those calculated from viscosity measurements with use of Lennard-Jones or Stockmayer potentials and the relation, $s_{ij}^2 = \sigma_{ij}^2[\Omega^{*(2,2)}(\epsilon_{ij}/T, \delta_{max})]$ where σ_{ij} is the Lennard-Jones parameter and $\Omega^{*(2,2)}(\epsilon_{ij}/T, \delta_{max})$ is tabulated for both nonpolar collisions[3] ($\delta_{max} = 0$), and for polar–polar collisions[6] ($\delta_{max} > 0$). Molecular beam scattering cross sections for Lennard-Jones gases have usually been calculated by the use of the relation

$$Q_{ij} = 8.08(C/g)^{2/5} \qquad (3)$$

where C is the constant multiplying the r^{-6} term in the potential ($4\epsilon_{ij}\sigma_{ij}^6$, in the Lennard-Jones expression). In general, for molecular beam scattering, C has not been taken from viscosity-derived potentials but has been calculated from the molecular polarizability and dipole-induced dipole effects. C is taken to be equal to the sum of a dispersion term and an induction term. The dispersion term is given by the Slater–Kirkwood approximation and the induction term by the Debye relation. That is

$$C = C_{disp} + C_{ind} \qquad (4)$$

where

$$C_{disp} = \frac{25.2 \times 10^{-24}\alpha_i\alpha_j}{[(\alpha_i/N_i)^{1/2} + (\alpha_j/N_j)^{1/2}]}$$

and

$$C_{ind} = \alpha_i\mu_j^2 + \alpha_j\mu_i^2$$

the α's are the polarizabilities, the N's are the number of outer shell electrons, and the μ's the dipole moments of the molecules.

Dipole–dipole forces have been treated by several general approaches. In the Keesom–Linder approximation,[11] the dipole–dipole orientations are given their Boltzmann weightings, and the potential is averaged over the orientations. This approach was used by Bernstein, Rothe, and Schumacher[12] (BRS) in the treatment of beam scattering. A second approach[13] invokes the sudden approximation and yields very large cross sections.[7] A third treatment by Cross and Gordon[7] used the Born approximation in first-order perturbation theory and yields cross sections smaller than those calculated from the sudden approximation, but usually larger than those calculated using the Keesom–

(10) K. Berkling, R. Helbing, K. Kramer, H. Pauly, C. Schlier, and P. Toschek, *Z. Phys.*, **166**, 406 (1962).

(11) W. Keesom, *ibid.*, **22**, 129 (1921); B. Linder, *J. Chem. Phys.*, **44**, 265 (1966).

(12) (a) E. W. Rothe and R. B. Bernstein, *ibid.*, **31**, 1619 (1959); (b) H. Schumacher, R. B. Bernstein, and E. W. Rothe, *ibid.*, **33**, 584 (1960).

(13) H. G. Bennewitz, H. H. Kramer, U. Paul, and J. P. Toennies, *Z. Phys.*, **177**, 84 (1964); H. H. Kramer and R. B. Bernstein, *J. Chem. Phys.*, **44**, 4473 (1966).

Linder approximation; these cross sections are strongly dependent on the rotational periods of the colliding molecules. The Keesom–Linder approximation is a choice based on convenience and previous use. It is not a part of modern scattering theory, although second-order perturbation theory gives rise to terms which have a weaker dependence on rotational resonance and somewhat resemble the results of the Keesom–Linder expression.[7b]

The method of Bernstein and Rothe[12a] for treating nonpolar collision pairs has given fair agreement with experiment for collisions between alkali metals and a variety of gases; the agreement is best for simple molecules. The treatments of dipole–dipole interactions involving preaveraging have given fair agreement with molecular beam experiments when the cross-section contribution due to dipole–dipole interactions was comparable to that due to dispersion forces.[8,12] The treatment of Cross and Gordon has given better results when the cross sections calculated from dipole–dipole interactions is much larger than that due to dispersion forces.[7]

In this work, scattering collision diameters have been calculated with use of the Keesom–Linder approximation[12b] and by using the method of Cross and Gordon[7] as applied to classical dipoles by Cross, Gislason, and Herschbach[8] (CGH). Asymmetric top molecules were approximated as linear molecules whose rotational moment of inertia was equal to the mean moment about the axes perpendicular to the dipole. Where microwave spectra were available, the rotational moments were taken from these; where no spectra were available, the moments were approximated as for the fully extended configuration, with all masses concentrated at points along the molecular axis. Fortunately, the instances where these approximations are worst are the cases where errors in moments of inertia have the least effect on the calculated values.

Collision diameters have also been calculated from the viscosity-derived potentials in two ways. The hard-sphere diameters that would yield equivalent viscosities have been computed, as in the unimolecular reaction energy-transfer work.[2] Also, collision diameters have been calculated from the attractive potential

$$C = -[4\epsilon_{ij}\sigma_{ij}^6 + {}^2/_3\mu_i^2\mu_j^2/kT] \qquad (5)$$

as in the treatment of BRS, but using viscosity-derived potential parameters. These parameters have also been calculated for collisions at 280°, the temperature of the energy-transfer work.

Cross sections calculated from the attractive potentials are the normal ones for comparing with molecular beam scattering results. Hard-sphere viscosity-related diameters are included for comparison with the energy-transfer conditions; they can reveal the effect of heavily weighting the large angle scattering (weighting of $\Omega^{*(2,2)}$ by $\sin^2\phi_{cm}$, where cm ≡ center-of-mass coordinate system). The weighting given to the large angle scattering, which results from the low resolution of our apparatus, while not as great as in viscosity measurements is greater than in high-resolution scattering experiments. The parameters used in calculating the cross sections are given in Table II.

Table II: Some Molecular Parameters

	σ_{ii},[a] 10^{-8} cm	ϵ_{ii}/k,[a] °K	α_i,[a] 10^{-24} cm³	μ_i,[a] D	I, 10^{-40} g cm²
CH_3CN	4.47	380	4.27	3.97	90.9[c]
CH_3NC	4.47	380	4.47	3.80	83.2[c]
C_3H_8	5.06	254	6.29	0.0	
C_2H_2	4.22	185	3.33	0.0	
C_3H_4	4.74	261	5.0	0.75	95[d]
C_4H_6	5.25	310	6.7	0.81	200[e]
C_5H_8	5.75	310[b]	8.5	0.86	390[e]
C_6H_{10}	6.25	310	10.5	0.88	750[e]
C_7H_{12}	6.75	310	12.4	0.87	1250[e]
C_8H_{14}	7.25	310	14.3	0.87	1800[e]
C_9H_{16}	7.75	310	16.2	0.87	2600[e]
HCN	3.93	320	2.59	2.95	18.9[f]
CD_3CN	4.47	380	4.27	3.97	115[g]
C_2H_5CN	5.00	380[b]	6.07	4.03	198[h]
C_3H_7CN	5.50	380	7.8	4.07	390[i]
C_4H_9CN	6.00	380	9.6	4.12	750[j]
$C_5H_{11}CN$	6.50	380	11.5	4.2	1250[j]
$C_6H_{13}CN$	7.00	380	13.4	4.2	1800[j]
$C_7H_{15}CN$	7.50	380	15.4	4.2	2600[j]
Ne	2.79	36	0.392	0.0	
CD_4	3.8	144	2.6	0.0	
NH_3	3.15	358	2.26	1.47	4.37[f,k]
ND_3	3.15	358	2.26	1.47	8.86[f,k]
N_2	3.68	92	1.76	0.0	
C_2H_5OH	4.50	300	4.9	1.69	140[l]
C_5H_{12}	5.77	325	9.95	0.0	

[a] See ref 2 for sources. [b] An alternative choice for ϵ_{ii} for higher homologs, which increases with boiling point, was also tested. It led to no significant change in the behavior of Figures 2–5; hence the values of ref 2 were adopted. [c] H. Ring, H. Edwards, M. Kessler, and W. Gordy, *Phys. Rev.*, **72**, 1262L (1947). [d] R. Trambarulo and W. Gordy, *J. Chem. Phys.*, **18**, 1613 (1950). [e] Estimated from the moments of the similar nitrile. [f] G. Herzberg, "Molecular Spectra and Molecular Structure II Infrared and Raman Spectra of Polyatomic Molecules," D. Van Nostrand, Princeton, N. J., 1945. [g] Calculated from the known geometry of CH_3CN. [h] R. G. Lerner and B. P. Dailey, *J. Chem. Phys.*, **26**, 678 (1957). [i] E. Hirota, *ibid.*, **37**, 2918 (1962). [j] Estimated as discussed in the text. [k] The more nearly resonant rotation about the dipole axis was used. [l] B. Bak, E. S. Knudsen, and E. Madsen, *Phys. Rev.*, **75**, 1622L (1949).

Correction for Finite Resolution. The cross sections calculated from eq 3 are those that would be measured on a high-resolution apparatus, since there exists a limiting cm angle, α_0, within which the cross section is nearly independent of angle[14]

(14) H. Pauly and J. P. Toennies, *Advan. At. Mol. Phys.*, **1**, 201 (1965).

$$\alpha_0 = \frac{h}{2M_i v_i}(\pi/Q_{tot})^{1/2} \quad (6)$$

where M_i is the mass of the primary beam molecule, v_i is its velocity, and Q_{tot} is the total cross section. For the systems studied here, α_0 ranges between 0.01 and 0.2°, whereas the angular resolution of the apparatus was 0.75° (lab, *i.e.*, laboratory coordinates), or 1–3° (cm).[15] Experimentally, cross sections measured on an apparatus with angular resolution equal to α_0 are low by 5–10%.[14] It was necessary to correct for the finite resolution of the apparatus.[9]

The error in our absolute measurements is as much as a factor of four, although the effect on the relative cross sections is much smaller, 10–20%, if the correction is made using the expressions given by CGH for low-resolution experiments. These corrections take the form

$$Q_c(\theta_R) = Q_c(0)(A + B/\rho^{1/3}) \quad (7)$$

where $Q_c(\theta_R)$ is the cross section calculated at the experimental resolution, $Q_c(0)$ is the cross section calculated for infinite resolution, A and B are constants given by the form of the potential, and ρ is the resolution parameter given by

$$\rho = M_i v_i Q_c(0)^{1/2} W/lh$$

where M_i is the mass and v_i the velocity of the primary beam particle (taken as the most probable velocity),[16] h is Planck's constant, W is the width of the beam at the detector, and l is the distance from the source to the detector. For scattering from an r^{-6} potential, $A = 0.0814$ and $B = 0.5804$. For scattering resulting from dipole–dipole interactions calculated on the Born model,[8] $A = -0.0270$ and $B = 0.6018$. The Keesom–Linder approximation converts the dipole–dipole interaction to an r^{-6} form. Relative collision diameters calculated on this basis are given in the tables as $\sigma_c(\theta)$. It should be noted that these approximate corrections were developed[9] for experiments of better resolution than the present ones and may be less accurate as applied here.

Results

Table III gives collision diameters for the pair acetonitrile-d_3–acetonitrile. All diameters for other pairs are given relative to the pair, acetonitrile-d_3–acetonitrile. Comparisons of the data are presented in Figures 2–8; relative collision diameters of members of a homologous series are plotted against the number of skeletal atoms; collision diameters for molecules in groups of near-equal mass, which were chosen to minimize the effects of approximations in the treatment of the velocity dependence of the collision diameters and the correction for finite resolution, are plotted in order of increasing cross section.

Table III: Magnitudes of CH_3CN–CD_3CN Collision Diameters (Å)

σ_{obsd}[a]	$\sigma_{obsd(v)}$[a]	σ_{CGH}[b]	σ_{BRS}[b]	$\sigma_{BRS'}$[b,c]	σ_η[d]
		(40.4)	(26.9)	(28.1)	
9.1	8.0	16.6	13.9	14.5	7.21

[a] The absolute value of the experimental collision diameter has order-of-magnitude significance only. [b] The parenthetic value is the cross section calculated for high resolution; the lower value includes the finite resolution correction. [c] BRS treatment using viscosity-derived long-range potential. [d] Hard-sphere equivalent viscosity-based collision diameter.

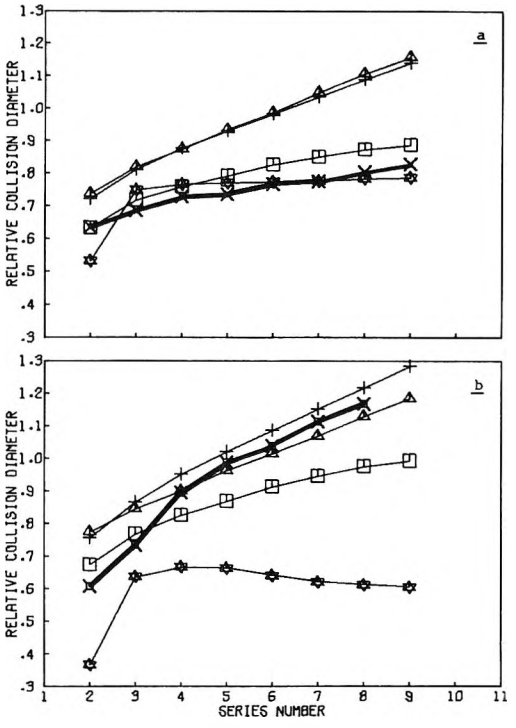

Figure 2. (a) Relative collision diameter *vs.* series number for the series alkynes *vs.* CH_3CN at 294°K: ×, scattering collision diameter; △, hard-sphere-equivalent viscosity-based collision diameter; +, collision diameter calculated from viscosity based-attractive forces; □, BRS collision diameter; ✡, CGH collision diameter. (b) Relative collision diameter *vs.* series number for the series alkynes *vs.* CH_3NC at 554°K: ⌑, energy transfer collision diameter; △, hard-sphere-equivalent viscosity-based collision diameter; +, collision diameter calculated from viscosity-based attractive forces; □, BRS collision diameter; ✡, CGH collision diameter.

In judging the goodness of fit amongst the curves in each of the figures that follow, it should be borne in mind that it is probably quite reasonable to conceive of small vertical displacements of the experimental curves as might be occasioned by residual errors in the data treatment.

Alkynes–Acetonitrile. Figure 2a shows the experimental relative collision diameters and the calculated

(15) P. Kusch, *J. Chem. Phys.*, **40**, 1 (1964).

(16) Thermal averaging over primary beam velocities of the resolution correction, as opposed to use of the most-probable-velocity correction, had less than a 0.5% effect on the relative collision diameters.

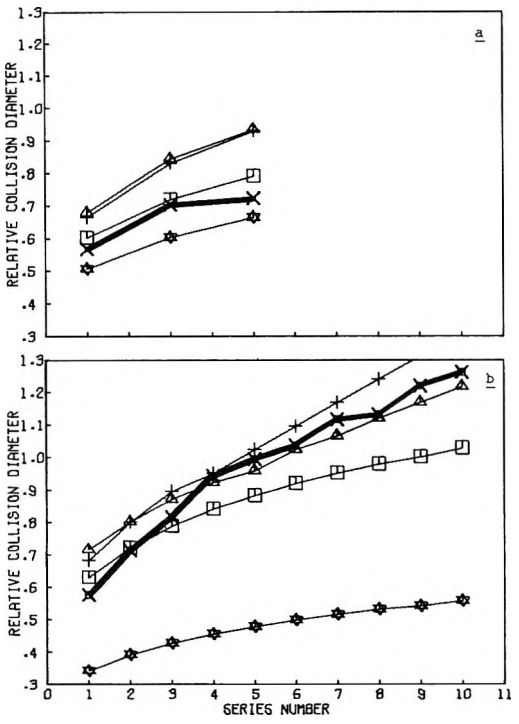

Figure. 3. (a) Relative collision diameter *vs.* series number for the series alkanes *vs.* CH_3CN at 294°K. Same symbols as in Figure 2a. (b) Relative collision diameter *vs.* series number for the series alkanes *vs.* CH_3NC at 554°K. Same symbols as in Figure 2b.

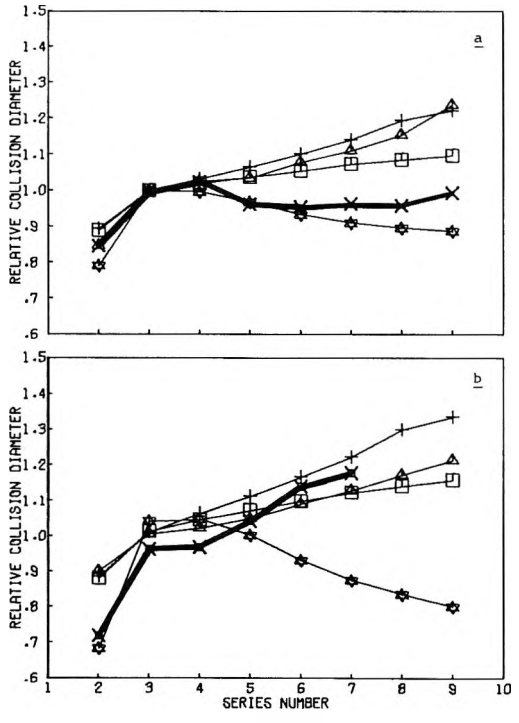

Figure 4. (a) Relative collision diameter *vs.* series number for the series nitriles *vs.* CH_3CN at 294°K. Same symbols as in Figure 2a. (b) Relative collision diameter *vs.* series number for the series nitriles *vs.* CH_3NC at 554°K. Same symbols as in Figure 2b.

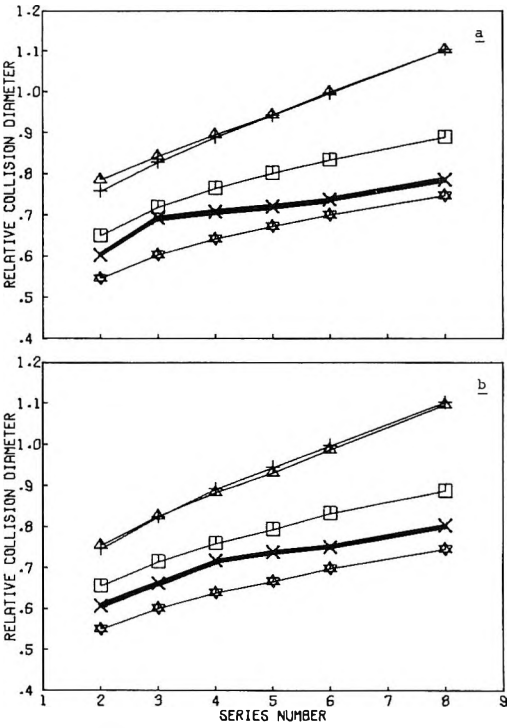

Figure 5. (a) Relative collision diameter *vs.* series number for the series nitriles *vs.* C_3H_8, at 294°K. Same symbols as in Figure 2a. (b) Relative collision diameter *vs.* series number for the series alkynes *vs.* C_3H_8 at 294°K. Same symbols as in Figure 2b.

resolution-corrected relative collision diameters for alkyne–acetontrile collisions. The experimental quantities are in better agreement with those calculated from the model of BRS than with that of CGH. The behavior for the smaller molecules suggests that CGH over estimates the contribution of weak dipole–dipole interactions to the cross section. Calculations based on the viscosity-derived potentials do not agree with the experimental diameters in any part of the range.

Figure 2b shows the reported behavior of the alkyne series for energy transfer in CH_3NC isomerization. The agreement with viscosity-derived values is good for all except the smallest alkynes; however, the known collisional inefficiency of the latter,[2] $\beta < 1$, *should* cause the energy-transfer cross sections to drop below those based simply on viscosity. As was expected, the models of CGH and BRS do not fit the data.

Alkanes–Acetonitrile. Methane, propane, and pentane were studied in collisions with acetonitrile. The results are seen in Figure 3a. Here the agreement is best with the BRS values. The results from CH_3NC energy-transfer experiments are summarized in Figure 3b; again, the larger molecules, having $\beta = 1$, give good agreement with the viscosity-derived values.

Nitriles–Acetonitrile. The results of the nitrile–acetonitrile scattering experiments are given in Figure 4a. The maximum observed in the experimental diameters at acetonitrile-d_3 and propionitrile is well repro-

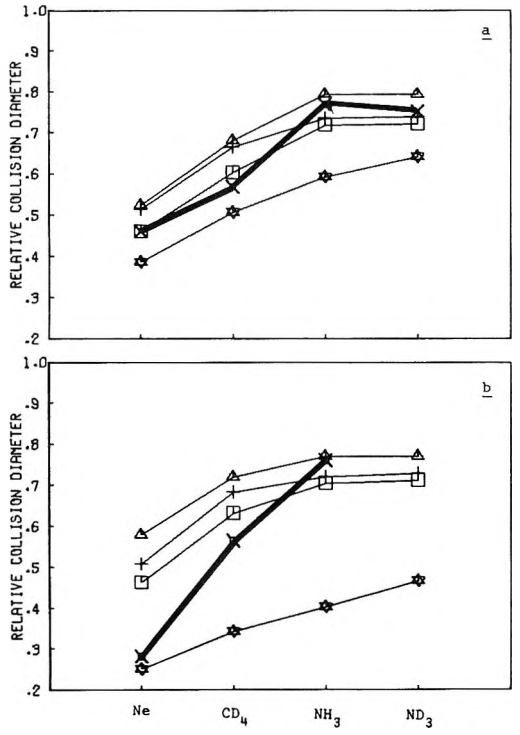

Figure 6. (a) Relative collision diameters for the series of molecules of mass near 20 in collision with CH_3CN at 294°K. Same symbols as in Figure 2a. (b) Relative collision diameters for the series of molecules of mass near 20 in collision with CH_3NC at 554°K. Same symbols as in Figure 2b.

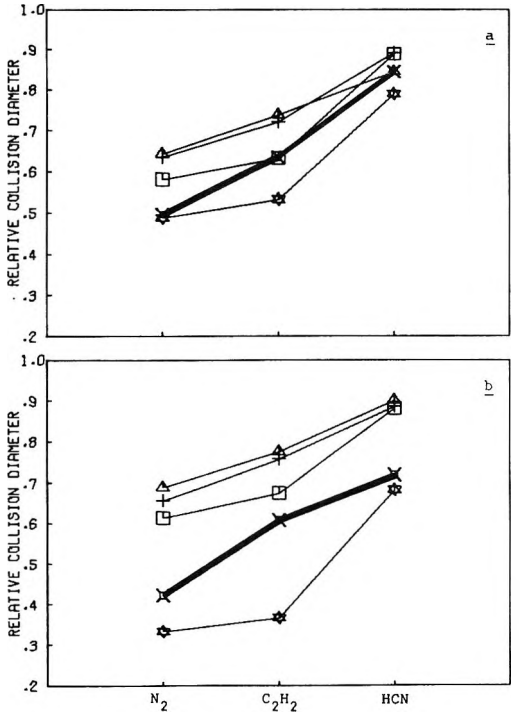

Figure 7. (a) Relative collision diameters for the series of molecules of mass near 28 in collision with CH_3CN at 294°K. Same symbols as in Figure 2a. (b) Relative collision diameters for the series of molecules of mass near 28 in collision with CH_3NC at 554°K. Same symbols as in Figure 2b.

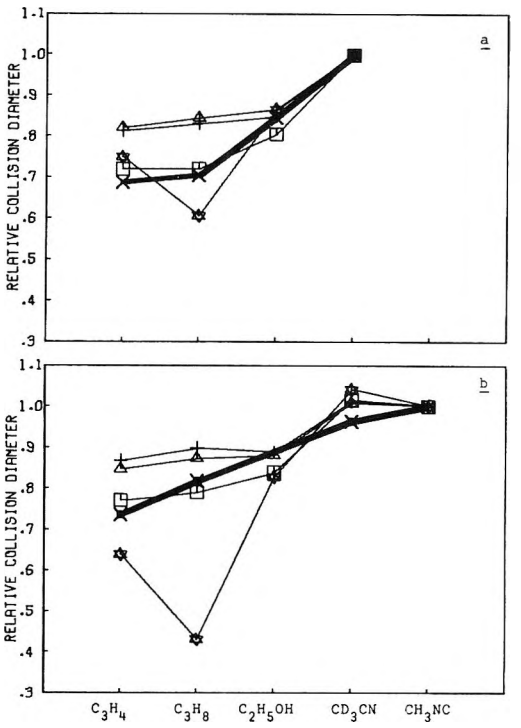

Figure 8. (a) Relative collision diameters for the series of molecules of mass near 42 in collision with CH_3CN at 294°K. Same symbols as in Figure 2a. (b) Relative collision diameters for the series of molecules of mass near 42 in collision with CH_3NC at 554°K. Same symbols as in Figure 2b.

duced by CGH; however, the values for the largest nitriles are not as well reproduced. The other models do not agree as well with experiment. The source of the maximum in the CGH cross sections is near-resonant rotational energy transfer; the model seems to underestimate nonresonant interactions of strong dipoles.

The CH_3NC energy-transfer results are shown in Figure 4b. Here no model fits the data well, although the viscosity-based diameters most nearly fit most of the data. The enhancement of the acetonitrile-d_3 collision diameter is similar to the scattering behavior and suggests a coupling of dipoles near rotational resonances. Vibrational resonance might enter into the explanation of this behavior: although the trideuteration of the d_3 compound substantially destroys any higher frequency vibrational resonances between excited methyl isocyanide and acetonitrile-d_3, the low-lying bending near-resonances still persist. However, the importance of vibrational resonance in this phenomenon is still not clear.[2,17]

Alkynes and Nitriles vs. Propane. To verify that the observed qualitative differences between the collisional behavior of the alkyne series (Figure 2a) and the nitrile series (Figure 4a) with a polar collision partner were a result of the dipole–dipole interaction, the behavior of the alkynes (Figure 5a) and nitriles

(17) Y. N. Lin and B. S. Rabinovitch, *J. Phys. Chem.*, **74**, 3151 (1970).

(Figure 5b) in collision with propane, a nonpolar gas of about the same mass and complexity as acetonitrile, was studied. As all of the models predicts, the behavior of the two series was similar, and similar to alkyne–acetonitrile and alkane–acetonitrile scattering. The agreement between experiment and calculation was fair for the relative collision diameters calculated from the BRS and CGH models. Obviously, the treatment of the dipolar interaction affected only the reference collision diameter, acetonitrile-d_3–acetonitrile, since propane is nonpolar.

Some Molecules of Equal Mass vs. Acetonitrile. The effects of any inadequacy in the handling of the corrections for resolution and for relative motion of the scattering particles are minimized in studies of small series of nearly equimassive molecules.

The molecules Ne, CD_4, NH_3, and ND_3, all near mass 20, were studied in collision with acetonitrile. The results are shown in Figure 6a. The calculated BRS values seem to be in good agreement with the experiment. Figures 6b gives the behavior of the relative collision diameters in energy-transfer (isocyanide isomerization) collisions. Here the apparent collision diameters, which include an inefficiency factor $\beta < 1$, are not expected to agree with any model.

The molecules N_2, C_2H_2, and HCN, all of mass near 27, were studied in acetonitrile scattering experiments. The results are given in Figure 7a. None of the models fit particularly well, although the BRS and CGH models give reasonable fits. Figure 7b shows the isocyanide collision diameters. Again no model agrees well with the experiment. And again, the explanation includes collisional inefficiency effects.

Another series of nearly equimassive molecules was studied, and the acetonitrile scattering results for propyne, propane, ethanol, and acetonitrile-d_3 are given in Figure 8a. The agreement with the calculations from BRS is fairly good. The isocyanide relative collision diameters are given in Figure 8b. All models yield fair agreement with experiment.

Discussion

The acetonitrile scattering behavior of the nitriles and of ethanol is well described by the theory of CGH. However, the dipole contributions to the collision diameters of weakly dipolar molecules with near-resonant rotational periods (*e.g.*, propyne, butyne) is overestimated and the cross sections of strongly dipolar molecules far from rotational resonance (*e.g.*, NH_3, ND_3, and, to a lesser extent, HCN and the largest nitriles) are underestimated. This observation agrees with the findings of CGH, who found that the model gave good results if the contribution to the cross section from the dipolar interaction was significantly greater than that from dispersion forces, but that the Keesom–Linder approximation gave better results when the contribution from dispersion forces was comparable to, or greater than, that from the dipole–dipole interaction. This may result from difficulties in determining the damping zones for the various contributions to the cross sections.[8] This difficulty is increased by the low resolution of our apparatus.

The relative collision diameters for nonpolar gases are given moderately well by the model of Bernstein and Rothe,[12a] but are in poor agreement with those calculated from viscosity. However, the energy-transfer cross sections fit well to the viscosity-derived quantities for all gases except for the simplest ones (where collisional inefficiency causes much of the difference between energy transfer and viscosity values), and for aceto- and propionitriles.

The theories used to calculate collision properties are essentially liquid droplet theories in which the potentials add to create a central scattering element. Although the longer chain molecules in a *n*-alkyl homologous series are not spherical, their cross sections calculated on the basis of the droplet model are predicted to be the same as those of their branched analogs; disparities could arise since scattering elements distributed over an appreciable volume shield each other less than do centrally packed scattering centers.[18] The latter expectation is borne out by energy-transfer data,[19] but not by diffusion data[18] nor probably by our scattering data.[20] The liquid droplet models predict a cross-sectional dependence on series number, n, of form $A + Bn^{2/3}$, for the larger molecules, where A and B are constants. The energy-transfer data reveal a stronger dependence on n than does the scattering. The explanation evidently lies with the range and nature of the interactions involved in the various kinds of experiment. Scattering depends on very weak interactions and the forces are long range compared to molecular dimensions. Energy transfer depends on stronger interactions and forces of range comparable to molecular dimensions. Thus, the results of the two types of experiment suggest that vibrational energy transfer in thermal unimolecular reactions depends primarily on strong, shorter range interactions which are nearly additive in the larger molecules, whereas scattering depends on long-range forces which increase as the approximate two-fifths power of the primary beam polarizability. However, the behavior of the lower nitriles in both types of experiment suggests that a coupling of dipoles plays a significant role in both phenomena.

(18) E. Fuller, K. Ensley, and C. Giddings, *J. Phys. Chem.*, **73**, 3679 (1969).

(19) L. Spicer and B. S. Rabinovitch, *ibid.*, **74**, 2445 (1970).

(20) An effect similar to this has recently been suggested as a possible source of larger-than-theoretical cross sections measured for the scattering of LiBr by Ar, Kr, and N_2 at very high resolution: see E. Richman and L. Wharton, *J. Chem. Phys.*, **53**, 945 (1970).

Gas-Phase Addition Reactions of CF_3 and CH_3 Radicals in Hexafluoroazomethane–Acetone Mixtures. I

by Joseph D. Reardon and Chas. E. Waring*

Department of Chemistry, University of Connecticut, Storrs, Connecticut 06268 *(Received June 22, 1970)*

Publication costs assisted by the University of Connecticut

Hexafluoroazomethane (HFAM) was employed as a source of CF_3 radicals to react with acetone at temperatures below which the latter decomposes. In a 1:2 HFAM–acetone mixture at 347°, mass peaks, not previously reported, corresponding to the addition compounds $(CF_3)_2N–N(CF_3)(CH_3)$ (250) and $(CH_3)(CF_3)N–N(CF_3)(CH_3)$ (196) and/or $CF_3(CH_3)_2COCF_3$ (196) were observed with an AEI MS-12. Large peaks at *m/e* 250 and 196 were also observed in 1:2 mixtures of HFAM–CH_4 at 347° and HFAM–di-*tert*-butyl peroxide at 170°. In the latter two mixtures, the mass peak at 196 could be due only to the hydrazine addition compound and not the ether. For the HFAM–acetone mixture, a theoretical calculation indicates that the formation of the hydrazine (196) is 150 times more probable than the ether. Subsequent analyses of the products of a 1:2 HFAM–acetone mixture at 347° with a high-resolution CEC 21-110 mass spectrometer confirmed the presence of a hydrazine of mass 196.043; no peak was observed at *m/e* = 196.032, the mass of the ether. The reasons as to why expected H-atom abstractions by methyl radicals and certain radical–radical recombinations do not occur in these systems are discussed.

Introduction

Hexafluoroazomethane (HFAM) has been employed often as a convenient source of CF_3 radicals in gas-phase studies.[1–5] In the pyrolysis[2] and photolysis[5–7] of HFAM alone, $(CF_3)_2N–N(CF_3)_2$ (I) has been reported as the addition product of CF_3 radicals to HFAM. In several gas phase investigations of HFAM in the presence of CH_3 radicals, the ultimate fate of the methyl radicals has been a matter of uncertainty and speculation. Batt and Pearson,[8] for example, decomposed di-*tert*-butyl peroxide, a CH_3 radical source, in the presence of HFAM below the decomposition temperature of the latter. They found no evidence for such expected products as CF_3CH_3 or C_2H_6 but postulated CH_3 addition to HFAM to give the stable $(CH_3)(CF_3)N–\dot{N}CF_3$ radical which subsequently added another CH_3 radical to form $(CH_3)(CF_3)N–N(CF_3)(CH_3)$ (II). Their evidence for this, however, was admittedly inconclusive.

More recently, McGee and Waring[4] investigated the reaction of CF_3 radicals with methyl ethyl ketone at temperatures below which MEK decomposes. Like Batt and Pearson, they found no evidence for CF_3CH_3, CH_4, C_2H_6, nor for I. Since McGee and Waring were unable to obtain a mass balance for all the available CF_3 and CH_3 radicals, they ascribed the deficiency as due to the formation of polymeric compounds.

Results and Discussion

Preliminary results in our current investigation of the reaction of CF_3 radicals with acetone, at temperatures below which acetone decomposes, both confirm and extend those previous studies. Major products from the reaction of a 1:2 HFAM–acetone mixture at 347° were N_2, CF_3H, CO, CH_2CO, and $CF_3CH_2COCH_3$. Trace amounts of CH_4, CO_2, C_2H_6, CF_3CH_3, and $CH_3COC_2H_5$, but no I, were observed only at 88% decomposition (by gc and mass spectrometry), 90-min reaction time. Employing an AEI MS-12 mass spectrometer, peaks were observed at *m/e* 250, 231, 196, 195, and 181. The presence of substances having masses corresponding to these spectra have not been reported previously in HFAM–methyl radical systems.

In the present system, there can be little doubt that the mass peaks at 250 and 231 are due to the ions $[(CF_3)_2N–N(CF_3)(CH_3)]^+$ (III) and $[(CF_3)_2N–N(CF_2)(CH_3)]^+$ resulting from the addition reactions

$$CF_3 + CF_3N{=}NCF_3 \longrightarrow (CF_3)_2N{-}\dot{N}CF_3 \text{ (rate step)} \quad (1)$$

$$CH_3 + (CF_3)_2N{-}\dot{N}CF_3 \longrightarrow (CF_3)_2N{-}N(CF_3)(CH_3) \text{ (fast)} \quad (2)$$

(III)

(1) W. G. Alcock and E. Whittle, *Trans. Faraday Soc.*, **61**, 662 (1965).

(2) G. O. Pritchard, H. O. Pritchard, and A. F. Trotman-Dickenson *Chem. Ind.*, 564 (1955).

(3) D. Clark and H. O. Pritchard, *J. Chem. Soc.*, 2136 (1956).

(4) T. H. McGee and C. E. Waring, *J. Phys. Chem.*, **73**, 2838 (1969).

(5) G. O. Pritchard, H. O. Pritchard, H. I. Schiff, and A. F. Trotman-Dickenson, *Trans. Faraday Soc.*, **52**, 849 (1956).

(6) J. R. Dacey and D. M. Young, *J. Chem. Phys.*, **23**, 1302 (1955).

(7) J. R. Dacey, R. F. Mann, and G. O. Pritchard, *Can. J. Chem.*, **43**, 3215 (1965).

(8) L. Batt and J. M. Pearson, *Chem. Commun.*, 575 (1965).

There are, however, two possibilities for the species corresponding to the mass peaks at 196, 195, and 181. The first would be addition reactions similar to (1) and

$$CH_3 + CF_3N{=}NCF_3 \longrightarrow (CH_3)(CF_3)N{-}\dot{N}CF_3 \text{ (rate step)} \quad (3)$$

$$CH_3 + (CH_3)(CF_3)N{-}\dot{N}CF_3 \longrightarrow (CH_3)(CF_3)N{-}N(CF_3)(CH_3) \text{ (fast)} \quad (4)$$

(II)

(2) Masses 195 and 181 would then be attributed to the ions $[(CH_3)(CF_3)N{-}N(CF_3)(CH_2)]^+$ and $[(CH_3)(CF_3)N{-}NCF_3]^+$, respectively.

The other possibility that could equally as well account for these mass peaks would be addition reactions to form an ether

$$CF_3 + CH_3COCH_3 \longrightarrow CH_3{-}\overset{\displaystyle O}{\overset{|}{\dot{C}}}{-}CH_3 \text{ (rate step)} \quad (5)$$

$$\qquad\qquad\qquad\qquad\qquad\quad CF_3$$

$$CF_3 + CH_3{-}\overset{\displaystyle O}{\overset{|}{\dot{C}}}{-}CH_3 \longrightarrow CH_3{-}\overset{\displaystyle O}{\overset{|}{C}}{-}CH_3 \text{ (fast)} \quad (6)$$

$$\qquad\qquad\qquad\qquad\quad CF_3$$

(IV)

Again, the loss of an H atom or a CH_3 radical from the ether would also give rise to mass peaks of 195 and 181.

It is of interest to note that Pritchard and Steacie[9] and Giles and Whittle[10] have investigated the reaction between methyl radicals and hexafluoroacetone and report the formation of 1,1,1-trifluoroacetone according to

$$CH_3 + CF_3COCF_3 \longrightarrow$$

$$CF_3{-}\overset{\displaystyle O}{\overset{|}{\dot{C}}}{-}CF_3 \longrightarrow CH_3COCF_3 + CF_3 \quad (7)$$

$$\qquad\qquad\quad CH_3$$

By analogy, one might reasonably expect the addition compound in reaction 5 to behave similarly. However, since the presence of 1,1,1-trifluoroacetone was never observed in any of our product analyses, one can state with some certainty that the reaction

$$CF_3 + CH_3COCH_3 \longrightarrow$$

$$CH_3{-}\overset{\displaystyle O}{\overset{|}{\dot{C}}}{-}CH_3 \longrightarrow CH_3COCF_3 + CH_3 \quad (8)$$

$$\qquad\qquad\quad CF_3$$

does not occur to any measurable extent in the present system.

In order to gain additional information concerning the reaction of CH_3 radicals with HFAM, a 1:2 mixture of HFAM and CH_4 was allowed to react at 347.5°. Analysis of the reaction products in the MS-12 gave major peaks corresponding to the masses of compounds I, II, and III. Other products, identified by gas chromatography were CF_3H and C_2F_6; definitely absent were CF_3CH_3 and C_2H_6.

In another experiment, a 1:2 mixture of HFAM and di-*tert*-butyl peroxide (DTBP) were allowed to react at 170°, a temperature below that at which HFAM decomposes. Gas chromatographic analysis gave no evidence for the presence of CF_3H, C_2F_6, CF_3CH_3, or CH_4. Surprising was the fact that very little C_2H_6 was present at this temperature. The peak corresponding to that suspected of being due to the compound II was sufficiently large to enable a good separation. Subsequent analysis on the MS-12 gave a $m/e = 196$.

The important consequences of these two experiments are: (1) the absence of ethane in the one case and the presence of very little in the other, together with the absence of methane, indicate that HFAM is an unusually good methyl radical trap; (2) the mass peaks at 196 must be due to compound II and hence reaction 4 could occur in the HFAM–acetone mixture. On the basis of this mass spectral evidence, however, it is not possible to determine whether II or IV, or both are actually responsible for the mass peak at 196 in the HFAM–acetone system. A theoretical approach to this problem suggests a possible answer to this question.

From bond energy[11] considerations it can be shown that the enthalpy change for reaction 5 is 9.9 kcal/mol. Since the activation energy cannot be less than the endothermicity, one may assume this as a minimum value for E_5. For a reaction analogous to 5,

$$CF_3 + CF_3COCF_3 \longrightarrow CF_3{-}\overset{\displaystyle O}{\overset{|}{\dot{C}}}{-}CF_3 \quad (9)$$

$$\qquad\qquad\qquad\qquad\quad CF_3$$

Gordon[12] reports an activation energy of 9.7 kcal/mol. Since the same bonds are broken and formed in (9) as are in (5), the close agreement between the calculated (E_5) and observed (E_9) activation energies is not too surprising. The activation energy of reaction 3 cannot be approximated by bond energy calculations, unfortunately, since these show the enthalpy change to be exothermic.

(9) G. O. Pritchard and E. W. R. Steacie, *Can. J. Chem.*, **35**, 1216 (1957).

(10) R. D. Giles and E. Whittle, *Trans. Faraday Soc.*, **61**, 1425 (1965).

(11) T. L. Cottrell, "The Strength of Chemical Bonds," 2nd ed, Butterworths, London, 1958, pp 270–289.

(12) A. S. Gordon, *J. Chem. Phys.*, **36**, 1330 (1962).

Pritchard, *et al.*,[3] however, report an activation energy of 3.5 kcal/mol for reaction 1. Since, as in reactions 5 and 9, the same bonds are broken and formed in (3) as in (1), the assumption that the value for E_3 is essentially the same as that for E_1, may not be wholly unjustified.

If one makes the not unreasonable assumption that the frequency factors of reactions 3 and 5 would be of the same order of magnitude, then at 347°

$$k_3/k_5 = \frac{e^{-3500/RT}}{e^{-9700/RT}} = e^{6200/RT} = 1.5 \times 10^2 \quad (10)$$

This indicates that reaction 3 should be at least 150 times as probable as reaction 5.

Support for this theoretical conclusion was obtained in the following manner. The products from a 1:2 HFAM–DTBP mixture at 170°, and products from two 1:2 HFAM–acetone mixtures at 347°, were separately analyzed in a CEC 21-110 high-resolution mass spectrometer. Polyfluorokerosine was employed as the reference sample, and the spectrometer was operated at maximum sensitivity and at a resolution of 20,000. In the HFAM–DTBP mixture, a large peak appeared at mass 196.043, corresponding to the mass of II. No peak was observed at m/e = 196.032, the mass corresponding to the ether (IV). In both samples of the HFAM–acetone products, a small peak appeared at m/e = 196.043. Again, not even a baseline disturbance could be observed at m/e = 196.032. This evidence indicates without question that compound II, and not IV, is one of the addition compounds formed in the HFAM–acetone reaction.

The results of these experiments help clarify the reason why such expected compounds as CH_4, C_2H_6, CF_3CH_3, etc., do not appear as products in HFAM–acetone and related systems. Since ketene is one of the major products of the HFAM–acetone reaction, it is formed, unquestionably, as the result of the dissociation of acetonyl radicals, together with equivalent amounts of methyl radicals

$$CH_2COCH_3 \longrightarrow CH_2CO + CH_3 \quad (11)$$

In an acetone-rich system, the methyl radicals would be expected to abstract hydrogen atoms readily from the ketone. The fact that H-atom abstraction does not occur to any significant extent in this, nor in the HFAM–MEK system, means that the activation energy for methyl radical additions to HFAM must be appreciably lower than 9.7 kcal/mol[13] the activation energy for H-atom abstraction by CH_3. In view of the absence (or traces only) of such compounds as C_2H_6 and CF_3CH_3, it also suggests that the activation energy for methyl radical additions to HFAM must also compete rather favorably with the activation energy for such radical–radical recombinations.

Research is currently in progress to determine the activation energies of certain of the addition reactions and to obtain relative amounts of the various addition compounds present in the HFAM–DTBP and HFAM–acetone mixtures.

Acknowledgment. The authors are grateful to Mr. Maurice L. Bazinet of the Army Natick Laboratories, Natick, Mass., for the high-resolution mass spectrographic analyses of our samples.

(13) A. F. Trotman-Dickenson and G. S. Milne, "Tables of Bimolecular Gas Reactions," NSRDS-NBS 9, 1967.

Electron Spin Resonance Study of Radicals Produced in Irradiated Aqueous Solutions of Amines and Amino Acids[1]

by P. Neta and Richard W. Fessenden*

Mellon Institute Radiation Research Laboratories and Department of Chemistry, Carnegie-Mellon University, Pittsburgh, Pennsylvania 15213 *(Received September 11, 1970)*

Publication costs assisted by Carnegie-Mellon University and the U. S. Atomic Energy Commission

The radicals produced by reaction of hydroxyl radicals with some amines, amino acids, and related compounds in aqueous solutions have been studied by esr. Irradiation with high-energy electrons was carried out directly in the esr cavity. In most cases aminoalkyl radicals were formed by hydrogen abstraction from the carbon bearing the amino group. The radicals $\dot{C}H_2NH_2$, $\dot{C}H_2NHCH_3$, and $\dot{C}H_2N(CH_3)_2$ produced from mono-, di-, and trimethylamine have been observed in the pH range 7–13.5. In acid solutions no radicals with the expected structure $R\dot{C}HNH_3^+$ have been observed. In the cases of di- and trimethylammonium ions secondary reactions leading to radicals of the type $R_2\dot{N}H^+$ take place. The radical found in acid solutions of glycine is best described by the structure $NH_2\dot{C}HCOOH$ as supported by experiments in D_2O. In alkaline solutions of all amino acids radicals of the type $H_2N\dot{C}RCO_2^-$ were observed. In the case of α-aminoisobutyric acid a different radical, probably of type $R\dot{N}H$, was also observed at pH 13 and low concentration of solute. The results are consistent with a mechanism involving the reaction $RCH_2NH_3^+ + H$ or $OH \rightarrow R\dot{C}HNH_3^+ + H_2$ or H_2O in acid solution and the two competing reactions $RCH_2NH_2 + OH \rightarrow R\dot{C}HNH_2 + H_2O$ and $RCH_2NH_2 + OH \rightarrow RCH_2\dot{N}H + H_2O$ in alkaline solution. The latter reaction must be followed by a fast secondary step, $RCH_2\dot{N}H + RCH_2NH_2 \rightarrow RCH_2NH_2 + R\dot{C}HNH_2$, which causes the disappearance of $RCH_2\dot{N}H$ in most cases.

Introduction

The radicals produced from amines and amino acids have been studied under various conditions. Both γ radiolysis[2-6] and photolysis[4,7] of single crystals[2-5] and polycrystalline and glassy samples[6-8] have been used for the formation of radicals which were subsequently studied by esr. Direct, *in situ* esr observation has been employed to study the radicals produced from such materials by the Ti^{3+}–H_2O_2 method[9-13] in aqueous solutions. Aqueous solutions of amines[14,15] and amino acids[16] have also been investigated by the pulse radiolysis technique utilizing kinetic spectrophotometry to follow the radicals produced initially by the electron pulse. Finally, product analysis of γ-irradiated solutions has been used to infer the mechanisms of formation and reaction of the amino acid radicals.[17] Although the latter two methods have provided a considerable amount of information, they lack the specificity of radical identification which is obtained by esr.

Esr studies of radicals in aqueous amino acid solutions have been carried out using Ti^{3+}–H_2O_2 to generate OH in acid solutions[10,12] and Ti^{3+}–EDTA–H_2O_2 in neutral and slightly alkaline solutions.[11,13] Generally it was found that in alkaline solutions hydrogen abstraction takes place from the position α to the amino group, whereas in acid solution the abstraction is mainly from positions further away from the ammonium group which strongly deactivates the adjacent position.

In acid solutions of methylamine the radical $\cdot CH_2\overset{+}{N}H_3$ has been observed by pulse radiolysis[15] but could not be detected by esr.[10] A similar difference exists for acid solutions of glycine where the results of pulse radiolysis experiments suggest[16] the radical $^+H_3N\dot{C}H$-

(1) Supported in part by the U. S. Atomic Energy Commission.

(2) D. K. Ghosh and D. H. Wiffen, *Mol. Phys.*, **2**, 285 (1959); *J. Chem. Soc.*, 1869 (1970).

(3) R. P. Kohin and P. G. Nadeau, *J. Chem. Phys.*, **44**, 691 (1966).

(4) P. B. Ayscough and A. K. Roy, *Trans. Faraday Soc.*, **64**, 582 (1968).

(5) H. C. Box, E. E. Budzinski, and H. G. Freund, *J. Chem. Phys.*, **50**, 2880 (1969).

(6) D. Cordischi and R. Di Blasi, *Can. J. Chem.*, **47**, 2601 (1969).

(7) S. G. Hadley and D. H. Volman, *J. Amer. Chem. Soc.*, **89**, 1053 (1967).

(8) W. Snipes and J. Schmidt, *Radiat. Res.*, **29**, 194 (1966).

(9) W. A. Armstrong and W. G. Humphreys, *Can. J. Chem.*, **45**, 2589 (1967).

(10) H. Taniguchi, K. Fukui, S. Ohnishi, H. Hatano, H. Hasegawa, and T. Maruyama, *J. Phys. Chem.*, **72**, 1926 (1968).

(11) R. Poupko, B. L. Silver, and A. Lowenstein, *Chem. Commun.*, 453 (1968).

(12) P. Smith, W. M. Fox, D. J. McGinty, and R. D. Stevens, *Can. J. Chem.*, **48**, 480 (1970).

(13) H. Paul and H. Fischer, *Ber. Bunsenges. Phys. Chem.*, **73**, 972 (1969).

(14) A. Wigger, W. Gruenbein, A. Henglein, and E. J. Land, *Z. Naturforsch. B*, **24**, 1262 (1969).

(15) M. Simic, P. Neta, and E. Hayon, *Int. J. Radiat. Phys. Chem.*, in press.

(16) P. Neta, M. Simic, and E. Hayon, *J. Phys. Chem.*, **74**, 1214 (1970).

(17) See review by W. M. Garrison in "Current Topics in Radiation Research," M. Ebert and A. Howard, Ed., North-Holland Publishing Co., Amsterdam, 1968, p 43.

COOH while the esr spectrum has been attributed to the species $H_2N\dot{C}HCOOH$.[10,12]

Esr spectroscopy has been used in this laboratory for the study of a number of radicals during continuous *in situ* radiolysis of aqueous solutions.[18-21] Radiolytic generation of radicals was found to have the advantage, relative to other chemical or photochemical means, of permitting the study of reactions of e_{aq}^- and of applicability over the full pH range. We have recently reported[20] an esr study of the deamination of a number of amino acids by e_{aq}^-. A disadvantage of this technique compared to pulse radiolysis is noticeable in those cases where secondary reactions can take place to form radicals which are long-lived compared with the primary radicals. In these cases only the secondary radicals are observed. The two methods are thus complementary to each other. We intend in this study to examine the reactions of OH radicals with amines and amino acids in aqueous solutions, with special emphasis on those points which could not be fully resolved by pulse radiolysis.

It should be noted that in cases where comparison of results is possible the esr spectra obtained here are essentially identical with those obtained with the Ti^{3+}–H_2O_2 system. In these cases (namely, with the amino acids previously studied) we have, therefore, only extended the results to higher pH. In terms of signal intensity (*i.e.*, radical concentration) our method is somewhat inferior to the use of Ti^{3+}–H_2O_2 although our resolution is somewhat better. The results reported here for amines are all new and provide important reference points for discussing the several problems encountered in interpretation of the amino acids results.

Experimental Section

The amino acids used were of the purest grade commercially available from Calbiochem, Cyclo Chemical, and Baker. Gaseous amines were obtained from Matheson. All the inorganic materials were Baker Analyzed reagents. Water was doubly distilled[18] and in the second distillation the vapor was passed with oxygen through a silica tube at ~600°. The pH was adjusted using potassium hydroxide, perchloric acid, sodium phosphates, and sodium tetraborate. Solutions were deoxygenated by bubbling with nitrous oxide. At pH > 3, N_2O scavenges practically all the hydrated electrons to form OH radicals. At lower pH values the competing reaction of e_{aq}^- with H_3O^+ takes place to form H atoms. Both OH radicals and H atoms can abstract hydrogen from the organic solutes. At pH > 3, ~90% of the reacting radicals are OH, and at pH < 2, ~50% are OH. In most cases of hydrogen abstraction the same radical is expected to be formed by either OH or H attack.

The irradiation was carried out in the esr cavity as previously described.[18,19] A flat silica cell of 0.5-mm internal spacing was used, and during irradiation the solution was driven through the cell at a flow rate of 1 cm^3/sec. In most cases no effect of flow rate on the spectrum could be observed at rates between 0.5 and 3 cm^3/sec. The solution was cooled slightly, before entering the cell, and all measurements pertain to about 15°. The total electron beam current was ~8 μA and that collected at an electrode in the solution was ~1 μA. Second-derivative spectra were recorded by use of two modulation frequencies. This method helps to minimize the interference by the signal from the silica cell so that only the region from 3 to 10 G above the center of the radical spectrum is obscured.

Results and Discussion

The two most probable paths for reaction of OH radicals with the basic form of amines and amino acids are hydrogen abstraction from either the α-alkyl group or the amino group

$$RCH_2NH_2 + OH \rightarrow \begin{cases} R\dot{C}HNH_2 & \text{(1a)} \\ RCH_2\dot{N}H & \text{(1b)} \end{cases} + H_2O$$

The amino alkyl radical can also be formed indirectly by

$$RCH_2\dot{N}H + RCH_2NH_2 \longrightarrow RCH_2NH_2 + R\dot{C}HNH_2 \quad (2)$$

Chemical analysis of irradiated aqueous solutions of amines and amino acids[17,22] shows that most products are formed from radicals of the type $R\dot{C}HNH_2$. There is, however, also some evidence from this source[22] for reaction 1b. The occurrence of both (1a) and (1b) is supported by recent pulse radiolysis experiments.[15,16] Reaction 2 is expected to be relatively more important in these esr experiments than in pulse radiolysis because in the present esr work radical lifetimes are much longer (~1 msec) so that reaction 2 can compete more effectively with radical–radical reactions.

Because there will be considerable discussion of the dissociation constants of various amine radicals, it is useful to review the existing data. Pulse radiolysis studies of amino acids[16] and amines[15] utilizing the initial optical absorption of the transient have been carried out. These studies show a change in absorption centered at about pH 5 for solutions of $CH_3NH_3^+$ and attributed the change to the equilibrium $\dot{C}H_2NH_3^+ \rightleftarrows \dot{C}H_2NH_2 + H^+$. With glycine two partially compensating changes in absorption occur between pH 3 and

(18) K. Eiben and R. W. Fessenden, *J. Phys. Chem.*, **72**, 3387 (1968).

(19) K. Eiben and R. W. Fessenden, *ibid.*, submitted.

(20) P. Neta and R. W. Fessenden, *ibid.*, **74**, 2263 (1970).

(21) P. Neta and R. W. Fessenden, *ibid.*, **74**, 3362 (1970).

(22) G. G. Jayson, G. Scholes, and J. J. Weiss, *J. Chem. Soc.*, 2594 (1955).

Table I: Structure and Coupling Constants of Radicals Produced in Irradiated Aqueous Solutions of Amines[a]

Amine	pH	Radical	g factor	a^N	a_{NH}^H	a_α^H	a_β^H	a_γ^H
Monomethylamine	7–13.5	$\dot{C}H_2NH_2$	2.00282	4.98	4.40 (2)	15.30 (2)		
Dimethylamine	7–13.5	$\dot{C}H_2NHCH_3$	2.00280	5.84	6.35 (1)	10.91 (2)		4.21 (3)
Trimethylamine	7–13.5	$\dot{C}H_2N(CH_3)_2$	2.00274	7.03		11.61 (2)		4.06 (6)
Dimethylamine	1	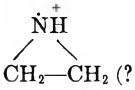	2.00360	19.22	21.90 (1)		33.56 (4)	
Trimethylamine	1	$CH_3\text{–}\dot{N}H\text{–}CH_3$	2.00360	20.53	$\mp$28.28 (1)[b]		$\pm$28.56 (6)	

[a] Hyperfine constants are given in gauss and are accurate to $\pm$0.03 G. The g factors are measured relative to the peak from the silica cell and are accurate to about $\pm$0.00005. Second-order corrections have been made [R. W. Fessenden, *J. Chem. Phys.*, **37**, 747 (1962)]. The number of hydrogen atoms displaying the hyperfine constant is given in parentheses. [b] From the second-order pattern this hyperfine constant must have a sign opposite that of a_β^H.

6. These changes have been interpreted as arising from the two protonations of $H_2N\dot{C}HCO_2^-$. The change of the pK associated with the amino group in going from the parent compound to the radical seems to lie in the range 4–6 units. On the basis of these studies it appears that the radical in acid solutions of glycine is $^+H_3N\dot{C}HCO_2H$.

Amines, amino acids, and several related compounds have been irradiated in aqueous solutions saturated with nitrous oxide at different pH values, and the esr spectra were recorded during the irradiation. For every compound the known[23] or estimated rate constants for reactions with OH radicals and H atoms have been used to choose a concentration high enough to ensure scavenging of most of the primary radicals. In many cases several different concentrations were used to verify that full scavenging occurred. In certain compounds no spectra could be observed, *e.g.*, from isopropylamine, *tert*-butylamine, tetramethylammonium hydroxide, acetylalanine, and aminomalonamide. This result is thought to be due to the large number of splittings which divide the intensity among many lines and as a result reduce the line intensities to near or below the noise level. Another possible reason for the absence of lines from acid solutions is the chemical exchange of the protons of the ammonium group. As discussed below, this exchange can cause line broadening in radicals having the structure $>\dot{C}\overset{+}{N}H<$, and in fact no radical of this type has been observed in solution. Such radicals are expected to be formed in acid solutions of mono-, di-, and trimethylamine and some amino acids. In contrast, spectra were detected when the amino group was in a position further away from the unpaired electron or when the amino group was in the basic form.

Amines. The structure and coupling constants of the radicals observed in irradiated aqueous solutions of amines are summarized in Table I, and two representative spectra are presented in Figure 1. The esr spectra observed with neutral and alkaline solutions of mono-, di-, and trimethylamine could be assigned to the aminoalkyl radicals formed by hydrogen abstraction from a methyl group.

$$CH_3NR_2 + OH \longrightarrow \dot{C}H_2NR_2 + H_2O \qquad (3)$$

This assignment is based on the number of equivalent protons of each type and on the magnitudes of the hyperfine constants. The symmetry implicit in these groupings and the consistency of the hyperfine constants for these three radicals make it very probable that the spectra belong to the expected reaction products. These hyperfine constants parallel those found here and in previous work[11,13] for the radicals in neutral and basic solutions of amino acids. In particular the value of a_α^H is quite small (10–15 G) and a^N is $\sim$5 G. Both the small a_α^H and the large a_γ^H can be taken to indicate a relatively large spin density on the nitrogen and a consequent lowering of the carbon spin density. However, it seems unlikely that this spin density could be as low as 0.5 (using $Q_\alpha \cong 23$ G), and it is possible that the three bonds around the carbon are not in plane. The pronounced effect of substitution of the nitrogen in reducing a_α^H from 15.3 to 10.9 G seems also to support this idea. Such a large change seems unlikely for a planar radical site, but if the substitution were to change the departure of the radical from planarity, a much larger effect on a_α might occur. The greater electron donating power of $-NHCH_3$ as compared to $-NH_2$ would favor a more bent structure.

Because no change in the spectra of $\dot{C}H_2NH_2$, $\dot{C}H_2NHCH_3$, and $\dot{C}H_2N(CH_3)_2$ could be found between pH 7 and 13.5, it can be concluded that over this region the radicals are always in the basic form as a result of the lower pK of the radical as compared to that of the parent molecule.[15] The appearance of radicals of the type $\dot{C}H_2NR_2$ at pH 7 demonstrates that reactions 4 and 5 must occur.

$$CH_3\overset{+}{N}HR_2 + OH \longrightarrow \dot{C}H_2\overset{+}{N}HR_2 + H_2O \qquad (4)$$

(23) M. Anbar and P. Neta, *Int. J. Appl. Radiat. Isotopes*, 18, 493 (1967).

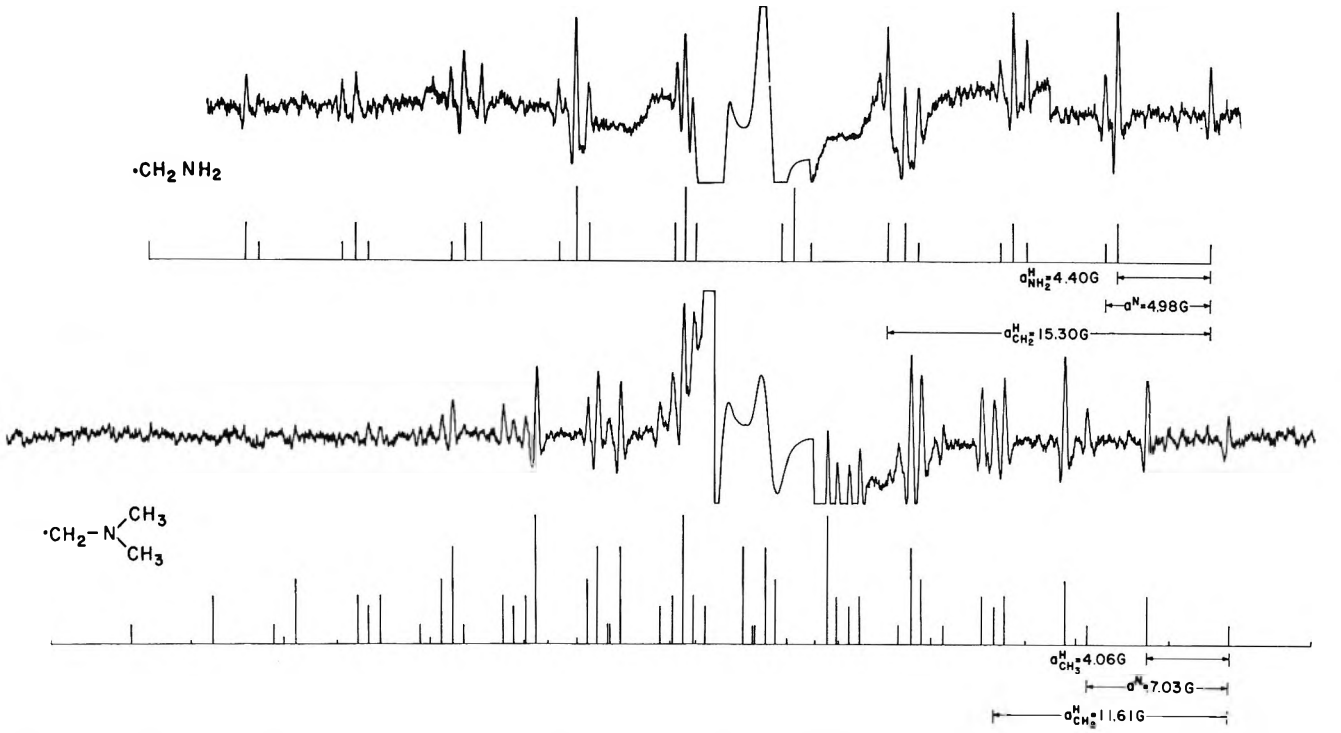

Figure 1. Second-derivative esr spectra of aqueous solutions of monomethylamine (top) and trimethylamine (bottom) saturated with N_2O at pH 12 during irradiation with 2.8-MeV electrons. Magnetic field increases to the right. The stick spectra show the relationship of the lines. The large signal from the silica cell is seen just above the center of the spectrum and is recorded at a gain 100 times less than the other portions. The low-field portion of the bottom spectrum was also recorded under conditions giving a somewhat higher signal-to-noise ratio, but no continuous scan of that is available. Both of these spectra show a pronounced intensity effect in that the high-field lines are considerably stronger than their low-field counterparts.

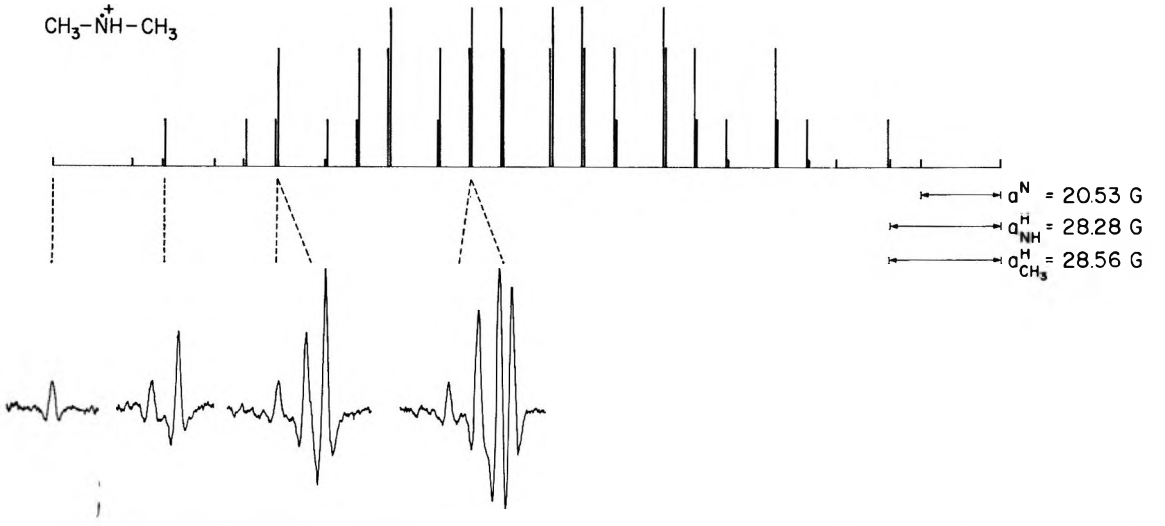

Figure 2. A schematic representation of the spectrum observed during radiolysis of a 0.1 M solution of trimethylamine at pH 1. Because of the large number of line groups, it is not possible to reproduce a continuous scan. Portions of the spectra with resolved second-order structure are shown. Similar line groups were observed at the other designated positions.

$$\dot{C}H_2\overset{+}{N}HR_2 \longrightarrow \dot{C}H_2NR_2 + H^+ \qquad (5)$$

Although the reaction of OH with methylamines in acid solutions must form aminoalkyl radicals (eq 4) the protonated forms of the radicals could not be observed (possibly as a result of the line broadening by chemical exchange of the $\overset{+}{N}H$ protons). Instead, the esr spectra observed in strongly acid solutions of dimethylamine and trimethylamine could be assigned to radicals produced by secondary reactions.

The spectra detected from irradiated acid solutions (pH 1) of di- and trimethylamine ($\sim$0.1 M) are different from those found in all other cases in that a large nitrogen splitting of about 20 G is evident (see Table I and Figure 2). These spectra clearly *cannot* be assigned to the radicals $\dot{C}H_2\overset{+}{N}H_2CH_3$ and $\dot{C}H_2\overset{+}{N}H(CH_3)_2$. The

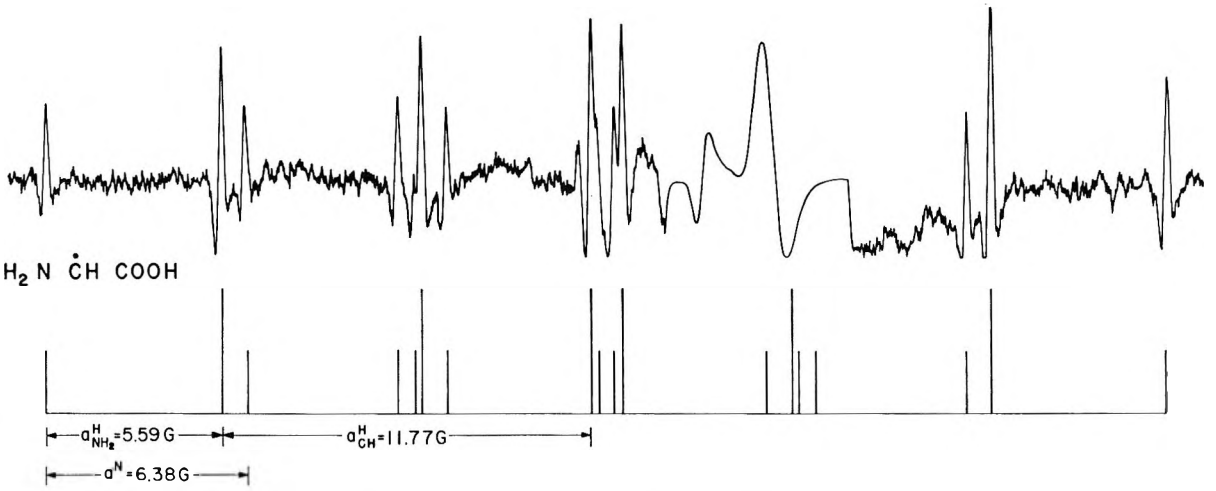

Figure 3. Esr spectrum of an aqueous solution of glycine (0.1 *M*) at pH 1 during irradiation. All lines are explained by the stick spectrum excepting one to the left of the center group.

most likely radicals with such a splitting are of the type $R_3\dot{N}^+$. The species $\dot{N}H_3^+$ and $(CH_3)_3\dot{N}^+$ are known from work on irradiated solids and the hyperfine constants are $a^N = 19.5$, $a_{NH}{}^H = 25.9$[24] and $a^N = 18.0$, $a_{CH}{}^H = 26.7$ G,[25] respectively, for the two radicals. In the case of trimethylamine the spectrum consists of 24 line groups and well-resolved second-order structure is present. From the number of line groups there must be one nitrogen splitting (20.53 G) and seven approximately equal proton splittings of about 28 G. The second-order structure is typical of *six* equivalent protons, however. This situation can arise if there are six equivalent protons with a coupling constant of one sign and another of nearly the same magnitude but of opposite sign.[26] The radical $(CH_3)_3\dot{N}H^+$ seems uniquely to satisfy these requirements ($a_\alpha{}^H$ should be negative while $a_\beta{}^H$ is positive). From the coupling constants for $^+\dot{N}H_3$ and $(CH_3)_3\dot{N}^+$ it is clear that such a chance equivalence of the magnitudes of the α and β constants would be possible.

The spectrum from solutions of dimethylamine also shows second-order structure (typical of four equivalent protons), and this spectrum can be fit to a high degree of accuracy by the hyperfine constants given in Table I. The previously developed computer program[27] was used for this purpose and using 36 of the total of 54 lines an rms deviation of 0.02 G was obtained. This deviation is about that expected from the accuracy of the line position measurements. The nitrogen hyperfine constant and g factor of this radical are very similar to those of the radical discussed immediately above so that the structure must be similar. To have four equivalent protons a structure of the type $RCH_2\dot{N}^+HCH_2R$ seems most probable and the lack of any further splittings suggests $\underline{CH_2\dot{N}^+HCH_2}$. The value of $a_\beta{}^H$ is larger than for the methyl protons in the same position as is the case when either a cyclic or straight-chain radical is compared to ethyl radical.[28] The splitting for the (presumably) NH proton is somewhat smaller than in $(CH_3)_2\dot{N}H^+$ or $\dot{N}H_3^+$. It should be noted that the cyclic structure is isoelectronic to cyclopropyl radical which has the abnormally low $a_\alpha{}^H$ of 6.5 G. If the cyclic structure is in fact correct, the bonds at the radical site must be more nearly in a plane than is the case for cyclopropyl radical.[28] The lack of exchange of the NH^+ proton in both radicals is consistent with the results on $N_2H_4{}^+$.[29]

The radicals from di- and trimethylamine can hardly be the result of any simple reaction and some secondary process is necessary. In support of this contention a reduction in signal height with increased flow rate is observed. No reasonable mechanism has been found for the formation of either of the two radicals suggested to explain the spectrum from solutions of dimethylamine. In the case of trimethylamine, however, a rather tentative mechanism can be suggested. It has been noted that the radical $\cdot CH_2N^+H(CH_3)_2$ must be formed in acid solutions although its spectrum is not observed (probably because of its broadened esr lines). If this radical undergoes disproportionation the compound $CH_2{=}N^+(CH_3)_2$ should be formed as suggested for amino acids.[17] The double bond will be very reactive toward OH addition so that this intermediate product can compete with the unreactive parent ammonium

(24) T. Cole, *J. Chem. Phys.*, **35**, 1169 (1961).

(25) A. J. Tench, *ibid.*, **38**, 593 (1963).

(26) With the values given in Table I overlap of pairs of second-order patterns (from the six equivalent protons) will occur in such a way as to give essentially no new lines. (A partially resolved line of unit intensity should appear between the first and second lines of each group in Figure 2.) This is possible because the second-order patterns all have common splittings. Some attempts at synthesizing the line shapes have been made, and although exact agreement has not been obtained no serious discrepancies are evident at this time.

(27) R. W. Fessenden, *J. Mag. Res.*, **1**, 277 (1969).

(28) R. W. Fessenden and R. H. Schuler, *J. Chem. Phys.*, **39**, 2147 (1963).

(29) J. Q. Adams and J. R. Thomas, *ibid.*, **39**, 1904 (1963).

Table II: Structure and Coupling Constants of Radicals Produced in Irradiated Aqueous Solutions of Amino Acids[a]

Compd	pH	Radical	g factor	a^N	a_{NH}^{H1} a_{NH}^{H2}	a_α^H	a_β^H	a_γ^H	a_δ^H
Glycine	1	$NH_2\dot{C}HCOOH$	2.00340	6.38	5.59 (2)	11.77 (1)			
Glycine	1 (in D_2O)	$ND_2\dot{C}HCOOH$	2.00340	6.21	0.87 (2)[b]	12.00 (1)			
Glycine	7–13.5	$NH_2\dot{C}HCOO^-$	2.00340	6.11	3.38 2.87	13.76 (1)			
α-Alanine	11–13.5	$NH_2\dot{C}(CH_3)COO^-$	2.00334	5.07	1.93 <0.2		13.86 (3)		
β-Alanine	11–13	$NH_2\dot{C}HCH_2COO^-$	2.00277	6.27	3.91 (2)	15.60 (1)	17.65 (2)		
Iminodiacetic acid	11–13	$^-OOCCH_2N\dot{C}HCOO^-$	2.00337	6.84	5.13 (1)	12.77 (1)		5.61 (2)	
Nitrilotriacetic acid	9–13	$(^-OOCCH_2)_2N\dot{C}HCOO^-$[c]	2.00340	6.96		11.64 (1)		3.8–4.0 (4)[d]	
α-Aminoisobutyric acid	5	$H_3{}^+N-\dot{C}(CH_3)_2-COO^-$	2.00255	3.51		22.24 (2)		0.44 (3)	
α-Aminoisobutyric acid	11–13	$NH_2-\dot{C}(CH_3)_2-COO^-$	2.00249	2.97		21.94 (2)		0.72 (3)	
α-Aminoisobutyric acid	13 (low concn only)	$H\dot{N}-C(CH_3)_2-COO^-$	2.00282	10.44	<0.2			1.28 (6)	
Acetylglycine	8	$CH_3CONH\dot{C}HCOO^-$	2.00333	0.51	1.32 (1)	17.33 (1)			2.74 (3)
Acetylglycine	13.5	$CH_2{=}CNHCHCOO^-$	2.00333	0.44	<0.2	19.91 (1)			3.48 (2)
Acetamide	9	$\cdot CH_2CONH_2$	2.00293	1.76	2.12 2.53	21.36 (2)			
N-Methylacetamide	1–13	$CH_3CONH\dot{C}H_2$	2.00281	2.20	<0.2	19.05 (2)			4.07 (3)

[a] Hyperfine constants are given in G and are accurate to +0.03 G. The g factors are measured relative to the peak from the silica cell and are accurate to about ±0.00005. Second-order corrections have been made [R. W. Fessenden, *J. Chem. Phys.*, **37**, 747 (1962)]. The number of hydrogen atoms displaying the hyperfine constant is given in parentheses. [b] This value of a_{NH}^D when corrected by the ratio of proton to deuteron magnetic moments becomes 5.67 G in excellent agreement with the value in the proton containing radical. [c] Paul and Fischer[13] report a small additional splitting of 0.15 G at pH 9 and give the structure as $(^-OOCCH_2)_2N\dot{C}HCOOH$. We did not observe this splitting, but this result could be a consequence of proton exchange. No change in the spectrum was observed upon going to stronger base. [d] See Figure 6.

ion $CH_2{=}N^+(CH_3)_2 + OH \rightarrow HOCH_2\dot{N}^+(CH_3)_2$. Because this species has both a hydroxyl group and a nitrogen on the same carbon some transformation such as $HOCH_2\dot{N}^+(CH_3)_2 \rightarrow OCH_2 + HN^+(CH_3)_2$ could occur leading to the observed radical. The acid conditions (pH 1) might contribute by catalyzing the reaction.

Amino Acids. The spectrum obtained from an irradiated solution of glycine at pH 1 is presented in Figure 3; the coupling constants (Table II) are in good agreement with previous values.[10,12] With this compound no lines could be observed at pH 3. However, at pH 5–7 the alkaline solution spectrum was present with many additional lines. Because of the complexity of the spectrum and weakness of the line intensities, no successful analysis of the additional contribution was possible. In acid solutions (pH 1–3) of iminodiacetic and nitrilotriacetic acids no spectra could be observed, again possibly as a result of the exchange of protons of the ammonium group.

The radical produced by the reaction of OH with glycine in acid solution seems to be $NH_2\dot{C}HCOOH$ as concluded in several previous studies[10,12] and in the present work. The hyperfine constants for this species are similar to those for the radical $H_2N\dot{C}HCOO^-$ which is formed in basic solution, but the two NH protons appear equivalent and have a somewhat larger coupling constant (the two NH protons in $H_2N\dot{C}HCOO^-$ are not equivalent). Protonation of the carboxyl group could readily account for the difference. This result is not in agreement with the conclusions drawn from the pulse radiolysis experiments discussed earlier which suggest that the radical should exist in the form $^+H_3N\dot{C}HCO_2H$. The assignment of the esr spectrum observed at pH 1 to the radical $H_2N\dot{C}HCOOH$ would imply a $pK < 1$ and a change of the pK of the NH_3^+ group of more than 8 units from the parent compound. This disagreement is serious enough to require a search for alternative explanations.

One possibility is that the lines of $^+H_3N\dot{C}HCOOH$ are broadened by exchange of the $-NH_3^+$ protons and that the spectrum observed is from some other radical, possibly a product of secondary reactions. Reference to the hyperfine constants of Table II shows that it is possible for the CH_2 protons of a radical of the form $RCH_2NH\dot{C}HCOO^-$ to have a coupling constant of the size assigned to the NH_2 protons of $H_2N\dot{C}HCOOH$. To test if such a radical were responsible for the spectrum in acid solutions of glycine an experiment was performed with a D_2O solution to determine if the protons having the 5.59-G hyperfine constant would be exchanged. The spectrum obtained in this case did in fact, have the 5.59-G proton triplets replaced by 0.87-G quintets of intensity 1:2:3:2:1 as expected for two deuterium nuclei. This result shows that the protons in question are located on a nitrogen because of their ready exchange and further substantiates the interpretation of the spectrum in terms of the hyperfine constants. Based on the esr results alone there seems little doubt, therefore, that the radical detected in acid solutions of glycine is $H_2N\dot{C}HCOOH$.

It should be noted that in no case (neither from amines nor amino acids) have radicals of the form $H_3\overset{+}{N}\dot{C}R_2$ been observed in aqueous solution. No radicals were detected from methylamine and iminodiacetic and nitrilotriacetic acids and from di- and trimethylamines the only radicals found seemed clearly to be the result of secondary reactions. Similar results have been reported for other systems.[10,13] The possibility that spectra of radicals with an α-NH_3^+ group are undetectable because of line broadening caused by exchange of the NH_3^+ protons has been mentioned above. Here we would like to discuss this point more fully.

The hyperfine constants for radicals of the type $^+H_3N\dot{C}R_2$ as found in irradiated solids[2,3] are quite different from those for the basic forms, and depending on the kinetics of the proton exchange process this difference could lead to a large increase in line width. Proton exchange in alcohol radicals has been considered several times,[30,31] but in those cases the splitting by the exchangeable proton is small ($\sim$1 G). Furthermore the exchange is acid-catalyzed $\dot{R}OH + H^+ \rightleftharpoons \dot{R}OH_2^+$ and can be made very rapid in strong acid. In the case of a radical $\dot{R}NH_3^+$ the exchange reaction should be

$$\dot{R}NH_3^+ \underset{k'}{\overset{k}{\rightleftharpoons}} \dot{R}NH_2 + H^+$$

If the pK of the acid form is like that determined from the pulse work on methylamine, then the equilibrium will be to the left at pH 1 and the lifetime of the spin state of the radical $\dot{R}NH_3^+$ will be limited by the first-order dissociation. To estimate this rate we will use the relation $K = k/k'$ where K is the equilibrium constant. With the values $k' = 10^0$ and $K = 10^{-4}k$ becomes 10^6. To cause a line width increase to 1 G the first-order rate would have to be approximately 2×10^7 sec^{-1} (the equivalent of 1-G line width in radians sec^{-1}). With a lower pK and a higher value for k' such a value of k is possible. On the basic side of the equilibrium the lifetime of the spin state of $\dot{R}NH_2$ is limited by the protonation rate, k'. To avoid line broadening to 1 G the product $k'[H^+]$ must be less than 2×10^7, or at pH 1 k' must be less than 2×10^8 M^{-1} sec^{-1}. Again line broadening is possible. At this time it is not clear if such a line broadening is in fact occurring.

The structure and coupling constants of the radical produced in irradiated alkaline solutions of several other amino acids are summarized in Table II, and some representative spectra are presented in Figures 4–9. With all of the amino acids which give sufficiently

(30) H. Fischer, *Mol. Phys.*, 9, 149 (1965).

(31) H. Zeldes and R. Livingston, *J. Chem. Phys.*, 47, 1465 (1967).

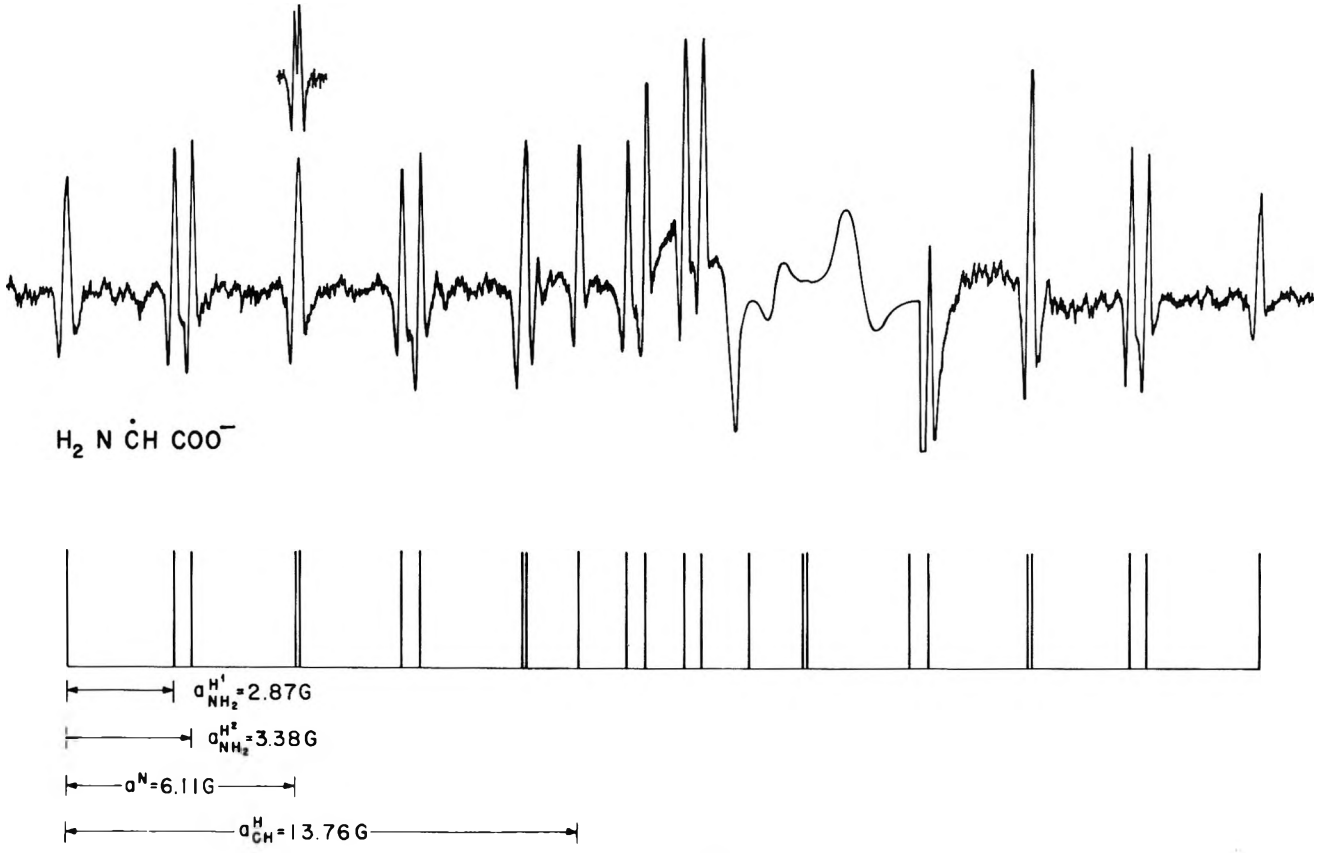

Figure 4. Esr spectrum of an aqueous solution of glycine (0.01 M) at pH 12 during irradiation. The fourth and fifth lines (of the stick spectrum) were resolved at a lower modulation as shown above the spectrum.

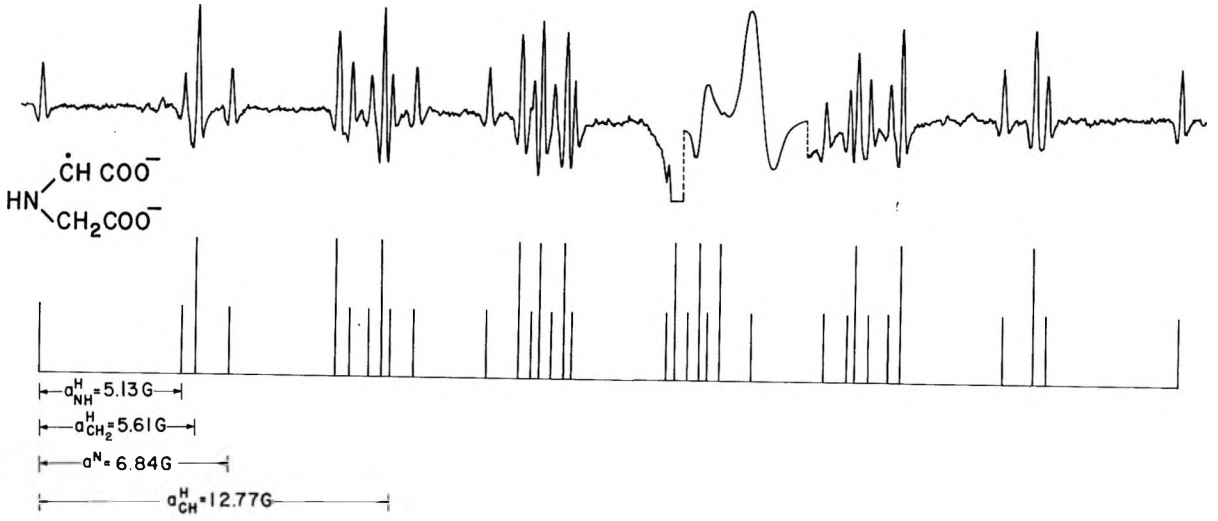

Figure 5. Esr spectrum of an aqueous solution of iminodiacetic acid (0.01 M) at pH 13 during irradiation.

intense spectra to be analyzed the aminoalkyl radical is observed. Furthermore, abstraction occurs to produce the α-aminoalkyl radical $R_2\dot{C}NH_2$ whenever a hydrogen α to the amino group exists. In the case of α-aminoisobutyric acid no such hydrogen is available and abstraction is at the β position producing $\dot{C}H_2C(NH_2)(CH_3)$-COO^-. Some of these radicals (from glycine, α-alanine, nitrilotriacetic acid, and acetylglycine) were produced previously by the Ti^{3+}–EDTA–H_2O_2 method,[13] and the coupling constants reported here are in good agreement with those values. We have followed the assignments given by Paul and Fischer[13] for most of the amino acids and from the consistency of the values among the various radicals see no reason to question their assignments. All of the amino acids studied were also irradiated at pH > 13; in most cases no changes in the spectra were observed. However, a different spectrum than that found in neutral solution was ob-

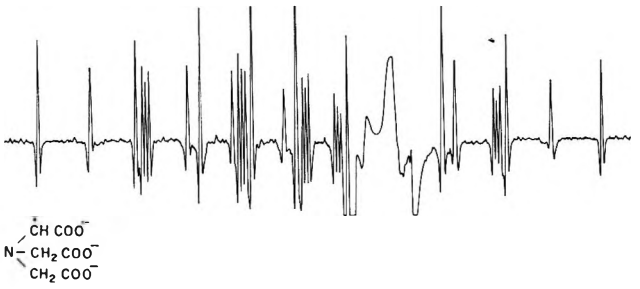

Figure 6. Esr spectrum of an aqueous solution of nitrilotriacetic acid (0.01 M) at pH 13 during irradiation. The varying peak heights reflect in part, varying line widths which are assumed to be a result of hindered internal rotation. No complete interpretation has been made. This spectrum is similar to that found by Paul and Fischer[13] but is better resolved.

served with strongly alkaline acetylglycine (see below).

The results obtained here are consistent with the overall mechanism given above, but because of the effect of reaction 2 there is little evidence of reaction 1b. In order to demonstrate the occurrence of reaction 1b it is necessary to choose a compound with a relatively slow reaction 2. It is reasonable to assume that the rate of reaction 2 would parallel that of (1a) and also be effected by the activating amino group. Compounds having no CH bonds in a position α to the amino group would be less reactive. For this reason α-aminoisobutyric acid and t-butylamine were chosen to demonstrate this effect after the experiments with glycine and alanine at low concentrations failed to show the RṄH radicals. Unfortunately, the spectrum obtained with t-butylamine did not have strong enough lines to be analyzed (see above). With solutions containing only low concentrations of α-aminoisobutyric acid a second spectrum was observed in addition to that of $\dot{C}H_2C(NH_2)(CH_3)COO^-$ (Figure 7). As well as can be determined this radical has six equivalent protons with a hyperfine constant of 1.28 G and a nitrogen with a^N = 10.44 G. The size of the proton splitting seems clearly to indicate that these nuclei are in a γ or comparably distant position and the size of the nitrogen splitting suggests a new type of radical. The only radical with this configuration which can be produced without considerable rearrangement is $HN\dot{C}(CH_3)_2COO^-$ or its dissociated form $^-N\dot{C}(CH_3)_2COO^-$. These species are also suggested by the chemical arguments given above. The latter radical must be considered because of the absence of a splitting in the spectrum by the NH proton. This radical, however, is isoelectronic to an alkoxy radical and might be expected to have a large g-factor anisotropy and broad lines even in solution.[32] The form $HN\dot{C}(CH_3)_2COO^-$ should show an extra splitting from the NH proton, but it is quite possible that rapid exchange of this proton could average this splitting to zero. In this connection it should be mentioned that the splitting by the OH proton of $(CH_3)_2\dot{C}OH$ is averaged out[19] at a pH of about 10, two units below the pK of this radical. It does not seem possible at this time to estimate the pK of the radical $HN\dot{C}(CH_3)_2COO^-$ and so to choose on this basis between these two alternatives. The fact that a nitrogen centered radical is observed only at millimolar concentrations demonstrates the importance of reaction 2 in our experiments.

Relatively little is known about this type of nitrogen centered radical. Recently Danen and Kensler[33] have reported solution spectra of $R_2\dot{N}$ radicals formed photolytically. These possess nitrogen splittings of 14 G consistent with our assignment here. It should be noted that the radicals $R_2C{=}\dot{N}$ also have similar nitrogen splittings.[21] Species with the structure RṄH have been invoked to explain the esr spectra observed from photolyzed frozen amines[7] and nitrogen hyperfine constants of ~30 G rather than the 10 G seen here were required to explain the spectra. This apparent discrepancy can be explained by reference to the full hyperfine tensor for nitrogen in the radical $H_2C{=}\dot{N}$. This radical has an isotropic hyperfine constant in the solid[34] of ~9.5 G, but the splitting in the powder spectrum corresponds to the parallel value of the hyperfine tensor, namely 34.4 G. It is reasonable to assume a similar anistropy for radicals of the type RṄH. Thus the isotropic hyperfine constant of 10.44 G assigned here to the radical $HN\dot{C}(CH_3)_2COO^-$ and the ~30-G splitting found for RṄH in the solid are both of the magnitude one should expect.

Amides. Experiments were performed with acetamide and N-methylacetamide because the hyperfine constants of the radicals $\dot{C}H_2CONH_2$ and $CH_3CONH\dot{C}H_2$ (Table II) were considered useful in deciding what radical is formed from acetylglycine. The radical from acetamide has been observed previously,[35] and our hyperfine constants as given in Table II are in good agreement. The radical from N-methylacetamide could be either $CH_3CONH\dot{C}H_2$ as indicated or $\dot{C}H_2CONHCH_3$. Chemical arguments favor the former in that the hydrogens of the CH_3 group on nitrogen are more activated. Recent pulse radiolysis experiments[36] support this view. A comparison of hyperfine constants of other radicals derived from amides[13,35] also leads to this choice. The absence of a splitting from the NH proton does not seem disturbing because of the small size and variable nature of this type of splitting (the radical from α-alanine shows only one splitting).

(32) M. C. R. Symons, *J. Amer. Chem. Soc.*, **91**, 5924 (1969).

(33) W. C. Danen and T. T. Kensler, *ibid.*, **92**, 5235 (1970).

(34) J. A. Brivati, K. D. J. Root, M. C. R. Symons, and D. J. A. Tinling, *J. Chem. Soc. A*, 1942 (1969).

(35) R. Livingston and H. Zeldes, *J. Chem. Phys.*, **47**, 4173 (1967).

(36) E. Hayon, T. Ibata, N. N. Lichtin, and M. Simic, *J. Amer. Chem. Soc.*, **92**, 3898 (1970).

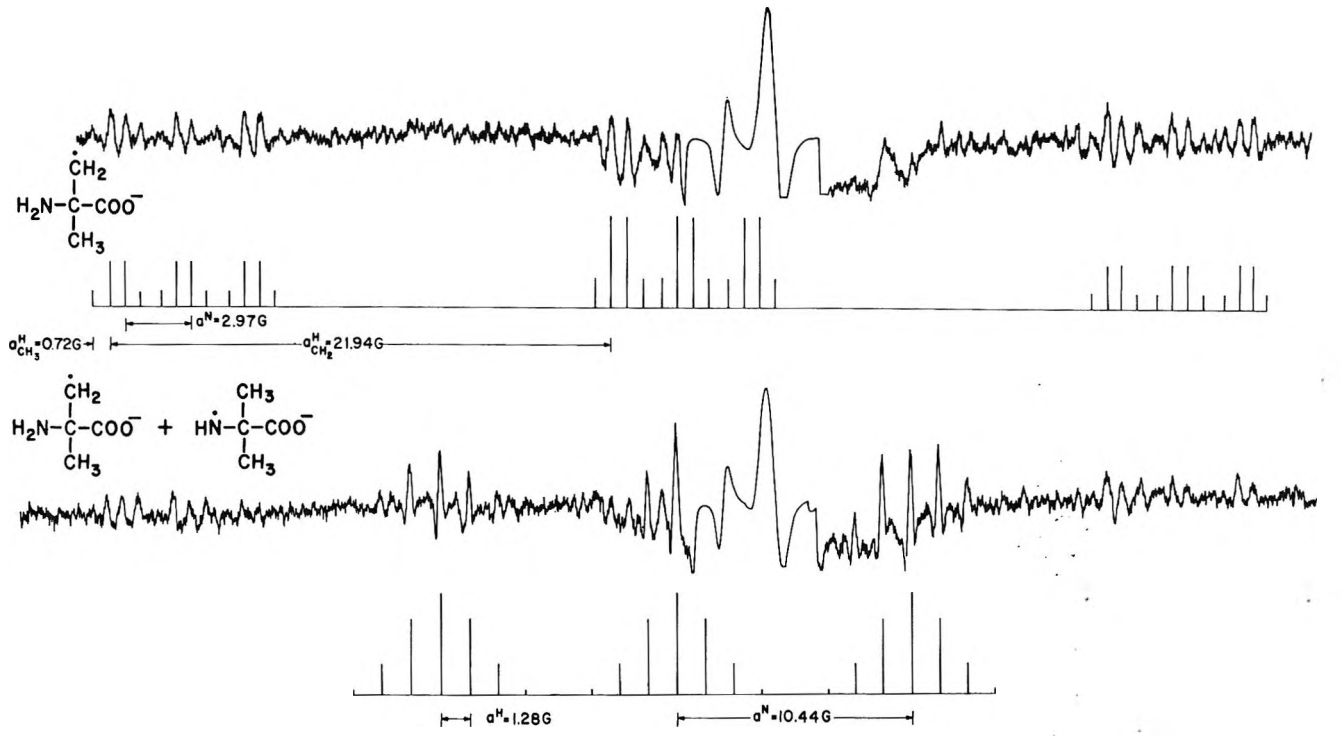

Figure 7. Esr spectra of aqueous solutions of α-aminoisobutyric acid (top, 0.1 M; bottom, 2.5×10^{-3} M) at pH 13.3. The stick spectrum at the top shows the relationship of the lines of the $\cdot CH_2C(NH_2)(CH_3)COO^-$ radical which is present at both concentrations. The stick spectrum at the bottom shows the lines of the $HNC(CH_3)_2COO^-$ radical formed only at the low concentration.

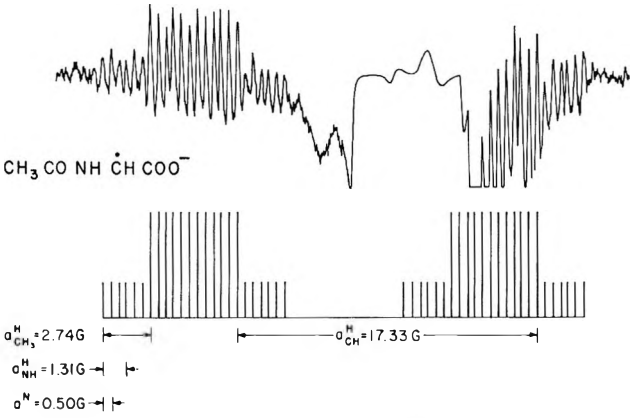

Figure 8. Esr spectrum of an aqueous solution of acetylglycine (0.01 M) at pH 8 during irradiation.

At pH 8 acetylglycine gives a radical with hyperfine constants similar to those of the radical from *N*-methylacetamide. The radical must be $CH_3CONH\dot{C}HCOO^-$. Paul and Fischer[13] have also detected this radical and give the same assignment. In stronger base (pH 13) a different spectrum is obtained (Figure 9). This spectrum has similar parameters to those found in the less alkaline solution (without the splitting by the NH proton) but is distinguished by having only a triplet splitting of ~3 G rather than the quartet from the terminal CH_3 group. At this time it is not clear whether this is a different form of the same radical or a new radical formed in some secondary reaction. Because no transformation of the starting material occurs in this pH range it is difficult to see why the species $CH_3CONH\dot{C}HCOO^-$ would *not* be formed. Therefore, either this radical undergoes some change or for some reason the lines become broad and unobservable while a new radical is formed. The first alternative seems the more reasonable. The species $CH_2{=}C(O^-)NH\dot{C}HCOO^-$ which is equivalent to dissociation of the OH proton from enol form $CH_2{=}C(OH)NH\dot{C}HCOO^-$ is suggested as at least consistent with the hyperfine constants.

Conclusion

The results obtained are consistent with the radical formation mechanism defined by reactions 1a, 1b, and 2. Because reaction 2 is usually fast, there is little direct evidence for reaction 1b in most cases. Only in the case of α-aminoisobutyric acid was a nitrogen centered radical detected which is believed to come from reaction 1b. In general the results obtained in very alkaline solutions of amines and amino acids are not different than those obtained in milder base (~pH 9) both in this work and previously.[13]

In agreement with previous results no radicals of the type $R_2\dot{C}NH_3^+$ were found in acid solutions of amino acids. This observation has been extended to solutions of the methylamines. The absence of such a spectrum cannot be explained by a lack of reactivity on the part of the acid form of the amine because secondary product

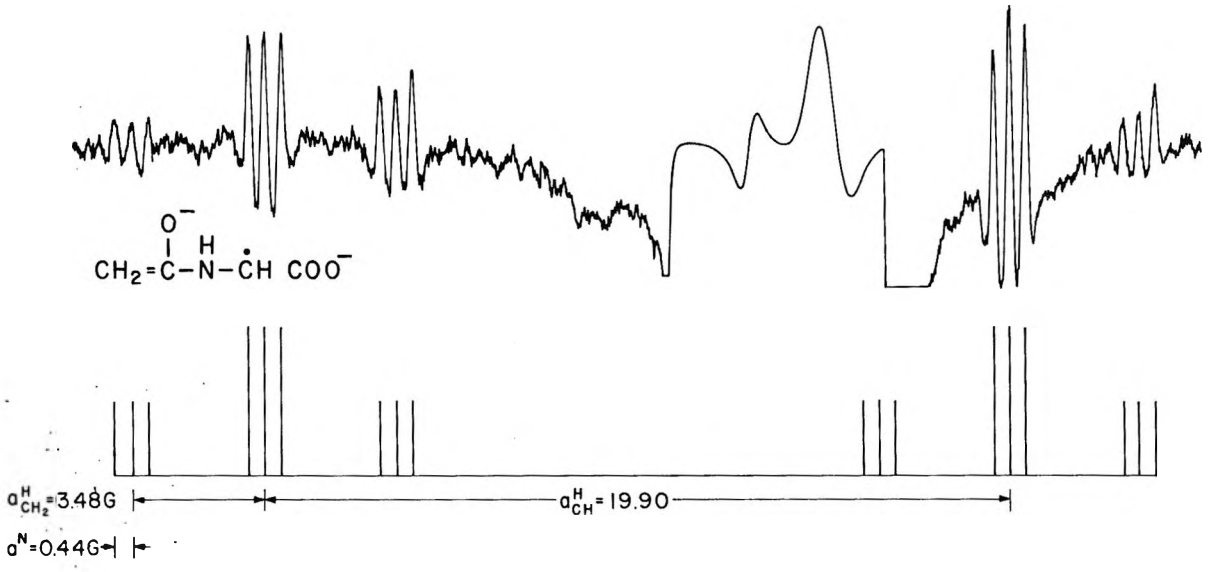

Figure 9. Esr spectrum of an aqueous solution of acetylglycine (0.01 *M*) at pH 13.5 during irradiation.

radicals were observed in the cases of di- and trimethylamine. It is possible that proton exchange in the radical $R_2\dot{C}NH_3^+$ broadens the lines of the esr spectrum making them unobservable. Finally, we are forced to agree with earlier workers that the esr spectrum observed in strongly acid solutions of glycine is best attributed to the radical $H_2N\dot{C}HCOOH$ although this assignment does not seem in agreement with the results of pulse radiolysis experiments. We believe this disagreement merits further investigation.

Acknowledgment. The authors wish to acknowledge several helpful discussions with H. Fischer.

Pulse Radiolysis of Oxalic Acid and Oxalates

by N. Getoff, F. Schwörer, V. M. Markovic, K. Sehested,*[1] and S. O. Nielsen

Danish Atomic Energy Commission, Research Establishment Risö, DK-4000 Roskilde, Denmark, and Max-Planck-Institut für Kohlenforschung, Abteilung Strahlenchemie, D-433 Mülheim a.d. Ruhr, F.R. Germany
(Received June 22, 1970)

Publication costs assisted by the Danish Atomic Energy Commission

Pulse radiolyses of oxalic acid and oxalates in aqueous solution were carried out. The following rate constants were determined: $k(e_{aq}^- + HC_2O_4^-) = (3.2 \pm 0.6) \times 10^9\ M^{-1}\ sec^{-1}$ and $k(e_{aq}^- + C_2O_4^{2-}) = (1.7 \pm 0.5) \times 10^7\ M^{-1}\ sec^{-1}$. With CNS^- ions as competitive solutes $k(OH + H_2C_2O_4) = (1.0 \pm 0.1) \times 10^6\ M^{-1}\ sec^{-1}$; $k(OH + HC_2O_4^-) = (3.2 \pm 0.1) \times 10^7\ M^{-1}\ sec^{-1}$, and $k(OH + C_2O_4^{2-}) = (5.3 \pm 0.3) \times 10^6\ M^{-1}\ sec^{-1}$ were also obtained. With N_2O as a scavenger for e_{aq}^- and H_2 (45 atm) for OH the absorption spectra of several radicals were obtained. Their absorption maxima are between 230 and 250 nm. Reaction mechanisms and kinetic data of the radicals are discussed.

1. Introduction

Aqueous oxalic acid has been studied extensively and used as a reliable radiation dosimeter.[2a] It has also been used as a scavenger for OH radicals for determination of the pH effect on the primary products of water radiolysis.[2b,3] The rate constants of the reactions of OH radicals,[4] e_{aq}^- and H atoms[5] with oxalic acid have been determined by means of competition reactions under steady-state conditions only. It has been found that oxalic acid is a very good scavenger of e_{aq}^-

$$k[e_{aq}^- + H_2C_2O_4\ (HC_2O_4^-;\ C_2O_4^{2-})] = 2.6 \times 10^{10}(3.4 \times 10^9;\ 4.8 \times 10^7)\ M^{-1}\ sec^{-1}\ [5]$$

The OH radicals react more slowly with the oxalic acid and with both oxalate forms

$$k[OH + H_2C_2O_4\ (HC_2O_4^-;\ C_2O_4^{2-})] = 5 \times 10^6\ (3.5 \times 10^7;\ 6 \times 10^6)\ M^{-1}\ sec^{-1}\ [4]$$

The corresponding rate constants for the reactions of H atoms were found to be extremely low

$$k[H + H_2C_2O_4\ (HC_2O_4^-;\ C_2O_4^{2-})] \leq 10^6\ M^{-1}\ sec^{-1}\ [5]$$

Some preliminary pulse radiolysis experiments with oxalic acid were made by Nielsen, Sehested, Pagsberg (Risö), and Christensen (AB Atomenergi, Sweden), and those experiments initiated the present investigations.

The formation and the kinetics of the decay as well as the absorption spectra of the short-lived intermediates of irradiated aqueous oxalic acid and oxalates are still unknown. In order to obtain more insight into this subject, we carried out pulse radiolysis of oxalic acid and oxalates at different pH values and under various experimental conditions. We determined $k(e_{aq}^- + HC_2O_4^-)$ and $k(e_{aq}^- + C_2O_4^{2-})$ by following the decay of e_{aq}^-. The rate constants for the reactions of OH radicals with the three forms of oxalic acid were determined with CNS^- and I^- ions as competing species.

2. Experimental Section

Preparation of the Solutions. The solutions were prepared by dissolution of analytical grade oxalic acid and potassium oxalates (E. Merck AG, Darmstadt) in triply distilled water. The pH of the solutions was adjusted by means of high-purity perchloric acid (G. F. Smith, Chemical Corp., Columbus, Ohio). The solutions were saturated by bubbling at room temperature (for 45 min) with high-purity argon or N_2O in 100-ml Summit syringes made of Pyrex. All glassware was baked for several hours at 470°.

Pulse Irradiation and Optical Detection. Most of the pulse irradiations were carried out with the 10-MeV Linac at Risö. The solutions were irradiated with 0.5-μsec electron pulses (dose: 3.5 krads/pulse) in a Suprasil quartz cell (light path length 5.2 cm, i.d. 1.5 cm) at room temperature. Some experiments were carried out with a special pressure cell (light path length 7.1 cm) under 45 atm H_2. The description of the cell as well as the technique has been given by Pagsberg, *et al.*[6]

The details concerning the pulse irradiation and the optical and electronic equipment are found elsewhere.[6,7]

(1) To whom correspondence should be addressed at Danish Atomic Energy Commission, Research Establishment Risö, DK-4000 Roskilde, Denmark.

(2) (a) N. W. Holm and I. G. Draganić, *Atompraxis*, **14**, 11/12, 495 (1968); (b) Z. D. Draganić, I. G. Draganić, and M. M. Kosanic, *J. Phys. Chem.*, **68**, 2085 (1964).

(3) Z. D. Draganić, I. G. Draganić, and M. M. Kosanic, *ibid.*, **70**, 1418 (1966).

(4) Z. D. Draganić, M. M. Kosanic, and M. T. Nedadovic, *ibid.*, **71**, 2390 (1967).

(5) O. Mićić and I. Draganić, *Int. J. Radiat. Phys. Chem.*, **1**, 287 (1969).

(6) P. Pagsberg, H. Christensen, J. Rabani, G. Nilsson, J. Fenger, and S. O. Nielsen, *J. Phys. Chem.*, **73**, 1029 (1969).

The dose absorbed in the irradiated samples was determined by means of a 10^{-3} M $Fe(CN)_6^{4-}$ solution saturated with N_2O and containing a small amount of air.[6,8] The absorption of the radiation-induced $Fe(CN)_6^{3-}$ was measured at 420 nm (ϵ_{420} = 1000 M^{-1} cm^{-1}),[8] and the absorbed dose was calculated by the use of $G[Fe(CN)_6^{3-}] = 5.25$.

The rate constants for the reactions of e_{aq}^- and OH radicals with both oxalate forms were determined by means of the 3-MeV Van de Graaff accelerator (High Voltage Eng. Co., type K) of the Max-Planck-Institut in Mülheim/Ruhr. Electron pulses (1.3 μsec) were used. The dose was varied from 0.9 to 3.6 krads/pulse.

The first-order decay of the electron absorption was followed either at 600 nm (Photomultiplier, 1P28) or at 720 nm (Photodiode, SD 100, Edgerton, Grier and Germeshausen). The dose was 0.9 krad/pulse, small enough to minimize undesired secondary reactions. Further details about this pulse irradiation facility have been reported previously.[9,10]

Measurement of Absorption Spectra. Since oxalic acid and both oxalates absorb light strongly in the ultraviolet region, it was not possible to work with concentrations higher than 10 mM even when a flashed Xe lamp[7] was used. This concentration is not high enough to ensure the complete scavenging of radicals. Furthermore the OH radicals also absorb in the same wavelength region.[6] Therefore, a computer program was used in each case to calculate the concentrations of radicals formed at a given reaction mechanism and set of rate constants at a given time after the electron pulse. The same calculations gave the necessary corrections for OH absorption. In order to ensure the validity of this method several concentrations of oxalic acid were always used, usually between 1 and 10 mM, as well as matrix solutions containing no solute.

The computer program used for solving the differential equations representing the course of the radiolytic reactions[11] was based on a fifth-order Runge-Kutta method. The computations were carried out on the Risö computer GIER.[12,13]

3. Results and Discussion

3.1. Reactions with Solvated Electrons. The rate constants for the reactions of e_{aq}^- with both oxalate forms were determined by the pseudo-first-order decay of the electron absorption. Oxalate solutions (0.6–10 mM) at pH 5 and 9, containing 10 mM of ethanol as scavenger for the OH radicals and saturated with O_2-free argon, were used. The rate constants, $k(e_{aq}^- + \text{oxalate})$, were calculated from the slopes of the straight lines, obtained by the plotting of $-\ln$ OD *vs.* time. Appropriate matrix corrections were applied. In the case of pH $\sim$ 5 (*ca.* 16% $HC_2O_4^-$ and 84% $C_2O_4^{2-}$) a correction for $k(e_{aq}^- + C_2O_4^{2-})$ is about 2% and the correction for $e_{aq}^- + H_3O^+$ is about 10%. pK_1 = 1.25 and pK_2 = 4.28 for oxalic acid dissociation were used in the calculations. The results obtained are shown in Table I together with literature data. The

Table I: Rate Constants for the Reaction of e_{aq}^- with Oxalic Acid and Oxalates

Solute	Rate constant	k in M^{-1} sec^{-1} This work	k in M^{-1} sec^{-1} Mićić and Draganić[a]
$H_2C_2O_4$	k_1	Not determined	$(2.5 \pm 0.5) \times 10^{10}$
$HC_2O_4^-$	k_2	$(3.2 \pm 0.6) \times 10^9$	$(3.4 \pm 0.4) \times 10^9$
$C_2O_4^{2-}$	k_3	$(1.7 \pm 0.5) \times 10^7$	$(4.8 \pm 0.3) \times 10^7$

[a] See ref 5.

rate constants determined by means of competition reactions under steady-state conditions[5] are in reasonable agreement with our data. As was to be expected, the rate constants decrease appreciably with the dissociation degree of oxalic acid.

It is assumed that the electron is added preferably to an undissociated carboxylic group and a radical-ion is formed

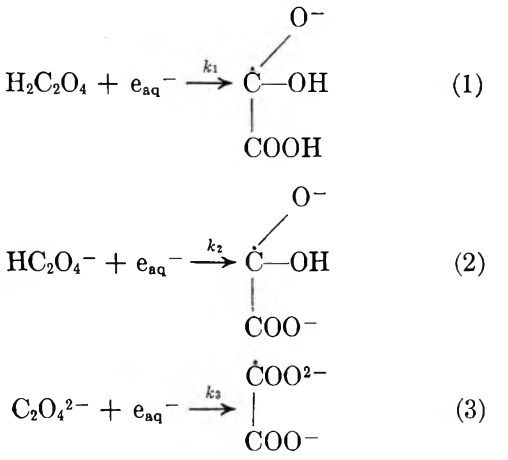

The first two rate constants, k_1 and k_2, conform neither to Brønsted's acid catalysis law, applied to reactions between acids and solvated electrons,[14] nor to the influence of the groups adjacent to the –CO– group, as described by Hart, *et al.*[15]

(7) H. C. Christensen, G. Nilsson, P. Pagsberg, and S. O. Nielsen, *Rev. Sci. Instrum.*, **40**, 786 (1969).

(8) J. Rabani and M. S. Matheson, *J. Phys. Chem.*, **70**, 761 (1966).

(9) G. O. Schenck and F. Schwörer, "Jahrbuch des Landesamtes für Forschung des Landes Nordrhein-Westfalen," Westdeutches Verlag, Köln, 1964, p 435.

(10) N. Getoff and F. Schwörer, *Radiat. Res.*, **41**, 1 (1970).

(11) H. Fricke and J. K. Thomas, *Radiat. Res. Suppl.*, **35**, 4 (1964).

(12) K. Sehested, O. L. Rasmussen, and H. Fricke, *J. Phys. Chem.*, **72**, 626 (1968).

(13) K. Sehested, E. Bjergbakke, O. L. Rasmussen, and H. Fricke, *J. Chem. Phys.*, **51**, 3159 (1969).

(14) J. Rabani, *Advan. Chem. Ser.*, **No. 50**, 242 (1965).

(15) E. J. Hart, E. M. Fielden, and M. Anbar, *J. Phys. Chem.*, **71**, 3993 (1967).

The radical-ions formed according to reactions 1–3 will be called RA1, RA2, and RA3, respectively.

3.2. Reactions with OH Radicals. The rate constants for the reactions of OH radicals with oxalic acid and with both oxalate forms were determined by the method developed by Adams, *et al.*[16] As competitive solute CNS^- ions and in some cases also I^- ions were used.

The transient, $(CNS)_2^-$, has a strong absorption at 475 nm (ϵ_{475} = 7600 M^{-1} cm^{-1}) and the I_2^- radical ions at 380 nm.[17] All thiocyanate solutions as well as mixtures of thiocyanate and oxalate (pH 3 and 9.3) were saturated with nitrous oxide (2×10^{-2} M) for scavenging of e_{aq}^-. At each pH value at least three different ratios of concentrations were irradiated with 0.9-μsec electron pulses. By plotting of the ratios of the optical densities with and without oxalic acid (respective oxalates) as a function of the concentration ratios of oxalic acid (respective oxalates) and thiocyanate, straight lines were obtained. From the slopes (S) of the straight lines the corresponding rate constants were calculated, *i.e.*

$$k(\mathrm{OH} + \text{oxalate}) = S \times k(\mathrm{OH} + \mathrm{CNS}^-)\ M^{-1}\ \mathrm{sec}^{-1} \quad (4)$$

At pH 0.5 there is about 85% of $H_2C_2O_4$ and 15% of $HC_2O_4^-$, whereas at pH 3 only $HC_2O_4^-$ and at pH > 6 only $C_2O_4^{2-}$ is present. Consequently the rate constants, $k(OH + HC_2O_4^-)$ and $k(OH + C_2O_4^{2-})$, were obtained directly, whereas the value for $k(OH + H_2C_2O_4)$ was calculated from the k value at pH 0.5 and corrected for the contribution of $HC_2O_4^-$.

The mean values of several determinations are given in Table II for $k(OH + CNS^-) = 7.5 \times 10^9\ M^{-1}\ sec^{-1}$ [18]

Table II: Rate Constants for the Reaction of OH Radicals with Oxalic Acid and Oxalates

Solute	Rate constant	k in M^{-1} sec^{-1}: This work	Draganić, *et al.*[a]
$H_2C_2O_4$	k_5	$(1.0 \pm 0.1) \times 10^6$	5×10^6
$HC_2O_4^-$	k_6	$(3.2 \pm 0.1) \times 10^7$	3.5×10^7
$C_2O_4^{2-}$	k_7	$(5.3 \pm 0.3) \times 10^6$	5×10^6

[a] See ref 2.

together with literature data.[4] These values, as well as those based on $k(OH + CNS^-) = 6.6 \times 10^9\ M^{-1}$ sec^{-1},[19] are in fair agreement with steady-state competition measurements,[4] while those based on $k(OH + CNS^-) = 2.8 \times 10^{10}$ and $k(OH + I^-) = 3.4 \times 10^{10}$ [17] are about four times as high.

It is well known that the reaction of OH radicals with a –COOH group is very slow, the adjacent group being very often the preferred point of attack.[16] It is difficult to say whether H abstraction or OH addition takes place. However, it is assumed that the overall reaction is

$$H_2C_2O_4 + OH \xrightarrow{k_5} H_2O + \begin{array}{l}\dot{C}OO\\ |\\ COOH\end{array} \quad (5)$$

The reaction with a dissociated carboxylic group is somewhat faster than that with an undissociated one, and most probably electron transfer occurs

$$HC_2O_4^- + OH \xrightarrow{k_6} OH^- + \begin{array}{l}\dot{C}OO\\ |\\ COOH\end{array} \quad (6)$$

$$C_2O_4^{2-} + OH \xrightarrow{k_7} OH^- + \begin{array}{l}\dot{C}OO\\ |\\ COO^-\end{array} \quad (7)$$

The radicals formed by the reaction of OH radicals with oxalic acid or oxalates (reactions 5–7) are denoted RB1, RB2, and RB3, respectively.

3.3. Reactions with H Atoms. For a study of these reactions solutions of 5 mM oxalic acid at pH 1.5 and 3 were irradiated under hydrogen pressure (45 atm). No appreciable absorption of short-lived species was observed in the optical region between 240 and 300 nm at pH 1.5, which confirms the very low rate of reactions reported.[15]

The addition of H may be regarded as the first step in the reaction with oxalic acid and oxalate ions

$$H_2C_2O_4 + H \xrightarrow{k_8} \begin{array}{l}\dot{C}(OH)_2\\ |\\ COOH\end{array} \quad (8)$$

$$HC_2O_4^- + H \xrightarrow{k_9} \begin{array}{l}\dot{C}(OH)_2\\ |\\ COO^-\end{array} \quad (9)$$

$$C_2O_4^{2-} + H \xrightarrow{k_{10}} \begin{array}{l}O^-\\ /\\ \dot{C}—OH\\ |\\ COO^-\end{array} \quad (10)$$

Since, under our experimental conditions, the rate constants for these three reactions (8–10) could not be determined by direct pulse radiolysis measurements,

(16) G. E. Adams, J. W. Boag, J. Currant, and B. D. Michael in "Pulse Radiolysis. Proceedings of the International Symposium," M. Ebert, J. P. Keene, A. J. Swallow, and J. H. Baxendale, Ed., Manchester, April 21–23, 1965, Academic Press, London, 1965, pp 131–143.

(17) J. H. Baxendale, P. L. T. Bevan, and D. A. Stott, *Trans. Faraday Soc.*, 64, 2389 (1968).

(18) C. L. Greenstock, I. W. Hunt, and M. Ng, *ibid.*, 65, 3279 (1969).

(19) G. E. Adams, J. W. Boag, J. Currant, and B. D. Michael in "Pulse Radiolysis. Proceedings of the International Symposium," M. Ebert, J. P. Keene, A. J. Swallow, and J. H. Baxendale, Ed., Manchester, April 21–23, 1965, Academic Press, London, 1965, pp 117–131.

we took the previously determined values for our computations, namely $k_8 \sim k_9 \sim k_{10} = 1 \times 10^6\ M^{-1}$ sec^{-1}.[5] For simplification, we shall call these radicals RC1, RC2, and RC3, respectively.

3.4. Absorption Spectra and Kinetics. The attack of the primary products of water radiolysis on oxalic acid and oxalates leads to the formation of a number of intermediates. It was established that they all absorb in the optical region from 230 to 350 nm. The radicals will be discussed in groups.

The RA-Type Radicals. As already mentioned, these species are formed by reactions of e_{aq}^- with oxalic acid and with both oxalate ions in argon-saturated solutions. Apart from the above-mentioned reactions (1–3 and 5–10) the following processes are assumed

$$e_{aq}^- + H_3O^+ \xrightarrow{k_{11}} H + H_2O \qquad k_{11} = 2.3 \times 10^{10}\ M^{-1}\ sec^{-1}\ [20] \quad (11)$$

$$H + H \xrightarrow{2k_{12}} H_2 \qquad 2k_{12} = 1.6 \times 10^{10}\ M^{-1}\ sec^{-1}\ [6] \quad (12)$$

$$H + OH \xrightarrow{k_{13}} H_2O \qquad k_{13} = 1.0 \times 10^{10}\ M^{-1}\ sec^{-1}\ [6] \quad (13)$$

$$OH + OH \xrightarrow{2k_{14}} H_2O_2 \qquad 2k_{14} = 1.1 \times 10^{10}\ M^{-1}\ sec^{-1}\ [6] \quad (14)$$

The computations for this system at pH 3 (argon-saturated solution) show that reaction 2 is almost completed during the pulse under our conditions. When the pulse ends, no significant amount of other radicals, except RA2, has been formed. The concentrations of RA2 and OH radicals at the pulse end, computed for a system of eq 2, 6, 9, and 11–14 are given in Table III.

Table III: Computed Yields of RA2 and OH Radicals at Pulse End for Three Oxalate Solutions (saturated with argon) at pH 3, Pulse Length 0.5 μsec, Dose 3.5 krads

	Computed values		
$[HC_2O_4^-]$, mM	RA2 $\dot{C}(O^-)(OH)COO^-$, μM	OH, μM	Correction for OH absorption, %
1	1.2	9.7	Max 45
2.5	2.6	9.6	Max 25
5	4.1	9.4	Max 17

The spectrum of RA2 radicals was obtained after correction for OH absorption and is shown in Figure 1.

The results obtained with three different oxalate concentrations agree very well within ±10%.

The fate of the RA2 radical was followed in a hydrogen-saturated solution (45 atm) at pH 3. Because of the very low rate constant for the reaction of H atoms with $HC_2O_4^-$ practically only RA2 radicals are formed

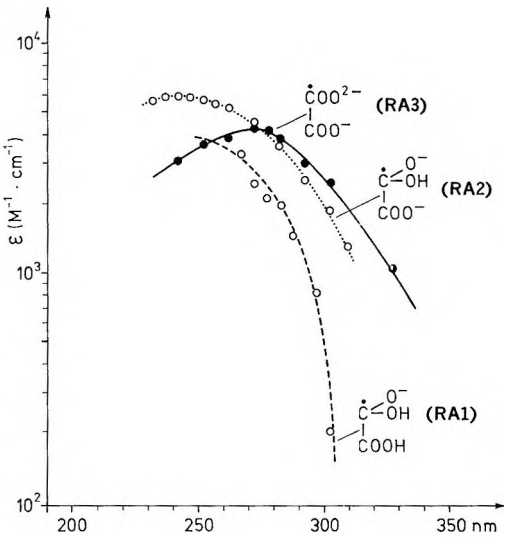

Figure 1. The absorption spectra of intermediates obtained by reaction of e_{aq}^- with oxalic acid and both oxalate ions.

under these conditions. The kinetic measurements were carried out at 260 and 280 nm.

It was possible to resolve the observed decay into two consecutive processes. At the beginning, for about 80 μsec, first-order decay with a half-life $T_{1/2} = 22.5$ μsec, was ascribed to the reaction

$$\dot{C}(O^-)(OH)COO^- \xrightarrow{k_{15}} \dot{C}OCOO^- + OH^-$$

$$k_{15} = (3.1 \pm 0.3) \times 10^4\ sec^{-1} \quad (15)$$

Assuming a protonation of the radical instead of reaction 15, one may calculate a first-order rate constant $k = 3 \times 10^7\ sec^{-1}$, which we consider to be too low for a protonation process. The radical formed in (15), however, most probably hydrates before recombination, but our experiments have not given enough information to be able to state which of the two reactions is the rate-determining step. The first-order decay was followed by a second-order decay of the radical ions, lasting from about 100 μsec to about 2.5 msec after the end of the pulse

$$2\,\dot{C}OCOO^- \text{ or } 2\,\dot{C}(OH)_2COO^- \xrightarrow{2k_{16}} \left[C(OH)_2COO^-\right]_2 \quad (16)$$

$$\frac{2k_{16}}{\epsilon_{280}} = 3.1 \times 10^5\ cm\ sec^{-1}$$

On the assumption that no significant decay of the $^-OOC\text{–}\dot{C}(OH)_2$ radical occurs before completion of reaction 15, the following molar extinction coefficients at 260 and 280 nm were calculated.

(20) S. Gordon, E. J. Hart, M. S. Matheson, J. Rabani, and J. K. Thomas, *Discuss. Faraday Soc.*, **36**, 193 (1963).

$$\epsilon_{260} = 2.6 \times 10^3\ M^{-1}\ \text{cm}^{-1}$$

and

$$\epsilon_{280} = 1.65 \times 10^3\ M^{-1}\ \text{cm}^{-1}$$

This gives

$$2k_{16} = 5.1 \times 10^8\ M^{-1}\ \text{sec}^{-1}$$

The spectrum of the RA3 radical (reaction 3) was obtained from argon-saturated $C_2O_4^{2-}$ solutions (5 and 10 mM) at pH 9.4. The spectra obtained were corrected for OH and RB3 absorption. The concentrations of these two radicals were computed at a time 10 μsec after the pulse end, and the reactions 3, 7, 10, 12, 13, 14, and also the following equations were taken into consideration.

$$e_{aq}^- + e_{aq}^- \xrightarrow{2k_{17}} H_2 + 2OH^- \qquad 2k_{17} = 9.0 \times 10^9\ M^{-1}\ \text{sec}^{-1}\ ^{21} \quad (17)$$

$$e_{aq}^- + H \xrightarrow{k_{18}} H_2 + OH^- \qquad k_{18} = 2.5 \times 10^{10}\ M^{-1}\ \text{sec}^{-1}\ ^{21} \quad (18)$$

$$e_{aq}^- + OH \xrightarrow{k_{19}} OH^- \qquad k_{19} = 3 \times 10^{10}\ M^{-1}\ \text{sec}^{-1}\ ^{21} \quad (19)$$

The computed values are given in Table IV.

The molar extinction coefficients of RA3 for different wavelengths are given in Figure 1.

Table IV: Computed Yields of RA3, RB3, and OH Radicals 10 μsec after the Pulse for Two Concentrations of Oxalate Solutions (saturated with argon) at pH 9.4, Pulse Length 0.5 μsec, Dose 3.5 krads

	Computed values			
$[C_2O_4^{2-}]$, mM	RA3 $\dot{C}OO^{2-}$ | COO^-, μM	RB3 $C\dot{O}O$ | COO^-, μM	C·H, μM	Total correction for OH and RB3 absorption, %
5	2.7	1.4	2.0	Max 50
10	3.8	2.2	1.7	Max 35

The species formed at pH 9.4 in argon-saturated $C_2O_4^{2-}$ solutions follow approximately second-order decay with slope $S = 9 \times 10^4$ cm sec^{-1} at the beginning and $S = 6 \times 10^4$ cm sec^{-1} after a few hundred microseconds. These slopes, however, are followed for a relatively small change in optical densities (less than 2 half-lives in both cases), and they are considered less accurate than the other kinetic data given in this paper.

Here, both radicals, RA3 and RB3, are present at the beginning. The second radical decays much faster than the first (see later) and has a much smaller molar extinction coefficient at 280 nm (Figure 2). Therefore the second slope probably corresponds to the recombination of the RA3 radical only, in accordance with the reaction

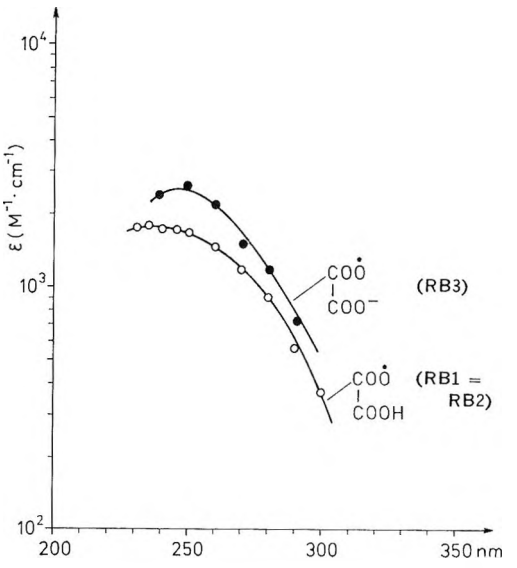

Figure 2. The absorption spectra of intermediates obtained by reaction of OH radicals with oxalate ions.

$$2\ \dot{C}OO^{2-} \xrightarrow{2k_{20}} \text{products}\ 2k_{20} \leq 2 \times 10^8\ M^{-1}\ \text{sec}^{-1} \quad (20)$$

An attempt has been made to determine the absorption spectrum of RA1 radicals at pH 2 (16% $H_2C_2O_4$ and 84% $HC_2O_4^-$). In this case the corrections for OH and RA2 radicals are too large (60–80%). The spectrum is, however, presented in Figure 1 for comparison. The ϵ values are probably too low, and the spectrum may be identical with that of the RA2 radical. An alcohol as OH scavenger might have improved the determinations.

The RB-Type Radicals. These radicals are formed as a result of the attack of OH radicals on oxalic acid and both oxalate ions. The determination of the absorption spectrum of the RB1 radical is difficult. However, in writing reactions 5 and 6 it was assumed that RB1 and RB2 are identical.

The absorption spectrum of RB2 was obtained for solutions containing various concentrations (1–10 mM) of $HC_2O_4^-$ in N_2O-saturated solutions at pH 3. In this case there is competition between N_2O and $HC_2O_4^-$ for e_{aq}^-. Most of the e_{aq}^-, however, are transformed into OH radicals according to the reaction

$$e_{aq}^- + N_2O \xrightarrow{k_{21}} N_2 + OH + OH^- \qquad k_{21} = 5.6 \times 10^9\ M^{-1}\ \text{sec}^{-1}\ ^{22} \quad (21)$$

Therefore, only a small amount of RA2 radicals is formed. The corrections for RA2 and OH radicals

(21) M. S. Matheson and J. Rabani, *J. Phys. Chem.*, 69, 1324 (1965).

(22) J. P. Keene, *Radiat. Res.*, 22, 1 (1964).

were computed for the system of eq 2, 6, 9, 11–14, and 21. The results are given in Table V.

The absorption spectrum of the RB2 radical (Figure 2) was obtained from various concentrations of $HC_2O_4^-$ corrected according to the data in Table V. Here again very good agreement was obtained for several different concentrations. Only mean values are presented. They were obtained with about ±10% standard deviation.

Table V: Computed Yields of RB2, RA2, and OH Radicals at Pulse End for Several Concentrations of N_2O-Saturated Oxalate Solutions at pH 3, Pulse Length 0.5 μsec, Dose 3.5 krads

	Computed values			
$[HC_2O_4^-]$, mM	RB2 $\dot{C}OO$-COOH, μM	RA2 $\dot{C}(O^-)$-OH-COO^-, μM	OH, μM	Correction for OH and RA2 absorption, %
1	3	0.14	4.3	Max 38
2	5.4	0.3	3.3	Max 26
5	10.1	0.7	1.5	Max 26
10	13.4	1.3	0.3	Max 26

The kinetics of these radicals are complex (Figure 3). At pH 3 the OH radicals are practically consumed within about 20 μsec.

Figure 3 shows for two oxalate concentrations the second-order decay, starting after a few hundred microseconds. At the beginning an increase of optical absorption is observed, followed by a subsequent decrease, which indicates the transformation of radicals with lower molar extinction coefficient into radicals with higher coefficient. The position of the maximum of the absorption (minimum on curve A, Figure 3) is shifted to shorter times with an increase of the oxalate concentration (Figure 3, curve B).

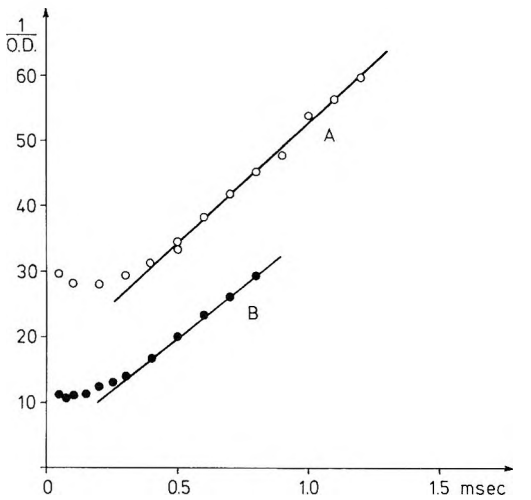

Figure 3. Mixed- and second-order decay at λ 270 nm of radicals formed in N_2O-saturated oxalate solutions at pH 3: A, (○) 2.5 mM $HC_2O_4^-$; B, (●) 10 mM $HC_2O_4^-$.

The reaction of radical RB2 with oxalic acid, yielding radical RC1, is suggested as an explanation of the yield of dihydroxytartaric acid and CO_2 measured in deaerated solutions of oxalic acid at pH 1 and 3.[23]

At pH 1

$$\begin{matrix}\dot{C}OO \\ | \\ COOH\end{matrix} + \begin{matrix}COOH \\ | \\ COOH\end{matrix} \xrightarrow{2k_{22}} 2CO_2 + \begin{matrix}\dot{C}(OH)_2 \\ | \\ COOH\end{matrix} \qquad (22)$$

This reaction may explain the first part of the curves in Figure 3. The RC1 radical is the hydrated form of the $CO \cdot COO^-$ radical ion and may be assumed to have the same molar extinction coefficient. Hence the RB2 radical is transformed into a radical with about twice the molar extinction coefficient at 270 nm. The second-order decay, then, corresponds to the recombination of RC1 radicals

$$2\begin{matrix}\dot{C}(OH)_2 \\ | \\ COOH\end{matrix} \xrightarrow{2k_{16}} \left[\begin{matrix}C(OH)_2 \\ | \\ COOH\end{matrix}\right]_2 \qquad (16)$$

Figure 3 gives

$$\frac{2k_{16}}{\epsilon_{270}} = 1.6 \times 10^5 \text{ cm sec}^{-1}$$

With $\epsilon_{270} \leq 2100\ M^{-1}\text{ cm}^{-1}$ (see section 3.4) the following rate constant was calculated

$$2k_{16} \leq 3.4 \times 10^8\ M^{-1}\text{ sec}^{-1}$$

This value is lower than 5.1×10^8 calculated earlier (see section 3.4) probably due to the interference of reaction 22 on the decay.

Before complete decay of the radical RB2 its reaction with RC1 also starts to contribute[23]

$$\begin{matrix}\dot{C}OO \\ | \\ COOH\end{matrix} + \begin{matrix}\dot{C}(OH)_2 \\ | \\ COOH\end{matrix} \longrightarrow 2CO_2 + H_2O + \begin{matrix}CHO \\ | \\ COOH\end{matrix} \qquad (23)$$

The influence of oxalic acid concentration on the first part of the curves in Figure 3 supports reaction 22. This reaction is quickly masked by reactions 16 and 23, and thus the accurate determination of k_{22} is prevented. An estimate, however, can be made, giving an upper limit to k_{22} of a few times $10^6\ M^{-1}\text{ sec}^{-1}$.

The rate constant for the recombination of RB2 radicals seems to be much lower than $10^7\ M^{-1}\text{ sec}^{-1}$, and this reaction can probably be neglected in the presence of oxalic acid in concentrations above 1 mM.

By radiolysis of a $C_2O_4^{2-}$ solution saturated with N_2O at pH 9.4, only RB3 radicals are produced. Corrections for the OH radicals have been computed as before

(23) V. Markovic, K. Sehested, and E. Bjergbakke, unpublished work.

for the system of eq 7, 10, 12, 13, 14, and 22. For a 5 mM $C_2O_4^{2-}$ solution saturated with N_2O the following values were calculated at 10 μsec after the pulse end: [OH] = 5.12 μM and [RB3] = 3.34 μM. From the measured absorption spectrum of RB3, corrected for OH radicals, the corresponding molar extinction coefficients, shown in Figure 2, were calculated. The correction for the OH absorption is in this case below 25%.

The kinetics of decay showed no indication of the deviation from the second order that was observed at pH 3. This probably means that the RB3 radical hardly reacts with oxalate.

A pure second-order decay of the $C_2O_4^-$ radical ion was observed

$$2\begin{vmatrix}\dot{C}OO\\ COO^-\end{vmatrix} \xrightarrow{2k_{24}} \text{products} \qquad (24)$$

with

$$\frac{2k_{24}}{\epsilon_{280}} = 8 \times 10^5 \text{ cm sec}^{-1}$$

and

$$2k_{24} = 9.6 \times 10^8 M^{-1} \text{ sec}^{-1}$$

It might be of interest to compare this value with the corresponding data for the CO_2^- radical ion and the COOH radical. For $2k(CO_2^- + CO_2^-) = 1 \times 10^9 M^{-1}$ sec^{-1} [24] we calculate $2k/\epsilon_{280} = 4.2 \times 10^5$ cm sec^{-1} and for $2k$(COOH + COOH) $= 4 \times 10^9$ M^{-1} sec^{-1}, $2k/\epsilon_{280} = 3 \times 10^6$ cm sec^{-1}.[25]

From this comparison it can be concluded that reaction 25

$$\begin{vmatrix}\dot{C}OO\\ COOH\end{vmatrix} \longrightarrow CO_2 + \dot{C}OOH \qquad (25)$$

does not take place at pH 3, and probably not at pH 9.

The RC-Type Radicals. The reactions of oxalic acid and both oxalates with H atoms, as discussed above, are very slow ($k \leq 10^6 M^{-1}$ sec^{-1}),[5] and therefore the determination of the corresponding absorption spectra is very difficult. No appreciable absorption could be detected in 5 mM oxalic acid under 45 atm of H_2 at pH 1.5.

3.5. Peroxy Radicals. A few series of pulse radiolysis experiments were carried out with oxygen present and with various concentrations of oxalic acid and oxalates at different pH values. The absorption spectra of the short-lived species are rather complex. Further investigations of these intermediates are necessary in order to distinguish between the various peroxy radicals.

Acknowledgments. We wish to thank O. L. Rasmussen for computer calculations. The help given by the accelerator staff at Risö and the technical assistance by P. L. Genske and M. Wille are gratefully acknowledged. Two of us (N. G. and V. M.) thank the Danish Atomic Energy Commission for the fellowships granted.

(24) J. P. Keene, Y. Raef, and A. J. Swallow in "Pulse Radiolysis. Proceedings of the International Symposium," M. Ebert, J. P. Keene, A. J. Swallow, and J. H. Baxendale, Ed., Manchester, April 21–23, 1965, Academic Press, London, 1965, pp 99–106.

(25) N. Getoff, B. D. Michael, and E. J. Hart, unpublished results.

The Radiolysis of Colloidal Sulfur. A Mechanism for Solubilization[1,2]

by G. W. Donaldson and F. J. Johnston*

Department of Chemistry, University of Georgia, Athens, Georgia 30601 *(Received July 24, 1970)*

Publication costs assisted by The Atomic Energy Commission

Colloidal sulfur suspensions having a narrow range of particle sizes have been irradiated with γ rays from cobalt-60. The particles are solubilized upon irradiation and the reaction has been followed by light scattering measurements. The total dose of radiation which is required to produce a given change in particle size in a particular suspension depends upon the durations of the irradiation periods and of the waiting or recovery periods between irradiations, the temperature, and the particle concentration. At the highest dose rates studied, solubilization rates are independent of radiation intensity. The results are consistent with a mechanism in which sulfur in the solution phase undergoes reaction upon irradiation and the particles dissolve as the system attempts to establish equilibrium. Reaction at the particle surface is evidently of negligible importance. The mechanism has been formulated in terms of n, the particle population, D, the diffusion coefficient for the species diffusing away from the particle surface, C_s, the effective saturation concentration of homogeneously dissolved or dispersed sulfur in the liquid phase, and k_1, a pseudo-first-order rate constant for the reaction upon irradiation of sulfur in the liquid phase. Our results indicate a value of 25° for the product DC_s of 5.7 to 5.9 $\times 10^{-13}$ with D in cm^2 sec^{-1} and C_s in g cc^{-1}. It is not possible to assign unique values to D and C_s; however, our results suggest that $D \sim 5.9 \times 10^{-6}$ cm^2 sec^{-1} and $C_s \sim 1.0 \times 10^{-7}$ g cc^{-1}. Based upon the suggested mechanism for the process and the above value for C_s, the reaction rates indicate an initial G value for reaction by sulfur in the solution phase of 2.6 atoms reacting per 100 eV of absorbed energy.

Introduction

In earlier reports[3,4] we have described the behavior of colloidal sulfur suspensions upon absorption of ionizing radiation. When subjected to γ radiation from ^{60}Co, the colloidal material is solubilized with the with the apparent formation of sulfuric acid. The reaction is inhibited by O_2, H_2O_2, Fe^{2+}, and Br^- and is accelerated by the addition of n-propyl alcohol.

In a more comprehensive study of the radiation-induced reaction we have found that solubilization rates depend upon the duration and frequency of irradiation periods and upon the length of the waiting period between irradiations. At dose rates above approximately 8×10^{15} eV cc^{-1} sec^{-1}, reaction rates are independent of radiation intensity and for irradiation schedules in which the ratio of irradiation time to recovery time is small (less than approximately 0.2) there is a marked dependence upon particle concentration.

This report summarizes the results of our experiments in which particle solubilization rates were measured as a function of "pulsing" schedule, radiation intensity, and particle concentration. A mechanism is proposed which is consistent with the experimental results and which involves a reaction by homogeneously dissolved or dispersed sulfur. Our results indicate that reaction at the particle surface is of negligible importance.

Experimental Section

Preparation of Colloidal Sulfur Suspensions. The preparation and properties of colloidal sulfur suspensions having a narrow range of particle sizes (La Mer sols) have been thoroughly described by La Mer and coworkers and references to these articles may be found in ref 4. All of the colloids used in our experiments were prepared by mixing prefiltered solutions of $Na_2S_2O_3$ and HCl at 25°. Reactant concentrations were 5×10^{-4} M $S_2O_3^{2-}$ and 4×10^{-3} M HCl. The colloid growth reaction was stopped by titration with saturated aqueous Br_2. Samples of the suspension to be irradiated were placed in light scattering–radiolysis cells, thoroughly degassed on a vacuum line, and sealed off *in vacuo* prior to irradiation.

Irradiations. Irradiations were carried out in a ^{60}Co source loaded with approximately 5000 Ci of ^{60}Co. During irradiations, the reaction cells were placed in a jacket through which water from a thermostatically controlled bath was circulated. Unless otherwise indicated, the irradiations were performed at 25 ± 0.5°. When lead shields were used, temperature control was not feasible and irradiations were at ambient source temperature (approximately 35°). Dose rates in the jacketed cell were 1.42×10^{16} to 1.46×10^{16} eV cc^{-1} sec^{-1} at 25°.

Particle Size Determinations. Particle radii were obtained from measurements of the intensities of horizontally and vertically polarized light scattered from the colloidal suspensions as a function of scattering

(1) This work has been supported in part by AEC Research Grant AT-(40-1)-2826 and in part by PHS Grant EC 00077-07.

(2) G. W. Donaldson, Ph.D. Thesis, University of Georgia, Athens, Ga., 1970.

(3) F. J. Johnston, *J. Phys. Chem.*, 69, 2805 (1965).

(4) G. W. Donaldson and F. J. Johnston, *ibid.*, 72, 3552 (1968).

angle.[5] The experimental details have been described in our earlier report. A computer program, CONTOU2, developed by workers[6-8] at Clarkson College of Technology, was used to recover particle radii from the experimental polarization ratios. This program utilizes an assumed zeroth-order log normal distribution function for particle size that is characterized by the parameters r_m and σ_0. These quantities are defined by the distribution function

$$f(\alpha) = \frac{\exp\left[-\frac{(\ln \alpha - \ln \alpha_m)^2}{2\sigma_0^2}\right]}{2\pi\sigma_0\alpha_m \exp(\sigma_0^2/2)}$$

$\alpha = 2\pi r/\lambda'$, where r is the particle radius and λ' the wavelength of light in the medium. r_m, the modal radius, and the distribution breadth parameter, σ_0, are defined through the above equation. σ_0 is approximately related to the standard deviation, σ, of the modal size by $\sigma_0 = \sigma/r_m$. The program compares theoretical polarization ratios, based upon Mie scattering theory, with experimental ratios from the 19 scattering angles. The program output consists of a plot of the size parameter, α_m, *vs.* the distribution parameter, σ_0, in the format of a topographical mapping. We have used in our calculations and in our plots the value of r_m corresponding to the minimum σ_0. For small particles of less than approximately 0.3 μ, the modal radii obtained from this treatment were usually in good agreement with those obtained from Figure 6 in ref 5. For bigger particles, the computer treatment gave larger radii and for the suspensions that we used having $r_m \sim 0.45$ μ, modal radii were approximately 10–20% larger than those obtained from ref 5.

Particle Concentrations. Particle concentrations were estimated from transmission measurements on the colloidal suspensions. These were obtained with a Cary 15 spectrophotometer using a 10-cm cell. Particle populations were evaluated from the measured turbidities, τ, and the scattering factors, K,[9a,b] corresponding to the modal radii. The number of particles per cubic centimeter, n, is given by

$$\tau = \pi r^2 n K$$

Apparent particle concentrations obtained by this procedure for the suspensions used in this work were from 1.2 to 2.5 $\times 10^6$ cc^{-1} with most of the values between 1.7 and 2.1 $\times 10^6$ cc^{-1}. These must be considered as approximations since the method assumes monodispersity.

Rowell, *et al.*,[10] have used measurements of absolute scattering intensities to determine number concentrations and size distributions in colloidal sulfur suspensions grown at different reactant concentrations from those used in our work. For a typical colloid grown from a solution 0.002 *M* each in $S_2O_3^{2-}$ and HCl, they obtained a total population of 5.4 $\times 10^6$ particles/cc with over 95% of these having radii within 10% of the modal value.

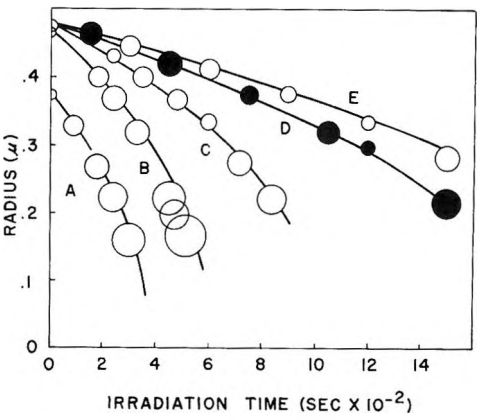

Figure 1. Particle radii as a function of total irradiation time at 25° for sulfur suspensions subjected to irradiation periods (t_1) of 30–300 sec duration. In each case the recovery period (t_2) was 208 sec. The dose rate was 1.4 $\times 10^{16}$ eV cc^{-1} sec^{-1}. The radii of the circles representing the experimental points correspond to the approximate standard deviations of the values. The initial radius, particle concentration and length of irradiation period were: A, 0.374 μ, 2.0 $\times 10^6$ cc^{-1}, 30 sec; B, 0.467 μ, 1.9 $\times 10^6$ cc^{-1}, 30 sec; C, 0.475 μ, 1.8 $\times 10^6$ cc^{-1}, 60 sec; D, 0.475, 1.8 $\times 10^6$ cc^{-1}, 150 sec; E, 0.475 μ, 1.8 $\times 10^6$ cc^{-1}, 300 sec. The smooth curves represent calculated values for the radii obtained using $D = 5.9 \times 10^{-6}$ cm^2 sec^{-1} and $C_s = 1 \times 10^{-7}$ g cc^{-1}. The value for k_1 was 0.2 sec^{-1}.

Results

Effect of the Length of the Irradiation Period. The experimental points in Figures 1 and 2 represent particle radii as a function of total irradiation time at 25° for colloidal sulfur suspensions subjected to periodic irradiations of 30 to 300 sec duration followed by recovery periods of 208 sec, which was the time required to remove the reaction cell from the radiation source, transfer it to the light scattering photometer, perform the angular intensity measurements, and return the cell to the radiation source. A small error in the value for the radius will result from any change in the particle size that occurs during the period of measurement. The radii of the circles representing the experimental points correspond to approximate standard

(5) M. Kerker and V. K. La Mer, *J. Amer. Chem. Soc.*, **72**, 3519 (1950).

(6) T. P. Wallace and J. P. Kratohvil, *J. Polymer Sci., Part C*, **25**, 89 (1968).

(7) M. Kerker, E. Daby, G. L. Cohen, J. P. Kratohvil, and E. Matijevic, *J. Phys. Chem.*, **67**, 2105 (1963).

(8) We appreciate the assistance of Dr. T. P. Wallace of the Rochester Institute of Technology in adapting the program to the University of Georgia computer.

(9) (a) R. O. Gumprecht and C. M. Sliepcevich, "Tables of Light Scattering Functions for Spherical Particles," Edwards Brothers, Inc., Ann Arbor, Mich., 1951. (b) In ref 4 we gave an incorrect expression for the turbidity of a monodisperse suspension. Equation 2 should read $\tau = \pi r^2 n K$.

(10) R. L. Rowell, T. P. Wallace, and J. P. Kratohvil, *J. Colloid Interface Sci.*, **26**, 494 (1968).

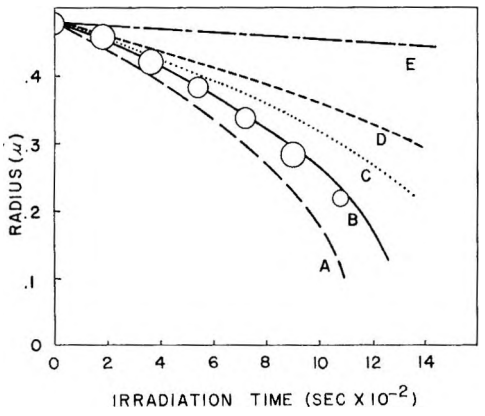

Figure 2. The experimental points represent particle radii for a sulfur suspension with $r_0 = 0.475\ \mu$ and an apparent $n = 1.8 \times 10^6$ cc^{-1} subjected to an irradiation schedule of $t_1 = 90$ sec and $t_2 = 208$ sec at 25°. The smooth curves illustrate the dependence of the calculated radii upon several choices of values for the reaction parameters. The values used were: A, $D = 5.9 \times 10^{-6}$ cm^2 sec^{-1}; $C_s = 1.0 \times 10^{-7}$ g cc^{-1}, $n = 0.45 \times 10^6$ cc^{-1}; B, $D = 5.9 \times 10^{-6}$, $C_s = 10^{-7}$, $n = 1.8 \times 10^6$; C, $D = 10 \times 10^{-6}$, $C_s = 5.9 \times 10^{-8}$, $n = 1.8 \times 10^6$; D, $D = 5.9 \times 10^{-6}$, $C_s = 1.0 \times 10^{-7}$, $n = 5.4 \times 10^6$; E, $D = 5.9 \times 10^{-6}$, $C_s = 1.0 \times 10^{-8}$, $n = 1.8 \times 10^6$. The value of k_1 was 0.2 sec^{-1}.

deviations of the modal radii as obtained from the computer analyses of the polarization ratio data. These results show that a given dose of radiation is more effective in producing solubilization when absorbed in short "pulses" than when administered in fewer exposures of longer duration. For a suspension having an apparent concentration of 1.8×10^6 particles/cc with radii of 0.475 μ, the total irradiation time (with recovery periods of 208 sec) required for complete solubilization increases from 720 to approximately 2300 sec as the irradiation periods increase from 30 to 300 sec.

Effect of the Length of the Recovery Period. Because of the time required to perform the light scattering measurements, we were not able to follow particle size changes from irradiation schedules which involved recovery periods of less than 208 sec. A turbidity measurement could be made within 40 sec, however, and it was possible to determine the irradiation time required for the complete solubilization of a suspension for a given irradiation schedule by measuring the time at which the turbidity decreased to that of a homogeneous solution. With experience, it could be predicted when this would occur during the irradiation period following a given measurement and this period was shortened to better define the total irradiation time. It was found that this procedure gave a convenient and reliable measure of the reaction rate. In Figure 3 are shown experimental total reaction times for three suspensions as functions of recovery time. Samples of suspensions A, B, and C were subjected to periodic irradiations of 30, 60, and 100 sec duration, respectively, with recovery

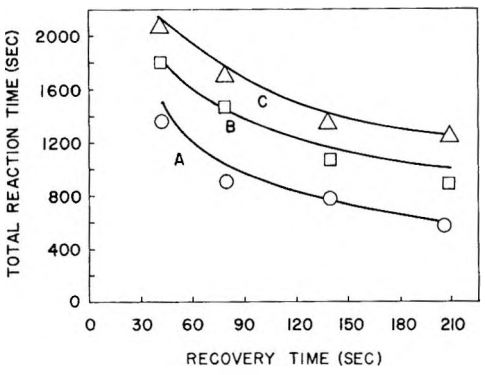

Figure 3. The effect of recovery time on the total irradiation time required to solubilize colloidal sulfur suspensions at 25°. For suspension A, $r_0 = 0.467\ \mu$, $n = 1.9 \times 10^6$ cc^{-1} and $t_1 = 30$ sec. For B, $r_0 = 0.441\ \mu$, $n = 2.1 \times 10^6$ and $t_1 = 60$ sec. For C, $r_0 = 0.420\ \mu$, $n = 2.5 \times 10^6$ and $t_1 = 100$ sec. The symbols represent experimental values for the three suspensions. The smooth curves represent calculated times corresponding to $D = 5.9 \times 10^{-6}$ cm^2 sec^{-1} and $C_s = 1.0 \times 10^{-7}$ g cc^{-1}.

periods of from 40 to 208 sec. For a given irradiation period, the shorter recovery times resulted in a less efficient utilization of the absorbed energy. Recovery periods of longer than 208 sec were not tested. However, the results suggest that for periods slightly longer than this, the total dose of radiation required for solubilization will be almost independent of the duration of the recovery period. It is evident that after absorbing a pulse of ionizing radiation, a significant time must elapse before the system can most efficiently respond to a further exposure.

The Effects of Temperature, Radiation Intensity, and Particle Concentration. The experimental points of Figure 4 represent particle radii as a function of irradiation time for samples of one suspension irradiated at 25, 35, and 44.6°. The decrease in the initial radius with increasing temperature is a reflection of the increased solubility of sulfur at the higher temperature.

The effect of radiation intensity on the particle solution rate was studied by performing irradiations of the colloidal suspensions in lead shields and in a radiation source of lower intensity in the Biological Sciences Building.[11] Temperature control was not feasible and the experiments were carried out at ambient source and room temperature (The mean temperature was estimated to be 30° for these experiments.) Total reaction times for particle solubilization were measured for several suspensions for a range of intensities. Irradiation scheduling was comparable although not exactly the same among the series at the different intensities, and the results are summarized in Table I. The long recovery period was a consequence of the time required to transport the low dose rate samples from one building to another between irradiation and light scattering

(11) We appreciate the cooperation of Dr. D. A. Crossley of the Department of Entomology in the use of this source.

Table I: The Effect of Radiation Intensity on Total Solubilization Time for Several Colloidal Sulfur Suspensions (the Mean Temperature Was Approximately 30°)

Dose rate × 10^{16}, eV cc^{-1} sec^{-1}	Suspension A,[a] t(obsd), sec	Suspension B,[a] t(obsd), sec	Suspension C[b] t(obsd) sec	k_1, sec^{-1}	t(calcd),[c] sec
1.60	480	425	700	0.24	720
0.82	490			0.12	720
0.40		455		0.060	810[d]
0.31	675	660		0.047	810[d]
0.20	860		980	0.030	990
0.13	950		1100	0.020	1260

[a] Initial suspension incompletely characterized: $r_0 \sim 0.32$ μ (from growth time); $t_1 = 100$ sec; $t_2 = 1500$ sec. [b] $r_0 = 0.433$ μ, $n = 2 \times 10^6$ cc^{-1}, $t_1 = 100$–200 sec, $t_2 = 1500$ sec. [c] Using D and C_s, corrected from 25°, as 7.25×10^{-6} cm^2 sec^{-1} and 1.2×10^{-7} cm cc^{-1}, respectively. [d] Calculated radii became zero during the same recovery period.

measurements. The results indicate that only at dose rates below 0.4 to 0.8 × 10^{16} eV cc^{-1} sec^{-1} is there a significant dependence of solubilization time upon dose rate.

In order to determine the effect of particle concentration on the solubilization times for irradiated suspensions, reaction times were compared for diluted samples of stock suspensions. Dilutions were made with millipore-filtered aliquots of the original colloid growth solution in which the reaction had been stopped before the appearance of turbidity. This was done to minimize particle size changes upon dilution. Suspensions at high dilutions were solubilized very rapidly upon irradiation. Variable irradiation schedules were used in attempting to determine as closely as possible the total irradiation time required for solubilization. Table II summarizes the results of two such series of experiments.

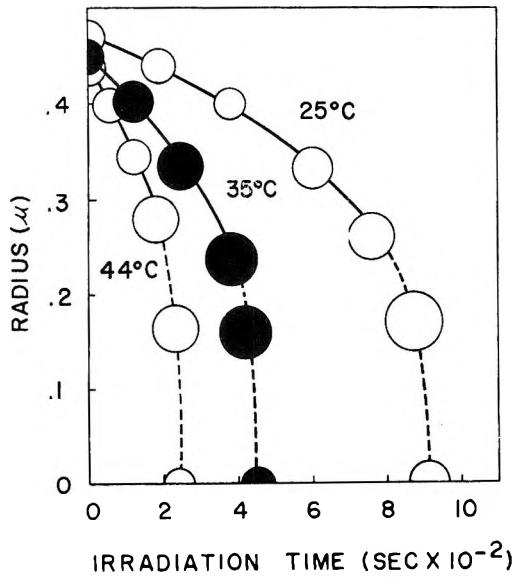

Figure 4. The effect of temperature on the radiation-induced solubilization of a colloidal sulfur suspension. The apparent particle concentration was $n = 1.8 \times 10^6$ cc^{-1}. The initial radii, r_0, were at 25°, 0.477 μ; at 35°, 0.451 μ; and at 44.6°, 0.441 μ. The circles represent experimental points and the smooth curves represent calculated values using at 25°, $D = 5.9 \times 10^{-6}$, $C_s = 1.0 \times 10^{-7}$; at 35°, $D = 8.8 \times 10^{-6}$, $C_s = 1.5 \times 10^{-7}$; and at 44.6°, $C = 10.5 \times 10^{-6}$ and $C_s = 2.2 \times 10^{-7}$; $k_1 = 0.2$ sec^{-1}. For the portions of the experiments represented by the continuous curves, $t_1 = 60$ sec and $t_2 = 220$ sec. The dashed portions correspond to variable irradiation periods.

Table II: The Effect of Particle Concentration upon the Total Irradiation Time Required for Solubilization of Colloidal Sulfur Suspensions at 28°

Suspension	r_0, μ	n	t(obsd), sec	t(calcd),[g] sec
A (undiluted)[a]	0.436	1.8×10^6	400	400
(1–1.67)[b]	0.436	1.1×10^6	270	285
(1–3.75)[c]	0.415	0.48×10^6	170	170
B (undiluted)[d]	0.337	n_0	332	
(1–1.33)[e]	0.337	$0.75n_0$	235	
(1–2.0)[f]	0.332	$0.50n_0$	175	

[a] $t_1 = 100, 50, 50, 50, 35, 30, 25, 25, 20, 15$ sec, $t_2 = 600$ sec. [b] $t_1 = 50, 50, 100, 35, 20, 15$ sec, $t_2 = 600$ sec. [c] $t_1 = 40, 40, 40, 30, 10$ sec, $t_2 = 600$ sec. [d] $t_1 = 70, 90, 95, 55, 10, 5, 7$ sec, $t_2 = 400$ sec, particle concentration unknown. [e] $t_1 = 50, 102, 50, 20, 8$ sec, $t_2 = 400$ sec. [f] $t_1 = 60, 90, 20, 10$ sec, $t_2 = 400$ sec. [g] Based upon the actual irradiation schedule and using $D = 6.5 \times 10^{-6}$ cm^2 sec^{-1}, $C_s = 1.1 \times 10^{-7}$ g cc^{-1} and $k_1 = 0.2$ sec^{-1}.

These results contrast with those obtained for the chemical consumption of the suspension by reaction with sulfite.[12] Here reaction rates were independent of particle concentration. For shorter recovery periods, the dependence of the radiolysis reaction upon particle number became less marked and suggested that for a continuous radiolysis an independence of particle concentration would also be realized.

The Radiolysis Reaction in the Presence of Oxygen. The radiation-induced solubilization reaction is inhibited by oxygen. The experimental points of curve A in Figure 5 represent particle radii as a function of irradiation time for a suspension irradiated in the presence of atmospheric oxygen at 25°. The suspension had an apparent population of 2.0×10^6 cc^{-1} with an initial radius of 0.420 μ and the irradiation schedule was comprised of 100-sec irradiation periods followed by 300-sec recovery periods. The points of curves B and C correspond to irradiations of 1–2 and 1–3 dilutions of the original suspension subjected to the same irradiation schedule.

(12) G. W. Donaldson and F. J. Johnston, *J. Phys. Chem.*, **73**, 2064 (1969).

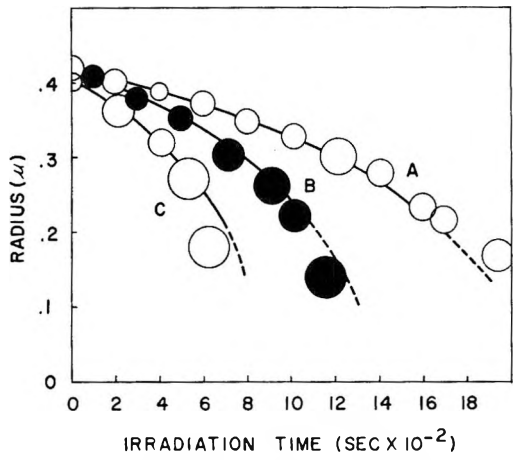

Figure 5. The radiolysis of colloidal sulfur in the presence of O_2 at 25°. Curves B and C represent two- and sixfold dilutions of the suspension of curve A. For A, $r_0 = 0.420\ \mu$, and $n = 2.0 \times 10^6$ cc^{-1}; for B, $r_0 = 0.420\ \mu$, $n = 1.0 \times 10^6$; for C, $r_0 = 0.405\ \mu$, and $n = 0.33 \times 10^6$. The circles represent experimental points and the smooth curves represent calculated values for $D = 5.9 \times 10^{-6}$ cm^2 sec^{-1}, $C_s = 1.0 \times 10^{-7}$, and $k_1 = 0.01$ sec^{-1}.

Discussion

There are several possible mechanisms to consider in discussing the radiation-induced solubilization of colloidal sulfur suspensions. One of these, which involves a direct absorption of energy in the particles themselves, may be discounted immediately because of the extremely high ($\sim 10^5$) G value which would be required to explain the observed rates. Mechanisms in which the reaction occurs as a result of attack at the particle surface by radicals or other intermediates produced by the radiation will result in rates limited by diffusion of reactants to the particle surface and/or by diffusion of products away from the surface. The effects of radiation periodicity and intensity may be explained in terms of such pictures. Such processes, however, will give rates independent of particle concentration unless each sulfur particle effectively scavenges reactive intermediates from a volume of solution that is approximately 10^6 to 10^8 times that of the particle itself. This, we feel, is highly improbable. We have interpreted our results in terms of the simplest picture that is consistent with all of our experimental results. This mechanism involves a radiation-induced reaction which involves only homogeneously dissolved or dispersed sulfur followed by a solution of the colloidal particles. This mechanism is discussed in detail below.

Reaction Model. Our experimental results are best explained on the basis of the following picture for the mechanism by which colloidal sulfur is solubilized upon irradiation. When aqueous suspensions of colloidal sulfur absorb ionizing radiation, homogeneously dissolved or dispersed sulfur is oxidized to sulfate by reaction with intermediates produced from water. The suspended material dissolves as the system attempts to reestablish equilibrium. At dose rates of 1.4×10^{16} eV cc^{-1} sec^{-1} in deaerated systems, the concentration of sulfur in the homogeneous phase is reduced to effectively zero within approximately 3–5 sec and for irradiation periods that are long compared with this time, the solution process occurs through a diffusion of material away from the particle surface. When removed from the radiation source, the solution process will continue until an equilibrium concentration is reached. According to this picture, the irradiation time required to produce a given change in particle size in a suspension subjected to periodic irradiation will depend critically upon the relative durations of irradiation and recovery periods.

The mathematical formulation of this mechanism is similar in form to that for the dissolution rates of gas bubbles in liquids which are undersaturated in the gas. The latter process has been treated by several workers[13–15] and has been used by Krieger, *et al.*,[15] to determine diffusion coefficients of gases in liquids. As applied to the irradiated sulfur suspensions, this treatment is summarized below.

The rate at which the mass of a dissolving, spherical particle of density ρ decreases with time is determined by the outward flux, J (in g cm^{-1} sec^{-1}), of molecules at the particle surface.

$$dm/dt = 4\pi r^2 \rho dr/dt = -4\pi r^2 J \tag{1}$$

The rate of decrease in particle radius is then

$$dr/dt = -J/\rho \tag{2}$$

J may be expressed in terms of Fick's first law

$$J = -D\frac{\partial C}{\partial r} \tag{3}$$

In this expression, D is the diffusion coefficient for the species diffusing away from the particle surface and $\partial C/\partial r$ is the corresponding concentration gradient at the particle surface. The latter quantity has been obtained from the solution of Fick's second law for a spherically symmetrical geometry. The result is[13]

$$\left(\frac{\partial C}{\partial r}\right)_{r=r'} = -\frac{(C_s - C)}{r'}\left[1 + \frac{r'}{(\pi Dt)^{1/2}}\right] \tag{4}$$

C_s represents the saturation solubility of the material comprising the particle and C the actual concentration in the solution phase. For particle sizes and times such as those of our experiments, the term in brackets is very close to unity and eq 4 becomes

$$\left(\frac{\partial C}{\partial r}\right)_{r=r'} = -\frac{(C_s - C)}{r'} \tag{5}$$

(13) P. S. Epstein and M. S. Plesset, *J. Chem. Phys.*, **18**, 1507 (1950).

(14) L. Liebermann, *J. Appl. Phys.*, **28**, 205 (1957).

(15) I. M. Krieger, G. W. Mulholland, and C. S. Dickey, *J. Phys. Chem.*, **71**, 1123 (1967).

The rate at which the particle radius changes with time will be

$$\frac{dr}{dt} = -\frac{D}{\rho}\frac{(C_s - C)}{r} \quad (6)$$

According to the reaction mechanism that we have suggested, $C \sim 0$ during irradiation periods of approximately 60 sec or longer at high radiation intensities. If the particle radius at the beginning of such a period is r_0, then after an irradiation time t

$$r = \left[r_0^2 - \frac{2DC_s t}{\rho}\right]^{1/2} \quad (7)$$

At lower radiation intensities ($<8 \times 10^{16}$ eV cc^{-1}) and for short irradiation periods the reaction rate of dissolved sulfur must be considered. For concentrations at which the reacting solute is scavenging radiation-produced species, reaction rates are zero order in that solute. It seems unlikely that this can be the situation with dissolved sulfur and we have assumed that the homogeneous reaction is pseudo-first order in sulfur. The rate at which the sulfur concentration changes during an irradiation will then be

$$\frac{dC}{dt} = -k_1 C + 4\pi r n D(C_s - C) \quad (8)$$

In this expression, k_1 is a pseudo-first-order constant which will be a function of the radiation intensity, and n is the particle concentration.

When the suspension is removed from the radiation source, the sulfur concentration in the homogeneous phase increases according to

$$\frac{dC}{dt} = 4\pi r n D(C_s - C) \quad (9)$$

and the decrease in particle radius is described by (6). Under experimental conditions of high intensity and long irradiation periods, integrated expressions for r as a function of time are readily obtained from (6) and (9) after expressing C in terms of n and r. We have, however, found it more generally useful to generate particle radii as a function of time directly from eq 6, 8, and 9 by iterative processes using a remote computer terminal. This was done for one or two second time increments for trial values of n, D, C_s, and, for certain of the experiments, k_1. The approximations that are involved in such a treatment are well within the experimental uncertainties.

Reaction Parameters. The mathematical picture includes a discouraging number of quantities that are either unknown or are known only approximately. Particle populations, n, given by our transmission measurements on suspensions of known modal radii were initially considered to be only approximations because of the assumption of monodispersity. n was, therefore, treated as a variable parameter with values of from $^1/_2$ to 2 times the measured value.

Of the unknown parameters, C_s, the effective saturation concentration of sulfur in the homogeneous phase is least susceptible to estimation. The term effective is used because it is doubtful that the species in equilibrium with the colloidal particles whose behavior we are following is truly molecularly dispersed material. As a starting point, the value obtained by Reiss and La Mer[16] for the critical supersaturation concentration, 4.7×10^{-6} g-atom l.$^{-1}$ (1.5×10^{-7} g cc^{-1}) at 25° was used. The effective equilibrium solubility of sulfur in the colloidal systems such as we have studied must approach this value. This is indicated from particle size changes which occur upon dilution of suspensions which are comprised of initially small particles. In one experiment, for example, a colloidal suspension consisting of particles with radii of 0.26 μ and in which the growth reaction was stopped by titration with Br_2 was diluted with an equal volume of distilled water. A decrease in the particle radius to 0.23 μ resulted. If a particle population of 2×10^6 cc^{-1} is assumed, the change corresponds to a solubility of approximately 0.8×10^{-7} g cc^{-1}. We have varied C_s over the range of 10^{-8} to 2.7×10^{-7} g cc^{-1}, in attempting to describe our experimental results in terms of eq 6–9.

In a theoretical study of the diffusional processes involved in colloid growth, Reiss and La Mer[16] have obtained a value of 2.0×10^{-6} cm^2 sec^{-1} for the diffusion coefficient of the sulfur units diffusion to the surface of a growing particle. They suggested that this was a larger unit than S_8. If it is assumed that the entities diffusing away from the surface of the dissolving particles are S_8 molecules, kinetic theory estimations suggest values for D of from 5 to 7×10^{-6} cm^2 sec^{-1} depending upon the assumed configuration. We have considered variations in D from 2 to 10×10^{-6} cm^2 sec^{-1} at 25°.

k_1, the pseudo-first-order constant for the reaction in the homogeneous phase, is, according to the mechanism we are suggesting, sufficiently large that for irradiation periods of 60 sec or longer, the particles are dissolving into a medium of effectively zero sulfur concentration. Under these conditions, C_s, D, and n become the only variable parameters. An approximate value for k_1 was obtained from the effects of radiation intensity.

Particle radii generated by the computer program proved to be compatible with the experimental values only for fairly narrow ranges of values for the above quantities. As is evident from eq 6–9, D and C_s occur predominately as a product, DC_s. Using the experimental estimations of n from transmission measurements, results were consistent with a range of values for this product from approximately 5.7 to 5.9 $\times 10^{-13}$ g cm^{-1} sec^{-1}. The use of values of n which were markedly different from those obtained from the transmission measurements required, for agreement with a given experiment, a value for DC_s which was

(16) H. Reiss and V. K. La Mer, *J. Chem. Phys.*, **18**, 1 (1950).

inconsistent with the results of, for example, an experiment utilizing a different irradiation schedule. The most satisfactory correlation between the simulated and experimental behavior was obtained by using throughout the particle concentrations given by the transmission measurements. The theoretical radii obtained for a given schedule are fairly insensitive to the specific values assigned to D and C_s as long as the above product range is not extended. The data were well reproduced by values for D of from 3.85×10^{-6} cm^2 sec^{-1} to 5.90×10^{-6} cm^2 sec^{-1} with C_s varied correspondingly from 1.5×10^{-7} to 1.0×10^{-7} g cc^{-1}. When D and C_s were varied significantly beyond these limits, even though the product range for DC_s of 5.9×10^{-13} was maintained, discrepancies between the calculated and experimental results occurred. For all of our comparisons with the experimental results at 25° we have used for the value of D, 5.9×10^{-6} cm^2 sec^{-1} and for C_s, 1.0×10^{-7} g cc^{-1}.[17]

In Figure 2 experimental radii for a suspension subjected to an irradiation schedule at 25° consisting of 90-sec irradiation periods and 208-sec recovery periods are compared with calculated radii for this schedule using several different values for the parameters D, C_s, and n. The calculated radii should also more properly be represented as points but are shown as smooth curves for clarity. The smooth curve B, in good agreement with the experimental results, was obtained using the measured particle concentration of 1.8×10^6 cc^{-1}, $D = 5.9 \times 10^{-6}$ cm, and $C_s = 1.0 \times 10^{-7}$ g cc^{-1}.

The smooth curves of Figure 1 represent calculated radii for the different irradiation schedules corresponding to the measured initial radii, the apparent particle concentrations, and the above values for D and C_s.

The smooth curves of Figure 3 correspond to calculated irradiation times for complete solubilization as a function of the length of the recovery period for three suspensions subjected to irradiation periods of 30, 60, and 100 sec. The experimental behavior is very closely reproduced.

The smooth curves in Figure 4 represent calculated radii as a function of irradiation time for three samples of a single suspension irradiated at 25, 35, and 44.6°. The values of D used in making the calculations were based on our suggested value at 25° by assuming a linear dependence upon T/η where T is the absolute temperature and η is the coefficient of viscosity of water. Values of C_s were adjusted to best fit the experimental data. These values are very tentative and have been used only to estimate corrected values of D and C_s for experiments at 28 and 30°.

According to the mechanism that we have suggested, k_1 will be a function of the radiation intensity. We have no experimental basis for predicting the form of this dependence and have assumed a linear dependence of k_1 upon the dose rate. This corresponds to a production by radiation of reactive intermediates, the concentration of which is not determined predominantly by a recombination with like species. In column 6 of Table I are listed reaction times calculated for suspension C using $k_1 = 0.24$ sec^{-1} at a dose rate of 1.60×10^{16} eV cc^{-1} sec^{-1} and a value at other dose rates based upon the linear dependence. This treatment describes the observed behavior of the suspensions when irradiated at the different intensities. The values of D and C_s used in the calculations were corrected to 30° on the basis of our measured rates at 35 and 44°. The value $k_1 = 0.2$ sec^{-1} was used in treating the experiments at an intensity of 1.4×10^{16} eV cc^{-1} sec^{-1}.

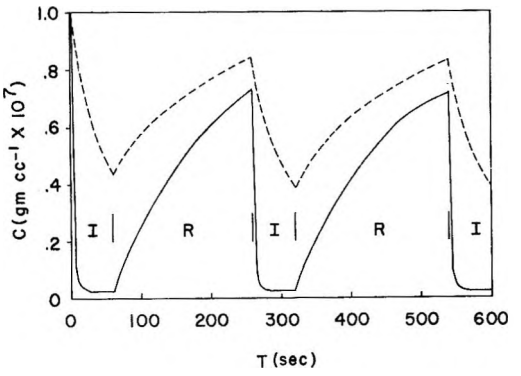

Figure 6. The calculated variation in dissolved sulfur concentration as a function of time in a colloidal system subjected to successive irradiation periods of 60 sec and recovery periods of 200 sec. The colloid was assumed to consist of 1.8×10^6 particles/cc with initial radii of 0.475 μ. The values of $D = 5.9 \times 10^{-6}$ cm^2 sec^{-1} and $C_s = 1.0 \times 10^{-7}$ g cc^{-1} were used. The continuous curve corresponds to $k_1 = 0.2$ sec^{-1} (for 1.4×10^{-16} eV cc^{-1} sec^{-1}) and the dashed curve to $k_1 = 0.017$ sec^{-1} (for 0.12×10^{16} eV cc^{-1} sec^{-1}).

These values for the parameters also predict a dependence of the reaction times upon the particle concentration that agrees with observation (Table II, column 5).

The inhibition of the reaction by oxygen must, according to our suggested mechanism, result from a competition by oxygen with the homogeneously dispersed sulfur for reactive species produced upon irradiation. This will result in a lower effective value for k_1. The smooth curves in Figure 5 correspond to calculated radii for the indicated irradiation schedule and particle populations with $D = 5.9 \times 10^{-6}$, $C_s = 1.0 \times 10^{-7}$, and $k_1 = 0.01$ sec^{-1}.

The Reaction of Dissolved Sulfur. The chemical behavior of dissolved sulfur upon irradiation can only be inferred from the measured changes in the colloidal particles. The proposed mechanism assumes a first-

(17) In ref 2, a less sensitive computational program was used which assumed average radius values over each irradiation and recovery period and then corrected these following each period. In addition, the value for D given in ref 16 was assumed to be applicable here also and was not treated as a variable. A representation of the experimental data was obtained which was less satisfactory than that obtained in the present treatment and which required a value for C_s of 2.7×10^{-7} g cc^{-1}.

order rate of decrease in sulfur concentration during irradiation periods and a rate of increase during recovery which is determined by the solution rate of the particles. Figure 6 shows the calculated variation in dissolved sulfur concentration with time during irradiation of a suspension containing 1.8×10^6 particles/cc with initial radii of 0.475 μ. Reaction parameters obtained from our experiments were used and irradiation periods of 60 sec and recovery periods of 200 sec were assumed. The smooth curve corresponds to a dose rate of 1.4×10^{16} eV cc^{-1} sec^{-1} and the dashed curve to a dose rate of 0.12×10^{16} eV cc^{-1} sec^{-1}.

Assuming that $C_s = 10^{-7}$ g cc^{-1} and that $k_1 = 0.2$ sec^{-1} at the highest dose rate used at 25°, dissolved sulfur undergoes reaction at an initial rate of 0.2×10^{-7} g cc^{-1} sec^{-1}. This corresponds to an initial G value for the reaction of 2.6 atoms of S per 100 eV absorbed.

The Reaction with Chlorine. In attempting to find a different reagent than Br_2 for stopping the colloid growth reaction, aqueous Cl_2 was used for titration of the reaction mixture. When present in stoichiometric excess, reaction with sulfur occurred resulting in the solubilization of the colloid. The reaction was studied quantitatively in order to make a comparison with the radiation-induced reaction. We observed that above approximately 10^{-3} M Cl_2, solubilization rates were independent of the Cl_2 concentration. This result suggested a process analogous to the radiation-induced reaction in which the measured decrease in particle size is determined by the solution rate for the colloidal particles. If this is correct then the dependence of particle size upon the time of reaction with Cl_2 should be described by eq 7 with the values for D and C_s the same as those used to describe the radiation-induced reaction.

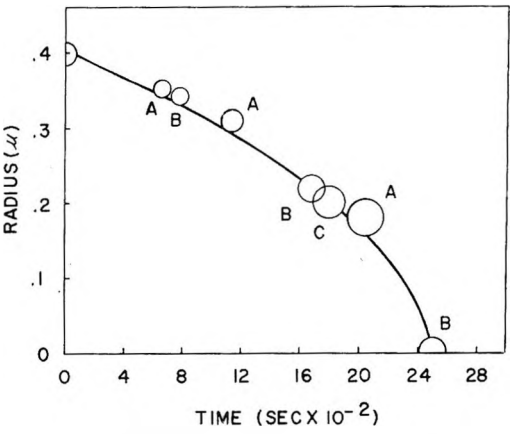

Figure 7. The solubilization of a colloidal sulfur suspension by reaction with Cl_2 at 25°. The points labeled A correspond to a sample made 2.3×10^{-3} M in Cl_2; those labeled B, 1.03×10^{-3} M in Cl_2; and C, 1.6×10^{-3} M in Cl_2. The original colloid contained 2.4×10^6 particles/cc and the initial radius was 0.40 μ. The smooth curve was calculated from eq 7 using $D = 5.9 \times 10^{-6}$ cm^2 sec^{-1} and $C_s = 1.0 \times 10^{-7}$ g cc^{-1}.

The experimental points in Figure 7 show the results of experiments at 25° in which known aliquots of an aqueous Cl_2 solution were added to different samples of a colloidal sulfur suspension. The Cl_2 concentrations ranged from 1.0 to 2.3×10^{-3} M. The smooth curve corresponds to radius values calculated according to eq 7 and using $D = 5.9 \times 10^{-6}$ cm^2 sec^{-1} and $C_s = 1.0 \times 10^{-7}$ g cc^{-1}. The good agreement between the calculated and measured values is evidence for the basic similarity of the radiolytic and chemical reaction, *i.e.*, the chemical reaction corresponding to a continuous radiolysis in which the particles are dissolving into a medium in which the sulfur concentration is effectively zero.

The Chemiluminescent Reaction of Hydrated Electrons with Optically Excited Fluorescein Dyes[1a]

by A. F. Rodde, Jr.,[1b] and L. I. Grossweiner*[1c]

Department of Radiation Therapy, Michael Reese Hospital and Medical Center, Chicago, Illinois 60616
(Received October 16, 1970)

Publication costs assisted by the National Institutes of Health

It has been shown with a flash photolysis–pulse radiolysis technique that hydrated electrons react with a photochemical product of aqueous eosin or fluorescein in a chemiluminescent process. The emission has been identified with the fluorescent state, where the intensity varies linearly with the electron pulse dose and with the square of the initial triplet concentration. It is proposed that triplet–triplet interactions lead to a loosely bound triplet–singlet complex which reacts with e_{aq}^- to generate the excited singlet state of the monomer and the dye semiquinone.

Introduction

Early work of Sommermeyer, *et al.*,[2a] reported that X-ray irradiation of several aromatics and dyes in aqueous solution induces light emission with the spectrum of the uv-excited fluorescence. However, the yield was enhanced by low concentrations of iodide ion and quenched by nitrate ion and fructose, which do not influence the fluorescence. Sommermeyer and Prütz[2b] proposed that the hydrated electron e_{aq}^- is involved in the emission process, which was confirmed by pulse radiolysis measurements of Prütz, *et al.*,[3] who found that e_{aq}^- scavengers quench the radiation-induced luminescence. However, the emission is quenched also by hydroxyl radical scavengers and high iodide ion concentrations, which indicates that an OH· reaction product of the dye is involved as well. Prütz and Land[4] proposed that OH· oxidizes the dye and then e_{aq}^- reduces the oxidized dye product to the fluorescent state

$$S_0 + OH\cdot \longrightarrow S_{ox} \quad (1)$$

$$S_{ox} + e_{aq}^- \longrightarrow S_1^* \quad (2)$$

Pulse radiolysis studies of eosin and fluorescein[5-7] have shown that OH· reacts to form both the ring adduct SOH· and a phenoxyl type semioxidized radical X. An attempt was made to distinguish between these two oxidation products in earlier work by generating the X radical with a xenon light flash prior to irradiation with a 35-MeV electron pulse.[8] The triplet dye T_1 formed by intersystem crossing reacts with itself and unexcited dye *via* known quenching and electron transfer processes

$$S_0 + h\nu \longrightarrow S_1^* \quad (3)$$

$$S_1^* \longrightarrow T_1 \quad (4)$$

$$T_1 + T_1 \longrightarrow T_1 + S_0 \quad (5)$$

$$T_1 + T_1 \longrightarrow R + X \quad (5')$$

$$T_1 + S_0 \longrightarrow 2S_0 \quad (6)$$

$$T_1 + S_0 \longrightarrow R + X \quad (6')$$

where R is the dye semiquinone.[9-11] It was found that prior application of the light flash has no effect on the luminescence yield and it was concluded that the OH· adduct of fluorescein or eosin (formed only by the electron pulse) is responsible for the emission

$$SOH\cdot + e_{aq}^- \longrightarrow S_1^* + OH^- \quad (2')$$

A different type of emission was observed in the work of ref 8 that requires optical excitation prior to the electron pulse. In this case scavenging of OH· has no quenching effect and it was proposed that e_{aq}^- reacts with the triplet state of the dye to form the excited state of the dye semiquinone. The present work was

(1) (a) Supported by NIH Grant GM-12716. (b) Based in part on the thesis of A.F.R. submitted in partial fulfillment of the requirements for the Ph.D. degree in physics to Illinois Institute of Technology. (c) Physics Department, Illinois Institute of Technology, Chicago, Ill. 60616.

(2) (a) K. Sommermeyer, V. K. Birkwald, and W. Prütz, *Strahlentherapie*, **116**, 354 (1961); (b) K. Sommermeyer and W. Prütz, *Z. Naturforsch. A*, **21**, 1081 (1966).

(3) W. Prütz, K. Sommermeyer, and E. J. Land, *Nature*, **212**, 1043 (1966).

(4) W. Prütz and E. J. Land, *Biophysik*, **3**, 349 (1967).

(5) J. Chrysochoos, J. Ovadia, and L. I. Grossweiner, *J. Phys. Chem.*, **71**, 1629 (1967).

(6) P. Cordier and L. I. Grossweiner, *ibid.*, **72**, 2018 (1968).

(7) L. I. Grossweiner, *Advan. Chem. Ser.*, **No. 81**, 277 (1968).

(8) L. I. Grossweiner and A. F. Rodde, Jr., *J. Phys. Chem.*, **72**, 756 (1968).

(9) L. Lindqvist, *Arkiv Kemi*, **16**, 79 (1960).

(10) V. Kasche and L. Lindqvist, *Photochem. Photobiol.*, **5**, 507 (1965).

(11) T. Ohno, S. Kato, and M. Koizumi, *Bull. Chem. Soc. Jap.*, **39**, 232 (1966).

undertaken to explore the new emission process under improved experimental conditions. In particular, new optics and circuitry made it possible to measure the emission at low electron pulse dose where the bimolecular e_{aq}^- reactions do not complicate the kinetics analysis. The results prove that the earlier identification of the luminescence precursor with the dye triplet state is incorrect and indicate that a new dye species is involved with the properties of a loosely bound complex between the triplet state and ground state dye.

Experimental Details

The experiments were performed with a modified linear accelerator pulse radiolysis arrangement which permits optical absorption and emission measurements after irradiation of the sample with a flash lamp and subsequent application of the 35-MeV electron pulse. The electron pulse duration used was 0.2 μsec at 10–500 rads per pulse, as measured for each run with a pulse current transformer calibrated with the modified Fricke dosimeter.[12] An E.G. & G. FX-33 flashtube operated at 36 J input provided a 10 μsec ($1/e$) light flash. The timing circuits made it possible to trigger the electron pulse at any time delay after the light flash and display both the emission signal and the optical absorption transient on appropriate time scales with a Tektronix Type 556 dual beam oscilloscope.[13] The sample was contained in a 5 cm long, 25 mm o.d. cell of Supracil quartz and could be evacuated to 5×10^{-6} Torr by pumping and shaking. Beam profile studies showed a uniform dose distribution over the cell face. Two-channel optical absorption measurements were made by focusing the monitoring light from an Osram XBO 450-W xenon arc through the cell in two passes with front surfaced mirrors and dividing the beam between a Jarrell Ash 0.25-m grating monochromator and the Hilger E 498 quartz prism spectrograph with the E 720 photoelectric scanning unit, followed by RCA 1P28 photomultipliers at their exit slits. A separate monitoring channel using a University Labs Model 240 He–Ne laser with solid state detector was available at 633 nm. The flash lamp was located immediately adjacent and parallel to the irradiation cell. Emission measurements were made with the same pulse radiolysis optical system by blocking the xenon arc. Commercial Eosin Y was purified with the chromatographic method of Koch[14] to give ϵ_{max}(518 nm) = 9.7×10^4 M^{-1} cm^{-1}, and the disodium salt of fluorescein was crystallized twice to give ϵ_{max}(491 nm) = 8.2×10^4 M^{-1} cm^{-1}. Other chemicals were reagent grade and triply distilled water was used for all solutions.

Experimental Results and Analysis

Typical data showing the chemiluminescent process investigated in this work are reproduced on a single time base in Figure 1 for the case of 10 μM eosin (pH 9.0) in the presence of 0.01 M formate to scavenge OH· radicals. The application of the xenon light flash at zero time ($\lambda > 350$ nm) generates the dye triplet state measured by its absorption at 633 nm (curve b). The decay of the triplet is accompanied by the growth of absorption at 405 nm (curve a) attributed to the dye semiquinone dianion (R) formed by the T–S and T–T electron-transfer reactions 5′ and 6′. The application of a 0.2-μsec electron pulse (520 rads) at 250-μsec time delay after the light flash leads to a fast increase in the R concentration accompanied by strong light emission at 550 nm (curve c). The absorptivity at 633 nm shows a spike due to e_{aq}^- followed by the continuation of triplet decay. However, the 405 nm R absorption continues to grow slowly from additional dye reduction by CO_2^-, produced by the scavenging of OH· by formate.[5] Measurements of the emission decay on a faster time scale show that it is exponential in time with a decreasing lifetime at higher dye concentrations and parallels the disappearance of e_{aq}^-. However, the luminescence buildup is "instantaneous" for the 0.1 μsec time resolution of the apparatus.

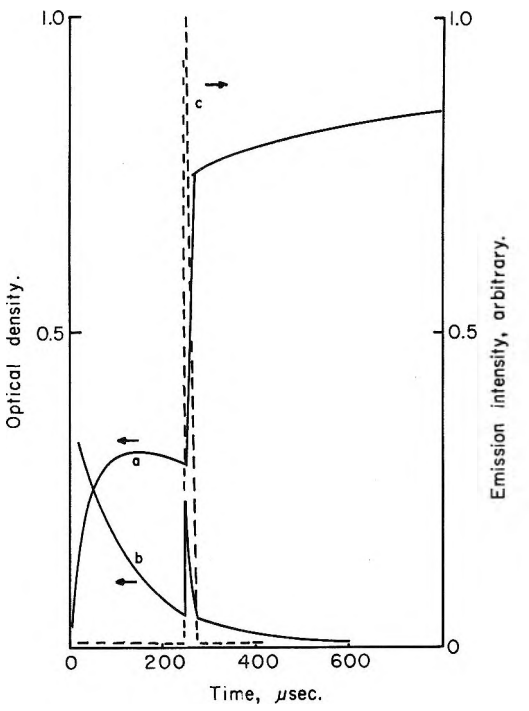

Figure 1. Typical transient signals from deaerated 10 μM eosin (pH 9.0) in the presence of 0.01 M formate. The flash lamp was triggered at $t = 0$ and the 35-MeV electron pulse applied at $t = 250$ μsec: curve a, optical density at 405 nm; curve b, optical density at 633 nm; curve c, luminescence at 550 nm.

(12) L. M. Dorfman and M. S. Matheson, *Progr. React. Kinet.*, **3**, 237 (1965).

(13) A. F. Rodde, Jr., Ph.D. Thesis, Illinois Institute of Technology, Dec 1970.

(14) L. Koch, *J. Assoc. Offic. Agr. Chem.*, **39**, 397 (1956).

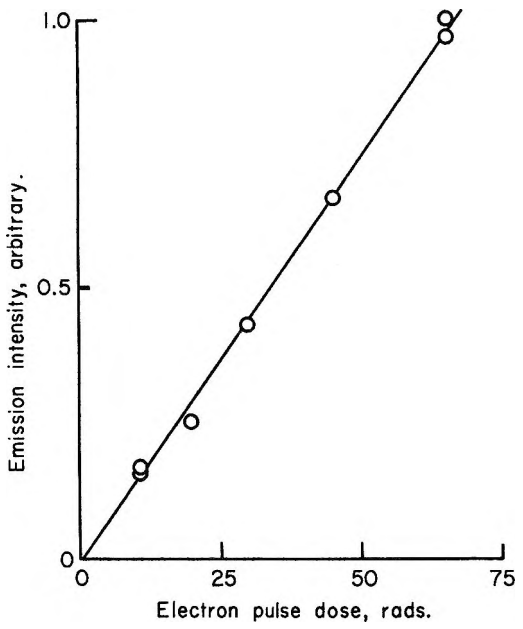

Figure 2. Dependence of emission intensity at 110 μsec delay on electron pulse dose: deaerated 10 μM eosin in the presence of 0.01 M formate (pH 9.0).

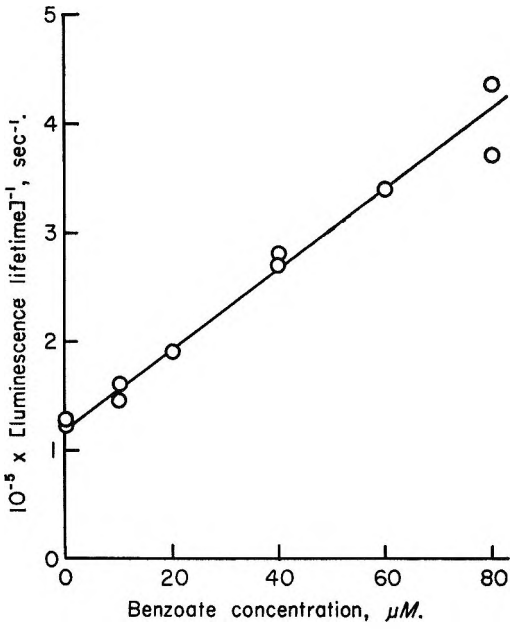

Figure 3. Quenching of emission by benzoate: deaerated 5 μM eosin in the presence of 0.01 M formate (pH 9.0), 30 rads/pulse.

It was deduced in the earlier report[8] that e_{aq}^- is responsible for the emission because H· and OH· are scavenged by the added formate. This conclusion is supported by the data in Figure 2 showing that the emission intensity is a linear function of the pulse dose, which argues against the participation of more than one type of water radiolysis radical. Additional evidence has been obtained by adding sodium benzoate to compete with the fast reaction between e_{aq}^- and the dye. Although OH· reacts rapidly with benzoate [k(OH + benzoate) = (3.2 ± 0.5) × 10^9 M^{-1} sec^{-1} (average of values in ref 15)] the scavenging by 0.01 M sodium formate [k(OH + formate) = 2 × 10^9 M^{-1} sec^{-1} [16]] controls at the low benzoate concentrations employed. The measurements were made by observing the effect of added benzoate on the emission decay lifetime, with all others factors held constant, *i.e.*, the flash lamp energy, electron pulse dose, dye concentration, and delay time. A semiempirical fit to the data obtains by assuming that e_{aq}^- reacts with the dye, benzoate, and the unknown dye precursor of the emission process P with the second-order rate constants k_D, k_B, and k_P, respectively. The assumption that the lifetime of P is much longer than that of the actual emitting state (shown below to be the first excited singlet state) leads immediately to the following relationship for the decay of luminescence

$$I(t) \sim k_p[e_{aq}^-]_0[P]_{av}e^{-\{k_D[D]+k_B[B]+k_p[P]+k_0\}t} \quad (I)$$

where $[e_{aq}^-]_0$ is the initial e_{aq}^- concentration produced by the electron pulse, $[P]_{av}$ is the average concentration of the precursor during the emission process, and k_0 is the e_{aq}^- decay constant in the buffer solution under the experimental conditions. The linear plot of reciprocal emission lifetime against the benzoate concentration in Figure 3 follows the form of eq I. The slope leads to k_B = 3.6 × 10^9 M^{-1} sec^{-1} in good agreement with the average of published values: (3.3 ± 0.3) × 10^9 M^{-1} sec^{-1}.[17] The intercept gives $k_D \lesssim 2.3 \times 10^{10} M^{-1}$ sec^{-1} for the reaction of e_{aq}^- with eosin, in good agreement with the pulse radiolysis result of 2.2 × 10^{10} M^{-1} sec^{-1},[7] noting that $k_0 \simeq 6 \times 10^3$ sec^{-1} is much smaller than k_D[D] and P must be present in quite low concentrations (see below).

Although this analysis confirms that e_{aq}^- is a principal reactant in the luminescent process, the identification of the coproduct P has proven to be more difficult. It was believed at first that P is the dye triplet state, in which case the emitting species must be the excited state of the dye semiquinone. However, Figure 4 shows that the luminescence emission spectra for eosin and fluorescein (points) are identical with the usual fluorescence excited by visible light ($\lambda > 450$ nm) under the pulse radiolysis spectrophotometric conditions. An approximate correction for photomultiplier sensitivity indicates that emission yield from eosin is 1.5 ± 0.5 times as high as fluorescein. Ruling out the triplet state itself, information about the precursor P has been obtained by measuring the emission intensity as a function of the delay time between the light flash and electron pulse for dye concentrations from 2.5 to 15 μM. A typical result is shown in Figure 5 for 10 μM eosin. The time delay

(15) M. Anbar, D. Meyerstein, and P. Neta, *J. Phys. Chem.*, **70**, 2660 (1966).

(16) M. S. Matheson, *Ann. Rev. Phys. Chem.*, **13**, 77 (1962).

(17) M. S. Matheson and L. M. Dorfman, "Pulse Radiolysis," M. I. T. Press, Cambridge, Mass., 1969, p 121.

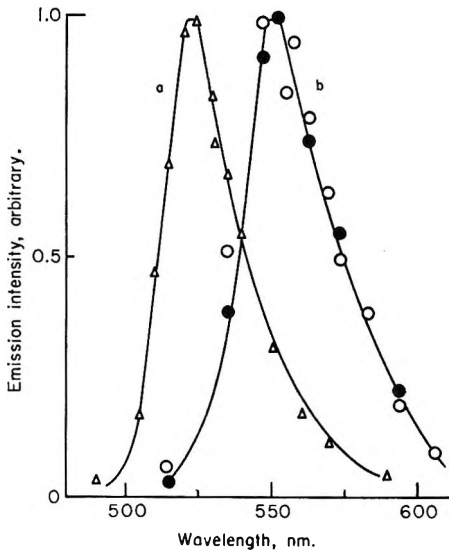

Figure 4. Comparison of electron-pulse induced emission spectra with ordinary fluorescence: curve a, fluorescence from 10 μM fluorescein (pH 11.8) (solid line); emission in the presence of 0.01 M formate (△); curve b, fluorescence from 10 μM eosin (pH 9.0) (solid line); emission in the presence of 0.01 M formate (○), and 0.01 M glucose (●).

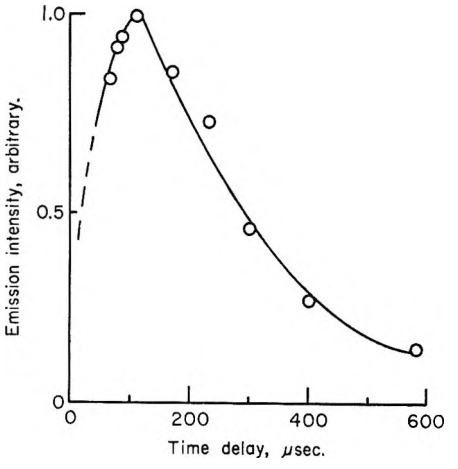

Figure 5. Dependence of emission intensity from deaerated 10 μM eosin (pH 9.0) in the presence of 0.01 M formate on delay time between light flash and 40-rad electron pulse.

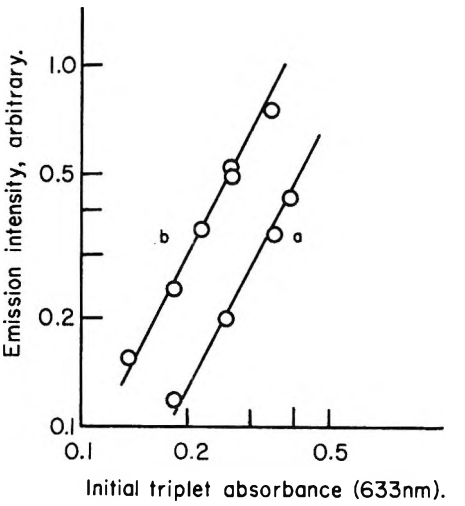

Figure 6. Dependence of emission intensity (40 rads/pulse) from deaerated 10 μM eosin (pH 9.0) in the presence of 0.01 M formate on the initial triplet absorbance. Line a, 80-μsec time delay; line b, 130-μsec time delay. The lines correspond to slope 2.0 on the logarithmic plot.

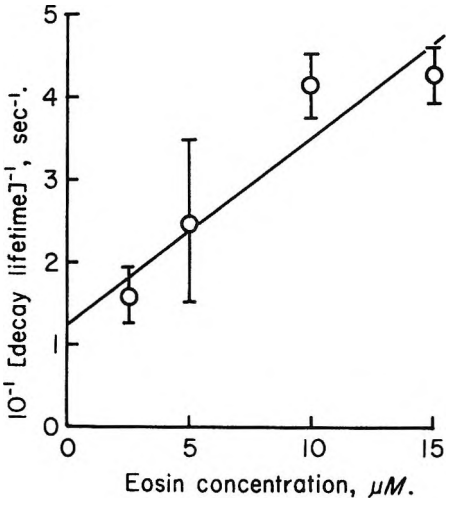

Figure 7. Dependence of precursor lifetime on initial eosin concentration.

required for maximum emission decreases from 160 μsec at 2.5 μM dye to 95 μsec at 15 μM dye. These data provide a direct measurement of the P growth and decay rate at the different dye concentrations. In another series of experiments the initial triplet yield generated by the light flash was varied with neutral density filters and it was found that the emission intensity at constant delay time depends on the *square* of the initial triplet concentration, Figure 6. This result effectively rules out X as the precursor because the T–S electron-transfer reaction 6′ makes the major contribution to X formation compared to the T–T reaction 5′, particularly at the initial triplet concentrations less than 2 μM. Furthermore, the dependence of the luminescent intensity on delay time shows that the decay of product P is considerably slower than the disappearance of the triplet state and faster than the decay of R and X. (This was shown directly by plotting the emission intensity against the triplet, R, and X concentrations at the time of the electron pulse for different dye concentrations.) The decay of P is accelerated by the dye, where the halftime ranges from 400 μsec at 2.5 μM eosin to 150 μsec at 15 μM eosin. A straightforward analysis based on the assumed decay law

$$-\mathrm{d[P]}/\mathrm{d}t = k'[\mathrm{P}] + k''[\mathrm{P}][\mathrm{D}] \qquad \text{(II)}$$

predicts that the decay halftime should vary inversely with the eosin concentrations. The experimental data in Figure 7 lead to $k' \simeq 1300$ sec^{-1} and $k'' \simeq 2 \times 10^8$ M^{-1} sec^{-1}.

A careful search was made for the absorption spectrum of P by flash photolysis of aqueous eosin to no avail. It appears that the yield of the T–T reaction responsible for its production must be low compared with reaction 5′ or that the P absorption is masked by that of T, R, or X. Apparently the luminescent process is more selective than absorption spectroscopy because of the high exothermicity when P reacts with e_{aq}^-.

Discussion

The experimental results show that triplet eosin (or fluorescein) engages in a T–T reaction leading to the unknown product P which reacts with e_{aq}^- to generate the excited singlet state of the dye as the emitting species. The simplest model consistent with these observations is the formation of an unstable TS complex as the product of the T–T quenching reaction. The subsequent chemiluminescent reaction can be represented as the spin conserving process

$$T(\uparrow\uparrow)\ldots S(\uparrow\downarrow) + e_{aq}^-(\downarrow) \longrightarrow R(\uparrow\uparrow\downarrow) + S_1^*(\uparrow\downarrow) \quad (7)$$

In a previous flash photolysis study of eosin-sensitized photochemical oxidation of aromatics[18] it was estimated that $\Delta F'$ of the reaction

$$e_{aq}^- + S_1 + H^+ \longrightarrow R$$

is approximately −34 kcal/mol at pH 8. Taking the eosin singlet–triplet splitting as 40 kcal/mol from phosphorescence measurements[19] leads to $\Delta F' \simeq (-19 +$ binding energy) for reaction 7. The binding energy of the complex is not likely to be larger than 10 kcal/mol so that the reduction process should be exothermic.

The formation of an intermediate complex involving the eosin or fluorescein triplet states is not surprising in view of the well known ground-state complexing leading to the D band[20] and the complexing of the semiquinone with the unexicted dye observed in recent pulse radiolysis measurements.[6] The formation of short-lived charge-transfer complexes between triplet eosin and a reductant has been suggested also in flash photolysis studies.[11] In particular, Kira and Kato[21] observed a transient in the flash photolysis of ethanolic eosin with absorption components in the region of the R (410 nm) and X (450 nm) bands with the properties of a charge-transfer intermediate between these species. The identification of the emission band in the present work with the monomer dye fluorescence indicates that the TS complex is loosely bound, in contrast to aromatic hydrocarbon excimers with characteristic fluorescence spectra and lifetimes. The value of k'' for the reaction between the complex and eosin is comparable to the T–S quenching rate constant of $3 \times 10^8\ M^{-1}\ sec^{-1}$, but considerably slower than $1.1 \times 10^9\ M^{-1}\ sec^{-1}$ for T–T quenching.[10] Furthermore, k' is the same magnitude as the reported values for the triplet eosin first-order decay constant of 420 sec^{-1} [22] and 540 sec^{-1}.[10] The correspondence in both cases is consistent with a loosely bound TS complex in which the intersystem crossing rate of the triplet moiety is not strongly perturbed.

Prütz and Land[4] estimated the luminescence yield of reaction 2 as the order of 10^{-5} quanta per eV of radiation absorbed for $10^{-6}\ M$ acriflavin, rhodamine B, or fluorescein, which is about 50 times as efficient as the fluorescence yield produced by direct electron impact at much higher dye concentrations. The emission intensity in the present work varies with the square of the triplet concentration and linearly with the pulse dose, which precludes the definition of a simple yield parameter. However, noting that the actual triplet yield from eosin was about 3 times as large as from fluorescein under the experimental conditions and taking the corresponding fluorescence efficiencies as 0.19 and 0.92,[23] the expected ratio of the emission intensities is $9 \times (0.19/0.92) \sim 2$, in fair agreement with the observed value 1.5 ± 0.5.

In summary, eosin or fluorescein engage in two chemiluminescent reactions involving hydrated electrons. In one process investigated in detail by Prütz and Land[4] the fluorescent state is formed by the reaction between e_{aq}^- and a dye oxidation product. Recently, the same workers[24] proposed that the quenching effect of halogen ions is due to oxidation of the dye by the halogen atom (or dihalide ion) followed by the reaction of e_{aq}^- with the oxidized dye. The process studied in the present work requires the prior formation of the dye triplet state and is not quenched by OH· scavengers. It is proposed that a triplet–singlet dye complex reacts with e_{aq}^- to form one molecule of the dye semiquinone, leaving the other dye molecule in the excited singlet state. The precursor is formed by the T–T interaction but not the T–S, so that this process is efficient only at high triplet concentrations and is not likely to be significant in ordinary photochemical reaction sensitized by these dyes.

(18) J. Chrysochoos and L. I. Grossweiner, *Photochem. Photobiol.*, **8**, 193 (1968).

(19) C. A. Parker and C. G. Hatchard, *Trans. Faraday Soc.*, **57**, 1894 (1967).

(20) B. Soederberg, *Ann. Phys.*, **41**, 381 (1913).

(21) A. Kira and S. Kato, *Sci. Rep. Tohoku Univ., Ser. 1*, **48**, 142 (1965).

(22) E. F. Zwicker and L. I. Grossweiner, *J. Phys. Chem.*, **67**, 549 (1963).

(23) P. G. Bowers and G. Porter, *Proc. Roy. Soc. Ser. A*, **297**, 348 (1967).

(24) W. Prütz and E. J. Land, *J. Phys. Chem.*, **74**, 2107 (1970).

The Decomposition of Ammonia and Hydrazine by Electron Impact

by H. Bubert and F. W. Froben*

Max-Planck-Institut für Spektroskopie, Göttingen, Germany *(Received November 16, 1970)*

Publication costs assisted by Max-Planck-Gesellschaft

In a crossed-beam experiment, fluorescence from excited fragments of ammonia and hydrazine are observed at low pressure. The spectra originate from $NH(^3\Pi)$, $NH(^1\Pi)$, $N_2^+(^2\Sigma_u^+)$, H (Balmer series), and $NH_2(^2A_1)$. In the primary reactions only $NH(^3\Pi)$, $NH(^1\Pi)$ (not from hydrazine), and $N_2^+(^2\Sigma_u^+)$ (not from ammonia) are produced.

Introduction

The formation of free radicals and stable products in ammonia and hydrazine has been studied in an electric discharge,[1,2] by photolysis,[3-5] and by electron impact.[6] Since in these experiments[1-6] secondary reactions occur during the exposure time, it is difficult to decide which reactions are the primary ones. By reducing the gas pressure and the collision volume in a crossed-beam apparatus it is possible to observe primary reactions more accurately, which leads to information about the excitation functions and the appearance potentials for the excited species.

Experimental Section[7]

The apparatus is shown in Figure 1. Electrons from an oxydcathode C (PL 505) are focused by an electron optical system L, to a collision volume of a few mm^3 where they interact with a molecule beam coming from an inlet, J. The emission is measured by means of a 0.5-m Jarrell Ash Monochromator and a 56 UVP (Valvo) photomultiplier, or photographically by a Medium Hilger Spectrograph. In both cases the spectral bandwidth is 1 Å. The energy of the electrons can be varied between 1 and 250 eV.

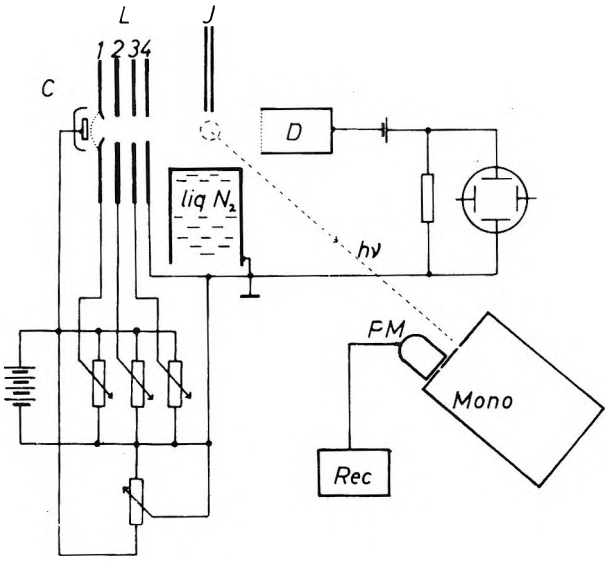

Figure 1. Equipment used for the excitation (for a description see text).

For energy calibration the $3p^3P \rightarrow 2s^3S$ transition of He at 3888.65 Å is used. Its upper level is at 23.0 eV and it has a very steep excitation function. The energy distribution is measured to have a half width $\leq$ 1.8 eV. This distribution is obtained by deflection of the electron beam using an ac modulated capacitor. The beam then sweeps across a perpendicularly aligned grid of single wires and causes pulses on each of them, from which the energy distribution of the electrons can be obtained. The number of electrons entering the collision volume is of the order of 10^{15} sec^{-1} and the number of molecules 10^{17} to 10^{18} sec^{-1}.

The electron gun and the collision volume are connected to two different vacuum systems to slow down the poisoning of the cathode and to maintain a pressure of less than 10^{-5} Torr in the electron gun.

Ammonia, Matheson 99.99% purity, was used without further purification. Hydrazine hydrate (Merck) was used after removal of water by distillation over KOH.

Results and Discussion

Emission resulting from the transitions listed in Table I was observed. Besides this emission there were a number of weak identified lines with less than 1% of the intensity of the lines given in Table I.[8]

The excitation functions of NH^* $(^3\Pi)$ and N_2^{+*} at 3360 and 3914 Å, respectively, are shown in Figure 2. For the 0,0 and 1,1 bands of the $A^3\Pi \rightarrow X^3\Sigma$ transition

(1) E. F. Logan and J. M. Marchello, *J. Chem. Phys.*, **49**, 3929 (1968).

(2) D. C. Carbaugh, F. J. Mumo, and J. M. Marchello, *ibid.*, **47**, 5211 (1967).

(3) K. H. Becker and K. H. Welge, *Z. Naturforsch.*, **19a**, 1006 (1964).

(4) H. Okabe and M. Lenzi, *J. Chem. Phys.*, **47**, 5241 (1967).

(5) K. A. Mantei and E. J. Bair, *ibid.*, **49**, 3248 (1968).

(6) E. Fink and K. H. Welge, *Z. Naturforsch.*, **19a**, 1193 (1964).

(7) H. Bubert, Ph.D. Thesis, University of Göttingen, 1970.

(8) J. R. McNesby, W. Braun, and J. Ball, "Vacuum Ultraviolet Techniques in Photochemistry," National Bureau of Standards, Washington, D. C., Dec 1968.

Table I: Transitions Observed in Ammonia and Hydrazine between 2000 and 4900 Å

Species	From	Transition	A.P.	eV, this work
$NH^*(^3\Pi)$	N_2H_4	$A^3\Pi \rightarrow X^3\Sigma$	5.92[6]	5.9
$NH^*(^3\Pi)$	NH_3	$A^3\Pi \rightarrow X^3\Sigma$	7.62[4]	8.0
$NH^*(^1\Pi)$	NH_3	$c^1\Pi \rightarrow a^1\Delta$	8.95[4,8]	8.5
$N_2^{+*}(^2\Sigma_u^+)$	N_2H_4	$B^2\Sigma_u^+ \rightarrow X^2\Sigma_g^+$	18.7	18.6
H	NH_3/N_2H_4		12.68	12.7

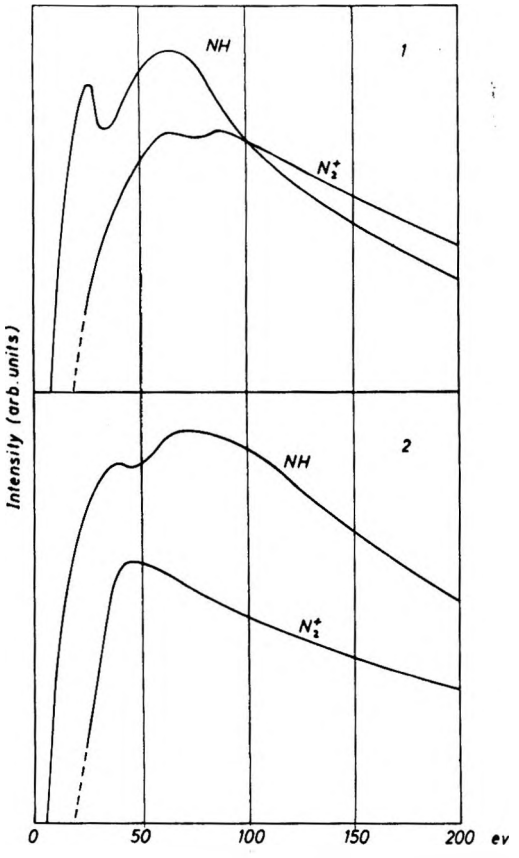

Figure 2. Excitation functions for NH measured at 3360 Å and for N_2^+ measured at 3914 Å: 1, in ammonia; 2, in hydrazine.

Table II: Decomposition by Electron Impact into Species Which Can Emit Light

	eV
Primary Reactions	
$N_2H_4 \xrightarrow{e^-} NH_2^*(^2A_1) + NH_2(^2B_1)$	3.87
$NH^*(^3\Pi) + NH_3$	5.92
$NH^*(^3\Pi) + NH(^3\Sigma) + H_2$	10.07
$NH^*(^3\Pi) + NH_2(^2B_1) + H$	10.42
$N_2^{+*}(^2\Sigma_u^+) + e^- + 2H_2$	18.7
$NH^*(^3\Pi) + NH_2(^2B_1) + H^*\ (n = 4)$	23.1
$NH_3 \xrightarrow{e^-} NH_2^*(^2A_1) + H$	5.70
$NH^*(^3\Pi) + H_2$	7.62
$NH^*(^1\Pi) + H_2$	8.95
Secondary Reactions	
$H \xrightarrow{e^-} H^*\ (n = 4)$	12.68
$H_2 \xrightarrow{e^-} H + H^*\ (n = 4)$	17.15
$N_2 \xrightarrow{e^-} N_2^{+*}(^2\Sigma_u^+) + e^-$	18.7

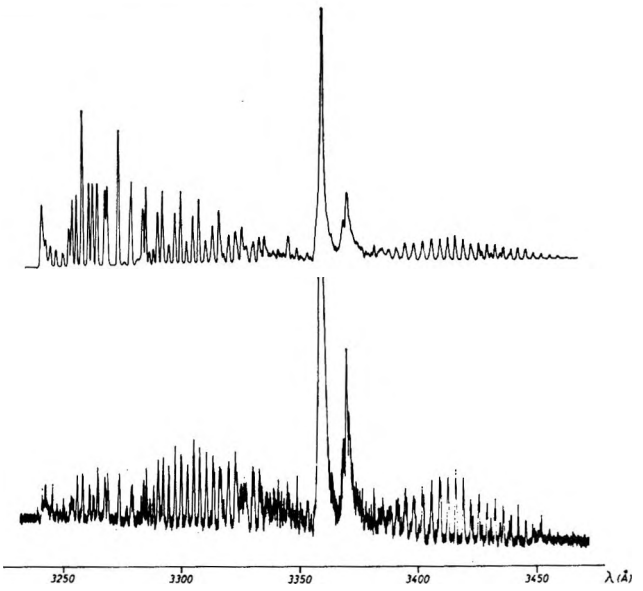

Figure 3. Part of the spectra of NH (excitation energy 70 eV): upper spectrum in ammonia; lower spectrum in hydrazine.

of NH, the excitation function is same as given in Figure 2. The intensity ratio of the 0,0 to 1,1 band is found to be 3. Following Avery[9] one obtains a vibrational temperature, $T_{vib} = 4000°K$ with ammonia as well as with hydrazine. Since the rotational structure of the transition $c^1\Pi$, $v' = 0 \rightarrow a^1\Delta$, $v'' = 0$ can be resolved, one can plot $I_J'/\nu^4\ S_J'$ over $B'J'(J' + 1)hc$, where I_J' is the intensity of the rotational line with the quantum number J' of the upper level, S_J' the line strength and B' the rotational constant. The semilogarithmic plot yields a straight line from which results a rotational temperature, $T_{rot.} = 1730°K$. The temperatures are independent of the energy of the impacting electrons. This fact points to the possibility that the resulting temperatures are characteristic for the decomposition of NH_3 and N_2H_4 into the excited states $A^3\Pi$ and $c^1\Pi$.

Reactions which lead to excitation of ammonia and hydrazine are tabulated in Table II together with their threshold energies. There is of course some contribution from secondary reactions because H_2 and N_2 do not condense at 77°K and will have a steady-state vapor pressure. It is remarkable that the $^1\Pi$ state of NH is not produced by impact on hydrazine. This effect may be seen in Figure 3. A small part of the NH spectrum is shown in this figure.

(9) H. E. Avery, J. N. Bradley, and R. Tuffnell, *Trans. Faraday Soc.*, **60**, 335 (1964).

Below 5.9 eV the excitation should lead to NH or NH_2 in the ground state or NH_2 in an excited state. The emission of $NH_2^*(^2A_1)$ can be seen only if the pressure in the reaction chamber is a factor of 100 higher than in the experiment here described. This shows that $NH_2^*(^2A_1)$ is not produced in a primary reaction.

The maximum in the excitation function of N_2^+ (Figure 2) from N_2H_4 is at a point where the excitation function for the emission of NH has a small minimum. That allows the conclusion that the formation of N_2^+ is a primary process. The excitation of H on the other hand cannot take place in a primary process, as such a process requires 16 eV.

In the case of the decomposition of NH_3, the form of the excitation function of NH may be related to different potential energy functions in the excited state. The energy distribution of the exciting electrons is too large to yield more specific results.

Statistical Mechanical Theory of Electrostriction in Dense Gases[1a,b]

by James F. Ely[1c] and Donald A. McQuarrie*

Department of Chemistry, Indiana University, Bloomington, Indiana 47401

Publication costs assisted by the Petroleum Research Foundation

Virial expansions are derived for the electrostriction of an imperfect gas in both a closed and an open system. A number of numerical calculations are presented in the form of eight figures.

I. Introduction

When a dielectric fluid is subjected to the influence of an externally applied electric field, either the pressure of the fluid will change if the system is closed or the density will change if the system is open. This phenomenon is known as electrostriction. One of the earliest molecular treatments of electrostriction is due to Scaife.[2] He considered the case of a spherical specimen of a fluid dielectric, showing that both the Lorenz–Lorentz and Debye theories lead to the result that the change in pressure in a closed system is zero and that it is necessary to use the statistical theories of Yvon and Kirkwood to obtain a nonzero result. Shortly afterwards, Hill[3] derived rigorous virial expansions for the polarization, Clausius–Mossotti function, dielectric constant, and electrostriction of an imperfect gas. The results are given in the form of series expansions which are closely related to the conventional virial expansions of an imperfect gas. McQuarrie and Levine[4] applied Hill's formal development to a calculation of the second and third dielectric virial coefficients of a system of nondipolar, anisotropically polarizable, axially symmetric, quadrupolar molecules such as CO_2 and N_2. Later they tabulated[5] the various integrals appearing in these dielectric virial coefficients for Lennard-Jones intermolecular potentials of the form 6–n, where n = 9, 12, and 15. The formulas for the virial expansion of electrostriction are very similar to those of the dielectric constant, and in this paper we shall present calculations of the pressure and density changes that occur when an imperfect gas is placed in a parallel plate capacitor.

II. Basic Formulas

Closed System. Following the development of Hill,[3] we consider a parallel plate capacitor with surface charge densities σ' and $-\sigma'$. The capacitor is filled from plate to plate with fluid and is assumed to have a large enough plate area so that edge effects may be ignored. We subtract any effects associated with the vacuum in absence of the fluid. Owing to this definition of the system, the pressure that we consider is operationally the transverse pressure defined by Koenig[6] and the external field (dielectric displacement in this case) is given by $D = 4\pi\sigma'$. The virial equation of state of an imperfect gas in this external field is

$$\frac{p}{kT} = \rho + \sum_{n\geq 2} B_n(T,D)\rho^n \qquad (1)$$

where ρ is the density and the B_n are the dielectric

(1) (a) This work was supported by the Petroleum Research Foundation; (b) contribution number 1902 from the chemical laboratories of Indiana University; (c) NDEA Predoctoral Fellow.

(2) B. K. P. Scaife, *Proc. Phys. Soc. B*, **69**, 153 (1956).

(3) T. L. Hill, *J. Chem. Phys.*, **28**, 61 (1958).

(4) D. A. McQuarrie and H. B. Levine, *Physica*, **31**, 749 (1965).

(5) H. B. Levine and D. A. McQuarrie, *J. Chem. Phys.*, **44**, 3500 (1966).

(6) F. O. Koenig, *J. Phys. Chem.*, **41**, 597 (1937).

pressure virial coefficients. For normal field strengths we may write

$$B_n(T,D) = B_n^{(0)}(T) + B_n^{(2)}(T)D^2 + O(D^4) \quad (2)$$

where we have realized that $B_n(T,D)$ must be an even function of D owing to symmetry. Defining Δp as the change in the thermodynamic pressure caused by the external field, we have from (1) and (2)

$$\Delta p = p(\text{field} = D) - p(\text{field} = 0)$$
$$= kTD^2[B_2^{(2)}(T)\rho^2 + B_3^{(2)}\rho^3 + \ldots] + O(D^4) \quad (3)$$

If the molecules in our system are axially symmetric and nonpolar but possess permanent quadrupole moments and anisotropic polarizabilities (with α_L and α_T being the longitudinal and transverse components, respectively), we may derive expressions for the virial coefficients in terms of a power series in the mean polarizability $\bar{\alpha} = (\alpha_L + 2\alpha_T)/3$ and the scalar quadrupole moment Θ. This was done in ref 4, from which the results for $B_2^{(2)}(T)$ and $B_3^{(2)}(T)$ are

$$B_2^{(2)}(T) = -4\pi\bar{\alpha}^3(1 + 2\kappa^2)\beta\int_0^\infty e^{-\beta\phi(r)} r^{-4}dr -$$
$$2\pi\bar{\alpha}^2\Theta^2\beta^2\left(1 + \frac{4}{5}\kappa^2\right)\int_0^\infty e^{-\beta\phi(r)}r^{-6}dr + \frac{4\pi\beta\bar{\alpha}^2}{3} \quad (4)$$

and

$$B_3^{(2)}(T) = -\frac{2\beta\bar{\alpha}^3}{V}(1 + 2\kappa^2)\iiint f(r_{13}) \times$$
$$f(r_{23})e^{-\beta\phi(r_{12})}r_{12}^{-6}\,d\vec{r}_1\,d\vec{r}_2\,d\vec{r}_3 -$$
$$\frac{\beta\bar{\alpha}^3}{V}\iiint f(r_{13})e^{-\beta\phi(r_{12})}e^{-\beta\phi(r_{23})}(3\cos^2\theta - 1) \times$$
$$r_{12}^{-3}r_{23}^{-3}\,d\vec{r}_1\,d\vec{r}_2\,d\vec{r}_3 - \frac{\beta^2\Theta^2\bar{\alpha}^2}{V}\left(1 + \frac{4}{5}\kappa^2\right) \times$$
$$\iiint f(r_{13})\,f(r_{23})e^{-\beta\phi(r_{12})}r_{12}^{-8}\,d\vec{r}_1\,d\vec{r}_2\,d\vec{r}_3 -$$
$$\frac{\beta^2\Theta^2\bar{\alpha}^2}{2V}\iiint f(r_{13})e^{-\beta\phi(r_{12})}e^{-\beta\phi(r_{23})}(5\cos^3\theta -$$
$$3\cos\theta)\,r_{12}^{-4}r_{23}^{-4}\,d\vec{r}_1\,d\vec{r}_2\,d\vec{r}_3 - \beta\bar{\alpha}^3\left(\frac{8\pi}{3}\right)^2 \quad (5)$$

In these equations $\beta = 1/kT$, $\kappa = (\alpha_L - \alpha_T)/3\bar{\alpha}$, V is the volume of the system, $\vec{r}_{ij}$ the vectorial distance between particles i and j, $r = |\vec{r}_{12}|$, θ the angle between $\vec{r}_{12}$ and $\vec{r}_{23}$, and $f(r_{ij})$ is the Mayer function of particles i and j interacting with an intermolecular potential $\phi(r_{ij})$

$$f(r_{ij}) = e^{-\beta\phi(r_{ij})} - 1$$

It is computationally convenient to write these equations in reduced form. If we use a Lennard-Jones 6–12 potential with well depth ϵ and hard-sphere diameter σ, we may define the reduced variables

$$\alpha^* = \bar{\alpha}/\sigma^3,\ \Theta^* = (\Theta^2/\epsilon\sigma^5)^{1/2};\ T^* = kT/\epsilon;$$
$$(x, y, z) = (r_{12}, r_{23}, r_{23})/\sigma,\ \phi^*(x) =$$
$$4(x^{-12} - x^{-6});\ \rho^* = \rho\sigma^3;\ D^* = D(\sigma^3/\epsilon)^{1/2} \quad (6)$$

Using these definitions eq 4 and 5 become (after some coordinate transformations)

$$B_E^* \equiv \frac{\epsilon T^* B_2^{(2)}(T^*)}{\sigma^6} = -4\pi\alpha^{*2}\left\{(1 + 2\kappa^2)\alpha^* I_2 + \frac{1}{2}\frac{\Theta^{*2}}{T^*}\left(1 + \frac{4}{5}\kappa^2\right)I_3 - \frac{1}{3}\right\} \quad (7)$$

and

$$C_E^* \equiv \frac{\epsilon T^* B_3^{(2)}(T^*)}{\sigma^9} = -16\pi^2\alpha^{*2} \times$$
$$\left\{2\alpha^*(1 + 2\kappa^2)J_4 + \alpha^* J_5 + \frac{\Theta^{*2}}{T^*} \times \left(1 + \frac{4}{5}\kappa^2\right)J_2 + \frac{\Theta^{*2}}{T^*}J_6 + \frac{4\alpha^*}{9}\right\} \quad (8)$$

The I_n's and J_n's are dimensionless integrals over the reduced intermolecular potential, $\phi^*(x)$, given by

$$I_1(T^*) = \int_0^\infty x^2 f(x)dx$$
$$I_2(T^*) = \int_0^\infty x^{-4}\exp\left[-\frac{\phi^*(x)}{T^*}\right]dx$$
$$I_3(T^*) = \int_0^\infty x^{-6}\exp\left[-\frac{\phi^*(x)}{T^*}\right]dx$$
$$I_4(T^*) = \int_0^\infty x^{-8}\exp\left[-\frac{\phi^*(x)}{T^*}\right]dx$$
$$I_5(T^*) = \int_0^\infty x^{-9}\exp\left[-\frac{\phi^*(x)}{T^*}\right]dx$$
$$J_1(T^*) = \int_0^\infty\int_0^z\int_{z-y}^{z+y} zf(z)yf(y)xf(x)dxdydz \quad (9)$$
$$J_2(T^*) = \int_0^\infty\int_0^z\int_{z-y}^{z+y} zf(z)yf(y)x^{-7} \times \exp\left[-\frac{\phi^*(x)}{T^*}\right]dxdydz$$
$$J_3(T^*) = \int_0^\infty\int_0^z\int_{z-y}^{z+y} zf(z)yf(y)x^{-9} \times \exp\left[-\frac{\phi^*(x)}{T^*}\right]dxdydz$$
$$J_4(T^*) = \int_0^\infty\int_0^z\int_{z-y}^{z+y} zf(z)yf(y)x^{-5} \times \exp\left[-\frac{\phi^*(x)}{T^*}\right]dxdydz$$

$$J_5(T^*) = \int_0^\infty \int_0^z \int_{z-y}^{z+y} (3W^2 - 1)z^{-2}y^{-2} \times \exp\left[-\frac{\phi^*(y) + \phi^*(z)}{T^*}\right] dx\,dy\,dz$$

and, finally

$$J_6(T^*) = \int_0^\infty \int_0^z \int_{z-y}^{z+y} (5W^3 - 3W)z^{-3}y^{-3} \times \exp\left[-\frac{\phi^*(y) + \phi^*(z)}{T^*}\right] dx\,dy\,dz$$

$$W = (z^2 + y^2 - x^2)/2zy$$

These integrals have been tabulated by Levine and McQuarrie.[5] Using the reduced quantities we may write eq 3 as

$$\Delta p = D^2\{B_E^*\rho^{*2} + C_E^*\rho^{*3} + \ldots\} \quad (10)$$

This is the pressure change experienced by a closed isotropic system when placed between the plates of a parallel plate capacitor.

Open Systems. In an open system the effect of the external field is to draw molecules into the field and hence give an increase in density. A possible experimental setup to measure this effect might be a parallel plate capacitor in a large container of gas. When there is no voltage across the capacitor, the density will be uniform throughout; when a potential difference is applied across the plates of the capacitor, the density between the plates will actually increase and should be measurable by a technique such as light scattering.

The equation defining the electrostrictive effect in an open system may be derived by differentiating ρ with respect to D at constant temperature and chemical potential. The result is

$$\frac{1}{\rho}\left(\frac{\partial\rho}{\partial D}\right)_{T,\mu} = D\left\{\frac{\bar{\alpha}}{kT} - \left(4B_2^{(2)} + 2B_2^{(0)}\frac{\bar{\alpha}}{kT}\right)\rho + \left[-3B_3^{(2)} + 8B_2^{(0)}B_2^{(2)} + \frac{\bar{\alpha}}{kT}(-3B_3^{(0)} + 4B_2^{(0)2})\right]\rho^2 + \ldots\right\} \quad (11)$$

The actual change in density associated with this effect may be found by either integrating this expression from ($\rho = \rho_0$, $D = 0$) to ($\rho = \rho$, $D = D$) or by simply expanding $\rho(D)$ in a Taylor series about $D = 0$. Equation 11 may then be used to evaluate the various derivatives of ρ with respect to D. Either way, one gets

$$\frac{\Delta\rho}{\rho_0} = \frac{\rho - \rho_0}{\rho_0} = \frac{1}{2}\frac{D}{\rho_0}\left(\frac{\partial\rho}{\partial D}\right)_{\rho=\rho_0}$$

This can be written in reduced form as

$$\frac{\Delta\rho}{\rho_0} = \frac{D^{*2}}{2T^*}\{\alpha^* - (4B_E^* + 2\alpha^*B_p^*)\rho_0^* + [3C_E^* + 8B_E^*B_p^* + \alpha^*(-3C_p^* + 4B_p^{*2})]\rho_0^{*2} + \ldots\} \quad (12)$$

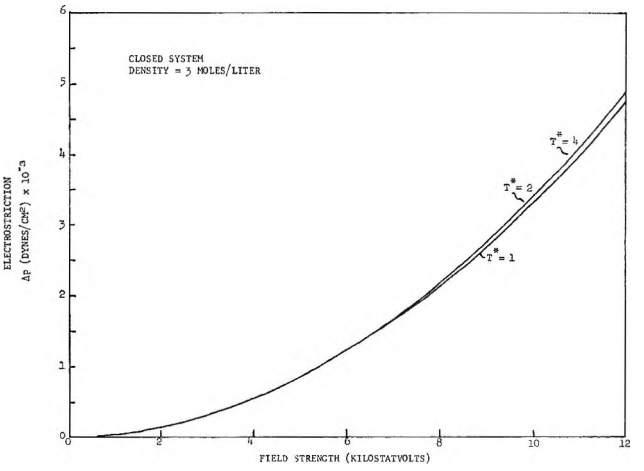

Figure 1. The change in pressure, Δp, given by eq 10 is plotted for argon gas as a function of the applied field, D. The density is fixed at 3 mol/l. and the reduced temperature T^* is defined in eq 6.

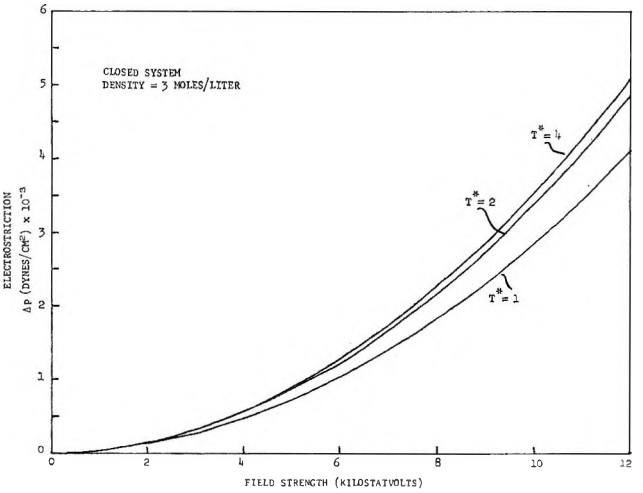

Figure 2. The change in pressure given by eq 10 is plotted for nitrogen gas as a function of the applied field. The density is fixed at 3 mol/l.

We have introduced two "new" quantities in these equations, *viz*, B_p^* and C_p^*, whose reduced forms are

$$B_p^* \equiv \frac{B_2^{(0)}(T^*)}{\sigma^3} = -2\pi I_1 - \frac{14\pi}{5}\frac{\Theta^{*4}}{T^{*2}}I_4 - \frac{6\pi\alpha^*\Theta^{*2}}{T^*}I_3 + \frac{72\pi}{25}\frac{\alpha^{*2}\Theta^{*2}}{T^*}\kappa^2 I_5 \quad (13)$$

and

$$C_p^* \equiv \frac{B_3^{(0)}(T^*)}{\sigma^6} = -\frac{16\pi^2}{3}J_1 - \frac{112\pi^2}{5}\frac{\Theta^{*4}}{T^{*2}}J_3 - \frac{48\pi^2}{T^*}\alpha^*\Theta^{*2}J_2 \quad (14)$$

The unreduced forms are given in ref 4.

Notice that the electrostrictive effect is zero for an ideal gas in a closed system but does not vanish for an

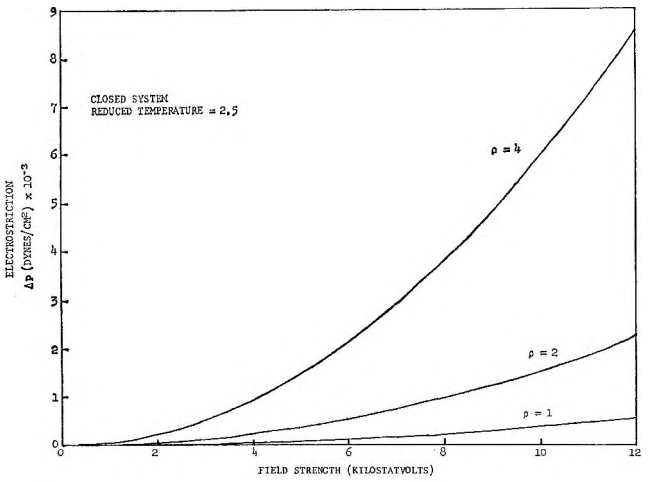

Figure 3. The change in pressure Δp is plotted for argon gas as a function of the applied field. The reduced temperature is fixed at 2.5.

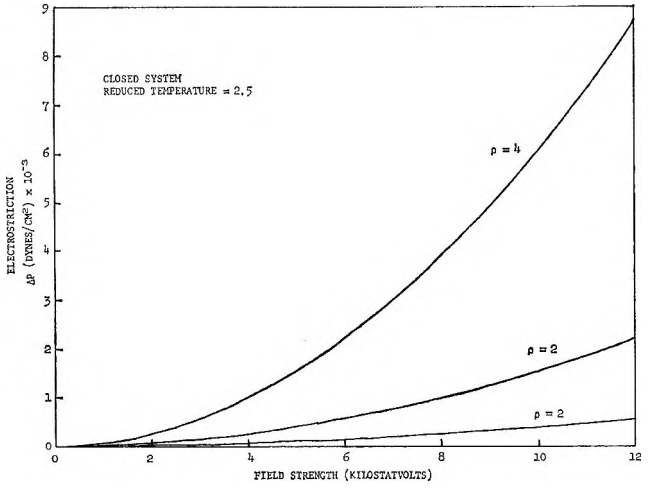

Figure 4. The change in pressure Δp is plotted for nitrogen gas as function of the applied field. The reduced temperature is fixed at 2.5.

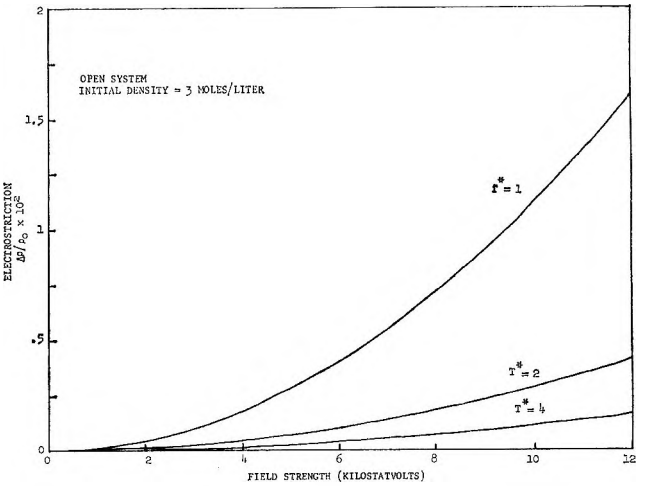

Figure 5. The fractional change in density $\Delta\rho/\rho_0$ given by eq 12 is plotted for argon gas as a function of the applied field D. The initial density is fixed at 3 mol/l. Notice that the temperature dependence in this system is reversed from that of the closed system.

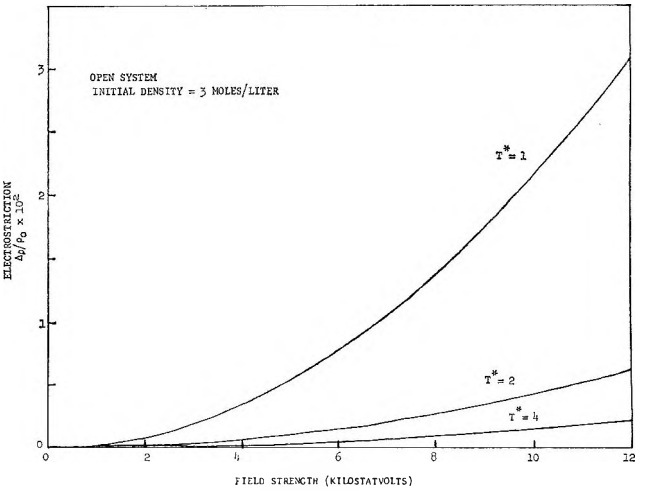

Figure 6. The fractional change in density in nitrogen gas given by eq 12 is shown as a function of the applied field. The initial density is 3 mol/l. and the reduced temperature T^* is defined in eq 6.

open system. In the open system, the gas imperfections contribute a small correction to a leading dominant term (*cf.* eq 11).

III. Results

The preceding equations relating the electrostrictive behavior to the dielectric virial coefficients were evaluated for two gases, argon and nitrogen. The parameters that enter the equations were from Hirschfelder, Curtis, and Bird[7] for argon and from Orcutt[8] for nitrogen. In both cases the Lennard-Jones parameters were fitted from viscosity data. To be more specific, for argon $\epsilon/k = 124°\text{K}$, $\sigma = 3.418\text{Å}$, and $\bar{\alpha} = 1.653\ \text{Å}^3$, and for nitrogen $\epsilon/k = 91.5°\text{K}$, $\sigma = 3.681\ \text{Å}$, $\bar{\alpha} = 1.73\ \text{Å}^3$ and $\Theta = 1.90 \times 10^{-26}$ esu cm^2.

Using these parameters it was found that the quadrupolar terms in eq 13 and 14 for B_p^* and C_p^* contribute less than 0.1% and in eq 7 and 8 for B_E^* and C_E^* they contribute approximately 15% of the total at a reduced temperature of 1.5. The values obtained from the equations for the virial coefficients were also found to compare favorably with those values existing in the literature.[9] The actual values of the parameters are not particularly crucial, however, since we only wish to present an idea of the magnitude of the effect and its dependence on temperature and density.

The eight figures show typical results of the calculations for open and closed systems. It appears that in a closed system the temperature dependence arises

(7) J. O. Hirschfelder, C. R. Curtis, and R. B. Bird, "Molecular Theory of Gases and Liquids," Wiley, New York, N. Y., 1954, pp 1110–1111.

(8) R. H. Orcutt, *J. Chem. Phys.*, **39**, 605 (1963).

(9) R. H. Orcutt and R. H. Cole, *Physica*, **31**, 1779 (1965). See also ref 7, Appendices I-B and I-C.

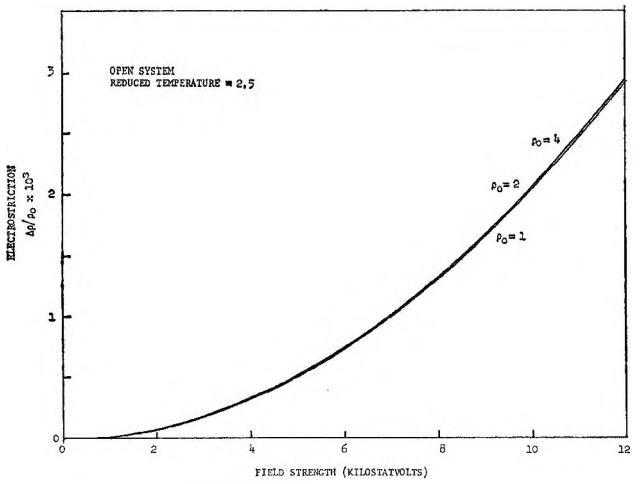

Figure 7. The electrostriction in an open system, $\Delta\rho/\rho_0$, is shown for argon gas as a function of the applied field D. The reduced temperature is fixed at a value of 2.5. Notice that the effect is virtually independent of the initial density ρ_0.

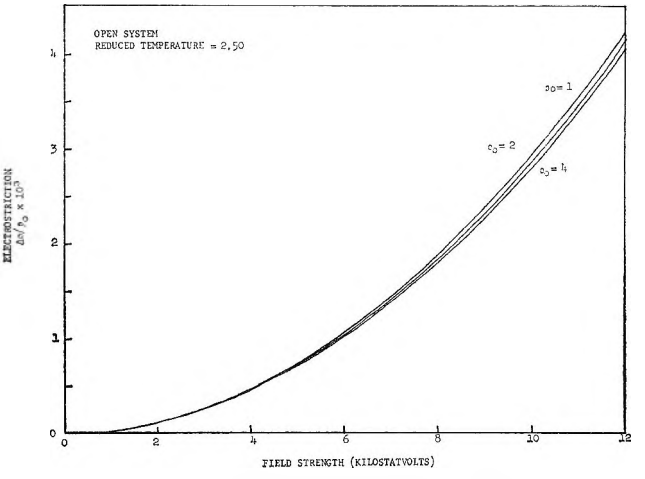

Figure 8. The effect of an applied field D on the density of an open system of nitrogen gas is shown at a fixed reduced temperature of 2.5.

mainly with the quadrupole moment, as can be easily seen from Figures 1 and 2. The results for argon appear to be very insensitive to the value of the temperature. We also see in Figures 3 and 4 that the quadrupole moment does not cause any appreciable change in the density dependence of the electrostriction.

As should be expected, the behavior is different in the open system. It is again apparent from Figures 5 and 6 that the quadrupole moment makes an appreciable effect on the temperature dependence, but notice that the system is far from temperature independent in the case of argon. We see in Figures 7 and 8 that the effect is virtually density independent in the open system since the leading and dominant term in eq 11 is density independent.

The results calculated here are well within the range of being able to be measured experimentally. The only experimental determination of the excess pressure produced by a fluid in an electric field, however, is a study of several liquids by Hakim and Higham.[10]

Acknowledgment. The authors wish to thank Dwain Diller of the National Bureau of Standards for suggesting these calculations.

(10) S. S. Hakim and J. B. Higham, *Proc. Phys. Soc.*, **80**, 190 (1962).

Chain Association Equilibria. A Nuclear Magnetic Resonance Study of the Hydrogen Bonding of *N*-Monosubstituted Amides. II. In Carbon Tetrachloride[1]

by Laurine L. Graham* and Chang Y. Chang

Department of Chemistry, Northern Illinois University, DeKalb, Illinois 60115 *(Received August 26, 1970)*

Publication costs assisted by Northern Illinois University

Thermodynamic parameters for hydrogen bonding through self-association in *N*-monosubstituted amides have been determined in carbon tetrachloride solution by nuclear magnetic resonance measurements in the temperature range 20 to 60°. The free energy and enthalpy changes for association decrease in the order: *N*-methylacetamide > *N*-isopropylacetamide > *N*-*tert*-butylacetamide. The results agree with recent molecular orbital calculations which predict that hydrogen bonds in higher linear aggregates of formamide are stronger than those in the dimer.

Introduction

Thermodynamic parameters for hydrogen bonding for highly self-associated species have been notoriously difficult to obtain, either by spectroscopic or by physicochemical measurements. The mathematics involved in the problem of infinite association requires either computer solutions or approximations such as that only one higher aggregate (for example, only tetramers) exists in equilibrium with the monomer.[2,3] Another assumption frequently used allows the presence of monomer, dimer, trimer, and higher aggregates, but assigns only one equilibrium constant to all types of association.[4] These objections have been overcome in some infrared,[5] vapor pressure,[6] and nuclear magnetic resonance (nmr) studies[7] of self-association by using K_{12} for the monomer–dimer equilibrium constant and a second constant, $\bar{K}$, to describe the next steps

$$\text{monomer} + n\text{-mer} \rightleftarrows (n+1)\text{-mer where } n \geq 2$$

In paper I, only the equilibrium constants for self-association were determined. In this work, temperature studies allow the calculation of enthalpies and entropies of hydrogen bond formation.

Of the two special cases discussed in the theoretical section of paper I, the inert solvent equations (eq 31–37) apply to the *N*-monosubstituted amides in carbon tetrachloride. The following equation was derived

$$\delta_0 = \frac{\bar{Y}}{Y}(\nu_M - \nu_D) + \nu_D \qquad (1)$$

Equation 1 relates the observed chemical shift (δ_0) of the nitrogen proton in the amides (CH_3CONHR'), which is a weighted average of all NH protons, bonded and free, to ν_M, the chemical shift of the free NH proton, ν_D, the shift of the hydrogen-bonded NH proton, and $\bar{Y}/Y$, a ratio which is derived from the stoichiometric concentration of the amide–carbon tetrachloride solution and which is related to K_{12} and $\bar{K}$. The values of K_{12} and $\bar{K}$ which give the smallest value for the sum of the squares of the deviations of δ_0 in the least-squares fit of eq 1 to a straight line are assumed to be the best set of equilibrium constants. The theory has been presented in detail;[7] however, it does seem worthwhile to mention here the assumptions made in arriving at eq 1. These are that all hydrogen-bonded protons in amide–amide linkages (–C=O....H–N<) will resonate at the same frequency, ν_D, and that all free NH protons, including those at the ends of the hydrogen-bonded chains, will resonate at the monomer frequency, ν_M.

The primary questions which we sought to answer were these: (1) What is the relative contribution of enthalpy and entropy to the driving force for hydrogen bond formation in amides? (2) How does changing

(1) This work was supported by a grant from the Academic Dean's Fund of Northern Illinois University. This work is taken in part from the dissertation of C. Y. C. submitted in partial fulfillment of the requirements for the M.S. degree, Northern Illinois University, 1970.

(2) M. Saunders and J. B. Hyne, *J. Chem. Phys.*, **29**, 253, 1319 (1958); **31**, 270 (1959).

(3) (a) E. Lippert, *Ber. Bunsenges. Phys. Chem.*, **67**, 267 (1963); (b) S. H. Marcus and S. I. Miller, *J. Amer. Chem. Soc.*, **88**, 3719 (1966).

(4) (a) O. Redlich and A. T. Kister, *J. Chem. Phys.*, **15**, 849 (1947); (b) G. Mavel, Doctoral Thesis, University of Paris, 1961; (c) E. T. Adams, Jr., "Fractions," No. 3, 1967 (a publication of and obtainable from the Spinco Division, Beckman Instruments, Inc., 1117 California Ave., Palo Alto, Calif. 94304).

(5) N. D. Coggeshall and E. L. Saier, *J. Amer. Chem. Soc.*, **73**, 5414 (1951).

(6) M. Davies and D. K. Thomas, *J. Phys. Chem.*, **60**, 767 (1956).

(7) L. A. LaPlanche, H. B. Thompson, and M. T. Rogers, *ibid.*, **69**, 1482 (1965). Referred to as Paper I.

the nitrogen alkyl substituent affect the free energy, the enthalpy, and the entropy? (3) How do the thermodynamics for adding another unit to a hydrogen-bonded aggregate differ from those for the monomer–dimer equilibrium?

Experimental Section

Two good reasons for the scarcity of nmr hydrogen bonding studies of amides are: (1) the amides are so highly associated[7] that extremely dilute solutions are needed to enter the range where monomer concentration becomes appreciable; (2) in the low concentration range, the nitrogen proton line width is so broad, due to the quadrupole relaxation of the ^{14}N nucleus, that without the use of a ^{14}N spin decoupler and/or a time averaging computer, measurements of the chemical shift can only be estimates.

Our instrumentation was a Varian A60-A nmr spectrometer, with variable temperature apparatus, an NMR Specialties Inc. HD-60B ^{14}N spin decoupler, and a Fabri-Tek Model 1062 computer.

N-Methylacetamide (NMA) and *N*-isopropylacetamide (NiPA) were purified by drying over anhydrous sodium sulfate and fractionally distilling *in vacuo*. *N-tert*-butylacetamide (NtBA) was recrystallized to a constant melting point. Carbon tetrachloride was dried over calcium sulfate and then fractionally distilled. After purification, all materials were kept in a dessicator. Samples were made up by weight inside a Glove Bag (I^2R Company) which had been flushed with dry nitrogen several times. The samples were transferred to A-60 nmr sample tubes, which had been flamed out on a vacuum line, and closed with a ground-glass stopper while inside the Glove Bag. The sample tubes were then degassed and sealed. A small amount of tetramethylsilane (TMS) had been added for use as an internal reference and for homogeneity adjustments at various temperatures.

Sample temperatures were determined from the separation of the proton peaks in the Varian-supplied methanol or ethylene glycol standards. The standard sample was kept in the probe while the temperature control was adjusted until the peak separation exactly corresponded to the desired temperature as given by the Varian chart. The error in the chart[8] in this temperature range is less than $\pm 1°$. This procedure was repeated before and after the recording of each spectrum.

Because use of the ^{14}N spin decoupler was found to raise the sample temperature by approximately 2°, the spin decoupler was left on during all measurements, including those of the methanol or ethylene glycol standards. Although a high level of radiofrequency power was used, complete decoupling of the ^{14}N proton was not attained. Nevertheless, the improvement in accuracy of measurement is significant. In one solution of NMA, the width at half-height of the NH peak narrows from about 0.33 ppm to about 0.23 ppm. As the amide solutions are made more dilute, the line width of the NH peak increases, compounding the difficulties of measurement. For this reason, the time averaging computer was used for solutions of concentration below 0.01 mole fraction amide. The lowest concentration recorded was 0.004 mole fraction in amide. In more dilute solutions, the error in measurement would have been greater than ± 1 Hz. A sweep width of 500 Hz was used to record the spectrum, and the NH peak was measured in Hz downfield from TMS. (In this paper, a chemical shift of 300 Hz means that the peak is 300 Hz downfield from TMS, at 60 MHz.) The calibration of the 500-Hz sweep width of the A-60A was frequently checked using a side band oscillator and frequency counter.

Results

Tables I–III contain the chemical shifts of the nitrogen proton in NMA, NiPA, and NtBA, respectively, as a function of temperature and concentration. These values were put into the computer program already described and the results are shown in Table IV. The

Table I: Concentration and Temperature Dependence of the Observed Chemical Shift[a] of the Nitrogen Proton in NMA–CCl_4 Solutions

X^b	$\delta_0(20°)$	$\delta_0(30°)$	$\delta_0(40°)$	$\delta_0(50°)$	$\delta_0(60°)$
0.1064	497	491	485	479	475
0.04072	482	475	464	453	441
0.02190	462	450	437	420	402
0.01530	448	435	418	400	380
0.01518	444	433	418	399	379
0.00998	420	406	389	362	349
0.00502	373	359	338	320	309

[a] In hertz from internal TMS, at 60 MHz. [b] Mole fraction of amide.

Table II: Concentration and Temperature Dependence of the Observed Chemical Shift[a] of the Nitrogen Proton in NiPA–CCl_4 Solutions

X^b	$\delta_0(20°)$	$\delta_0(30°)$	$\delta_0(40°)$	$\delta_0(50°)$	$\delta_0(60°)$
0.1490	490	483		466	459
0.09898	479	471.5	462.5	453	445
0.08529	481.5	472.5	462	452	441
0.02906	456	442	430	417	395
0.02210		438	422	407	380
0.01539	432	418	401	383	356
0.00739	383	367	344	332	315
0.00500	362	345	329	320	

[a] In hertz from internal TMS, at 60 MHz. [b] Mole fraction of amide.

(8) A. L. Van Geet, *Anal. Chem.*, **40**, 2227 (1966).

Table III: Concentration and Temperature Dependence of the Observed Chemical Shift[a] of the Nitrogen Proton in NtBA–CCl_4 Solutions

X^b	$\delta_0(20°)$	$\delta_0(30°)$	$\delta_0(40°)$	$\delta_0(50°)$	$\delta_0(60°)$
0.1503	457	448	438.5	428	417
0.1247	453	444	433.5	423.5	411.5
0.07776	442	431	418	406	392
0.06514	439	429	414.5	401	388
0.05062	428	417	403	389	375
0.03592	417	402	386.5	370.5	357
0.02354	396	381	365	349	336
0.01502	377	362	346	333	323
0.00996	359	344	331	320.5	311

[a] In hertz from internal TMS at 60 MHz. [b] Mole fraction of amide.

Table IV: Values of the Equilibrium Constants and Free (ν_M) and Hydrogen-Bonded (ν_D) Chemical Shifts[a] of the Nitrogen Proton in Amide–CCl_4 Solutions

	T, °C	K_{12}, mf^{-1}	$\bar{K}$, mf^{-1}	ν_M	ν_D
NMA	20	17 ± 0.6	270 ± 9	291	513
	30	15	240	286	507
	40	13	180	289	506
	50	10	140	284	503
	60	8	110	285	501
NiPA	20	11 ± 0.4	180 ± 13	323	500
	30	10	160	312	495
	40	9	130	304	489
	50	7	110	302	482
	60	6	70	300	480
NtBA	20	7.6 ± 0.3	67 ± 1.3	335	480
	30	6.0	60	324	473
	40	5.9	50	314	469
	50	4.7	41	308	463
	60	4.6	35	301	457

[a] In hertz from internal TMS at 60 MHz.

chemical shifts of the free and hydrogen-bonded NH proton are given by the slope and intercept of the least-squares treatment of eq 1. The thermodynamic parameters shown in Table V were determined from a least-squares plot of ln K_{12} (or ln $\bar{K}$) *vs.* $1/RT$. The errors given are the most probable errors in the slope and intercept of a straight line.[9]

Discussion

The Monomer–Dimer Equilibrium Compared with the n-mer Equilibria. The most obvious conclusion to be drawn from this work is that even in the concentration range studied (up to approximately 1 *M* amide in carbon tetrachloride) at least two equilibrium constants are necessary to adequately account for the complex hydrogen-bonding chain association in each of the amides. The equilibrium constant $\bar{K}$ is approximately ten times larger than K_{12}, indicating that the free energy change for the process monomer + *n*-mer → (*n* + 1)-mer is more favorable than for dimerization. Furthermore, the entropies and the enthalpies are also different for these steps in the hydrogen-bonding association (Table V). The enthalpy decrease upon the addition of an amide monomer to a dimer or longer chain is larger than for the dimerization of two monomers.

Two recent molecular orbital calculations,[10,11] both done by the CNDO/2 method, indicate that the average energy per hydrogen bond is lower for linear trimers than for linear dimers of formamide. In one of these calculations,[11] two structures for the NMA dimer, four structures for the formamide dimer, and two for the formamide trimer are considered. A comparison of calculated values for ΔH_{12} and $\Delta\bar{H}$ is therefore not possible for NMA, but in the formamide linear trimer, the energy per hydrogen bond is about 0.7 kcal/mol lower than for the formamide linear dimer. As Momany, *et al.*,[11] point out, this favors extended hydrogen-bonded structures in peptide systems and indicates that linear hydrogen bond formation is a cooperative process. The same argument would apply to the linear NMA aggregates.[12]

The hydrogen bonding by self-association in a few *N*-monosubstituted amides has been studied in benzene solution by vapor pressure measurements,[6] and the results indicate that when linear aggregates form, $|\Delta\bar{H}| > |\Delta H_{12}|$. (Therefore, the average energy per hydrogen bond for the higher aggregates is lower, or more negative, than for the dimer.) Similar results have been found for methanol[13] and in theoretical calculations of linear HF polymers.[14]

Earlier theoretical work[15] concerning only the entropy changes on self-association of solutes in inert solvents predicts that $|\Delta S_{12}| > |\Delta\bar{S}|$. The reasoning is that the decrease in entropy when two monomers form a dimer is larger than that for the process monomer + *n*-mer → (*n* + 1)-mer, where $n \geq 2$. Although we estimate an error in the change in entropy (Table V) of about 1 eu/mol, the trend is for $|\Delta S_{12}|$ to be greater than $|\Delta\bar{S}|$ for each amide. Therefore, both enthalpy and entropy factors (namely, that $|\Delta\bar{H}| > |\Delta H_{12}|$ and that

(9) H. Margenau and G. M. Murphy, "The Mathematics of Physics and Chemistry," 2nd ed, D. Van Nostrand Co., New York, N. Y., 1959, p 519.

(10) A. S. N. Murthy, K. G. Rao, and C. N. R. Rao, *J. Amer. Chem. Soc.*, **92**, 3544 (1970).

(11) F. A. Momany, R. F. McGuire, J. F. Yan, and H. A. Scheraga, *J. Phys. Chem.*, **74**, 2424 (1970).

(12) The average energy per hydrogen bond for the NMA trimer is $\frac{1}{2}(\Delta H_{12} + \Delta\bar{H})$, which is lower (*i.e.*, more negative) than ΔH_{12} (Table V).

(13) A. S. N. Murthy, R. E. Davis, and C. N. R. Rao, *Theor. Chim. Acta*, **13**, 81 (1969).

(14) P. A. Kollman and L. C. Allen, *J. Amer. Chem. Soc.*, **92**, 753 (1970).

(15) L. Sarolea-Mathot, *Trans. Faraday Soc.*, **49**, 8 (1953).

Table V: Thermodynamic Parameters[a] for the Hydrogen Bonding of NMA, NiPA, and NtBA in CCl_4 Solution

Amide	$-\Delta H_{12}$, kcal/mol	$-\Delta\bar{H}$, kcal/mol	$-\Delta S_{12}$,[b] eu/mol	$-\Delta\bar{S}$,[b] eu/mol	$-\Delta G_{12}$,[c] kcal/mol	$-\Delta\bar{G}$,[c] kcal/mol
NMA	3.7 ± 0.3	4.5 ± 0.3	6.8 ± 1.0	4.1 ± 0.9	1.7	3.3
NiPA	3.0 ± 0.3	4.3 ± 0.5	5.5 ± 0.9	4.3 ± 1.8	1.4	3.0
NtBA	2.4 ± 0.2	3.3 ± 0.1	4.3 ± 0.9	2.7 ± 0.5	1.2	2.5

[a] The free energy and entropy changes were calculated from K_{12} and $\bar{K}$ in mole fraction units. [b] Independent of temperature between 20 and 60°. [c] The value at 20° is given.

$|\Delta S_{12}| > |\Delta\bar{S}|$) contribute toward making $|\Delta\bar{G}| > |\Delta G_{12}|$. Within experimental error, the value of $\Delta\bar{G}$ is twice that of ΔG_{12} (Table V), leading to $\bar{K} \gg K_{12}$.

Varying the Nitrogen Alkyl Substituent. Changing the *N*-alkyl substituent from methyl to isopropyl to *tert*-butyl reduces the values of the equilibrium constants (Table IV). Although the entropy changes are small, and $\Delta\bar{S}$ for NMA and NiPA are the same within experimental error, there is still a trend toward a smaller negative value for the entropy change as the *N*-methyl group is replaced by larger groups. However, while the entropy change upon hydrogen-bond formation is becoming somewhat more favorable for the amides with bulkier substituents, the enthalpy change is becoming smaller (Table V) indicating weaker hydrogen bonds in NtBA than in NiPA, which in turn are weaker than in NMA. Since the change in the enthalpy is larger than the change in $|T\Delta S|$, the change in free energy decreases in the series NMA to NtBA, and thus the equilibrium constants, at a given temperature, are smaller (Table IV). We attribute this change in enthalpy predominantly to steric factors rather than to the inductive effect of the *N*-alkyl substituent since: (1) previous studies have shown that changing the *N*-alkyl substituent in amides has a small effect on the basicity[16,17] of the carbonyl oxygen atom; and (2) recent theoretical studies[11] of the NMA linear dimer indicate that in the lowest energy configuration, the monomers are aligned in the dimer in such a way as to bring the acetyl protons of one molecule and the *N*-methyl protons of the second molecule in close proximity. Replacing the *N*-methyl group by bulkier substituents such as isopropyl and *tert*-butyl would increase steric interaction with the acetyl protons. A second configuration, also of low energy, contains acetyl–acetyl and *N*-methyl–*N*-methyl interactions between the NMA monomers. Although further calculations would be needed to predict the preferred energy configurations of the NiPA and NtBA dimers, a possible result could be a lengthening of the hydrogen bond to reduce alkyl–alkyl group interactions. Many studies show a decrease of hydrogen bond energy as the bond length is increased.[11,18] Furthermore, Berkeley, and Hanna[19] have correlated hydrogen bond length with the quantity $(\nu_D - \nu_M)$ (which is discussed later), which supports the suggestion that the hydrogen bond energy is in the order NMA > NiPA > NtBA, while the hydrogen bond length is in the reverse order.

In a series of sixteen *N*-monosubstituted amides in CCl_4 solutions studied by infrared spectroscopy, steric factors were found to control the degree of association.[20] As the size of substituents on either the carbonyl carbon atom or on the nitrogen atom increased, the concentration ratio of associated molecules to monomers decreased. For 0.05 *M* solutions of NMA, NiPA, and NtBA, the values of this ratio at room temperature were found to be: 0.57 ± 0.10, 0.43 ± 0.10, and 0.23 ± 0.08, respectively.[20]

Chemical Shift of the Free Nitrogen Proton. The parameters ν_M and ν_D are not predetermined, but are obtained from the slope and intercept of the best straight line fit of eq 1. It was expected that ν_M, for a given amide, would be independent of temperature. Instead, as the temperature is raised, a value of ν_M to higher field is found (Table IV).

In hydrogen bonding studies of chloroform,[21] di-*tert*-butyl carbinol[22] and benzenethiol,[23,24] the chemical shift of the uncomplexed proton was experimentally determined and found to be nearly temperature independent. In extremely dilute solutions of water in CCl_4, however, where the self-association of water is negligible (below 1.5×10^{-3} mole fraction), ν_M for the water monomer is temperature dependent.[25] The variation is an upfield shift of 10.1 Hz (at 56.4 MHz) as the temperature is raised 59°. The error analysis[9] indicates that the most probable error in the intercept

(16) T. Higuchi, C. H. Barnstein, H. Ghassemi, and W. E. Perez, *Anal. Chem.*, **34**, 400 (1962).

(17) C. C. W. Chao, A. Veis, and F. Jacobs, *J. Amer. Chem. Soc.*, **89**, 2219 (1967).

(18) G. C. Pimentel and A. L. McClellan, "The Hydrogen Bond," W. H. Freeman, San Francisco, Calif., 1960, p 238.

(19) P. J. Berkeley, Jr., and M. W. Hanna, *J. Chem. Phys.*, **41**, 2530 (1964).

(20) R. L. Jones, *Spectrochim. Acta*, **22**, 1555 (1966).

(21) C. J. Creswell and A. L. Allred, *J. Phys. Chem.*, **66**, 1469 (1962).

(22) L. K. Patterson and R. M. Hammaker, *Spectrochim. Acta*, **23A**, 2333 (1967).

(23) R. Mathur, S. M. Wang, and N. C. Li, *J. Phys. Chem.*, **68**, 2140 (1964).

(24) R. Mathur, E. D. Becker, R. B. Bradley, and N. C. Li, *ibid.*, **67**, 2190 (1963).

(25) N. Muller and P. Simon, *ibid.*, **71**, 568 (1967).

(ν_D) is about ± 1 Hz and the most probable error in the slope ($\nu_M - \nu_D$) is about ± 2 Hz. Therefore, the observed variation in ν_M is outside of the estimated error range of ± 3 Hz. Furthermore, the trend of ν_M to appear to higher field with an increase of temperature precludes random error in the analysis. We have examined several reasons for this behavior. One is competition by another type of self-association possible in amides: dipole–dipole association. Although it has not been proved that *N*-monosubstituted amides self-associate in this manner in solution, there is experimental evidence that *N*,*N*-disubstituted amides do so.[26] The dipole moments of *N*-monosubstituted and *N*,*N*-disubstituted amides are similar and such asosciation is certainly possible. Theoretical calculations[11] indicate that such a dimer could be quite stable. Both types of dimers might exist in solution. To see whether or not this could cause the calculated value of ν_M to appear at higher magnetic field with an increase in temperature, one must examine a proposed structure for such a dimer. Molecular orbital calculations have been performed for an NMA "parallel plane dimer."[11] The most stable structure was found to be the one with the C–N bonds antiparallel and the C=O bonds aligned. This configuration places the nitrogen proton of each molecule in a plane above (or below) the plane containing the amide bond. Although the magnetic anisotropy of the amide bond is not precisely known, there is generally a deshielding effect in the plane of the amide molecule and a shielding effect above (or below) the plane.[27-29] We may tentatively assume that the nitrogen proton in the "parallel plane dimer" (define its chemical shift as ν_{pp}) would be shielded relative to the monomer NH proton. However, in the linear dimer (and also in the higher linear aggregates) proposed for NMA, the hydrogen-bonded proton is deshielded relative to the monomer NH proton. Since the equations in this study were developed[7] for linear structures only, it is possible that *if* the "parallel plane dimer" structure exists in solution for these amides, and *if* its concentration becomes more important at higher temperatures, the observed chemical shift of the NH proton would be shifted to higher field than it would be if only linear aggregates formed. Since the theory[7] provides for only two chemical shifts, ν_M and ν_D, the higher value for the observed chemical shift would be accounted for in the value determined for ν_M. (The quantity ν_D is determined when $\bar{Y}/Y \rightarrow 0$, which occurs at high amide concentrations. The concentration of a "parallel plane dimer" would be low at high amide concentrations because of the large value for $\bar{K}$ which promotes extended self-association. Therefore, the net result of a higher-field value for ν_{pp} would be to make the calculated value of ν_M appear to higher field than the true monomer chemical shift.) According to this explanation, the change in ν_M over the temperature range studied would be larger in NtBA and NiPA than in NMA because at a given temperature and concentration, there is more dissociation of the higher *n*-mers and therefore, perhaps, more of the parallel plane dimer in NtBA and NiPA.

Another attempt to explain the variation of the amide monomer chemical shift with temperature comes from a consideration of the known solvent effect of CCl_4. Nmr studies of the hydrogen-bonding equilibrium of NiPA in CCl_4 and cyclohexane (paper I) reveal quite different dilution curves in the two solvents: CCl_4 is considerably more efficient at breaking up the amide self-association. Schaefer, *et al.*, have noted that CCl_4 interacts with many molecules more strongly than does cyclohexane[30] and consequently affects the nmr chemical shift. The reaction field effect is too small to be responsible for the observed low-field shift[30] in CCl_4 relative to cyclohexane. Steric, charge, and shape effects in the solute molecules studied appear to be responsible for the low-field shifts.[30] Of these, the charge effect could influence the chemical shift of the NH proton in the amides. Schaefer, *et al.*,[30] suggest that CCl_4 molecules, with their highly polarizable CCl bonds, are regions of relatively high electron density and may be attracted to regions of relatively low electron density (in the amides, this would be the region of the NH bond). A net shift would occur only if the CCl_4 molecules were found near the NH bond of the amides more often than near the C–H bonds of the internal reference, TMS. The CCl_4 molecules would then remove more charge from the NH bond than from the CH bond of TMS and the result would be a low-field shift of the NH proton. If the amide were studied at only one temperature, this low-field shift would be quite small compared with the total hydrogen-bond shift. However, as the temperature is raised, the amount of time spent by the CCl_4 molecules in the vicinity of the amide NH bond would be reduced. The result would be a high-field shift of the NH proton as the temperature increases. This is exactly what was found in our determination of ν_M. Temperature effects upon this recently discovered solvent effect of CCl_4 have not yet been studied and this explanation must be regarded as speculative. At any rate, the charge effect does not appear to be large enough in itself to account for the total variation in ν_M. A steric solvent effect of CCl_4 has been previously proposed,[31] but this does not seem to apply to the amides.

(26) M. Rabinovitz and A. Pines, *J. Chem. Soc. B*, 1110 (1968).

(27) T. H. Siddall, III, and W. E. Stewart, *J. Mol. Spectrosc.*, **24**, 290 (1967).

(28) P. T. Narasimhan and M. T. Rogers, *J. Phys. Chem.*, **63**, 1388 (1959).

(29) D. L. Hooper and R. Kaiser, *Can. J. Chem.*, **43**, 2363 (1965).

(30) T. Schaefer, B. Richardson, and R. Schwenk, *ibid.*, **46**, 2775 (1968).

(31) D. H. Williams, J. Ronayne, and R. G. Wilson, *Chem. Commun.*, 1089 (1967).

Finally, the variation in ν_M with temperature could result from weak hydrogen bonding between the amide NH proton and CCl_4. In a study of hydrogen bonding and self-association in haloethanes and halomethanes[32] the self-association was disrupted by cyclohexane mainly through the dilution effect, while CCl_4 apparently was able to hydrogen bond to the solute through a chlorine atom. Since the nitrogen proton of an amide would be a better proton donor than the protons of haloethanes or halomethanes, weak hydrogen bonding to CCl_4 is a possibility. Then the calculated value of ν_M would represent not the free amide monomer, but the monomer weakly bound to a molecule of CCl_4 and would be to lower magnetic field than the value for the uncomplexed monomer. The variance of ν_M with temperature would be expected if it is the chemical shift of a hydrogen-bonded proton (as discussed in the next section).

Our measurements in very dilute solution are not extensive enough to enable us to decide among the several mechanisms offered to explain the temperature dependence of ν_M. However, for molecules in which it is not possible to extrapolate the chemical shift to infinite dilution experimentally, it does seem somewhat risky to assume that ν_M or $(\nu_D - \nu_M)$ is independent of temperature.

Chemical Shift of the Hydrogen-Bonded Nitrogen Proton. A variation in the chemical shift of the hydrogen-bonded protons with temperature was expected. The chemical shift of the intramolecularly hydrogen-bonded proton in 3,5-dichlorosalicylaldehyde in CCl_4 and in benzene-*d* solutions is temperature dependent with a temperature coefficient of 0.25 to 0.30 $\times 10^{-2}$ ppm/°C.[33] The chemical shift of the proton in the C=O···H—N hydrogen bond in the δ-valerolactam dimer in CCl_4 is also temperature dependent.[34] Muller and Reiter[35] attribute this dependence to an increase in the population of excited vibrational levels of the hydrogen-bond stretching mode with temperature. They calculate an upfield shift of 0.2 to 0.8 $\times 10^{-2}$ ppm per degree temperature rise depending upon various parameters used in the calculations. In the range 20 to 60°, we find a temperature coefficient (Table IV) for ν_D of 0.50, 0.83, and 0.95 $\times 10^{-2}$ ppm/°C for NMA, NiPA, and NtBA, respectively. In addition, Muller and Reiter find that the temperature coefficient increases as the dissociation energy of the hydrogen bond decreases.[35] This is precisely the order presented in Tables IV and V.

In many studies of hydrogen bonding, ν_M and ν_D are not found independently instead the quantity $(\nu_D - \nu_M)$, for a self-associated solute, or $(\nu_C - \nu_M)$, where ν_C is the frequency of the proton in a hydrogen-bonded complex, is reported. One might expect this quantity to correlate with the enthalpy of hydrogen bond formation, but conflicting results have been obtained. Kaiser[36] found that $(\nu_C - \nu_M)$ and the enthalpy increase monotonically in various chloroform-base complexes. In hydrogen-bonding studies of benzenethiol[24] the enthalpy decreases as $(\nu_C - \nu_M)$ increases. Other studies[37,38] show no definite correlation between hydrogen bonding chemical shifts and the enthalpies determined.

Berkeley and Hanna,[19,39,40] however, have theoretically and experimentally correlated $(\nu_C - \nu_M)$ with a number of properties for weak complexes of chloroform with nitrogen bases. A larger value of $(\nu_C - \nu_M)$ was found: (1) as the basicity of the base increased, (2) as the hydrogen bond length decreased, and (3) as the enthalpy of the hydrogen bond increased. Eyman and Drago[41] found good correlation between the observed nmr chemical shift of the phenol OH proton (δ_{obsd}) and the enthalpy of hydrogen-bond formation in a series of thirty bases in methylene chloride solvent. (The quantity δ_{obsd} is comparable to $(\nu_C - \nu_M)$ for reasons discussed by Eyman and Drago.[41,42])

In general, in cases where correlation of $(\nu_C - \nu_M)$ with some hydrogen-bond property was found, the proton donor was the same, and the proton acceptors did not differ greatly in their magnetic anisotropy, or else, corrections were made for differing anisotropies.[40,41]

One of the difficulties is that even if the anisotropy of the proton acceptor is accurately known, it may change upon hydrogen-bond formation. The reason for the good correlation of $(\nu_D - \nu_M)$ with enthalpy in this work may be due to the similar anisotropies of the three amides and to the similar solvent effects upon $(\nu_D - \nu_M)$ in CCl_4 solution. Because the quantities ν_M and ν_D both shift to high field with an increase in temperature (Table IV), the quantity $(\nu_D - \nu_M)$ shows little temperature dependence. Therefore, the five values obtained for each amide were simply averaged to compare with the enthalpy. Values for $(\nu_D - \nu_M)_{av}$ are 220 Hz for NMA, 180 Hz for NiPA, and 152 Hz for NtBA. The corresponding values of ΔH_{12} are: 3.7, 3.0, and 2.4 kcal/mol, respectively.

Experimental Values for the Enthalpy of Hydrogen-Bond Formation in NMA. Values for the enthalpies

(32) A. L. McClellan and S. W. Nicksic, *J. Phys. Chem.*, **69**, 446 (1965).

(33) T. Schaefer and G. Kotowycz, *Can. J. Chem.*, **46**, 2865 (1968).

(34) J. M. Purcell, H. Susi, and J. R. Cavanaugh, *ibid.*, **47**, 3655 (1969).

(35) N. Muller and R. C. Reiter, *J. Chem. Phys.*, **42**, 3265 (1965).

(36) R. Kaiser, *Can. J. Chem.*, **41**, 430 (1962).

(37) F. Takahashi and N. C. Li, *J. Phys. Chem.*, **69**, 1622 (1965).

(38) F. Takahashi and N. C. Li, *ibid.*, **69**, 2950 (1965).

(39) P. J. Berkeley, Jr., and M. W. Hanna, *ibid.*, **67**, 846 (1963).

(40) P. J. Berkeley, Jr., and M. W. Hanna, *J. Amer. Chem. Soc.*, **86**, 2990 (1964).

(41) D. P. Eyman and R. S. Drago, *ibid.*, **88**, 1617 (1966).

(42) Over a temperature range of 90°, ν_M for phenol in methylene chloride is assumed constant. This point might bear investigation, since phenol is capable of hydrogen bonding to methylene chloride as well as to itself.

of hydrogen-bond formation obtained for NMA in inert solvents are shown in Table VI. The thermodynamic parameters for NiPA and NtBA have not been previously determined.

Table VI: Enthalpies for Hydrogen Bonding by Self-Association of NMA in Inert Solvents[a]

Solvent	$-\Delta H_{12}$, kcal/mol	$-\Delta\bar{H}$, kcal/mol	Ref
CCl_4	4.2[b]		43
CCl_4	4.7		44
CCl_4	3.7	4.5	[d]
Benzene[c]	3.6	3.8	6

[a] A value recently quoted (ref 11) for the enthalpy of self-association of NMA as obtained from nmr studies (ref 38) is actually the enthalpy of formation of the *N,N*-dimethylacetamide–aniline complex measured in chloroform solution (ref 38). [b] See the text for the method of calculation of the enthalpy. [c] Two values of the enthalpy between 25 and 49° were averaged. [d] This work.

To analyze infrared data of the self-association of NMA in CCl_4, Klotz and Franzen[43] used two different equilibrium constants (similar to the method of Davies and Thomas[6] and that discussed in paper I); however, only K_{12} (their k_2) is given.[43] The enthalpy is not computed from the temperature dependence of k_2, but from α, the degree of association. The Klotz and Franzen value for the enthalpy (4.2 kcal/mol) falls between the values found in this work (3.7 and 4.5 kcal/mol for the dimerization and further self-association of NMA in CCl_4). The Bhaskar and Rao[44] value of 4.7 kcal/mol (Table VI) was based on an analysis of the infrared data assuming that only a monomer–dimer equilibrium exists.

Although benzene is no longer considered an inert solvent for many solutes, and has been shown to associate with amides,[45] it is included in Table VI because in these vapor pressure studies of NMA in benzene[6] $|\Delta H_{12}| < |\Delta\bar{H}|, |\Delta S_{12}| > |\Delta\bar{S}|$, and $\bar{K} > K_{12}$, the same order as found in this work for each of the amides studied.

Experimental Values for the Equilibrium Constants of Hydrogen-Bond Formation in NMA. Any experimental errors in the measurement of the chemical shift in very dilute solutions would affect the value of K_{12} more than that of $\bar{K}$. We know that the NH peak is sharper and can be measured more accurately in more concentrated solutions. Therefore, the value obtained for $\bar{K}$ is more reliable than the value obtained for K_{12}.

Table VII illustrates the range of values which have been obtained for the equilibrium constants for NMA in CCl_4 within the past 8 years. Two of the ir values for K_{12}[43,44] appear within the range of the values obtained from vapor pressure lowering experiments;[46] however, when one computes the enthalpies from these

Table VII: Equilibrium Constants for NMA in CCl_4

Method	T, °C	K_{12}[a]	$\bar{K}$[a]	Ref
vpl[b]	20	9.0	61.6	46
lve[c]	60	2.7	14.3	46
lve[c]	75	1.5	13.8	46
ir	25	4.7 (5.8)[d]		43
ir	26	5.4		44
ir[e]	20	1	45	47
nmr	20	1.5	24.0	*f*
nmr	60	0.7	9.8	*f*

[a] In l./mol. The values were converted from (mole fraction)$^{-1}$. [b] Vapor pressure lowering. [c] Liquid–vapor equilibrium method. [d] Two different methods of analysis were used. [e] Values extrapolated (ref 48) from ir studies at 25, 35, and 50° (ref 47). [f] This work.

equilibrium constants,[46] one finds: $\Delta H_{12} = 5.8$ and $\Delta\bar{H} = 7.1$ kcal/mol (using the 20° and 60° values) or $\Delta H_{12} = 9.2$ and $\Delta\bar{H} = 0.6$ kcal/mol (using the 60° and 75° values). Clearly then, obtaining equilibrium constants which seem reasonable can be misleading.

It will be interesting to examine recent ir studies[47] which evaluate both K_{12} and $\bar{K}$ at several temperatures. At this writing, this work was not available for further comparison.

As it becomes possible to study even more dilute solutions by nmr, the range will be reached where it is possible to extrapolate a plot of the experimental chemical shift *vs.* the concentration of amide to infinite dilution and obtain the value of ν_M. This will have the double advantage of removing one of the unknowns from the equations while enabling a more accurate determination of K_{12} to be made.

Acknowledgment. The authors wish to thank Lester Isbrandt for sample preparation and the staff of the Northern Illinois Computer Center for operation of the computer.

Appendix

At the time of publication of paper I the rate constants for hydrogen-bond formation in *N*-monosubstituted amides were not known. It was assumed, by comparison with other hydrogen-bonded dimers, that the rate was fast enough so that the observed chemical shift was a true weighted average of the frequencies of the monomer, dimer, and higher aggregates,

(43) I. M. Klotz and J. M. Franzen, *J. Amer. Chem. Soc.*, **84**, 3461 (1962).

(44) K. R. Bhaskar and C. N. R. Rao, *Biochim. Biophys. Acta*, **136**, 561 (1967).

(45) A. A. Sandoval and M. W. Hanna, *J. Phys. Chem.*, **70**, 1203 (1966).

(46) R. D. Grigsby, S. D. Christian, and H. E. Affsprung, *ibid.*, **72**, 2465 (1968).

(47) H. Lowenstein, H. Lassen, and A. Hvidt, *Acta Chem. Scand.*, **24**, 1687 (1970)

Table VIII: The Mean Degree of Association in CCl_4

X_{NMA}[a]	20°	30°	40°	50°	60°
0.1064	14.1	13.0	10.3	8.7	7.3
0.04072	6.9	6.3	5.1	4.2	3.6
0.02190	4.4	4.0	3.2	2.7	2.3
0.01530	3.3	3.1	2.5	2.1	1.8
0.01518	3.3	3.1	2.5	2.1	1.8
0.00998	2.5	2.3	1.9	1.6	1.4
0.00502	1.6	1.5	1.3	1.2	1.1
X_{NiPA}[a]					
0.1490	14.0	12.8		9.8	6.7
0.09898	10.2	9.3	7.9	7.1	4.9
0.08529	9.1	8.3	7.0	6.3	4.4
0.02906	4.0	3.7	3.1	2.8	2.0
0.02210		3.0	2.6	2.3	1.7
0.01539	2.5	2.3	2.0	1.8	1.4
0.00739	1.6	1.5	1.3	1.2	1.1
0.00500	1.3	1.2	1.1	1.1	
X_{NtBA}[a]					
0.1503	6.2	6.0	5.1	4.5	3.9
0.1247	5.4	5.1	4.4	3.9	3.4
0.07776	3.8	3.6	3.1	2.8	2.5
0.06514	3.4	3.2	2.8	2.4	2.2
0.05062	2.8	2.7	2.4	2.1	1.9
0.03592	2.3	2.1	1.9	1.7	1.6
0.02354	1.8	1.6	1.5	1.4	1.3
0.01502	1.4	1.3	1.3	1.2	1.1
0.00996	1.2	1.1	1.1	1.1	1.1

[a] Mole fraction of amide.

Table IX: The Value of m[a]

X_{NMA}[b]	20°	30°	40°	50°	60°
0.1064	40	38	30	25	22
0.04072	21	19	15	12	10
0.02190	13	12	9	7	6
0.01530	10	9	7	5	4
0.01518	10	9	6	5	4
0.00998	6	6	4	2	2
0.00502	3	2	2	1	1
X_{NiPA}[b]					
0.1490	40	37		29	19
0.09898	30	28	23	21	14
0.08529	27	25	21	19	13
0.02906	12	11	9	8	5
0.02210		8	7	6	4
0.01539	7	6	5	4	2
0.00739	2	2	2	1	1
0.00500	1	1	1	1	
X_{NtBA}[b]					
0.1503	17	17	14	12	11
0.1247	15	15	12	11	9
0.07776	11	10	8	7	6
0.06514	9	9	7	6	5
0.05062	8	7	6	5	4
0.03592	6	5	4	4	3
0.02354	4	3	3	2	2
0.01502	2	2	2	1	1
0.00996	2	1	1	1	1

[a] Less than 10% of the hydrogen-bonded polymers contain more than m monomer units. [b] Mole fraction of amide.

leading to eq 29 in paper I and ultimately to eq 1 in this work. Now these constants have been measured by ultrasonic absorption methods[48] and for NMA in CCl_4, using $K_{12} = 1$ l./mol and $\bar{K} = 45$ l./mol, the rate constants for dimerization and for association of the n-mer are 3.8×10^7 and 1.7×10^9 $(\text{mol/l.})^{-1}$ sec^{-1}. For the dissociation of the n-mer, the rate constant is 3.8×10^7 sec^{-1}. These rapid rates ensure that δ_0 is a true weighted average of all free and hydrogen-bonded protons.

In order to gain a better understanding of the degree of association experienced by the amides in CCl_4 solution, two quantities were calculated as a function of concentration and temperature: (1) the weight average molecular weight and (2) the value of m, where less than 10% of the hydrogen-bonded aggregates contain more than m units. The weight average molecular weight (M_W) can be related to $\bar{Y}$ and Y in eq 1, where

$$\bar{Y} + Y_1 + Y_2 + Y_3 + \ldots Y_n$$

and

$$Y = Y_1 + 2Y_2 + 3Y_3 + \ldots nY_n$$

The effective mole fraction of n-mer is defined by Y_n. Then

$$M_W = \frac{Y_1M_1 + Y_2M_2 + Y_3M_3 + \ldots Y_nM_n}{Y_1 + Y_2 + Y_3 + \ldots Y_n}$$

$$= \frac{M_1(Y_1 + 2Y_2 + 3Y_3 + \ldots nY_n)}{\bar{Y}}$$

$$= M_1\left(\frac{Y}{\bar{Y}}\right) = M_1 f$$

where M_1 is the molecular weight of the monomer and f is the mean degree of association.[49] Table VIII gives the value of f for each of the amides studied. Table IX gives the value of m.

(48) J. Rassing and F. Garland, submitted for publication in *Acta Chem. Scand.*

(49) M. Davies and D. K. Thomas, *J. Phys. Chem.*, **60**, 763 (1956).

Chain Association Equilibria. A Nuclear Magnetic Resonance Study of the Hydrogen Bonding of *N*-Monosubstituted Amides. III. In Dioxane[1,2]

by Laurine L. Graham* and Chang Y. Chang

Department of Chemistry, Northern Illinois University, DeKalb, Illinois 60115 *(Received August 26, 1970)*

Publication costs assisted by Northern Illinois University

Equilibrium constants for self-association through hydrogen bonding have been determined by nuclear magnetic spectroscopy for three *N*-monosubstituted amides in dioxane solution at five temperatures in the range 20 to 60°. The free energy and enthalpy changes for association decrease in the order: *N*-methylacetamide > *N*-isopropylacetamide > *N*-*tert*-butylacetamide. The measured equilibrium constants and enthalpies are much smaller in dioxane than in carbon tetrachloride. The low values for the enthalpies are interpreted as measuring the difference in energy between forming an amide–amide hydrogen bond and breaking an amide–dioxane hydrogen bond.

Introduction

A number of solvent pairs have been used to change protein conformations.[3] A common component of such solvent mixtures is dioxane, which is capable of hydrogen bonding to the nitrogen proton in the peptide bond through the lone pair electrons on the oxygen atom. In order to study this interaction in more detail, model amides were chosen to represent the peptide bond. The free energy, enthalpy, and entropy of hydrogen bond formation of these amides with dioxane was determined. It is hoped that the present study will enable the complex contributions to protein conformations to be better understood.

A method of computer analysis of the equilibrium constants for self-associated species from nmr chemical shift data has been developed and applied to two special cases: (a) the inert solvent, and (b) the hydrogen bonding solvent.[4] Paper II in this series[5] treats the self-association of *N*-methylacetamide (NMA), *N*-isopropylacetamide (NiPA), and *N*-*tert*-butylacetamide (NtBA) in carbon tetrachloride. In this work, the equilibrium constants for these amides are determined in a hydrogen bonding solvent, namely, a solvent which is capable of disrupting amide–amide hydrogen bonds by competing for one of the hydrogen-bonding sites of the amide molecule. Either a proton donor or a proton acceptor fulfills the solvent requirements for this method of analysis, since the former hydrogen-bonds to the carbonyl oxygen atom while the latter bonds to the nitrogen proton. The solvent must not self-associate.

The competitive solvent chosen was 1,4-dioxane for several reasons: (a) its zero dipole moment and low dielectric constant, (b) the closeness of the dielectric constants of dioxane and carbon tetrachloride (for comparison with the results of paper II), (c) the presence of only one proton resonance signal, well removed from the amide nitrogen proton resonance, (d) the negligible self-association of dioxane, and (e) the known proton-accepting capacity of dioxane.

The equilibria may be represented by eq 1 and 2.

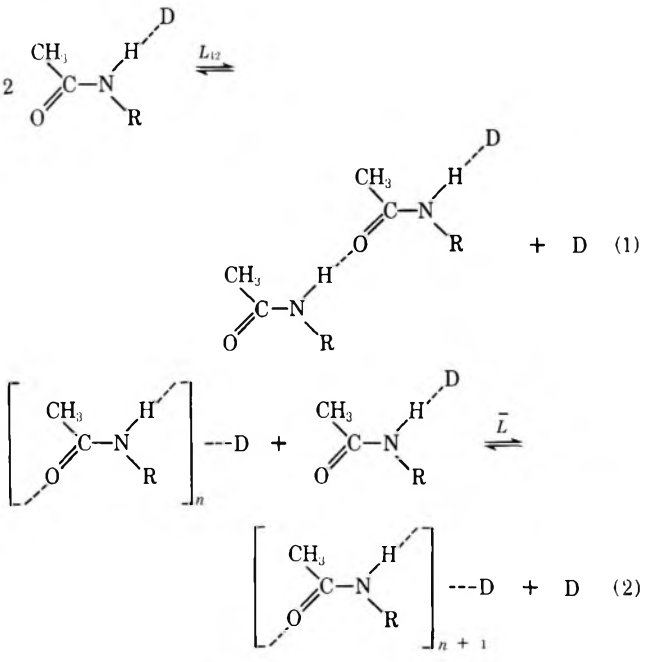

(1)

(2)

where R = CH_3– (NMA), $(CH_3)_2CH$– (NiPA), or $(CH_3)_3C$– (NtBA); $n \geq 2$ and D is dioxane bonding through the oxygen lone pair electrons.

(1) This work was supported by a grant from the Academic Dean's Fund of Northern Illinois University.

(2) This work is taken in part from the dissertation of C. Y. C. submitted in partial fulfillment of the requirements for the M.S. degree, Northern Illinois University, 1970.

(3) S. J. Singer, *Advan. Protein Chem.*, **17**, 1 (1962).

(4) L. A. LaPlanche, H. B. Thompson, and M. T. Rogers, *J. Phys. Chem.*, **69**, 1482 (1965). Referred to as Paper I.

(5) L. L. Graham and C. Y. Chang, *J. Phys. Chem.*, **75**, 776 (1971).

The use of two different constants, L_{12} and $\bar{L}$, to describe the equilibria has been discussed in paper II. It is assumed that all amide NH protons, either in the monomer or on the ends of self-associated amide n-mers, are hydrogen bonded to a molecule of dioxane. Thus one must ensure that the effective mole fraction of dioxane is larger than the sum of the effective mole fractions of each amide species. In addition, the equilibrium constant for the reaction: amide + dioxane $\rightleftharpoons$ amide···dioxane, must be large. This is the condition expressed in eq 38 of paper I, $K_S S \gg 1$, where S is the effective solvent mole fraction. Ethers are known to hydrogen bond strongly to NMA.[6] Dioxane, which is a stronger proton acceptor than tetrahydrofuran or ethyl ether,[7] has been complexed with various secondary amines. The equilibrium constants (in mf units) are large.[7] The computer-calculated value of S is between 0.82 and 0.99 for each of the solutions in this work. Therefore, it is likely that $K_S S \gg 1$ for each of the amides in dioxane.

Equation 3 (eq 52 in paper I) relates the observed chemical shift of the amide nitrogen proton, δ_0, to ν_C,

$$\delta_0 = \frac{\bar{Z}}{Z}(\nu_C - \nu_D) + \nu_D \qquad (3)$$

the chemical shift of all NH protons which are hydrogen bonded to dioxane; to ν_D, the chemical shift of all NH protons involved in amide–amide type hydrogen bonds; to $\bar{Z}$, the effective mole fraction of solvated amide n-mers ($\bar{Z} = Z_1 + Z_2 + Z_3 + \ldots + Z_n$, where Z_1 is the amide monomer bonded to dioxane, Z_2 is the amide dimer bonded to dioxane, etc.); and to Z, (where $Z = Z_1 + 2Z_2 + 3Z_3 + \ldots + nZ_n$). The values of $\bar{Z}$ and Z depend upon the equilibrium constants.[4] Estimates of L_{12} and $\bar{L}$ are fed into the computer and varied. The values of L_{12} and $\bar{L}$ which give the smallest value for the sum of the squares of the deviations in the least-squares fit of eq 3 to a straight line are assumed to be the best set of equilibrium constants. The values of ν_C and ν_D are found from the slope and intercept.

Experimental Section

Amide purification has been described.[4] Dioxane was dried over sodium, fractionally distilled, then kept in a dark bottle in a desiccator. Solutions were prepared in a Glove Bag (I^2R Co.) and run exactly as described in paper II. The ^{14}N spin decoupler and the time averaging computer were even more useful for measuring δ_0 in the dioxane solutions than in the CCl_4 solutions, due to a greater line width of the amide nitrogen proton in dioxane. In one extreme example, a 0.0948 mole fraction NMA–dioxane solution, the line width at half-maximum intensity of the NH proton was reduced from 0.67 to 0.28 ppm through the use of the ^{14}N spin decoupler (NMR Specialties, Inc.).

Results

Tables I–III contain the chemical shifts of the nitrogen proton in NMA, NiPA, and NtBA, respectively, as a function of temperature and concentration in dioxane. These values were put into the computer program already described and the results are shown in Table IV.

Table I: Concentration and Temperature Dependence of the Observed Chemical Shift[a] of the Nitrogen Proton in NMA–Dioxane Solutions

X^b	δ_0(20°)	δ_0(30°)	δ_0(40°)	δ_0(50°)	δ_0(60°)
0.4043	474	470	464	459	453
0.2524	460.5	456	449.5	445	438.5
0.1821	451.5	446	440	435	428.5
0.1299	440.5	436	429.5	424	417.5
0.09480	431	426	419.5	414.5	408.5
0.06471	419.5	416	409	404	399
0.03690	405	401	396	392	386
0.01734	393	390	384	381	374
0.01099	391	389	382	379	373
0.00601	389	386	381	378	372

[a] In hertz from internal TMS at 60 MHz. [b] Mole fraction of amide.

Table II: Concentration and Temperature Dependence of the Observed Chemical Shift[a] of the Nitrogen Proton in NiPA–Dioxane Solutions

X^b	δ_0(20°)	δ_0(30°)	δ_0(40°)	δ_0(50°)	δ_0(60°)
0.3220	459.5	455.5	450.3	445	438
0.1757	441	436.5	430	424.5	417
0.1588	438	433.5	427	421.5	414
0.05346	404.5	401	394	389.5	384
0.04159	399	395	389	384.5	379
0.01707	387	383	377	375	370
0.00815	382	380	373	370	367
0.00594	380	377	371	368	364

[a] In hertz from internal TMS at 60 MHz. [b] Mole fraction of amide.

The chemical shift of the NH proton hydrogen bonded to dioxane, ν_C, and to another amide molecule, ν_D, are given by the slope and intercept of the least-squares treatment of eq 3. The thermodynamic parameters shown in Table V were determined from a least-squares plot of ln K_{12} (or ln $\bar{K}$) *vs.* $1/RT$. The errors given are the most probable errors in the slope and intercept of a straight line.[8]

(6) S. Mizushima, M. Tsuboi, T. Shimanouchi, and Y. Tsuda, *Spectrochim. Acta*, **7**, 100 (1955).

(7) A. B. Sannigrahi and A. K. Chandra, *J. Phys. Chem.*, **67**, 1106 (1963).

(8) H. Margenau and G. M. Murphy, "The Mathematics of Physics and Chemistry," 2nd ed, D. Van Nostrand Co., Inc., New York, N. Y., 1959, p 519.

Table III: Concentration and Temperature Dependence of the Observed Chemical Shift[a] of the Nitrogen Proton in NtBA–Dioxane Solutions

X^b	δ_0(20°)	δ_0(30°)	δ_0(40°)	δ_0(50°)	δ_0(60°)
0.1363	412	406	400	393.5	387.5
0.09482	402.5	397	391	385	379
0.07451	396.5	391	385	380	374
0.05413	389.5	385	379	374.5	369
0.03125	381	376	371	367	361.5
0.01824	375	372	367	364	358
0.01123	373	369	364	360	355
0.00627	372	367	363	359	353
0.00443	371	366	362	357	351

[a] In hertz from internal TMS at 60 MHz. [b] Mole fraction of amide.

Table IV: Values of the Equilibrium Constants[a] and Chemical Shifts[b] for the Amides in Dioxane Solution

T, °C	L_{12}, (mf)$^{-1}$	L, (mf)$^{-1}$	ν_C	ν_D
		NMA		
20	4.3	11.8	385	499
30	3.9	10.6	383	497
40	3.8	10.2	377	491
50	3.6	9.5	374	487
60	3.4	9.3	369	481
		NiPA		
20	3.7	8.4	377	503
30	3.5	8.0	375	499
40	3.4	7.6	369	496
50	3.3	7.2	366	491
60	3.1	7.0	362	481
		NtBA		
20	3.2	4.8	369	500
30	3.0	4.6	365	495
40	2.9	4.5	360	486
50	2.8	4.2	357	478
60	2.8	4.1	351	473

[a] The estimated error is ±0.05 (mole fraction)$^{-1}$. [b] In hertz from internal TMS at 60 MHz. The NH proton is hydrogen bonded to dioxane (ν_C) or to another amide (ν_D). [c] mf = mole fraction.

Discussion

According to eq 1 and 2, the measured enthalpy is the difference between the enthalpy of formation of an amide–amide hydrogen bond and the enthalpy of dissociation of an amide–dioxane bond. It is, therefore, not surprising that the enthalpies are much smaller than those measured for the same amides in CCl_4.[5] The smaller enthalpies measured in hydrogen-bonding solvents such as dioxane are often said to denote weaker or less stabile hydrogen bonds.[3] While such a solvent could certainly be a destabilizing force to a given protein conformation, we feel that the hydrogen bond itself is not necessarily weaker; however, the degree of —N—H···O=C association in that solvent may be reduced considerably.

The Monomer–Dimer Equilibrium Compared with the n-mer Equilibria. Although there is a trend for $|\Delta\bar{H}|$ to be larger than $|\Delta H_{12}|$ (Table V) in each of the amides, as was found in CCl_4, the difference is only about 0.1 kcal/mol. It would be possible for the interamide hydrogen bonds to be about 1 kcal/mol stronger in the higher aggregates than in the dimers[9] (as they are in CCl_4); however, the bond to dioxane may also be stronger in the higher aggregate, and thus the difference may largely cancel.

Measuring the constants for the amide–dioxane equilibria is theoretically possible (see The General Case, paper I); however, four equilibrium constants and three chemical shifts would have to be extracted from the δ_0 *vs.* concentration data. Many more solutions would have to be studied to justify the use of seven independent parameters. In addition, the results of this work indicate that higher temperatures would be needed to observe amide–dioxane dissociation. For each of the amides, $|\Delta\bar{G}| > |\Delta G_{12}|$ (Table V) and thus the higher aggregates form more easily than the dimer. However, the difference between ΔG_{12} and $\Delta\bar{G}$ is not as large in dioxane as in CCl_4 and the degree of association beyond the dimer is therefore much higher in CCl_4.[5] The difference between $\Delta\bar{H}$ and ΔH_{12} is only 0.1 kcal/mol and therefore both $\Delta\bar{S}$ and ΔS_{12} have a significant effect in determining the values of ΔG_{12} and $\Delta\bar{G}$. To predict *a priori* the relative magnitudes of $\Delta\bar{S}$ and ΔS_{12} for the equilibria in eq 1 and 2 is difficult. The loss in entropy which occurs when a monomer hydrogen bonds to an n-mer could balance the gain in entropy by the freed dioxane molecule leading to a near-zero value for both $\Delta\bar{S}$ and ΔS_{12}.[10] The experimental results (Table V) show small positive values for $\Delta\bar{S}$ in NMA and NiPA and small negative values for ΔS_{12}. In NtBA, both quantities are positive, with $\Delta\bar{S} > \Delta S_{12}$. In each of the amides, then, a more favorable entropy change occurs during the formation of n-mers, where $n > 2$. Apparently, in dioxane as well as in CCl_4, the loss in entropy when a monomer hydrogen bonds to an n-mer (eq 2) is not as great as when two monomers form a dimer (eq 1). For the equilibria represented by eq 2, a net positive change in entropy is possible when the entropy gain by the freed dioxane molecule is larger than the loss in entropy of the amide monomer.

Varying the Nitrogen Alkyl Substituent. The relative effectiveness of dioxane in breaking amide–amide hydrogen bonds can be seen most clearly from a plot[11] of

(9) A dimer is an aggregate of two amide molecules and one dioxane molecule.

(10) N. Davies and D. K. Thomas, *J. Phys. Chem.*, **60**, 767 (1956).

(11) C. Y. Chang, M.S. Thesis, Northern Illinois University, DeKalb, Ill., 1970.

Table V: Thermodynamic Parameters[a] for the Hydrogen Bonding of NMA, NiPA, and NtBA in Dioxane Solution

	$-\Delta H_{12}$, kcal/mol	$-\Delta\bar{H}$, kcal/mol	ΔS_{12},[b] eu/mol	$\Delta\bar{S}$,[b] eu/mol	ΔG_{12},[c] kcal/mol	$\Delta\bar{G}$,[c] kcal/mol
NMA	1.07 ± 0.07	1.14 ± 0.09	−0.8 ± 0.3	1.0 ± 0.4	−0.85 ± 0.01	−1.44 ± 0.01
NiPA	0.80 ± 0.05	0.91 ± 0.03	−0.1 ± 0.2	1.1 ± 0.2	−0.76 ± 0.01	−1.24 ± 0.01
NtBA	0.66 ± 0.07	0.79 ± 0.05	0.1 ± 0.3	0.4 ± 0.2	−0.68 ± 0.01	−0.91 ± 0.01

[a] The free energy and entropy changes were calculated from L_{12} and $\bar{L}$ in mole fraction units. [b] Independent of temperature between 20 and 60°. [c] The value at 20° is given.

δ_0 *vs.* concentration for each of the three amides (values in Tables I–III). The plots resemble the plots for NMA, NiPA, and NtBA in chloroform solution (Figure 2 in paper I), except that in dioxane extrapolation to ν_C at infinite dilution is possible graphically as well as by computer calculation (the same results are obtained). The equilibrium constants found for NMA, NiPA, and NtBA in chloroform at 35° (L_{12} = 13.0, 4.5, 3.0 (mole fraction)$^{-1}$, and $\bar{L}$ = 14.0, 8.0, 4.0 (mole fraction)$^{-1}$, respectively)[4] are of the same order of magnitude as those found in dioxane solution (Table IV) indicating that chloroform, which competes for the carbonyl oxygen atom site of the amide for hydrogen bonding, and dioxane, which competes for the nitrogen proton site, are approximately equally effective in disrupting interamide hydrogen bonds. In both dioxane and chloroform, as well as in CCl_4,[5] the equilibrium constants for amide self-association decrease from NMA to NiPA to NtBA.

The net enthalpies of hydrogen bond formation (Table V) decrease in the order: NMA > NiPA > NtBA in dioxane as well as in CCl_4 solution.[5]

The effect of varying the nitrogen substituent upon ΔS_{12} or $\Delta\bar{S}$ does not appear to be significant. For NiPA and NtBA, ΔS_{12} is near zero; thus the gain in entropy by the freed dioxane molecule is nearly equal to the loss in entropy when the amide molecule joins an amide–dioxane complex to form a dimer (eq 1).

The Chemical Shift of the Amide Nitrogen Proton. Both ν_C, the chemical shift of the amide nitrogen proton hydrogen bonded to dioxane, and ν_D, the chemical shift of the amide proton hydrogen bonded to another amide molecule, are found to be temperature dependent (Table IV). A theory for temperature-dependent hydrogen bond chemical shifts has been proposed by Muller and Reiter[12] and application of the theory to the chemical shifts of amide hydrogen bonds has been discussed in paper II.

The temperature coefficients for ν_D in dioxane solution are very similar to those for ν_D in CCl_4.[5] In dioxane, the values are: NMA, 0.75 × 10^{-2}; NiPA, 0.91 × 10^{-2}; and NtBA, 1.1 × 10^{-2} ppm/°C. The temperature coefficients for ν_C are: NMA, 0.65 × 10^{-2}; NiPA, 0.63 × 10^{-2}; and NtBA, 0.73 × 10^{-2} ppm/°C.

The correlation of ($\nu_D - \nu_M$) with the enthalpy of the hydrogen bond was discussed in paper II. The quantity ($\nu_D - \nu_C$), which is obtained directly from the slope of eq 3, is temperature independent and is almost the same for each amide (Table IV). Averaged over the five temperatures, ($\nu_D - \nu_C$) is equal to 113 Hz for NMA, 124 Hz for NiPA, and 126 Hz for NtBA. If the chemical shift differences are related to hydrogen bond enthalpies, ($\nu_D - \nu_C$) in this study would represent the difference in energy between an amide–amide hydrogen bond and an amide–dioxane bond, after correcting the chemical shifts for anisotropy effects. The ν_D value would have to be corrected for the diamagnetic anisotropy of the carbonyl oxygen atom (estimated as 1.1 ppm in an amide hydrogen bond[13]), and the ν_C value would have to be corrected for the anisotropy of the dioxane oxygen atom. The similarity of the ($\nu_D - \nu_C$) values for the three amides may mean that the effect of changing the nitrogen alkyl substituent on the enthalpy of the amide–amide bond is similar to the effect on the energy of the amide–dioxane bond: (a decrease of about 0.3 kcal/mol from NMA to NiPA; a further decrease of about 0.1 kcal/mol from NiPA to NtBA.)

Values for the Thermodynamic Parameters of Hydrogen-Bond Formation of Amides in Dioxane. Although polypeptides are frequently studied in dioxane solvent mixtures, very few determinations of the thermodynamics of hydrogen bonding have been made for model peptides in dioxane. Using infrared, Klotz found a dimerization equilibrium constant of 0.58 l./mol [9.4 (mole fraction)$^{-1}$] at 25° for NMA in dioxane and an enthalpy of −0.8 kcal/mol.[14] The equilibrium constant is of the same order of magnitude as L_{12} and the enthalpy is in good agreement with that obtained in this work. An amide which forms cyclic dimers, δ-valerolactam, was also studied in dioxane solution in the infrared, and Susi found L_{12} = 4 (mole fraction)$^{-1}$ at 25° and an enthalpy of 0 ± 0.5 kcal/mol.[15] Susi explains the near-zero value of the enthalpy as representing the net enthalpy change of breaking two monomer–dioxane hydrogen bonds and then forming the two amide bonds in the cyclic dimer.

(12) N. Muller and R. C. Reiter, *J. Chem. Phys.*, **42**, 3265 (1965).

(13) D. P. Eyman and R. S. Drago, *J. Amer. Chem. Soc.*, **88**, 1617 (1966).

(14) I. M. Klotz and J. M. Franzen, *ibid.*, **84**, 3461 (1962).

(15) H. Susi and J. S. Ard, *Arch. Biochem. Biophys.*, **117**, 147 (1966).

Table VI: The Mean Degree of Association in Dioxane

	20°	30°	40°	50°	60°
X_{NMA}[a]					
0.4043	4.4	4.2	4.1	3.9	3.9
0.2524	3.0	2.8	2.8	2.7	2.7
0.1821	2.4	2.3	2.2	2.2	2.1
0.1299	2.0	1.9	1.8	1.8	1.8
0.09480	1.7	1.6	1.6	1.5	1.5
0.06471	1.4	1.4	1.4	1.3	1.3
0.03690	1.2	1.2	1.2	1.2	1.2
0.01734	1.1	1.1	1.1	1.1	1.1
0.01099	1.1	1.0	1.0	1.0	1.0
0.00601	1.0	1.0	1.0	1.0	1.0
X_{NiPA}[a]					
0.3220	3.0	3.0	2.9	2.8	2.8
0.1757	2.0	2.0	1.9	1.9	1.9
0.1588	1.9	1.9	1.8	1.8	1.8
0.05346	1.3	1.2	1.2	1.2	1.2
0.04159	1.2	1.2	1.2	1.2	1.2
0.01707	1.1	1.1	1.1	1.1	1.1
0.00815	1.0	1.0	1.0	1.0	1.0
0.00594	1.0	1.0	1.0	1.0	1.0
X_{NtBA}[a]					
0.1363	1.5	1.5	1.5	1.4	1.4
0.09482	1.3	1.3	1.3	1.3	1.3
0.07451	1.3	1.2	1.2	1.2	1.2
0.05413	1.2	1.2	1.2	1.2	1.2
0.03125	1.1	1.1	1.1	1.1	1.1
0.01824	1.1	1.1	1.1	1.1	1.1
0.01123	1.0	1.0	1.0	1.0	1.0
0.00627	1.0	1.0	1.0	1.0	1.0
0.00443	1.0	1.0	1.0	1.0	1.0

[a] Mole fraction of amide.

From measurements of ultrasonic attentuation, Hammes and Spivey[16] were able to study the kinetics of the cyclic dimerization of 2-pyridone. From the activation energy, the enthalpy was obtained. (Two hydrogen bonds are formed in a cyclic dimer.) In dioxane, ΔH is -1.7 kcal/mol, and in a 50 wt % CCl_4–dioxane solution, ΔH is estimated to be -4.6 kcal/mol. Although not directly comparable, the lowering of the measured enthalpy as the dioxane content of the solvent is increased parallels the results of these studies (paper II *vs.* III). An interesting result of the kinetic studies is that the dissociation rate constant for the dimer is very solvent sensitive. At 13°, it increases by a factor of about 200 as the solvent is changed from benzene to dioxane. This supports the idea that the mechanism of dioxane interaction with the peptide bond is through competition for the hydrogen bonds.

Acknowledgment. The authors wish to thank the staff of the Northern Illinois Computer Center for operation of the computer.

Appendix

The mean degree of association, f, for the three amides is given in Table VI as a function of temperature and concentration in dioxane. The weight average molecular weight, M_W, is equal to $M_1 f$, where M_1 is the molecular weight of the monomer and $f = Z/\bar{Z}$. The quantities Z and $\bar{Z}$ are defined in the text.

(16) G. G. Hammes and H. O. Spivey, *J. Amer. Chem. Soc.*, **88**, 1621 (1966).

Inelastic Light Scattering from Log Normal Distributions of Spherical Particles in Liquid Suspension

by Douglas S. Thompson

Engineering Physics Laboratory, Engineering Research Division, E. I. du Pont de Nemours & Company, Inc., Wilmington, Delaware 19898 *(Received October 12, 1970)*

Publication costs assisted by E. I. du Pont de Nemours & Company, Inc.

A theoretical expression for the inelastic light scattering spectrum arising from a polydisperse suspension of spherical, colloidal particles described by a log normal size distribution is presented. A simple graphical method for characterizing, by inelastic light scattering, a particulate suspension according to its average size and standard deviation (log normal parameters) is developed. The utility of the method is demonstrated by experimental characterization of a polytetrafluoroethylene dispersion.

Inelastic light scattering spectroscopy has been used to characterize the particle sizes of a variety of monodisperse colloidal suspensions.[1-3] However, its potential to characterize colloidal particulates with wide distributions of size has not been exploited to date. Such broad-distribution particulates are commonly encountered in emulsion polymerization, in colloidal precipitation reactions, and in dispersions attained by comminution. Previously, we have discussed a mathematical model that can be used to interpret inelastic light scattering spectra arising from polydisperse suspensions.[4] The present paper presents a scheme for reducing the general methods outlined in the previous paper to practical use.

Since the size distribution of many particulates of commercial importance is well described by the so-called log normal distribution function,[5] we shall use it to illustrate the method. The use of other size distributions simply requires a revision of some of the numerical computations. A graphical scheme to facilitate characterization of suspensions by two parameters, the average size and the standard deviation, is presented. This scheme has been tested by using inelastic light scattering spectra to obtain the geometric average size and standard deviation (the two parameters that completely characterize the log normal distribution) for dispersions of polytetrafluoroethylene (PTFE) in water.

When monochromatic light, at frequency ω_0, is scattered from a suspension of spherical, colloidal particles, the optical spectral density $I(\mathbf{K}, \omega - \omega_0)$ is broadened in frequency by the translational diffusive motion of the scattering particles. If the suspension is monodisperse and the scattering is monitored at an angle θ from the projected incident beam, the spectral density may be presented by the following Lorentzian function of $\Delta\omega = (\omega - \omega_0)$.[6,7]

$$I(\mathbf{K},\Delta\omega) = \frac{\Phi}{\pi}\left[\frac{K^2D}{(K^2D)^2 + (\Delta\omega)^2}\right] \qquad (1)$$

where the vector $\mathbf{K}$ is the difference between the propagation vectors of the incident and the scattered light and depends on both the wavelength of light in the medium and the scattering angle θ.

$$|\mathbf{K}| = \frac{4\pi}{\lambda}\sin\left(\frac{\theta}{2}\right) \qquad (2)$$

The kinetic diffusion coefficient D is related to the radius a of the spherical particles and the viscosity of the suspending liquid by the Stokes–Einstein relation[8]

$$D = \frac{k_B T}{6\pi\eta a} \qquad (3)$$

The effects of particle size are manifested through intraparticle interference as well as through D. These interference effects are taken into account by the function Φ. Intraparticle interference does not influence the *shape* of the spectral density and is not important for interpreting the spectra of monodisperse suspensions, but it does affect relative intensities and plays an important role in the development of mathematical expressions to represent the spectral density of scattering from polydisperse suspensions. The function Φ, for spherical, colloidal particles, can be obtained simply by using the methods of Rayleigh and Gans,[9] if: (1) the particles

(1) H. Z. Cummins, N. Knable, and Y. Yeh, *Phys. Rev. Lett.*, **12**, 150 (1964).

(2) S. B. Dubin, J. H. Lunacek, and G. B. Benedek, *Proc. Nat. Acad. Sci., U. S.*, **57**, 1164 (1967).

(3) F. T. Arecchi, M. Giglio, and U. Tartari, *Phys. Rev.*, **163**, 186 (1967).

(4) D. S. Thompson, *J. Chem. Phys.*, in press.

(5) G. Herdan, "Small Particle Statistics," 2nd rev ed, Butterworths, London, 1960.

(6) L. I. Komarov and I. Z. Fisher, *Zh. Eksp. Teor. Fiz.*, **43**, 1927 (1962); *Sov. Phys. JETP*, **16**, 1358 (1963).

(7) R. Pecora, *J. Chem. Phys.*, **40**, 1604 (1964).

(8) A. Einstein, "Investigations on the Theory of Brownian Movement," R. Fürth, Ed., Dover Publications, New York, N. Y., 1956.

(9) H. C. Van de Hulst, "Light Scattering by Small Particles," Wiley, New York, N. Y., 1957.

are not large compared with the wavelength of light, and (2) the ratio $\tilde{m}$ of the refractive index of the particles to that of surrounding medium is near unity. The result is

$$\Phi = \frac{n(\tilde{m} - 1)^2(\sin u - u \cos u)^2}{16R^2\kappa^2\left[\sin\left(\frac{\theta}{2}\right)\right]^6} \quad (4)$$

where

$$\kappa = \frac{2\pi}{\lambda} \quad (5)$$

and

$$u = 2\kappa a \sin\left(\frac{\theta}{2}\right) \quad (6)$$

R is the distance from the scattering center to the point of observation, and n is the number density of particles. Similar results have been obtained for scattering from polydisperse Gaussian polymer coils and rigid rods.[10,11]

If we take an heuristic approach to the problem of describing the spectral density of light scattered from a polydisperse suspension of spherical, colloidal particles, we consider the suspension to contain a very large number of particles and subdivide it into N classes of particulate species, each class being described by a particular radius a_i. If we let $f(a_i)$ be the number fraction of particles in a particular class with radius a_i, we may write the following expression for the homodyne spectral density of scattered light.[4]

$$S(\omega) = \left\{\left[\sum_{i=1}^{N}\sum_{j=1}^{N}\frac{\Omega_{ij}(\Gamma_i + \Gamma_j)}{(\Gamma_i + \Gamma_j)^2 + \omega^2}\right] \times \left[\sum_{i=1}^{N}\sum_{j=1}^{N}\Omega_{ij}\right]^{-1}\right\} \quad (7)$$

where

$$\Omega_{ij} = f(a_i)f(a_j)[(\sin u_i - u_i \cos u_i) \times (\sin u_j - u_j \cos u_j)]^2 \quad (8)$$

and

$$\Gamma_i = \mathbf{K}^2 D_i \quad (9)$$

The parameters D_i and u_i are obtained from eq 3 and 6 with a replaced by a_i. Equation 7 represents the homodyne spectral density from a polydisperse suspension of spherical, colloidal particles with a general size distribution function $f(a)$. At this point, we shall specialize the discussion to a specific form of the size distribution; namely, the log normal distribution.

The log normal distribution is commonly used to describe size distribution of particulates. This distribution fits the experimentally determined distribution of many particulate systems quite well and has several mathematical properties that make it especially attractive. Some of these properties are discussed by several authors,[5,12,13] so they will not be dwelt on here.

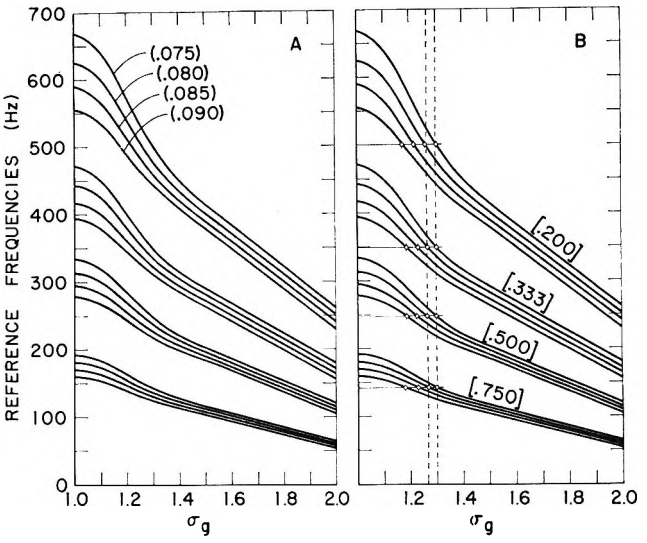

Figure 1. Reference frequencies *vs.* standard deviation σ_g for a log normal distribution with various average sizes $\bar{a}$ (in μm). The reference ratios are noted in brackets (B), and the values of $\bar{a}$ are in parentheses (A). Frequencies corresponding to experimental reference ratios from spectra of 0.02 wt % PTFE suspended in water at 22° and (θ = 90°) are shown as solid lines in (B). The points of intersection of the experimental frequencies and the calculated curves determine the best values of $\bar{a}$ and σ_g. The error bounds on σ_g are shown with dashed lines.

A convenient form of the log normal distribution of radius a is the following

$$f(a) = \frac{1}{\sqrt{2\pi}\, a \ln \sigma_g} \exp\left\{-\left[\frac{\ln a - \ln \bar{a}}{\sqrt{2} \ln \sigma_g}\right]^2\right\} \quad (10)$$

where $\bar{a}$ is the geometric mean radius, and σ_g is the geometric standard deviation. Monodisperse suspensions have $\sigma_g = 1$.

Families of "master" curves, with their parameters corresponding to various experimental situations, can be computed from eq 7 and its associated auxiliary equations. These master curves are specified by $\bar{a}$ and σ_g for any chosen set of values of scattering angle, solvent temperature, viscosity, and refractive index. There are several ways in which these master curves might be used to characterize experimental spectra. We have found the graphical scheme described in the following paragraphs to be quite easy to use.

The scheme we propose for fitting the best values of $\bar{a}$ and σ_g to experimental homodyne spectra is based on seeking a graphical solution to a system of transcendental equations that relate several specific values of spectral density and frequency to the parameters $\bar{a}$ and σ_g of a log normal distribution. First, we con-

(10) Y. Tagami and R. Pecora, *J. Chem. Phys.*, **51**, 3293 (1969).

(11) R. Pecora and Y. Tagami, *ibid.*, **51**, 3298 (1969).

(12) W. F. Espenscheid, M. Kerker, and E. Matijevic, *J. Phys. Chem.*, **68**, 3093 (1964).

(13) R. R. Irani and C. F. Callis, "Particle Size: Measurement, Interpretation, and Application," Wiley, New York, N. Y., 1963.

struct the sort of plot shown in Figure 1(A) from the master curves computed from eq 7. The reference frequencies are those, yielded by eq 7, at which the ratios of the spectral density $S(\omega)$ to its value at zero frequency $S(0)$ are $[S(\omega)/S(0) = 0.750, 0.500, 0.333,$ and $0.200]$. Values of these reference frequencies are taken from master curves with $\bar{a}$ fixed for various values of σ_g.

To characterize an experimental spectrum, one needs first to establish the value of the spectral density at zero frequency. Extrapolation of the reciprocal of the experimental spectral density plotted against the square of frequency seems to be a good way to get $S(0)$. This operation may be done manually or electronically.[14] The frequencies of the experimental power spectra at which $[S(\omega)/S(0)]$ is 0.750, 0.500, 0.333, and 0.200 are located on the frequency axis of the plot shown in Figure 1(B). Straight lines are drawn on the plot with these frequencies held constant. These lines will interesect various curves corresponding to different values of $\bar{a}$. The points of intersection with curves having a particular $\bar{a}$ will lie on a line of constant σ_g [shown dashed in Figure 1(B)] when a unique combination of $\bar{a}$ and σ_g can be used with a log normal distribution function to describe the suspension of particles giving rise to the inelastic light scattering. The method is illustrated by application to (PTFE) dispersions.

Experimental Section

Homodyne spectral densities of suspensions of PTFE in water were measured with the light mixing spectrometer previously described.[14] The suspensions were about 0.02% by weight. The spectra were presented as power spectral density *vs.* frequency and simultaneously as reciprocal spectral density *vs.* the square of the frequency. The latter representation is particularly useful for our method of analysis. The Rayleigh–Gans expression for Φ (eq 4) can be used for PTFE since $\tilde{m} = 1.025$.

Results and Discussion

The experimental frequencies at which $[S(\omega)/S(0)]$ has the values 0.750, 0.500, 0.333, and 0.200 are plotted in Figure 1(B). The values shown are average values of data points taken in six experiments. It can be seen that the spectral densities of polydisperse PTFE are best characterized by the log normal parameters $\bar{a} = 0.078 \pm 0.003$ μm and $\sigma_g = 1.28 \pm 0.02$. The same PTFE material, when characterized by sedimentation velocity experiments, is found to have a size distribution that is well represented (Figure 2) by a log normal distribution with a geometric mean radius of $\bar{a}_w = 0.112 \pm 0.003$ and $\sigma_g = 1.29 \pm 0.02$. The geometric mean radius averaged by weight, and the geometric mean radius averaged by number, may be related by the following version of Kapteyn's rule.[5]

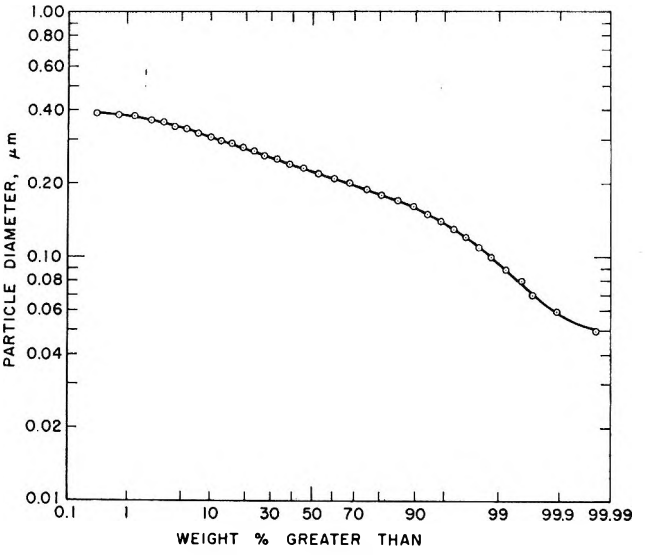

Figure 2. Weight per cent of particles with diameters greater than a given size (sedimentation data) *vs.* log particle diameter. This plot, linear on log probability scales for a log normal distribution (ref 5 and 9), is used to obtain the best values of $\bar{a}_w$ and σ_g from sedimentation data.

$$\bar{a}_w = \bar{a} \exp[3 \ln^2 \sigma_g] \quad (11)$$

The geometric standard deviation is invariant to averaging by weight or by number. Substituting $\bar{a}$ from inelastic light scattering into eq 11 and using $\sigma_g = 1.285$, we calculate $\bar{a}_w = 0.095 \pm 0.005$ μm.

It appears that inelastic light scattering can provide a rapid assay for the size distribution in colloidal suspensions that can be characterized by a unique distribution function. The log normal size distribution function is likely to be applicable in many cases.

Acknowledgments. I wish to thank Dr. C. S. Cope of the Plastics Department (E. I. du Pont de Nemours & Co., Inc.) for supplying the PTFE samples and the sedimentation data. I am grateful to D. Filkin for assistance with some of the numerical calculations and to M. Stasho for assistance with data collection.

(14) D. S. Thompson, *Rev. Sci. Instrum.*, 41, 1228 (1970)

The Reversible Hydration of Pyruvate Esters. Thermodynamic and Kinetic Studies[1]

by Y. Pocker,* J. E. Meany, and C. Zadorojny[2]

Department of Chemistry, University of Washington, Seattle, Washington 98105 *(Received June 29, 1970)*

Publication costs borne completely by The Journal of Physical Chemistry

The hydration of methyl and ethyl pyruvate has been investigated both by nmr and spectrophotometric techniques. From the temperature dependency of the equilibrium ratio R = [hydrated ester]/[pyruvate ester] the thermodynamic parameters have been determined for methyl pyruvate: $\Delta G^\circ = -0.62$ kcal mol^{-1}, $\Delta H^\circ = -5.4$ kcal mol^{-1}, and $\Delta S^\circ = -15.9$ eu; and for ethyl pyruvate: $\Delta G^\circ = -0.51$ kcal mol^{-1}, $\Delta H^\circ = -5.4$ kcal mol^{-1}, $\Delta S^\circ = -16.2$ eu; and these are compared to the corresponding values associated with several other reversible hydration reactions. In addition, a second-order dependence on water concentration is shown for the hydrations of methyl and ethyl pyruvates in contrast to the stoichiometry of the hydration process of pyruvic acid where three water molecules are involved. Kinetic investigations have also been carried out on these hydrations. The data show that general bases strongly promote the hydration of methyl pyruvate: $k_{CH_3CO_2^-} = 6.9$ l. mol^{-1} min^{-1}, $k_{HCO_2^-} = 5.3$ l. mol^{-1} min^{-1}; and that of ethyl pyruvate: $k_{CH_3CO_2^-} = 5.5$ l. mol^{-1} min^{-1}, $k_{HCO_2^-} = 4.3$ l. mol^{-1} min^{-1}. Specific acid catalysis was not observed. The magnitude of the spontaneous rate coefficients for methyl pyruvate, $k_0 = 1.98$ min^{-1}, and ethyl pyruvate, $k_0 = 1.55$ min^{-1}, is compared with that corresponding to the hydration of pyruvic acid. The significance of intramolecular acid catalysis in the hydration of pyruvic acid, a path not possible for the alkyl pyruvates, is discussed. For the hydration of methyl pyruvate and ethyl pyruvate, free energies, $\Delta G^\ddagger$, $\Delta H^\ddagger$, and entropies of activation, $\Delta S^\ddagger$, were deduced as -13.9 and -14.0 kcal mol^{-1}, -7.5 and -7.6 kcal mol^{-1}, and -21.3 and -21.4 eu, respectively.

Introduction

The reversible hydration reactions of carbonyl compounds occupy a central position in physiological systems.[3] The utility of many carbonyl compounds in studies pertaining to general acid–general base catalysis[4] and enzymatic catalysis[3,5,6] has caused such reactions to be both thermodynamically[7-9] and kinetically[10a-d] investigated. Several techniques have been utilized in recent years which have yielded thermodynamic data for reversible hydration reactions.[4,7-9,10c,11,12] Ultraviolet spectroscopy[4,8,9,10c] has greatly facilitated such investigations but for rapid hydrations this technique suffers from the uncertainty in the determination of the extinction coefficient of the unhydrated species prior to its reaction. Nmr has the advantage of allowing the ratio of the hydrated to unhydrated forms to be deduced directly by integration even for the very rapid processes.[4,8,9,11] ^{17}O nmr methods afford similar advantages but are generally less precise.[12] The main difficulty in correlating the results obtained from the various techniques often arises from the fact that few investigators take into consideration the influence of temperature or of the concentration of water on the ratio of the hydrated to unhydrated forms. Thus the first part of this paper is concerned with the second-order dependence on water concentration for the hydration of methyl and ethyl pyruvates[13] as well as with the corresponding standard free energies, heats, and entropies of hydration.[14]

The specific acid and spontaneous rates of hydration of pyruvic acid have been previously investigated[10d,15,16] and it has been suggested that the relatively high rate of spontaneous hydration of this compound is indicative of the participation of an intramolecular acid-catalyzed mechanism.[15,16] In order to test the validity

(1) This work was supported by U. S. Public Health Service Grants from the National Institutes of Health.

(2) National Science Foundation undergraduate research participant, 1969.

(3) R. P. Davis, *Enzymes*, **5**, 545 (1961).

(4) R. P. Bell, *Advan. Phys. Org. Chem.*, **4**, 1 (1966), and references quoted therein.

(5) Y. Pocker and J. E. Meany, *Biochemistry*, **4**, 2535 (1965); **6**, 239 (1967).

(6) Y. Pocker and D. G. Dickerson, *ibid.*, **7**, 1995 (1968).

(7) (a) R. Bieber and G. Trumpler, *Helv. Chim. Acta*, **30**, 1860 (1947); (b) R. P. Bell and J. C. Clunie, *Trans. Faraday Soc.*, **48**, 440 (1952); (c) R. P. Bell and A. O. McDougall, *ibid.*, **56**, 12 (1960).

(8) Y. Pocker, J. E. Meany, and B. J. Nist, *J. Phys. Chem.*, **71**, 4509 (1967).

(9) Y. Pocker, J. E. Meany, B. J. Nist, and C. Zadorojny, *ibid.*, **73**, 2879 (1969).

(10) (a) Y. Pocker and J. E. Meany, *ibid.*, **71**, 3113 (1967); (b) Y. Pocker and J. E. Meany, *ibid.*, **72**, 655 (1968); (c) Y. Pocker and D. G. Dickerson, *ibid.*, **73**, 4005 (1969); (d) Y. Pocker and J. E. Meany, *ibid.*, **74**, 1486 (1970).

(11) (a) E. Lombardi and P. B. Sogo, *J. Chem. Phys.*, **32**, 635 (1960); P. G. Evans, M. M. Kreevoy, and G. R. Miller, *J. Phys. Chem.*, **69**, 4325 (1965); (b) M. Becker, *Ber. Bunsenges. Physik. Chem.*, **68**, 663 (1964); (c) V. Gold, G. Socrates, and M. R. Crampton, *J. Chem. Soc.*, 588 (1964).

(12) P. Greenzaid, Z. Luz, and D. Samuel, *J. Amer. Chem. Soc.*, **89**, 749 (1967).

of this proposal, a comparison is made here between the spontaneous rates of hydration of pyruvate esters and that of pyruvic acid.

Experimental Section

The substrates, methyl and ethyl pyruvate, purchased from Aldrich Chemical Co., were distilled through a Vigreux column under nitrogen prior to use: bp (methyl pyruvate) 43° (19 mm); bp (ethyl pyruvate) 54° (19 mm). Buffer solutions were prepared in deionized water from reagent grade buffer components with the exception of diethylmalonic acid, the preparation of which was reported earlier.[17] For kinetics carried out at low values of pH (<1), the acidity of the reactions was adjusted by the addition of appropriate amounts of hydrochloric acid prior to the initiation of the run. The pH of these solutions was determined both before and after each run. Measurements of pH were carried out on a Beckman 101900 research pH meter. The spectrophotometric measurements were carried out on a Gilford high-speed recording spectrophotometer, Model 2000, which was equipped with a cell compartment[17] thermostated to ±0.02°. These investigations were conducted at 330 nm.

The hydrations were initiated by injecting 0.025 ml of the alkyl pyruvates, by means of a calibrated Hamilton syringe, into 3 ml of the reaction solution. Complete mixing was effected by rapid stirring at the time of injection. An immediate diminution of the absorbancy at 330 nm was recorded and excellent pseudo-first-order kinetics were observed. Linear results were obtained up to three half-lives when log $(A_t - A_\infty)$ was plotted against time (where A_t and A_∞ denote the absorbancies of the respective alkyl pyruvates at time t and at equilibrium). Due to the reversible nature of these reactions, the observed rate constant, $k_{obsd} = -2.3 \times$ slope, is actually the sum of first-order rate constants for the forward and reverse processes. The rate coefficient for the forward process, k_f, was evaluated by multiplying k_{obsd} by the appropriate value for the fraction of hydration, $\chi = (A_0 - A_\infty)/A_0$, which corresponded to the temperature at which the kinetic run was carried out and the concentration of alkyl pyruvate used (methyl pyruvate: 0.094 M; ethyl pyruvate: 0.075 M). The initial absorbancy, A_0, was deduced by extrapolation to the kinetic zero. The ratios of hydrated to unhydrated esters were deduced from the relationship: R = [hydrated ester]/[pyruvate ester] = $(A_0 - A_\infty)/A_\infty$. For temperatures exceeding 25.0°, it was assumed that the extinction coefficient was the same as at lower temperatures and the corresponding value of A_0 was employed in the calculations of R. This assumption proved to be valid as the mean extrapolated value of A_0 at these higher temperatures was identical, within experimental error, to that obtained at lower temperatures. In addition, the values of R as determined either by nmr or extrapolated from spectrophotometric data, when corrected for differences in the concentration of water, were found to be the same at 34°.

Nuclear magnetic resonance spectrometry was used to determine the equilibrium position of hydration as a function of water concentration. These measurements were carried out on either a Varian DA 60 IL or A 60 instrument over a sweep width of 500 cps. The relative quantities of hydrated and unhydrated forms of the pyruvates were determined directly through the integration of two signals associated with the hydrogens attached to the methyl group adjacent either to the gem diol group (as in the hydrated form) or the carbonyl group (as in the unhydrated form). These peaks were separated by approximately 0.9 ppm. The solutions prepared for these studies were tested immediately after mixing to avoid possible contamination arising from ester hydrolysis. However, it was noted that around neutral pH ester hydrolysis is rather slow so that even after several hours, no change in the nmr spectra occurred. The concentrations of the solutions ranged from 0.556 to 3.39 M and it was noted that the volumes of water and alkyl pyruvate were not strictly additive. Consequently, the solutions were prepared by weighing both components which made up a known final volume.

Results and Discussion

Thermodynamic Investigations. The reversible hydrations of methyl and ethyl pyruvate, eq 1, are

$$CH_3C(=O)CO_2R + (X + 1)H_2O \rightleftharpoons CH_3C(OH)_2CO_2R \cdot XH_2O \quad (1)$$

less complex than the corresponding process involving pyruvic acid because of the ionization of both pyruvic acid (pK_a = 2.2) and of its hydrate (pK_a =

(13) It should be noted that the results reported herein are based on concentrations rather than activities. Accordingly, the associated equilibrium constants may differ somewhat from the corresponding thermodynamic constants. However, due to the strict linearity of log R against log H_2O (Figure 2) over such a large range of concentrations we feel that the stoichiometry given by eq 2 is justified. Also the observed slope of precisely 2 (Figure 2) would be most coincidental if merely associated with differential solvent effects of the activity coefficients for the hydrated and unhydrated ester.

(14) These parameters were determined from measurements involving relatively low concentrations (Figure 3) of the substrates, in order to minimize any ambiguity arising from variations in activity coefficients.

(15) M. Eigen, K. Kustin, and H. Strehlow, *Z. Physik. Chem.*, **31**, 140 (1962).

(16) H. Strehlow, *Z. Elektrochem.*, **66**, 3921 (1962).

(17) Y. Pocker and J. E. Meany, *J. Amer. Chem. Soc.*, **89**, 631 (1967).

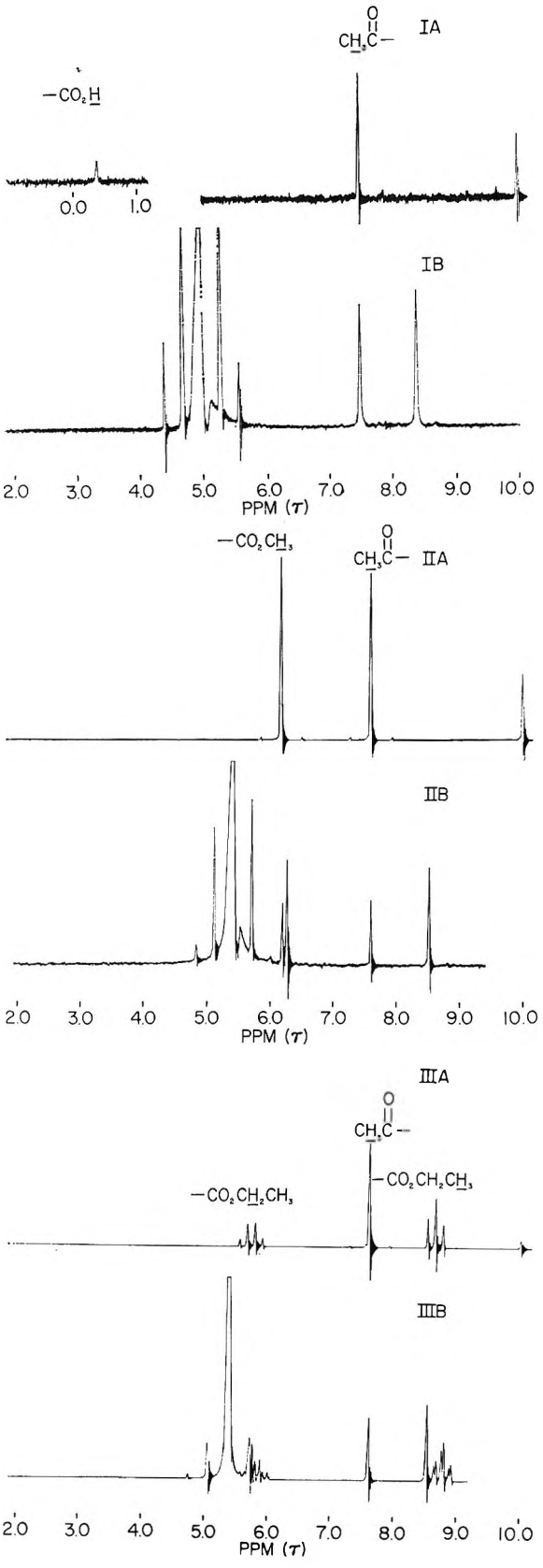

Figure 1. IA, nmr spectrum of pyruvic acid in carbon tetrachloride. IB, nmr spectrum of pyruvic acid in water. IIA, nmr spectrum of methyl pyruvate in carbon tetrachloride. IIB, nmr spectrum of methyl pyruvate in water. IIIA, nmr spectrum of ethyl pyruvate in carbon tetrachloride. IIIB, nmr spectrum of ethyl pyruvate in water.

3.6). Thus, for methyl and ethyl pyruvates, we have measured the extent of hydration in dilute HCl (pH 1–2), and in a series of buffers

$$(C_2H_5)_2C(CO_2H)_2\text{–}(C_2H_5)_2C\begin{matrix}CO_2H\\ \diagdown\\ \diagup\\ CO_2^-\end{matrix} \quad \text{(pH 2–3)}$$

$$HCO_2H\text{–}HCO_2^- \text{ (pH 3–4)}$$

$$HOAc\text{–}OAc^- \text{ (pH 4–6)}$$

$$\begin{matrix}CO_2H\\ \diagup\\ (C_2H_5)_2C\text{–}\\ \diagdown\\ CO_2^-\end{matrix}(C_2H_5)_2C(CO_2^-)_2 \text{ (pH 6–7)}$$

and have found no variation in the equilibrium positions in the pH range studied. It should be noted that the hydrolysis of the pyruvate esters is so slow under neutral or acidic conditions that their hydration may be studied long before hydrolysis occurs.[18a,b]

The nuclear magnetic resonance spectra of pyruvic acid, methyl pyruvate, and ethyl pyruvate both in carbon tetrachloride (IA, IIA, IIIA) and in H_2O (IB, IIB, IIIB) are shown in Figure 1. The spectra of these compounds are represented in IA, IIA, and IIIA in their unhydrated forms in carbon tetrachloride where TMS was used as an internal standard (τ 10). As will be noted from these spectra, the peaks around 7.6 ppm have been assigned to the methyl hydrogens adjacent to the unhydrated carbonyl group. Other peak assignments are indicated in the spectra and these are justified from consideration of shielding effects, splitting multiplicity, and the relative areas under the respective peaks. Each of the spectra in water (IB, IIB, and IIIB) has arbitrarily been offset such that the signals associated with the methyl hydrogens adjacent to the unhydrated carbonyl coincide with those as obtained in carbon tetrachloride. Upon hydrate formation in water, an additional peak arises slightly upfield due to an expected increase in shielding of the methyl hydrogens adjacent to the gem diol group. Each spectrum obtained from aqueous solution shows broad signals around 4.5–5.5 ppm which are due to water.

The nmr spectra of the alkyl pyruvates were obtained at various concentrations of water. Table I shows the results of these studies and Figure 2 demonstrates that plotting the data from Table I in the form of log R *vs.* log $[H_2O]$ for both methyl and ethyl pyruvate, a straight line of slope 2 is obtained. According to eq 1, a value of $X = 1$ yields the following expression

$$K_{eq} = \frac{[\text{hydrated ester}]}{[\text{pyruvate ester}][H_2O]^2} = \frac{R}{[H_2O]^2} \qquad (2)$$

(18) (a) A. Kirrmann, *Bull. Soc. Chim.*, [5] 1, 247, 254 (1934); (b) Y. Pocker and C. Zadorojny, unpublished results.

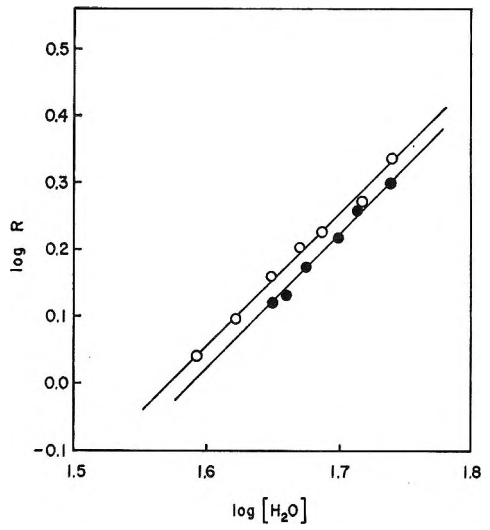

Figure 2. Log R plotted against log [H_2O] for ○, methyl and ●, ethyl pyruvate systems at 34°. Slope of straight lines is 2.0.

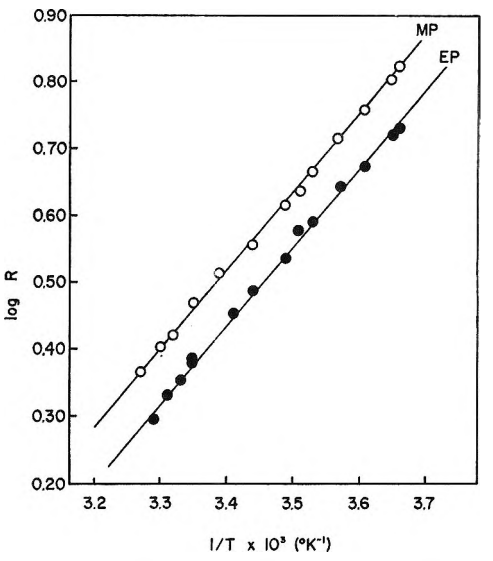

Figure 3. Log R plotted against reciprocal absolute temperatures for the hydrations of ○, 0.094 M methyl pyruvate and ●, 0.075 M ethyl pyruvate.

Consequently, the results from Figure 2 suggest that the stoichiometry of the hydration involves two water molecules.[13] It is interesting to note that similar studies have indicated that in the stoichiometry of hydration of pyruvic acid, three water molecules are involved.[9]

Table I: Second-Order Dependence of the Equilibrium Ratio, R = [Hydrated Ester]/[Pyruvate Ester], on Water Concentration for Methyl and Ethyl Pyruvate at 34°

[Ester], mol l.$^{-1}$	R	[H_2O], mol l.$^{-1}$	log [R]	log [H_2O]
		Methyl Pyruvate		
0.094[a]	2.16	55.1	0.335	1.741
0.566	1.86	52.0	0.270	1.716
1.130	1.68	48.6	0.226	1.686
1.700	1.59	46.7	0.202	1.670
2.260	1.45	44.6	0.160	1.649
2.830	1.26	41.8	0.099	1.622
3.390	1.09	39.2	0.040	1.593
		Ethyl Pyruvate		
0.075[a]	2.01	55.1	0.302	1.741
0.591	1.84	51.9	0.263	1.714
1.130	1.66	50.3	0.222	1.701
1.440	1.50	47.0	0.176	1.673
1.760	1.35	45.6	0.132	1.659
2.000	1.33	44.5	0.124	1.648

[a] Data taken from spectrophotometric work corresponding to 34°.

Values of R were determined as a function of temperature for methyl pyruvate (0.094 M) and ethyl pyruvate (0.075 M) using the spectrophotometric method previously described. These studies were carried out over a temperature range of 0.0–32.5° in acetate buffers, pH 4.6 at an ionic strength of 0.1 M. The linear plot of log R against $1/T$ shown in Figure 3 allowed the evaluation of the thermodynamic parameters for methyl and ethyl pyruvate.[14] These are compared with similar data as obtained for other hydration reactions in Table II. Greenzaid, *et al.*,[12] have determined the value R = 3.13 using 1 M total methyl pyruvate at 25° *via* ^{17}O nmr measurements. By converting our value of R at 0.094 M methyl pyruvate and 25° to 1 M at the same temperature we obtain R = 2.4. We calculate the same value by the extrapolation of our nmr data obtained at 1 M from 34 to 25°.

It will be noted that the standard entropies of hydration for methyl pyruvate ($\Delta S°$ = −15.9 eu) and for ethyl pyruvate ($\Delta S°$ = −16.2 eu) are not as highly

Table II: Thermodynamic Parameters for the Reversible Hydration Reactions of Carbonyl Compounds at 298.2°K

	$-\Delta H°$, kcal mol^{-1}	$-\Delta G°$, kcal mol^{-1}	$\Delta S°$, eu
Formaldehyde[a]	14.6	5.4	−30.8
Chloral[b]	12.7	3.68	−30.2
Pyruvic acid[c]	7.8	0.24	−25.4
s-Dichloroacetone[b]	5.7	1.27	−14.8
as-Dichloroacetone[b]	5.5	0.62	−16.4
Methyl pyruvate	5.4	0.62	−15.9
Ethyl pyruvate	5.4	0.51	−16.2
Acetaldehyde[d]	5.1	0.23	−16.4
Diacetyl[b]	4.5	0.72	−12.7
4-Pyridinecarboxaldehyde[e]	4.2	0.08	−13.9
2-Pyridinecarboxaldehyde[e]	3.8	−0.35	−13.8
Monochloroacetone[b]	2.0	−0.28	−7.7

[a] Reference 7a. [b] Reference 7c. [c] Reference 9. [d] Reference 7b; for other aliphatic aldehydes see reference 10c. [e] Reference 8.

negative as that corresponding to pyruvic acid ($\Delta S°$ = −25 eu).[9] This is consistent with the interpretation that a highly negative entropy of hydration is an indication of a highly structured form of the hydrate.

Generally speaking, it is apparent that the extent of hydration for various carbonyl compounds is dictated in part by the electron-withdrawing capacity of groups near the carbonyl group. However, a quantitative treatment of these effects, *viz.*, through a correlation of equilibrium constants by free energy relationships,[4,12] may be only qualitative unless account is taken of the sensitivity of such processes toward both temperature *and* water concentration. Whereas the latter consideration may be relatively unimportant at very low concentrations of substrate, or where substrates have a first-order dependency on water concentration, variations in the apparent standard free energies become more pronounced as the order of water dependency increases or when appreciable substrate concentrations are employed in the determination of $\Delta G°$. Thus, due care must be exercised when nmr or omr methods are employed in evaluating this thermodynamic parameter since these techniques generally necessitate considerably higher concentrations of substrate than the corresponding spectrophotometric methods. Accordingly, more meaningful free energy relationships should result when the equilibrium constants used are extrapolated to low concentrations of substrate.

Kinetic Investigations. For reactions subject both to general acid and general base catalysis, there exists a catalytic component for each acidic and basic species present in the reaction solution

$$k_f = k_0 + k_{H_3O^+}[H_3O^+] + k_{OH^-}[OH^-] + k_A[A] + k_B[B] \quad (3)$$

In the present studies, several series of kinetic runs were carried out in acetate buffers each at constant buffer ratio, r, while simultaneously varying the concentrations of acetic acid and the acetate anion. Rearranging eq 3 leads to eq 4

$$k_f = k_0 + k_{H_3O^+}[H_3O^+] + k_{OH^-}[OH^-] + (k_A + k_B/r)[A] \quad (4)$$

For each of these series, the forward rate constants, k_f, were plotted against the concentration of acetic acid (Figures 4 and 5). Linear results were obtained for each such series indicating the absence of catalytic components arising from the concerted action of both A and B. According to eq 4, the slopes of the straight lines thus obtained may be expressed as

$$S = k_A + k_B/r \quad (5)$$

and the intercepts as

$$I = k_0 + k_{H_3O^+}[H_3O^+] + k_{OH^-}[OH^-] \quad (6)$$

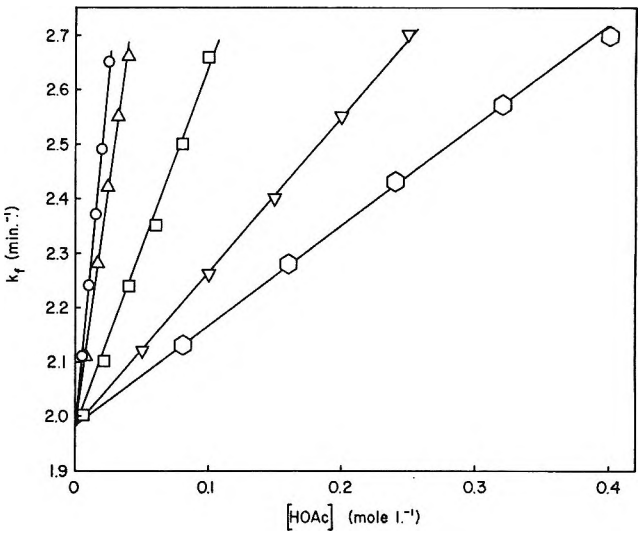

Figure 4. Methyl pyruvate: k_f against acetic acid concentration at 0.0°; μ = 0.1; ○ at r = 0.25; △ at r = 0.40; □ at r = 1.0; ▽ at r = 2.5; ○ at r = 4.0.

Table III gives the values of the slopes and intercepts obtained by carrying out such experiments at several different buffer ratios in acetic acid buffers and also at a buffer ratio of unity in formate buffers. These studies were carried out over a pH range of from 3.60 to 5.25.

Table III: Catalysis of Methyl and Ethyl Pyruvate Hydrations (at 0.0° and μ = 0.1)

		Methyl pyruvate[a]		Ethyl pyruvate[b]	
Buffer[c]	r	S, l. mol^{-1} min^{-1}	I, min^{-1}	S, l. mol^{-1} min^{-1}	I, min^{-1}
Formate	1	5.03	1.99	4.29	1.52
Acetate	0.25	27.3	1.97	22.7	1.57
Acetate	0.40	17.8	1.98	13.2	1.54
Acetate	1.0	6.74	1.97	5.64	1.54
Acetate	2.5	2.81	1.98	2.32	1.56
Acetate	4.0	1.83	1.98	1.60	1.54

[a] Forward rate constants used in deducing these data obtained from $k_f = \chi k_{obsd} = 0.867 k_{obsd}$. [b] Forward rate constants used in deducing these data obtained from $k_f = \chi k_{obsd} = 0.842 k_{obsd}$. [c] Ionic strengths adjusted using sodium chloride, μ = 0.1.

Since the intercepts given in Table III did not vary, it may be assumed that the catalytic contribution by either the specific acid or base in eq 6 is negligible. Consequently the average value of the intercepts was used to define the spontaneous rates of hydration for methyl pyruvate (k_0 = 1.98 min^{-1}) and ethyl pyruvate (k_0 = 1.55 min^{-1}).

The slopes, S, in eq 5, are a linear function of the reciprocal buffer ratio and accordingly Figure 6 allows the evaluation of the catalytic rate coefficients for the acetate anion for methyl pyruvate (k_{OAc^-} = 6.9 l.

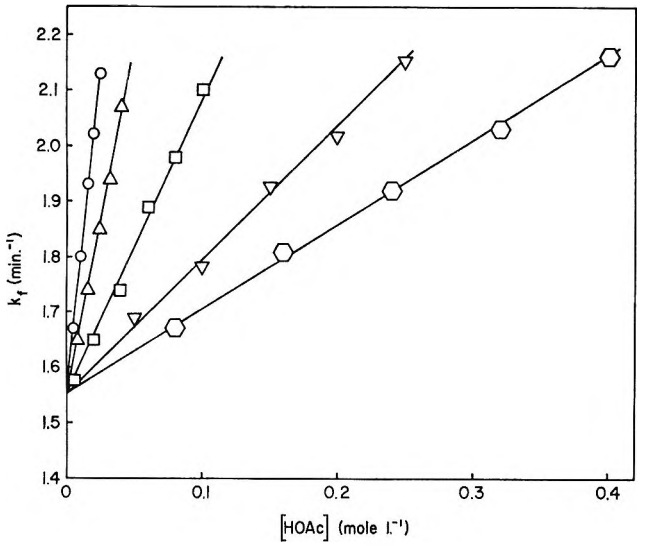

Figure 5. Ethyl pyruvate: k_f against acetic acid concentration at 0.0°; μ = 0.1; ○ at r = 0.25; △ at r = 0.40; □ at r = 1.0; ▽ at r = 2.5; ○ at r = 4.0.

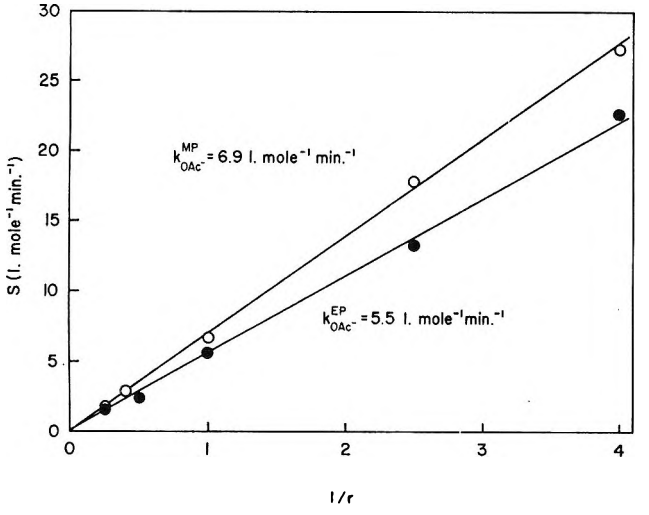

Figure 6. Determination of the specific rate coefficients for acetic acid and acetate ion: ○, methyl pyruvate; ●, ethyl pyruvate.

mol^{-1} min^{-1}) and ethyl pyruvate (k_{OAc^-} = 5.5 l. mol^{-1} min^{-1}). It will be noted that the intercepts cannot be distinguished from zero. This implies that the general acid catalyzed component for acetic acid is negligibly small for both hydrations.

If one assumes that for the formic acid buffers, the acid-catalyzed component is small at a buffer ratio of unity, the formate ion catalyzed hydrations may be approximated for methyl pyruvate ($k_{HCO_2^-}$ = 5.3 l. mol^{-1} min^{-1}) and ethyl pyruvate ($k_{HCO_2^-}$ = 4.3 l. mol^{-1} min^{-1}). This would appear to be a valid assumption since although formic acid (pK_a = 3.66) is a stronger acid than acetic acid (pK_a = 4.75), the acid-catalyzed component was still undetectable for the latter even at a buffer ratio of 4, *i.e.*, where there was a fourfold excess of acid over base.

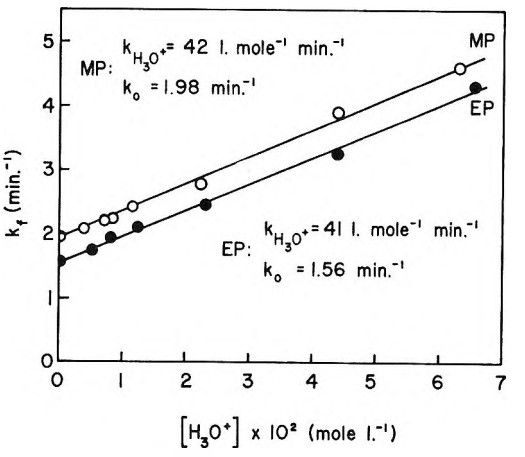

Figure 7. Catalysis of the hydration of H_3O^+: ○, methyl pyruvate; ●, ethyl pyruvate, at 0.0°.

The specific acid catalyzed component of hydration was determined in dilute standardized solutions of HCl[19] and also in very dilute diethylmalonic acid buffers (pK_1 = 2.21) having a total concentration of 0.01 M. It had independently been observed that at constant pH, doubling and quadrupling the concentration of the dilute diethylmalonate buffers had no effect on the observed rate constant and consequently the only detectable catalytic components in these buffers were those arising from water and the hydronium ion. Figure 7 shows the results of the plots of k_f against hydronium ion concentration for the alkyl pyruvates. The specific acid catalyzed components of hydration are deduced from the slopes of the straight lines obtained for methyl pyruvate, $k_{H_3O^+}$ = 42 l. mol^{-1} min^{-1} and ethyl pyruvate, $k_{H_3O^+}$ = 41 l. mol^{-1} min^{-1}. The fact that the specific acid catalyzed components are relatively small further justifies the previous assumption made in the evaluation of the formate-catalyzed hydration of methyl and ethyl pyruvate. Table IV summarizes the values for the catalytic rate coefficients determined for methyl and ethyl pyruvate.

Table IV: Catalytic Rate Coefficients for Acids and Bases in the Hydrations of Methyl and Ethyl Pyruvate at 0.0° and Ionic Strength of 0.1

Catalyst	k_c^{MP}, l. mol^{-1} min^{-1}	k_c^{EP}, l. mol^{-1} min^{-1}
$CH_3CO_2^-$	6.9	5.5
HCO_2^-	5.3	4.3
H_2O	1.98/55.5	1.55/55.5
H_3O^+	42	41

(19) When hydronium ion activities were determined from pH meter measurements, they were converted to concentrations using a mean activity coefficient of 0.77. The value f = 0.77 was calculated from the expression: $\log f_z = -0.49\, z^2\mu^{1/2}/(1 + 1.5\, \mu^{1/2})$, where μ and z stand for the ionic strength and charge, respectively.

Other studies which have been carried out in these laboratories are related to the hydration of pyruvate esters as catalyzed by metal ions and metalloenzymes (*e.g.*, carbonic anhydrase).[20] We find hydronium ion catalysis to be less powerful than that by divalent metal ions. This is not surprising since several reactions are known which involve substrates having the capacity to act as bidentate ligands in which metal ion catalysis greatly exceeds hydronium ion catalysis.[10b,d,17,21] We have also noted in the present studies that the subsequent hydrolysis of these α-ketoesters is significantly slower than their hydration[18b] but much faster than the hydrolysis of normal aliphatic esters.[18a] We are presently testing the sensitivity of these reactions to enzymatic and metal ion catalysis.

The relative insensitivity of the hydration of the pyruvate esters toward acid catalysis is not surprising since the nucleophilic attack by water is already facilitated to a large extent by the presence of adjacent groups which are strongly electron withdrawing. It is usually the case that not only does the extent of hydration increase when such substituents are directly bonded to the carbonyl group[4,12,22] but the rate of hydration is also enhanced.[23]

It will be noted that at 0.0° the spontaneous rate of hydration for methyl pyruvate (k_0 = 1.98 min^{-1}) is very nearly the same as that determined earlier for pyruvic acid (k_0 = 2 min^{-1}).[10d] Although the corresponding value for ethyl pyruvate is slightly lower (k_0 = 1.55 min^{-1}), this can be attributed to a steric effect caused by the presence of the bulky carbethoxy group. Strehlow[16] attributes the relatively powerful spontaneous rate of hydration of pyruvic acid to intramolecular catalysis by the neighboring carboxyl group

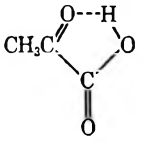

Were this the case it would appear difficult to explain the rapid spontaneous hydration of methyl and ethyl pyruvates, esters in which no such intramolecular acid-catalyzed path is possible.

The activation parameters for the spontaneous hydrations of methyl and ethyl pyruvates were determined. A series of kinetic runs were made at pH 4.5 in 0.005 *M* acetate buffers at various temperatures. From the data already presented, it will be noted that in this pH range and at this buffer concentration, the spontaneous rate coefficient accounts for more than 99% of the overall rate constant. The values of k_f were determined by multiplying the observed rate constants, k_{obsd}, by the value of the fraction of hydration, χ, which corresponds to the temperature at which the reactions were run. Table V lists the data for both methyl and ethyl pyruvates and Figure 8 shows the linearity of the resulting Arrhenius plots. The activation parameters for the spontaneous hydrations of methyl and ethyl pyruvates are given in Table VI.

Table V: Dependency of χ and k_0 on Absolute Temperature

	T, °K	χ	k_{obsd}, min^{-1}	k_0, min^{-1}
Methyl pyruvate	273.2	0.866	2.29	1.98
	273.8	0.862	2.36	2.03
	280.4	0.838	3.47	2.91
	285.0	0.817	4.48	3.67
	288.0	0.794	5.71	4.53
	298.8	0.768	7.28	5.59
	298.2	0.744	9.28	6.90
Ethyl pyruvate	273.2	0.844	1.84	1.55
	273.8	0.842	1.92	1.61
	280.4	0.810	2.80	2.27
	285.0	0.785	3.68	2.89
	288.1	0.762	4.68	3.57
	298.8	0.731	6.11	4.47
	298.2	0.703	7.64	5.37

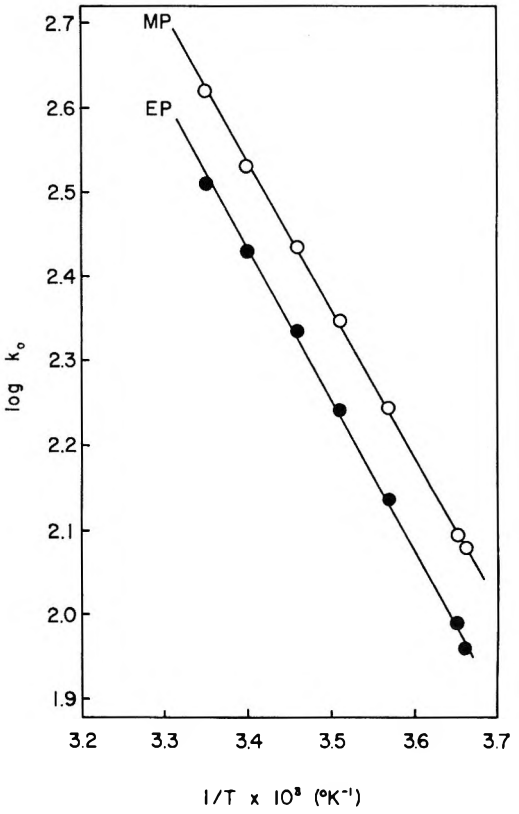

Figure 8. Arrhenius plot for: ○, methyl pyruvate and ●, ethyl pyruvate (values of k_0 in sec^{-1}).

(20) Y. Pocker and J. E. Meany, unpublished results.

(21) K. J. Pedersen, *Acta Chem. Scand.*, 2, 252 (1948); 6, 285 (1952); J. E. Prue, *J. Chem. Soc.*, 2331 (1952); M. L. Bender and B. W. Turnquest, *J. Amer. Chem. Soc.*, 79, 1889 (1957); M. D. Alexander and D. H. Busch, *ibid.*, 88, 1130 (1966).

(22) J. Hine, "Physical Organic Chemistry," 2nd ed, McGraw-Hill, New York, N. Y., 1962, p 249.

(23) M. M. Kreevoy and R. W. Taft, Jr., *J. Amer. Chem. Soc.*, 77 5590 (1955).

Table VI: Activation Parameters for the Spontaneous Hydrations of Methyl and Ethyl Pyruvates and Pyruvic Acid at 25.0°

	E_a,[a] kcal mol^{-1}	$\Delta H^{\ddagger}$, kcal mol^{-1}	log A[a]	$\Delta S^{\ddagger}$, eu	$\Delta G^{\ddagger}$, kcal mol^{-1}
Methyl pyruvate	8.1	7.5	8.57	−21.3	13.9
Ethyl pyruvate	8.2	7.6	8.55	−21.4	14.0

[a] From $\log k_0 = \log A - [E_a/(2.303RT)]$ where k_0, in sec^{-1}, is the spontaneous rate coefficient for the forward reaction.

The relative values of the entropies of activation associated with the spontaneous hydrations of methyl and ethyl pyruvate ($\Delta S^{\ddagger}$ = −21.3 and −21.4 eu, respectively) may be compared with the corresponding parameter for the hydration of pyruvic acid as recently reported by Patting and Strehlow ($\Delta S^{\ddagger}$ = −24 eu).[24] There indeed exists a parallel trend between the thermodynamic parameters (Table II) which also indicates a more highly negative entropy of hydration associated with pyruvic acid than with the esters. This is as expected since formation of a more highly ordered structure of hydrated pyruvic acid (involving three molecules of water) as compared to the hydrated esters (which involve only two) would also demand a greater degree of orientation during the development of the respective transition states.

(24) For pyruvic acid the spontaneous rate coefficient for forward reaction can only be determined through extrapolations of data obtained from acidic solutions since the compound does not hydrate appreciably in the region where acid catalysis becomes negligible. Such extrapolated values of k_0 were determined at four points over a temperature range of 0.0 to 20.0°. Further determinations at higher temperatures were precluded due to the extremely rapid kinetics. The estimated uncertainty in the evaluation of $\Delta S^{\ddagger}$ is ±10%. From pmr measurements at 23.5 and 39.5°, H. Patting and H. Strehlow, *Ber. Bunsenges Physik. Chem.*, **73**, 534 (1969), were able to deduce from the spontaneous hydration of pyruvic acid a $\Delta S^{\ddagger}$ value of −24 eu.

Complexes of Nickel(II) with Purine Bases: Relaxation Spectra[1]

by Richard L. Karpel, Kenneth Kustin,* and Michael A. Wolff

Department of Chemistry, Brandeis University, Waltham, Massachusetts 02154 *(Received September 11, 1970)*

Publication costs assisted by the National Institute of General Medical Sciences

The interactions of nickel(II) with 9-methylpurine, adenine, and hypoxanthine in aqueous solution at 25° and ionic strength ~0.1 M have been studied by the temperature-jump method. A kinetic analysis of the relaxation spectra of 9-methylpurine interacting with Ni^{2+} indicates formation of a 1:1 complex with the neutral form of this ligand. The complex formation rate constant, dissociation rate constant, and stability constant are $k_1 = (6.7 \pm 2.5) \times 10^3\ M^{-1}\ sec^{-1}$, $k_{-1} \simeq 75\ sec^{-1}$, and $K_1 \simeq 90\ M^{-1}$, respectively. The magnitude of the formation rate constant indicates normal substitution kinetics for nickel(II) ion. The temperature-jump results of the Ni(II)–adenine system are interpreted in terms of a mechanism in which the neutral form of the ligand attacks the metal ion. However, the anionic form of the ligand is postulated to be attached to the metal ion in the complex. The rate and stability constants which fit the data best are $k_1' = 3 \times 10^2\ M^{-1}\ sec^{-1}$, $k_{-1}' \simeq 1 \times 10^7\ M^{-1}\ sec^{-1}$, and $K_1 \simeq 2 \times 10^5\ M^{-1}$ for the formation, dissociation, and stability constants, respectively. Substitution for adenine with Ni^{2+} is slower than normal, an effect that may be due to rate-limiting ring closure if a bidentate chelate is formed. The relaxation spectra obtained for the Ni(II)–hypoxanthine system are not exponential, indicating the presence of multistep equilibria. Since these spectra were not resolvable into separate exponential functions, a quantitative kinetic analysis was not made.

Interactions of metal ions with nucleic acids and their components have recently become the subject of extensive study. Transition metal ions have been shown to affect the conformation of DNA by binding at specific sites on the macromolecule.[2] The purine bases of macromolecules, nucleotides, and nucleosides are known to bind metal ions.[3-5] To help elucidate the nature of this binding, we have studied the relaxation spectra of complexes formed between 9-methyl-

(1) The authors gratefully acknowledge support from Public Health Service Research Grant GM-08893-08 from the National Institute of General Medical Sciences.

(2) G. L. Eichhorn and Y. A. Shin, *J. Amer. Chem. Soc.*, **90**, 7323 (1968).

purine, adenine, and hypoxanthine and nickel(II) in aqueous solution at 25° by the temperature-jump method.

Although equilibrium studies have been reported for these complexes, the results are not in good agreement. For example, a comparison of the 1:1 stability constants of Ni(II) with adenine and with hypoxanthine obtained from potentiometric titration studies indicates a wide variation,[6-9] even accounting for differences in ionic strength and temperature (*cf.* Table I). The limited solubilities of these ligands and of their complexes is a complicating factor[7] and may partly explain the lack of agreement in the results.

Table I: Equilibrium Constants of Purine Bases in Aqueous Solution

A. Protolytic Constants

Ligand	pK_1^A	pK_2^A	Conditions	Reference
9-Methylpurine	2.27	...	20°	14
Adenine	4.22	9.80	25°, μ = 0.05 *M*	9
	4.25	9.83	20°	7
	4.18	9.7	25°	8
Hypoxanthine	...	8.83	25°, μ = 0.05 *M*	9
	1.98	8.94	20°	6

B. Stability Constants with Ni(II)

Ligand	log K_1	Conditions	Reference
Adenine	5.70	25°, μ = 0.05 *M*	9
	4.37	20°	7
	4.8	25°	8
Hypoxanthine	4.10	25°, μ = 0.05 *M*	9
	4.7	20°	6

In the stability constant determinations, higher order complexes were not postulated to interpret the data. On the other hand, a wide variation in concentration and pH, which would allow the attainment of conditions leading to the formation of such compounds, was precluded; consequently, the existence of 1:2 metal to base complexes, especially, cannot be dismissed. For 9-methylpurine, no stability constant information is available.

The proposed structures of purine base–metal ion complexes remain the subject of controversy. Reinert interpreted his results, principally the effect of *N*-methyl substitution on the base's affinity for metal ions, in favor of certain binding sites.[9] For instance, he found no evidence for 9-methyladenine and 9-methylhypoxanthine complexation with Cu(II). However, 7-methyladenine and 7-methylhypoxanthine exhibited complex formation with this metal ion. He therefore concluded that metal ions are most likely bound to the N(3) and N(9) groups of the purine bases. The results of a crystal structure analysis of a dinuclear 2:1 adenine–copper complex show N(3) and N(9) as the binding sites.[10] The same conclusion was reached following magnetic susceptibility, electron spin resonance, and optical studies on the same compound.[11] However, Harkins and Freiser proposed N(7) and the primary amino group of adenine as the sites of complexation with Cu(II).[8] Their conclusions were based on analogous interactions of copper with adenosine and ribose.

The possibility therefore exists that the purine bases possess multiple coordination sites, and that in aqueous solution linkage isomers may exist. In principle, higher order complexation could be distinguished from linkage isomerization (and other effects), by noting the effect on the relaxation spectra of concentration and pH. In the following we are reporting the results of such an analysis for nickel(II)–purine base systems.

Experimental Section

Adenine and hypoxanthine, obtained from Mann Research Laboratories, were used without further purification, as were all other chemicals. Professor E. Grunwald kindly provided us with 9-methylpurine, which he had obtained from Professor G. K. Helmkamp. Fisher Scientific $Ni(NO_3)_2 \cdot 6H_2O$ and Baker KNO_3 were both reagent grade. Indicators used were bromothymol blue and chlorophenol red (Fisher), methyl red and bromocresol green (Eastman), and bromochlorophenol blue (Matheson Coleman and Bell).

Solutions were prepared by dissolving weighed amounts of solid nickel(II) nitrate and ligand in 100- or 50-ml volumetric flasks containing distilled water. Indicator concentration and ionic strength were adjusted by the addition of appropriate amounts of stock solutions of indicator and KNO_3, respectively. The solutions were then diluted to the mark with distilled water (Belmont Springs) and degassed. The pH was adjusted by addition of dilute NaOH and/or HNO_3. A Corning Model 12 pH meter was used to measure the final pH value to ±0.01 pH unit. The measured hydrogen ion activity was divided by $\gamma_\pm = 0.79$ to obtain the H^+ concentration. The temperature in all experiments was 25 ± 1° and the ionic strength was 0.1 *M*, except where noted.

(3) R. Philips, *Chem. Rev.*, **66**, 501 (1966).
(4) G. L. Eichhorn, P. Clark, and E. D. Becker, *Biochemistry*, **5**, 245 (1966).
(5) H. Sternlicht, D. E. Jones, and K. Kustin, *J. Amer. Chem. Soc.*, **90**, 7110 (1968).
(6) A. Albert, *Biochem. J.*, **54**, 646 (1953).
(7) A. Albert and E. P. Serjeant, *ibid.*, **76**, 621 (1960).
(8) T. R. Harkins and H. Freiser, *J. Amer. Chem. Soc.*, **80**, 1132 (1958).
(9) H. Reinert, *Abh. Deut. Akad. Wiss. Berlin, Kl. Med.*, 373 (1964).
(10) E. Sletten, *Chem. Commun.*, 1119 (1967).
(11) D. M. L. Goodgame and K. A. Price, *Nature*, **220**, 783 (1966).

The temperature-jump apparatus has been described elsewhere.[12] The magnitude of the temperature perturbation was 10° except where noted below. All data reported fulfilled the requirement that blank experiments with ligand and indicator and with metal ion and indicator did not show any relaxation effects. Thus, all the spectra observed correspond to nickel(II)–ligand interactions.

Results and Treatment of Data

9-Methylpurine. Experiments were carried out with this purine derivative in the hope that the methyl group would block coordination at N(9), yielding simple spectra; the results showed the desired effect. Since no previous stability constants were known for this system, a method of treating the relaxation spectra which is independent of equilibrium data was used to obtain the rate and equilibrium constants.[13] In this method either metal ion or ligand is present in stoichiometric excess. Since excess ligand could result in the formation of higher order complexes, we chose to keep the metal ion in excess. Under these conditions it is safest to work at pH values below neutrality to prevent interference from hydroxo complexes. Very low pH's (<3) are also avoided, as the ligand becomes protonated in this pH range (*vide* Table I).

Therefore, at the pH's of the 9-methylpurine experiments, the predominant protolytic form of the ligand is the neutral species.[14] If only 1:1 complex formation occurs, the reaction is

$$Ni^{2+} + MeL \underset{k_{-1}}{\overset{k_1}{\rightleftharpoons}} NiMeL^{2+} \qquad (1)$$

where MeL is the neutral form of the ligand. As the metal ion is in excess, $[Ni^{2+}]_0 \gg [MeL]_0$ (where the subscript zero refers to total stoichiometric concentration), and this condition allows the approximation $[Ni^{2+}]_0 \approx [Ni^{2+}] \gg [MeL]$. A simplification in the relaxation expression for reaction 1 is obtained, leading to the following equation

$$1/\tau = k_1[Ni^{2+}]_0 + k_{-1} \qquad (2)$$

where τ is the relaxation time. The results are given in Figure 1 in graphical form.

Many indicators in the range $3 < pH < 6$ were tested and, with one exception, all showed relaxation effects for the metal–indicator blanks at the concentration levels where a metal–ligand effect could be observed. The one exception was bromochlorophenol blue, which gave no evidence for interaction with Ni(II). Use of a single indicator restricted the range of pH variation even further, however. In evaluating the relaxation spectra, allowance had to be made for the acid–base equilibria of indicator and ligand,[15] which are assumed to be very rapid in comparison to reaction 1.[16] Explicit calculations showed that, at the pH's of these studies, the rate constants are unaffected

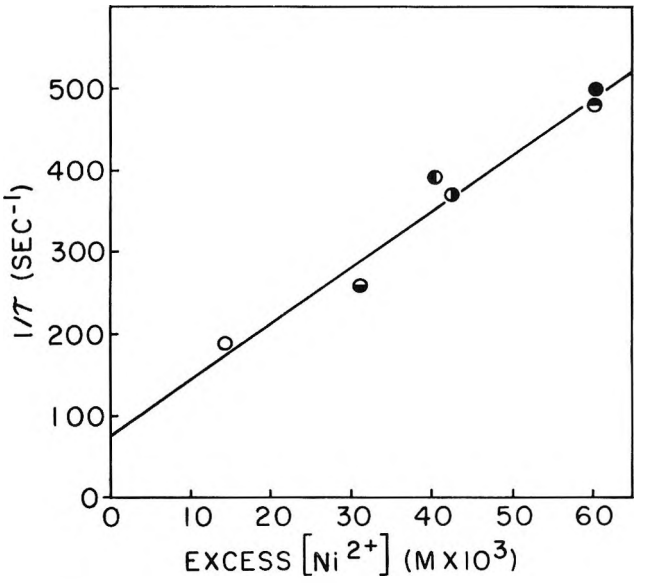

Figure 1. Plot of excess $[Ni^{2+}]$ *vs.* reciprocal relaxation time for the Ni(II)–9-methylpurine system. A preliminary treatment according to eq 2 indicated that the concentration of unbound nickel ion was more closely approximated by assuming virtually complete complex formation. Refinement using concentrations calculated from the graphically derived stability constant (=slope/intercept) did not lead to a further improvement. The stoichiometric amount of nickel(II) may be obtained from the relation [nickel(II)] = $[Ni]_0$ − $[MeL]_0$. The indicator used was bromochlorophenol blue, $pK_{HIn} = 4.0$ at 25° and $\mu = 0.1$ *M* [F. P. Cavasino, *J. Phys. Chem.*, **69**, 4380 (1965)]. Total ligand concentration $[MeL]_0$, pH, and ionic strength are: ○, $[MeL]_0 = 1.00 \times 10^{-3}$ *M*, pH 4.03, $\mu = 0.10$ *M*; ◒, $[MeL]_0 = 0.91 \times 10^{-3}$ *M*, pH 4.00, $\mu = 0.10$ *M*; ◑, $[MeL]_0 = 1.34 \times 10^{-3}$ *M*, pH 4.09, $\mu = 0.13$ *M*; ◐, $[MeL]_0 = 3.35 \times 10^{-3}$ *M*, pH 4.12, $\mu = 0.13$ *M*; ⊖, $[MeL]_0 = 1.01 \times 10^{-3}$ *M*, pH 4.50, $\mu = 0.18$ *M*; ●, $[MeL]_0 = 1.01 \times 10^{-3}$ *M*, pH 3.47, $\mu = 0.18$ *M*.

by these rapid equilibria. Although the ionic strength, μ, could not be maintained constant over the entire concentration range, the variation in rate constant due to an ionic strength dependence was well within the experimental error of the determination of individual relaxation times (±20% relative error). From Figure 1 we obtain $k_1 = (6.7 \pm 2.5) \times 10^3\ M^{-1}\ sec^{-1}$, $k_{-1} \simeq 75\ sec^{-1}$, $K_1 = k_1/k_{-1} \simeq 90\ M^{-1}$.

Adenine. The concentration range of temperature-jump experiments with Ni(II) and adenine was limited by the low solubilities of ligand and complex in aqueous solution. In general, these solutions were unstable, a condition reflected in the relative errors of the observed

(12) P. Hurwitz and K. Kustin, *Inorg. Chem.*, **3**, 823 (1964).

(13) G. Davies, K. Kustin, and R. F. Pasternack, *ibid.*, **8**, 1535 (1969).

(14) A. Albert and D. J. Brown, *J. Chem. Soc.*, 2060 (1954).

(15) G. G. Hammes and J. I. Steinfeld, *J. Amer. Chem. Soc.*, **84**, 4639 (1962).

(16) H. G. Busse and G. Maass, *Z. Phys. Chem.* (*Frankfurt am Main*), **66**, 92 (1969).

Table II: Relaxation Spectra of the Nickel(II)–Adenine System[a]

$[Ni^{2+}]_0 \times 10^3$ M	$[Adenine]_0 \times 10^3$ M	$[H^+] \times 10^6$ M	τ_{obsd}, msec	τ_{calcd}, msec
5.14	1.07	1.26[b]	9.4	13
2.96	2.89	1.20[b]	11	18
8.09	1.00	0.794[b]	12	7.3
4.50	1.00	3.02[b]	10	16
7.46	2.00	2.02[b]	8	11
8.00	2.00	8.32[c]	7.6	8.4
19.8	5.74	12.0[c]	6.4	5.3

[a] The subscript "0" refers to total stoichiometric concentration. [b] Indicator: chlorophenol red, 1.00×10^{-6} M, pK^A = 6.00 [I. M. Kolthoff, *J. Phys. Chem.*, **34**, 1466 (1930)]. [c] Indicator: methyl red, 1.00×10^{-5} M, pK^A = 5.00 [I. M. Kolthoff, *ibid.*, **34**, 1466 (1930)].

relaxation times listed in Table II, which have a rather high experimental deviation of ±25%.

The predominant form of uncomplexed adenine in all experiments is the neutral, protonated species.[6,8,9] The stability constant data of these investigators indicate that the unprotonated, negatively charged form of adenine is the complexing species. If we assume only 1:1 complex formation to be occurring, then the reaction is

$$Ni^{2+} - HL \underset{k_{-1}'}{\overset{k_1'}{\rightleftharpoons}} NiL^+ + H^+ \qquad (3a)$$

$$K_1' = k_1'/k_{-1}' = K_1K_2^A; \qquad K_1 = [NiL^+]/[Ni^{2+}][L^-] \qquad (3b)$$

where HL is the neutral form of adenine and L^- is the unprotonated, complexed species. The relaxation expression is[17]

$$\frac{1}{\tau} = k_1'\left[\frac{[Ni^{2+}]}{\delta[Ni^{2+}]/\delta[HL]} + [HL] + \left([H^+] + \frac{[NiL^{2+}]}{-\delta[Ni^{2+}]/\delta[H^+]}\right)\frac{1}{K_1K_2^A}\right] \qquad (4)$$

where δ indicates the deviation from equilibrium of a concentration variable and $(\delta[Ni^{2+}]/\delta[HL])$ and $(-\delta[Ni^{2+}]/\delta[H^+])$ can be calculated from the equilibrium data.

Equation 4 is sensitive to the value of the stability constant for formation of NiL^+. Since there is considerable disagreement about the value of K_1, a nonlinear least-squares computer program employing the protolytic constants of Reinert[9] (*vide* Table I) and stoichiometric concentrations (*vide* Table II) was used to determine both k_1' and K_1 from the experimentally determined relaxation times. The results are $k_1' \cong 3 \times 10^2$ M^{-1} sec^{-1}, $k_{-1}' \cong 1 \times 10^7$ M^{-1} sec^{-1}, and $K_1 \cong 2 \times 10^5$ M^{-1}. These values were then used to calculate the relaxation times. A comparison of observed *vs.* calculated τ, shown in Table II, gives an indication of how well the data have been fit by this process.

The relatively large uncertainty in these constants stems from a number of factors. First, the observed relaxation effects were generally of small magnitude, with unfavorable signal to noise ratios. Second, it was not possible to extend the range of conditions and carry out more experiments; therefore, the data are limited for this system. Third, as a consequence of the first two points, application of the iterative technique cannot yield accurate kinetic and equilibrium constants.

Hypoxanthine. As in the case of adenine, hypoxanthine is scarcely soluble in aqueous solution; the concentrations studied ranged from 5×10^{-4} to 3×10^{-3} M for hypoxanthine and from 3×10^{-3} to 8×10^{-3} M for Ni^{2+}. Although the temperature-jump experiments gave relaxation spectra of large amplitude, none of the observed effects were exponential displays.

The relaxation spectrum could not be resolved into a sum of exponential processes by using a nonlinear least-squares curve-fitting routine. The possibility that the magnitude of the temperature-jump perturbation (10°) produced a deviation from equilibrium that was too great to allow linearization of the rate equations without introducing appreciable error was considered. However, smaller perturbations (5°) still produced effects that could not be resolved. Similar experiments at a lower temperature (15°) also yielded nonresolvable spectra. Therefore, no kinetic analysis was attempted. The observed spectrum may be the result of a multistep mechanism, as for purine,[18] that yields two or more relaxations sufficiently close to one another not to permit separation.[19]

Discussion

It can be shown that the stability constant of 90 M^{-1} obtained for the 1:1 nickel(II)–9-methylpurine complex (Ia) correlates with the stabilities of ligands of similar structure. For example, consider 1-methylimidazole (Ib). Although the K_1 for the nickel complex of

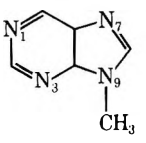

Ia

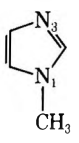

Ib

1-methylimidazole is not known, it should be similar to the value obtained for the nickel(II)–imidazole system, since the K_1 constants for the copper(II) complexes of these ligands are virtually identical.[20] The K_1 for the nickel(II)–imidazole complex is approxi-

(17) R. F. Pasternack and K. Kustin, *J. Amer. Chem. Soc.*, 90, 2295 (1968).

(18) R. Karpel, K. Kustin, and M. Wolff, unpublished data.

(19) M. Eigen and L. De Maeyer in "Technique of Organic Chemistry," Vol. VIII, part II, A. Weissberger, Ed., Interscience, New York, N. Y., 1963, p 895.

(20) L. G. Sillén and A. E. Martell, "Stability Constants," Special Publication No. 17, The Chemical Society, London, 1964.

mately 10^3 M^{-1}. However, the pK_A's of imidazole and 1-methylimidazole are both approximately 7,[20] but the pK_A for 9-methylpurine is less, being about 2.2. Therefore, one would expect a smaller stability constant for 9-methylpurine, and the measured value, being about an order of magnitude less, is in accord with this reasoning.

The forward rate constant for 9-methylpurine is also in accord with the results obtained in other studies of the rates of nickel(II) substitution reactions with neutral ligands.[21] Moreover, as a result of the experimental method, the rate constant we obtained is essentially independent of the stability constant. Like 9-methylpurine, ammonia, pyridine, and imidazole all yield rate constants of roughly 5×10^3 M^{-1} sec^{-1} with Ni^{2+}. For these (and other) systems, the absence of an appreciable k_1 dependence on specific ligand properties has been interpreted in terms of a dissociative (SN1) mechanism, in which the rate-determining step is the loss of a water molecule from the metal ion's inner coordination sphere.[22]

In this mechanism, outer-sphere complex formation is assumed to be very rapid (usually diffusion controlled). The rate-determining water loss proceeds with the formation of an activated complex of reduced coordination number. Attack of the ligand on the activated complex is then normally much more rapid. The overall rate constant, k_1, can be shown to be equal to the product of the outer-sphere complex association constant and water-loss rate constant if the steady-state approximation is applicable.[15] It may therefore be concluded that 9-methylpurine follows this mechanism.

The effect of methyl substitution at N(9) is very likely to block nickel ion binding at this site. If linkage isomers are formed; *i.e.*, if nickel is bound to N(7) in one complex and a different nitrogen in another complex, more than one relaxation time would result unless the binding properties of the three remaining nitrogens were equivalent. The poor complexing properties of pyrimidine derivatives[9] indicate that N(7) is the most likely binding site, a conclusion, however, not quite in keeping with Reinert's for *N*-methyl-substituted adenine derivatives. He determined that complexation occurs at N(9) and N(3) of unsubstituted adenine. In this case, both N(7) and N(9) are available for complexation, and both may participate in metal ion binding where neither is blocked.

Adenine (IIa) differs in many other respects from 9-methylpurine; it is the anionic form of adenine that binds the metal ion, and not the neutral form, as in the previous case. Therefore, it is not surprising that the stability constant is three orders of magnitude greater for adenine than for 9-methylpurine. The experimentally determined stability constant obtained in this study for the 1:1 nickel(II)–adenine complex falls within the range of values listed in Table I.

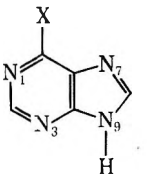

II

a, X = NH_2, adenine
b, X = OH, hypoxanthine

Another difference is that the formation rate constant for nickel(II)–adenine is more than an order of magnitude smaller than that for 9-methylpurine. If the dissociative mechanism is operative, the reduction in overall rate constant would have to be ascribed to a decrease in outer-sphere association constant. Since a neutral ligand is attacking in both cases, such a large variation in this constant for two ligands of rather similar structure is unlikely. Even allowing for the large relative errors of the adenine constants (±50%), the low value of k_1' for this ligand suggests the possibility of a change away from the rate-determining water-loss scheme described above.

When a ligand possesses more than one bonding group, it is known as a chelating agent and a dissociative mechanism implies that an intermediate exists with only a single metal ion binding site attached to the ligand. Before this site can be reoccupied by a water molecule, chelate ring closure occurs. If, however, repossession of the site is a faster process than ring closure, the rate-limiting step has shifted and the rate is no longer determined by the dissociative water-release rate constant. This mechanism has been termed sterically controlled substitution (SCS).[23]

If a chelate is formed at N(7) and the 6-amino group, ring closure may be the rate-determining step if it involves sufficient steric strain of the ligand. The rigidity of the aromatic pyrimidine ring may prevent the 6-amino group from binding as readily as it would had it been attached to a more flexible aliphatic chain. The result would be a smaller rate constant than that predicted from the dissociative mechanism, which is consistent with our findings.

The steric strain would be even greater if, as Reinert suggests, the nickel(II) was bound to N(9) and N(3). However, the formation of a five-membered chelate at N(7) and 6-amino group, though kinetically hindered, would be considerably more stable than a four-membered chelate at N(9) and N(3). The crystal structure study of Sletten[10] on the dinuclear 2:1 adenine–copper(II) complex shows metal ion binding at N(9) and N(3),

(21) K. Kustin and J. Swinehart in "Progress in Inorganic Chemistry, Vol. 13: Inorganic Reactions Mechanisms," J. Edwards, Ed., Wiley, New York, N. Y., p 107.

(22) M. Eigen and R. G. Wilkins, *Advan. Chem. Ser.*, **No. 49**, 55 (1965).

(23) K. Kustin, R. F. Pasternack, and E. M. Weinstock, *J. Amer. Chem. Soc.*, **88**, 4610 (1966).

but not to both these nitrogens on the same adenine molecule. Moreover, Ni^{2+} binding solely to N(9) or N(3) does not explain the low value of k_1'.

The possible existence of higher order complexes and linkage isomers formed in addition to the mono complex would make the relaxation expression derived for the adenine system a simplified, limiting case of a more complicated scheme. However, no information is available on the formation of such complexes in solution, and the limited amount of temperature-jump data does not permit a quantitative consideration of these factors. This complication might partly explain the relatively poor fit of observed to calculated relaxation times (*cf.* Table II). Nevertheless, the relatively low k_1' value would not be appreciably changed if the mechanism were incomplete in this way.

Higher order complexes and/or linkage isomers may be present in the nickel(II)–hypoxanthine (IIb) system. If the unresolvable, nonexponential effects for this ligand are the result of a multistep process, then this process may conceivably involve formation of more than one type of complex.

A Difference Spectrophotometric Method for the Determination of Critical Micelle Concentrations[1]

by Ashoka Ray and George Némethy*

The Rockefeller University, New York, New York 10021 *(Received April 18, 1970)*

Publication costs assisted by The National Science Foundation

A difference spectrophotometric method has been developed for the determination of critical micelle concentrations (cmc's). It is particularly useful for nonionic detergents. The method is based on observing the red shift, accompanying micelle formation, of the aromatic absorption band of a chromophore which is either part of the detergent molecule or added to the solution as an indicator. The cmc's so determined are in fair agreement with the values obtained by other available techniques. For detergents having very low cmc's, the more intense uv difference absorbance bands at still lower wavelengths are shown to be useful.

Introduction

Critical micelle concentrations (emc's) of nonionic detergents have most frequently been determined in the past by three different methods,[2] *viz.*, from the break in the static surface tension *vs.* logarithm of concentration curve, from the break in the turbidity *vs.* concentration curve, and by the iodine-solubilization technique.[3]

Since cmc's of nonionic detergents are generally much lower than those of ionic detergents of comparable hydrocarbon chain lengths, the time needed to reach equilibrium in each measurement of surface tension can be several hours.[4] The surface tension method thus becomes not only very time consuming, but may involve uncertainties[5] due to evaporation from the surface and stagnant layer formation.[6] The experimental difficulties involved in the precision determination of turbidities are well known,[7] though not insurmountable. The iodine-solubilization technique, although convenient, presumably involves some chemical reactions leading to the formation of hydrogen iodide[8-11] and therefore cannot be considered as too reliable.

(1) (a) This work was supported by Grants No. GB-5493 and GB-8410 of the National Science Foundation. (b) Presented in part before the Division of Colloid and Surface Chemistry at the 157th National Meeting of the American Chemical Society, Minneapolis, Minn., April 1969, and the IV Congresso Nazionale dell' Associazione Italiana di Chimica Fisica, Florence, Dec 1969.

(2) P. Becher in "Nonionic Surfactants," M. J. Schick, Ed., Marcel Dekker, New York, N. Y., 1967, p 478.

(3) S. Ross and J. P. Olivier, *J. Phys. Chem.*, **63**, 1671 (1959).

(4) P. H. Elworthy and C. B. MacFarlane, *J. Pharm. Pharmacol.*, **14**, 100T (1962).

(5) P. Mukerjee, *Advan. Colloid Interface Sci.*, **1**, 241 (1967).

(6) J. T. Davies and E. K. Rideal, "Interfacial Phenomena," Academic Press, New York, N. Y., 1961.

(7) P. H. Elworthy and C. B. MacFarlane, *J. Chem. Soc.*, 537 (1962).

(8) N. A. Allawala and S. Riegelman, *J. Pharm. Sci.*, **42**, 396 (1953).

(9) W. B. Hugo and J. M. Newton, *J. Pharm. Pharmacol.*, **15**, 731 (1963).

(10) P. G. Bartlett and W. Schmidt, *Appl. Microbiol.*, **5**, 355 (1957).

(11) T. Nakagawa in "Nonionic Surfactants," M. J. Schick, Ed., Marcel Dekker, New York, N. Y., 1967, p 588.

This paper reports the use of a difference spectrophotometric technique for the determination of cmc's of nonionic detergents. The method is rapid and has a precision of ±1%. It is based on the observation that the uv absorption of an aromatic chromophore, either built into the detergent molecules, such as in alkylphenoxy(polyethoxy)ethanols, or added as a third component of the solution, such as phenol used with alkyl polyethoxy ethanols, undergoes a red shift upon micelle formation in aqueous solution. The former class of detergents form micelles that are self-indicating, and thus provide suitable systems for studying the effects of various additives such as nonaqueous solvents,[12,13] salts,[14] etc., on them.

For detergents having no built-in aromatic chromophores, solubilized phenol was used as an indicator of micelle formation. In principle, the phenol-solubilization technique is similar to the past uses of water-soluble dyes[15,16] and iodine.[3] Like the latter methods, therefore, it is subject to the criticism that the addition of a third component may alter the structure and the stability of the micelles[11] in an undeterminable way, thereby making such methods less reliable. However, one advantage, possibly minor, is that the phenol molecule is much smaller than the dye molecules, and hence the effects may be smaller with phenol than with dyes. The same would be true for iodine, which is also small. However, the possibilities of chemical reactions[8-11] may render the use of iodine more objectionable than that of phenol.

The difference spectrophotometric technique has been extended to the determination of the cmc's of ionic detergents having built-in aromatic chromophores, such as alkylpyridinium halides, and should be applicable to alkyl benzenesulfonates and other similar detergents also. Similarly, the phenol-solubilization technique should, in principle, be applicable to ionic detergents having no intrinsic chromophores.

The uv absorption spectra of alkylphenoxy(polyethoxy)ethanols have been used in a somewhat different manner by Luck[17] and more recently by Gratzer and Beaven[18] for determining cmc's. Rehfeld[19] has recently determined the cmc of sodium dodecyl sulfate by a benzene-solubilization technique which is somewhat similar to the phenol technique presently described.

Experimental Section

A. Materials. Triton X-100 (OPE_{9-10}) and Triton X-102 (OPE_{12-13}) were supplied by the Rohm and Haas Co., and Igepal CO-630 (NPE_9) and Igepal CO-880 (NPE_{30}) were products of the General Aniline and Film Co. The samples were polydisperse with respect to the ethoxy chain lengths. The chain lengths, indicated above, represent mean values, as stated by the manufacturers.

The abbreviations OPE_{9-10} and OPE_{12-13} represent *p-tert*-octylphenoxy(polyethoxy)ethanols of mean ethoxy chain lengths of 9–10 and 12–13, respectively. Similarly, NPE_9 and NPE_{30} stand for *p-tert*-nonylphenoxy(polyethoxy)ethanols having mean polyethoxy chain lengths of 9 and 30, respectively.

The three homogeneous nonionic detergents, *n*-octyl-, *n*-decyl-, and *n*-dodecyl(hexaethoxy)ethanol (C_8E_6, $C_{10}E_6$, and $C_{12}E_6$), were highly pure samples obtained as kind gifts from Dr. J. M. Corkill.

Dodecylpyridinium bromide (DPB), a gift sample from Diversey (U.K.) Ltd., was quoted as homogeneous with respect to the alkyl chain length and was recrystallized from ether–acetone mixture before use.

Cetylpyridinium chloride (CPC) was of a practical grade obtained from Matheson Coleman and Bell.

Unless otherwise indicated, all detergents were used as obtained without further purification.

"Chromatoquality," reagent grade, ethylene glycol (Matheson Coleman and Bell) was used as obtained, without further purification.

B. Methods. 1. Uv Difference Spectrophotometry. (a) Formation of Self-Indicating Micelles. For the detergents having built-in aromatic chromophores, *viz.* alkylphenoxy(polyethoxy)ethanols and alkylpyridinium halides, the following experimental procedure was used.

Two carefully matched "split-compartment" mixing cuvettes[20] were placed in the reference and sample beams of a Cary 14 spectrophotometer (Figure 1). Each of these cuvettes consists of two compartments, A and B, with exactly equal path lengths, $l = 0.44$ cm. Appropriate solvent (1 ml) was placed in compartment A, and an exactly equal volume of a detergent solution of a known concentration, c_0, was placed in compartment B of each cell. The net difference absorbance is zero with such an arrangement, giving the base line (Figure 2). Next, the liquids in the two compartments of the *reference* cell were mixed thoroughly by sealing the top of the cell with parafilm and rocking the cell several times. For $c_0 \ll$ cmc, the subsequently observed difference absorbances were either zero or very small. However, as c_0 exceeded the cmc, the difference absorbance increased sharply. Figure 2 shows typical difference spectra obtained with an alkylphenoxy(polyethoxy)ethanol (NPE_{30}) at detergent concentrations well above the cmc. The first maximum in the difference spectrum appeared at 285–286 mμ for all the alkylphenoxy-

(12) A. Ray and G. Némethy, *J. Phys. Chem.*, **75**, 809 (1971).
(13) A. Ray and G. Némethy work in progress.
(14) A. Ray and G. Némethy, *Fed. Proc., Fed. Amer. Soc. Exp, Biol.*, **29**, 506 (1970).
(15) H. Lange, *Proc. Int. Congr. Surface Activ., 3rd*, **1**, 279 (1960).
(16) P. Becher, *J. Phys. Chem.*, **66**, 374 (1962).
(17) W. Luck, *Proc. Int. Congr. Surface Activ., 3rd*, **1**, 264 (1960).
(18) W. B. Gratzer and G. H. Beaven, *J. Phys. Chem.*, **73**, 2270 (1969).
(19) S. J. Rehfeld, *ibid.*, **74**, 117 (1970).
(20) J. A. Yankeelov, Jr., *Anal. Biochem.*, **6**, 287 (1963).

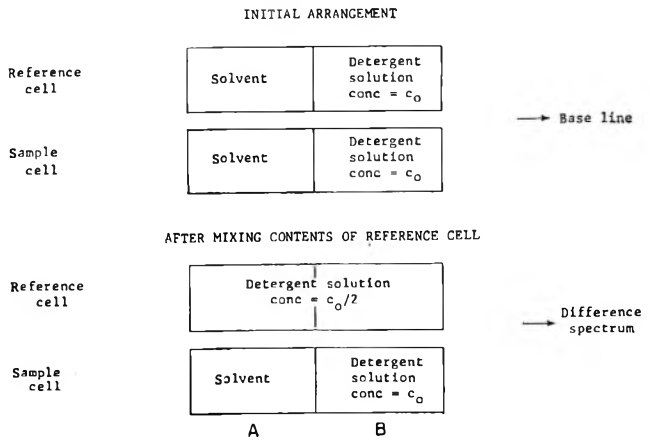

Figure 1. Schematic representation of the experimental arrangement used to obtain difference spectra with detergents forming "self-indicating" micelles.

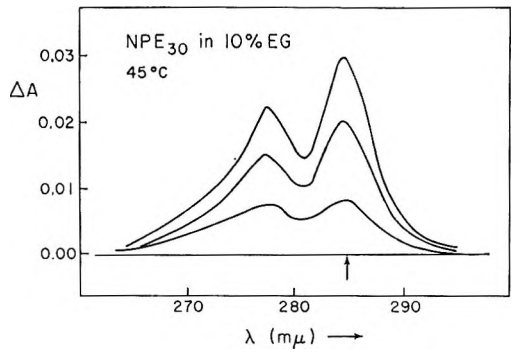

Figure 2. Difference absorption spectra of NPE_{30} in 10% ethylene glycol–water solution at 45°. The three spectra shown correspond to concentrations of 4.0×10^{-4}, 6.0×10^{-4}, and 7.1×10^{-4} M, respectively. The absorption at the difference peak at 285 mμ (indicated by arrow) was used to determine the cmc (*cf.* Figure 3a).

detergents. The difference absorbance, ΔA, at a wavelength near this maximum, when plotted as a function of the initial detergent concentration, c_0, shows a fairly sharp break at the cmc, followed by a linear rise (Figure 3a). We defined the cmc as the intercept of the straight line on the concentration axis, obtained by extrapolation. Although a better definition of the cmc might be the point at which two straight lines, joining the points well below and well above the cmc, intersect,[5] we preferred the former definition because the larger uncertainties in determining the small ΔA values below the cmc would have lowered the precision. Using the former definition, the cmc's could be reproduced within ±1% or better, but these were 8–12% lower than those obtained by the latter definition (Table I).

For the alkylpyridinium halides, DPB and CPC, the longest wavelength maxima appearing at 271.0 and 268.3 mμ, respectively, were utilized in the above manner to obtain the cmc's.

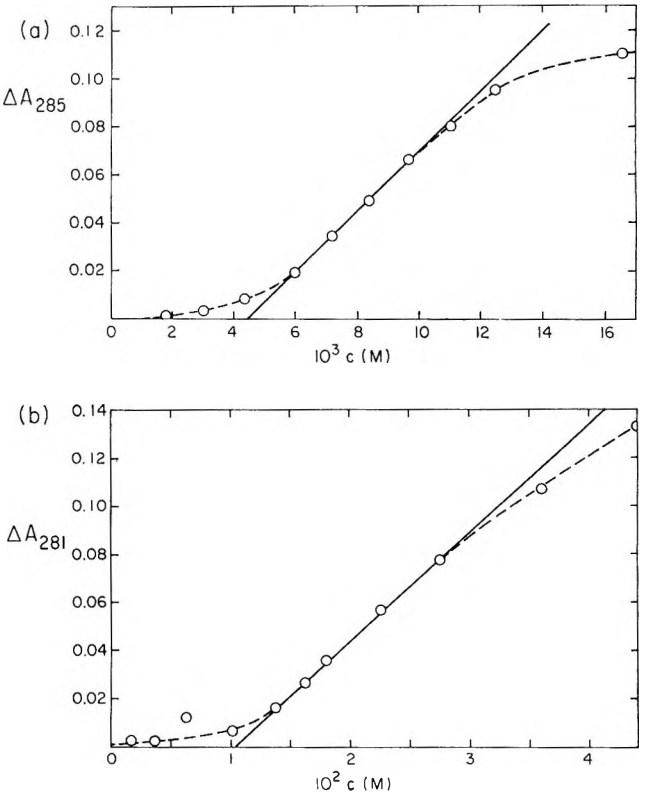

Figure 3. Example of the difference absorption plotted against detergent concentration to determine the cmc (defined as the abscissa intercept, see text): (a) for "self-indicating" micelle (NPE_{30} in 10% ethylene glycol–water at 45°) and (b) when phenol is used as an indicator (C_8E_6 in water at 25°).

(*b*) *Use of Phenol as an Indicator.* For detergents having no intrinsic chromophores, the above spectrophotometric technique was modified by dissolving phenol at a constant concentration of 1×10^{-3} M in the solvents in the A compartments, and mixing the liquids in the *sample* and not the reference cell. The spectrum prior to any mixing gives the base line as before. After mixing, a part of the phenol in the sample cell (5×10^{-4} M) is incorporated into the micelles, if present, and a difference spectrum, very similar to that observed for alkylphenoxy detergents, is obtained. The difference absorbance, ΔA, at the maximum, which occurs at 280–281 mμ, is plotted against $c_0/2$, where c_0 = initial detergent concentration in compartment B. The cmc is obtained as before from the intercept on the concentration axis.

All spectrophotometric measurements were carried out in a Cary 14 spectrophotometer equipped with a 0–0.1, 0.1–0.2 absorbance slide wire. The cell holders and the cell compartments were thermostated so that the temperatures of the solutions could be maintained constant within ±0.05°.

The detergent solutions were prepared by weight dilutions of stock solutions. The same pipet was used for delivering both the solvent and the detergent solution into the two compartments of the cuvettes.

Table I: Cmc Data in Water at 25°

Detergents	Cmc ($M \times 10^4$): Difference spectra[a] (mμ)	Cmc ($M \times 10^4$): Other techniques
Detergents with built-in aromatic chromophores		
OPE_{9-10}	2.64[b] (285.5)	2.66[d]
	2.64[b] (286.0)	2.59[e]
	2.40[c] (286.0)	2.56[f]
	2.68[b] (232.0)	
	2.40[c] (232.0)	
OPE_{12-13}	2.82[b] (286.0)	
	2.53[c] (286.0)	
NPE_9	0.459[c] (285.0)	0.56[g]
	0.459[c] (230.0)	
	0.459[c] (204.0)	
	0.454[c] (200.0)	
NPE_{30}	1.86[c] (285.0)	1.85[g]
		1.53[h]
		2.75[i]
DPB	117[c] (271.0)	121[j]
		114[k]
CPC	9.21[b] (268.3)	7.06[l]
	8.33[c] (268.3)	
Detergents with no built-in aromatic chromophores		
C_8E_6	104[c] (281.0)	99[m]
$C_{10}E_6$	8.5[c] (281.0)	9.0[m]
$C_{12}E_6$	0.83[c] (281.0)	0.87[m]

[a] Present work. Cmc's obtained for the same sample from measurements at various wavelengths indicated, as well as the use of different definitions of the cmc,[b,c] are shown. [b] Cmc defined from the intersection of two straight lines joining the points well below and well above the cmc, in the ΔA *vs.* c plots. [c] Cmc defined as the intercept on the concentration axis of the straight line joining the points above the cmc, in the ΔA *vs.* c plots (Figures 3a and 3b). [d] Uv spectrophotometry, this work. [e] Surface tension at 27.5°, this work. [f] Iodine-solubilization, ref 3. [g] Surface tension: M. J. Schick, S. M. Atlas, and F. R. Eirich, *J. Phys. Chem.*, **66**, 1326 (1962). [h] Iodine-solubilization, light-scattering: P. Becher, *J. Colloid Sci.*, **16**, 49 (1961). [i] Surface tension: L. Hsiao, H. N. Dunning, and P. B. Lorenz, *J. Phys. Chem.*, **60**, 657 (1956). [j] Uv spectrophotometry: P. Mukerjee and A. Ray, *ibid.*, **70**, 2150 (1966). [k] Conductometry: J. E. Adderson and H. Taylor, *J. Colloid Sci.*, **19**, 495 (1964). [l] Uv spectrophotometry: N. Sata and H. Sasaki, *Proc. Int. Congr. Surface Activ., 2nd*, **1**, 340 (1957). [m] Surface tension: ref 21.

2. Uv Absorption Spectrophotometry. The cmc of OPE_{9-10} was determined by a modified Gratzer and Beaven[18] method. Solutions of known detergent concentrations were prepared separately and their absorbances at 285.5 mμ were measured at 25°, using a 0.5-cm cell. These absorbances were then plotted against the detergent concentrations, and the cmc was determined from the intersection of the two straight lines joining the points below and above the cmc.

3. Surface Tension Measurements. Surface tensions of OPE_{9-10} and NPE_9 were measured using a Rosano surface tensiometer (Federal Pacific Electric Co., Newark, N. J.). The time allowed for equilibration varied from 1 to 2.5 hr, during which the solutions were kept covered with aluminum foil to minimize evaporation. The measurements were carried out at 27.5 ± 0.5°. The cmc's were determined from the breaks in the surface tension *vs.* logarithm of concentration curves.

Results and Discussion

When the particular experimental arrangements described in section *1* (*a*) are used with detergents forming self-indicating micelles, the following analysis can be made. Let c_0 = initial concentration of detergent in compartment B and l = path length of compartment A or B. After mixing in the reference cell, $c_0/2$ = final detergent concentration in both A and B of reference cell and $2l$ = path length of A + B. Therefore

$$\text{(stoichiometric concentration of detergent)} \times \text{(path length)} = c_0 l = \text{constant} \quad (1)$$

before and after mixing.

(*i*). When $c_0 \leqslant$ cmc, both cells should contain only monomers as the absorbing species after mixing in the reference cell, and hence no difference absorbance should be observed at all. This was found to be only approximately true, however. A small but definite difference absorbance always appeared below the cmc (Figure 3a), indicating possibly the existence of some premicellar aggregation.[5]

(*ii*). When cmc $< c_0 \leqslant$ 2cmc, no micelles should be present in the reference cell after mixing, since $c_0/2 \leqslant$ cmc. However, the sample cell contains detergent molecules in the micellar form at a concentration

$$c_m{}^s = c_0 - \text{cmc} \quad (2)$$

assuming that the change in free monomer concentration above the cmc is negligibly small. A difference absorbance, ΔA, is, therefore, observed in this concentration range

$$\Delta A = \Delta\epsilon(c_m{}^s)l = \Delta\epsilon(c_0 - \text{cmc})l \quad (3)$$

where $\Delta\epsilon$ is the difference in the extinction coefficients of the detergent monomer in aqueous solution and inside the micelle, and can be assumed to be constant. ΔA is a linear function of c_0 in this concentration range, as shown in Figure 3a.

(*iii*). When $c_0 >$ 2cmc, micelles are present in the sample cell in an effective path length l, as also in the reference cell (after mixing) in an effective path length $2l$. The concentration of micelles in the sample cell

is given, as before, by eq 2; that in the reference cell is given by

$$c_m^r = c_0/2 - \text{cmc} \quad (4)$$

Thus

$$\Delta A = \Delta\epsilon(c_m^s l - c_m^r(2l)) = \Delta\epsilon(\text{cmc})l = \text{constant} \quad (5)$$

The difference absorbance should ideally reach a maximal value at $c_0 = 2\text{cmc}$ and should stay constant with further increase in the detergent concentration. Figure 3a indicates that ΔA values tend to level off at $c_0 > 2\text{cmc}$, but just as the transition near the cmc occurs over a range of concentrations, so this leveling off is also gradual and not an abrupt one.

In the experiments described in section *1* (*b*), the difference absorbance, ΔA, results from a difference in the optical absorption of those molecules of the phenol which are incorporated into the micelles, after mixing in the sample cell, and that of an equivalent amount of phenol present in aqueous environment in the reference cell. As is evident from Figure 3b, very little phenol is removed from aqueous environment below the cmc. The subsequent rise in the observed ΔA shows that more and more phenol is incorporated into micelles, as the detergent concentration, $c_0/2$, is increased beyond the cmc. At very high detergent concentrations, a leveling of ΔA is observed. Presumably, this occurs when most of the phenol present in solution is contained in the micelles.

The cmc's of several nonionic and ionic detergents were determined by one of the two techniques described above. They are summarized and compared with the data obtained by other techniques in Table I. Molecular weights of OPE_{9-10} and OPE_{12-13} were assumed to be 624 and 756, respectively.

The cmc data for the three homogeneous pure nonionic detergents, C_8E_6, $C_{10}E_6$, and $C_{12}E_6$, obtained by the phenol solubilization method agree fairly well with the cmc's obtained by the surface tension method.[21] This seems to indicate that incorporation of phenol into the micelles does not alter strongly the cmc's of these detergents.

At least for C_8E_6, it is unlikely that more than one phenol molecule is incorporated into each micelle. The difference absorbance at constant phenol concentration (5×10^{-4} *M*) continues to increase (Figure 3b) even when the concentration of *micelles* exceeds that of phenol (assuming that the aggregation number of these micelles in the presence of phenol is about the same as in water,[22] *viz.*, 32). However, the possibility that more than one phenol molecule is incorporated into micelles

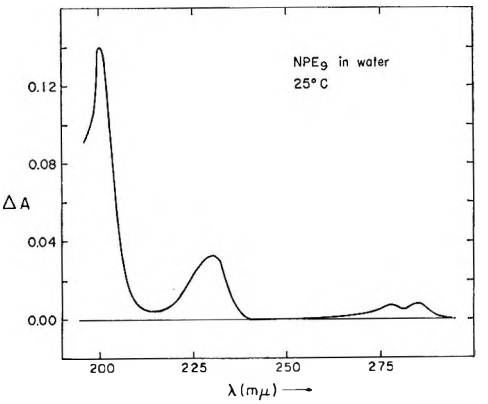

Figure 4. The difference absorption spectrum of NPE_9 in water at 25°, in the wavelength region 196–294 mμ. Concentration of NPE_9: $1.08 \times 10^{-4}M$.

of $C_{10}E_6$ and of $C_{12}E_6$ cannot be ruled out definitely, due to the much lower cmc (Table I) and the higher aggregation number.[23]

For alkylphenoxy(polyethoxy)ethanols having very low cmc's, the sensitivity of the present technique was considerably increased by using the difference absorbance bands at shorter wavelengths. Figure 4 illustrates the complete difference spectrum of NPE_9 in water at 25° in the wavelength region 196–294 mμ. The cmc's determined for this detergent using the various absorption bands are found to be in excellent agreement with each other (Table I). The 220–240 mμ difference absorption band was utilized for the determination of the cmc of OPE_{9-10} also. The cmc values obtained from ΔA measurements at 232 mμ (Table I) agree very well with the corresponding values obtained from ΔA measurements at longer wavelengths. However, the use of the shorter wavelengths is limited to solvents having low absorbances in these regions.

The shorter wavelength absorption bands can be useful in the phenol-solubilization method, too. This would allow the use of much lower phenol concentrations than used presently.

Acknowledgments. We wish to thank Miss Hilda Malodeczky for her competent technical assistance. We thank Dr. J. M. Corkill for his gift of highly pure detergents.

(21) J. M. Corkill, J. F. Goodman, and S. P. Harrold, *Trans. Faraday Soc.*, **60**, 202 (1964).

(22) J. M. Corkill, J. F. Goodman, and R. H. Ottewill, *ibid.*, **57**, 1627 (1961).

(23) R. R. Balmbra, J. S. Clunie, J. M. Corkill, and J. F. Goodman, *ibid.*, **58**, 1661 (1962); **60**, 979 (1964).

Micelle Formation by Nonionic Detergents in Water–Ethylene Glycol Mixtures[1]

by Ashoka Ray and George Némethy*

The Rockefeller University, New York, New York 10021 *(Received April 13, 1970)*

Publication costs assisted by The National Science Foundation

The critical micelle concentrations (cmc's) of several *p,tert*-alkyl phenoxy polyethoxy ethanols, with ethoxy chain lengths ranging from 9–10 to 30 residues, were studied in water–ethylene glycol mixtures over the concentration range from 0 to 60% ethylene glycol (by volume) at 25, 35, and 45°. The cmc increases with increasing glycol content. In water, the cmc decreases with increasing temperature, and a minimum appears to be approached at elevated temperatures. This is in agreement with what is expected for the hydrophobic interactions of the nonpolar tail of the detergent molecules. However, an additional effect, presumably due to partial changes in the solvent environment of the polar head of the molecule, modifies the enthalpy and entropy of micelle formation. In solutions containing ethylene glycol, the enthalpy of micelle formation becomes more negative, and the corresponding entropy becomes less positive, indicating that simple energetic interactions begin to predominate over hydrophobic effects. There is evidence for preferential solvation of the detergent molecules by ethylene glycol in solutions of low glycol content.

Introduction

In the study of the conformational stability of proteins, denaturation induced by solvent changes helps to elucidate the role of various kinds of noncovalent interactions. The effects of powerful denaturants, *e.g.*, urea and guanidinium salts, upon both proteins and model compounds have been studied extensively.[2] Much less information is available on the effects of weak denaturants,[2] although their studies may supply crucial information for the detailed understanding of the stabilization of conformations and of their changes. Distinctions between the effects of interactions which are comparable in strength may be swamped out by strong denaturants producing a general unfolding. On the other hand, such effects may be separated when weak denaturants are used.

Ethylene glycol is particularly interesting in this respect since it is one of the weakest organic denaturants. At moderate concentrations, even as much as 50%, it does not seem to have an effect on proteins.[2,3] It has been used, therefore, as a solvent perturbant in spectroscopic studies.[4] It can cause incomplete unfolding in the pure state or in 80–90% solution.[3,5] It has been shown that the solubility of hydrocarbons increases with glycol content in ethylene glycol–water mixtures, but that of peptide groups decreases.[6]

One can expect that ethylene glycol should be a very weak denaturant, due to many similarities with water: relative to monohydric alcohols and similar compounds, its molecules have the smallest ratio of nonpolar to polar components. The molecule is small, and presumably can form hydrogen-bonded networks, similar in nature to those in water, but considerably different in details of structure. Some of the physical properties[7] support this hypothesis very strongly: 1-propanol and ethylene glycol are very close in molecular weights, yet the latter has much higher melting and boiling points, heat of melting, and viscosity. Because of these similarities between water and ethylene glycol, the study of the latter is also important from the point of view of a better understanding of the structure of liquids, and of water in particular.

In order to elucidate the effect of ethylene glycol upon noncovalent interactions in proteins, it is useful to study the behavior of model compounds, where some of these interactions can be singled out. For this reason, the association of detergents into large micellar aggregates is of particular interest. In the present work, nonionic detergents were studied, in order to eliminate electrostatic effects and their dependence on local solvent structure around the micelle. The micellization of nonionic detergents, particularly alkyl- and alkylphenoxy(polyethoxy)alcohols, has been studied extensively,[8–18] but almost exclusively in pure water. Stud-

(1) (a) This work was supported by Grants No. GB-5493 and GB-8410 of the National Science Foundation. (b) Presented in part before the Division of Colloid and Surface Chemistry at the 157th National Meeting of the American Chemical Society, Minneapolis, Minn., April 1969, and the IV Congresso Nazionale dell'Associazione Italiana di Chimica Fisica, Florence, Dec 1969.

(2) Reviewed by C. Tanford, *Advan. Protein Chem.*, **23**, 121 (1968).

(3) C. Tanford, C. E. Buckley III, P. K. De, and E. P. Lively *J. Biol. Chem.*, **237**, 1168 (1962).

(4) T. T. Herskovitz and M. Laskowski, Jr., *ibid.*, **237**, 2481 (1962).

(5) M. L. Kientz and C. C. Bigelow, *Biochemistry*, **5**, 3494 (1966).

(6) Y. Nozaki and C. Tanford, *J. Biol. Chem.*, **240**, 3568 (1965).

(7) "Handbook of Chemistry and Physics," 50th ed, The Chemical Rubber Co., Cleveland, Ohio 1969.

(8) P. Becher, in "Nonionic Surfactants, M. J. Schick, Ed., Marcel Dekker, New York, N.Y., 1967, p 478.

ies of the effects of organic solvents are much less numerous.[19-21] Thus it seemed worthwhile to investigate the behavior of some of these detergents in water–ethylene glycol mixtures.

The nonionic detergents chosen for our study were *p,tert*-alkylphenoxy(polyethoxy)ethanols, having the general formula $C_mH_{2m+1}C_6H_4(OC_2H_4)_nOH$. Throughout this paper, they are abbreviated as RPE_n, where R = O (for *tert*-octyl), and N (for *tert*-nonyl), and n represents the mean ethoxy chain length, as these samples were polydisperse with respect to the latter. Gibbons[22] has pointed out the important distinction between "polydispersity" and "heterogeneity." On this basis, Becher[8] has argued that a great deal of useful information can be obtained from the study of the commercially available nonionic detergents of the (polyethoxy)ethanol type, which are polydisperse but not heterogeneous. This is particularly true when $n > 7$, as indicated[13] by the variation of cmc as a function of n. We, therefore, feel that the general thermodynamic conclusions made in this paper may be expected to be largely true for monodisperse materials as well, especially since n ranged from 9–10 to 30 in this work.

Experimental Section

The three detergents used for most of this work were Triton X-100 (OPE_{9-10}) and Triton X-102 (OPE_{12-13}), supplied by the Rohm and Haas Co., and Igepal CO-880 (NPE_{30}), produced by the General Aniline and Film Co. Some measurements in water were obtained with Triton X-305 (OPE_{30}), also supplied by the Rohm and Haas Co.

Ethylene glycol (Matheson Coleman and Bell, "Chromatoquality reagent grade") was used in all spectrophotometric measurements. It was found to be free of any impurities absorbing in the uv wavelength regions of interest, and was used without further purification.

The cmc's of the detergents in water and water–ethylene glycol mixtures were determined at three different temperatures, *viz.*, 25, 35, and 45°, by a difference spectrophotometric technique described in detail elsewhere.[23]

Results

The cmc data for the four nonionic detergents, OPE_{9-10}, OPE_{12-13}, OPE_{30}, and NPE_{30}, in water at 25, 35, and 45°, are summarized in Table I. The cmc's of OPE_{9-10}, OPE_{12-13}, and NPE_{30} in water–ethylene glycol mixtures at the corresponding temperatures are presented in Table II.

With all detergents, the cmc increases strongly at high ethylene glycol concentrations (Figure 1). The measurements were limited to 60% ethylene glycol (by volume) due to limitations of the experimental technique caused by high absorbances at detergent concentrations above about 10^{-2} *M*. The behavior of the detergents at higher glycol concentrations is not known. However, micelles were observed in several polar organic solvents,[24] including ethylene glycol,[25] in contrast to monohydric alcohols, in which no micelles occur in aqueous solutions containing more than 25–40% alcohol, depending upon the detergent.[20,26,27]

Table I: Cmc's and Thermodynamic Parameters of Micelle Formation for *p,tert*-Alkylphenoxy(polyethoxy)ethanols in Water

Temp, °C	Cmc, mol/l × 10^4	$\Delta G°$, kcal/mol	$\Delta H°$, kcal/mol	$\Delta S°$, cal/deg mol
		OPE_{9-10}		
25	2.40	−7.31	+2.1	+32
35	2.21	−7.61	+0.9	+28
45	2.17	−7.87	−0.0	+24
		OPE_{12-13}		
25	2.53	−7.29	+2.1	+32
35	2.38	−7.57	−0.0	+24
45	2.51	−7.78	−2.0	+18
		OPE_{30}		
25	7.73	−6.62	+4.3	+37
35	6.49	−6.95	+2.1	+29
45	6.16	−7.21	−0.0	+23
		NPE_{30}		
25	1.83	−7.48	+4.0	+38
35	1.55	−7.83	+2.1	+32
45	1.46	−8.12	+0.3	+26

(9) J. M. Corkill, J. F. Goodman, and R. H. Ottewil, *Trans. Faraday Soc.*, **57**, 1627 (1961).

(10) R. R. Balmbra, J. S. Clunie, J. M. Corkill, and J. F. Goodman, *ibid.*, **58**, 1661 (1962).

(11) M. J. Schick, S. M. Atlas, and F. R. Eirich, *J. Phys. Chem.*, **66**, 1326 (1962).

(12) M. J. Schick, *ibid.*, **67**, 1796 (1963).

(13) E. H. Crook, D. B. Fordyce, and G. F. Trebbi, *ibid.*, **67**, 1987 (1963).

(14) P. H. Elworthy and C. B. MacFarlane, *J. Chem. Soc.*, 537 (1962); 907 (1963)

(15) J. M. Corkill, J. F. Goodman, and S. P. Harrold, *Trans. Faraday Soc.*, **60**, 202 (1964).

(16) R. R. Balmbra, J. S. Clunie, J. M. Corkill, and J. F. Goodman, *ibid.*, **60**, 979 (1964).

(17) J. M. Corkill, J. F. Goodman, and J. R. Tate, *ibid.*, **60**, 996 (1964).

(18) E. H. Crook, G. F. Trebbi, and D. B. Fordyce, *J. Phys. Chem.*, **68**, 3592 (1964).

(19) M. J. Schick and A. H. Gilbert, *J. Colloid Sci.*, **20**, 464 (1965).

(20) P. Becher, *ibid.*, **20**, 728 (1965).

(21) W. B. Gratzer and G. H. Beaven, *J. Phys. Chem.*, **73**, 2270 (1969).

(22) R. A. Gibbons, *Nature*, **200**, 665 (1963).

(23) A. Ray and G. Némethy, *J. Phys. Chem.*, **75**, 804 (1971).

(24) A. Ray, submitted for publication.

(25) A. Ray, *J. Amer. Chem. Soc.*, **91**, 6511 (1969).

(26) A. F. H. Ward, *Proc. Roy. Soc. Ser. A*, **176**, 412 (1940).

(27) B. D. Flockhart, *J. Colloid Sci.*, **12**, 557 (1957).

Table II: Critical Micelle Concentrations of *p,tert*-Alkylphenoxy(polyethoxy)ethanols in Water–Ethylene Glycol Mixtures

Solvent, vol % EG	Cmc, mol/l. × 10^4 — OPE_{9-10} 25°	35°	45°	OPE_{12-13} 25°	35°	45°	Solvent, vol % EG	Cmc, mol/l. × 10^4 — NPE_{30} 25°	35°	45°
0.0	2.40	2.21	2.17	2.53	2.38	2.51	0.0	1.83	1.55	1.46
10.0	2.92	3.10	3.26	3.30	3.42	3.67	10.2	2.38	2.24	2.18
							10.6	2.37	2.31	2.33
							13.3	2.60	2.48	2.44
							13.9	2.64	2.57	2.52
							14.7	2.78	2.64	2.59
15.0	3.36	3.83	4.37	3.86	3.98	4.74	15.1	2.95	2.75	2.62
							15.9	2.85	2.83	2.81
20.0	3.89	4.54	5.16	4.49	4.86	5.70	19.8	3.30	3.38	3.56
							30.0	5.01	5.58	6.72
40.0	9.91	12.1	14.1	11.0	13.2	15.6	39.2	8.09	10.1	11.2
50.0	17.6	21.6	28.3	19.6	24.0	30.0	47.2	14.1	16.4	18.1
60.0	33.9	41.4	54.2	35.9	39.7	47.0	58.9	31.3	35.4	39.4

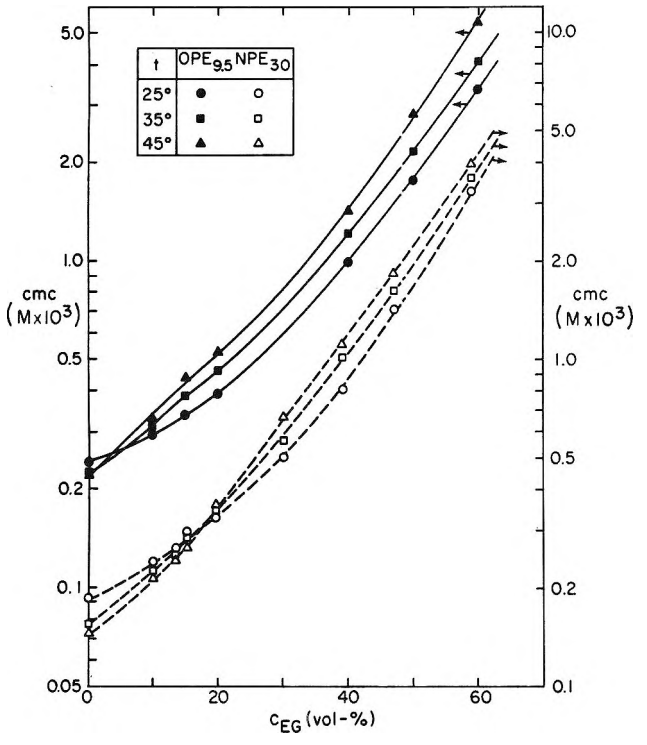

Figure 1. The cmc of OPE_{9-10} and NPE_{30} as a function of ethylene glycol content in water–ethylene glycol mixtures. Data for OPE_{12-13} resemble closely those of OPE_{9-10} and are not shown to avoid overcrowding of the graph.

Our data for OPE_{9-10} at 25° (Table II) can be compared with those obtained for the same detergent by Gratzer and Beaven.[21] While the cmc's measured by them are consistently higher than those reported here, the relative increments upon adding ethylene glycol agree closely for the two sets of measurements.

Assuming aggregation numbers to be 20–100 or more, a simple limiting expression for the free energy of micelle formation can be written[15,28]

$$\Delta G^\circ = RT \ln (\text{cmc}) \qquad (1)$$

The free energies so obtained are summarized in Tables I and IV. The difference absorption spectra provide some indirect evidence that the aggregation numbers of the micelles are not changed very strongly even at the highest glycol concentrations used here. The sharpness of the transitions of the curves of ΔA *vs.* detergent concentration at the cmc does not change with increasing glycol content. Furthermore, the slope of these curves above the cmc decreases only by 25–30% for the various detergents between water and 50% glycol. This change can be accounted for by the red shift and the increased extinction coefficient of the *monomeric* detergent molecules in the mixed solvent, as indicated by a comparison with spectral changes of model compounds in water–ethylene glycol mixtures.[29]

Enthalpies of micelle formation were obtained from the temperature variation of the cmc, by using a Clausius–Clapeyron type of equation[15,18,30]

$$\Delta H^\circ = -RT^2[\partial \ln (\text{cmc})/\partial T]_p \qquad (2)$$

Since ΔH° is not constant with respect to temperature, the data shown in Tables I, III, and IV were obtained by fitting quadratic functions of the form

$$\ln (\text{cmc}) = a/T^2 + b/T + c \qquad (3)$$

to the observed data and subsequent application of eq 2.

The enthalpies become more negative at high temperatures. Similar behavior is shown by monodisperse OPE_n's,[18] where n equals 1 to 10.

The entropies of micelle formation, ΔS°, were calculated from the ΔG° and ΔH° values, and are summarized in Tables I and IV.

(28) D. G. Hall and B. A. Pethica in Nonionic Surfactants," M. J. Schick, Ed., Marcel Dekker, New York, N. Y., 1967, p 516.

(29) G. Némethy and A. Ray, unpublished work.

(30) G. Stainsby and A. E. Alexander, *Trans. Faraday Soc.*, **46**, 587 (1950).

Table III: Enthalpies of Micelle Formation for *p,tert*-Alkylphenoxy(polyethoxy)ethanols in Water–Ethylene Glycol Mixtures[a] (kcal/mol)

Solvent, vol % EG	$\Delta H°$ OPE_{9-10} 25°	35°	45°	$\Delta H°$ OPE_{12-13} 25°	35°	45°	Solvent, vol % EG	$\Delta H°$ NPE_{30} 25°	35°	45°
0.0	2.1	0.9	−0.2	2.1	−0.0	−2.0	0.0	4.0	2.1	0.3
10.0	−1.1	−1.0	−0.9	−0.3	−1.0	−1.7	10.2	1.4	0.8	0.2
15.0	−2.3	−2.5	−2.7	−0.9	−2.0	−4.7	15.9	0.1	0.1	0.1
20.0	−3.0	−2.7	−2.3	−0.6	−2.3	−3.9	19.8	−0.1	−0.7	−1.3
							30.0	−1.1	−2.8	−4.4
40.0	−4.0	−3.3	−2.7	−3.4	−3.3	−3.2	39.2	−5.1	−3.0	−1.0
50.0	−2.9	−4.5	−6.0	−3.4	−4.0	−4.7	47.2	−3.2	−2.3	−1.5
60.0	−2.8	−4.5	−6.0	−1.0	−2.5	−4.0	58.9	−2.3	−2.2	−2.0

[a] Based on an assumed ±1% error in the cmc data, the uncertainty of the $\Delta H°$ values is estimated as ±0.2 kcal/mol at 35° and ±0.8 kcal/mol at 25 and 45°, excepting at 60%, where the errors may be considerably larger.

Table IV: Thermodynamic Parameters of Micelle Formation at 35° for *p,tert*-Alkylphenoxy(polyethoxy)ethanols in Water–Ethylene Glycol Mixtures[a]

Solvent, vol % EG	$\Delta G°$, kcal/mol	$\Delta H°$, kcal/mol	$\Delta S°$, cal/deg mol
	OPE_{9-10}		
0	−7.61	+0.9	+28
10	−7.36	−1.0	+21
15	−7.21	−2.5	+15
20	−7.07	−2.7	+14
40	−6.36	−3.3	+10
50	−5.94	−4.5	+5
	OPE_{12-13}		
0	−7.57	−0.0	+25
10	−7.30	−1.0	+20
15	−7.18	−2.0	+17
20	−7.03	−2.3	+15
40	−6.31	−3.3	+10
50	−5.88	−4.0	+6
	NPE_{30}		
0	−7.83	+2.1	+32
10.2	−7.55	+0.8	+27
15.9	−7.38	−0.1	+24
19.8	−7.25	−0.7	+21
39.2	−6.47	−3.0	+12
47.2	−6.12	−2.3	+12

[a] Estimated uncertainties are ±0.01 kcal/mol in $\Delta G°$, ±0.2 kcal/mol in $\Delta H°$, ±0.7 cal/deg mol in $\Delta S°$. No data are shown for 60% solutions because of much larger possible errors.

Discussion

A. Micelle Formation in Water. In pure water at low temperatures, the cmc's of all four detergents decrease with increasing temperature, corresponding to a positive enthalpy of micelle formation (Table I). Similar behavior has been observed by Corkill, *et al.*,[15] in monodisperse, and by Schick[12] in molecularly distilled alkyl(polyethoxy)ethanols, having ethoxy chain lengths ranging from 3 to 30, and by Crook, *et al.*,[18] in monodisperse OPE_n's, with n = 5 to 10. The sign of $\Delta H°$ in all these cases corresponds to that expected for stabilization of the micelle by hydrophobic interactions. The important difference between the purely alkyl and the alkylphenoxy compounds is that the cmc's of the former continue to decrease at the highest temperatures studied, *viz.* 45[15] and 55°,[12] whereas those of $OPE_{6\text{ to }10}$[18] show minima in the range 45–50°. For $OPE_{1\text{ to }5}$,[18] the minima in the cmc *vs.* temperature plots occur or seem to be approached at still lower temperatures, *viz* 15–38°. Thus the position of the cmc minimum is a rapidly varying function of the ethoxy chain length in the series OPE_n's, when n = 1 to 6, and is relatively independent of n, when n = 6 to 10. In the present work also, the cmc minima ($\Delta H°$ = 0) for OPE_{9-10}, OPE_{30}, and NPE_{30} appear to be around 45°, thus being almost independent of n, as well as of the alkyl chain length, m. OPE_{12-13}, however, shows a minimum at a somewhat lower temperature, which might be due to the presence of a relatively high concentration of lower ethoxy chain length components in this detergent sample.

The enthalpies of micelle formation, as determined from the temperature variation of the cmc's, are positive and independent of temperature for the alkyl(polyethoxy)ethanols,[12,15] but are found to vary with temperature for the alkylphenoxy derivatives, becoming more negative as the temperature increases[18] (Table I). This is not unexpected, because according to theory,[31] the strength of hydrophobic interactions should increase with a rise in temperature up to a certain temperature (about 55° for aliphatic and about 18° for aromatic hydrocarbons) and decrease at higher temperatures. The temperatures of observed minima are consistent with that for a hydrocarbon chain composed of both an aliphatic and an aromatic part. However, the dependence upon the ethoxy (EO) chain length, n (n = 1–6), of both the location of the minimum in cmc and the magnitude of the enthalpy indicates that

(31) G. Némethy and H. A. Scheraga, *J. Phys. Chem.*, 66, 1773 (1962).

the EO chain must contribute to the enthalpy of micelle formation as well. The shift of the minimum in cmc with increase in n to higher temperatures for n = 1–6 could be explained by assuming that there is considerable desolvation of the first six ethoxy groups of the EO chain upon micelle formation, presumably with the establishment of alkyl–alkyl contacts between EO chains, *i.e.*, the formation of additional hydrophobic interactions. The failure to observe such minima in the alkyl derivatives could be due to the fact that measurements were not extended to sufficiently high temperatures. This conclusion is supported by the observations of Corkill, *et al.*,[17] that the heats of micellization of monodisperse alkyl(polyethoxy)ethanols, determined calorimetrically and hence more accurate, do depend on the temperature, becoming less positive at the higher temperature. By extrapolating these enthalpy values to $\Delta H^\circ = 0$, the cmc minima are expected to occur in the range 70–90° for these detergents.

For each of the four detergents studied by us in water, the free energy of micelle formation, ΔG°, becomes more negative, and the entropy of micelle formation, ΔS°, becomes less positive, as the temperature is increased (Table I). This is consistent with the results obtained for the monodisperse nonionic detergents in water.[12,15,18]

The free energy, enthalpy, and entropy contribution of the hydrocarbon moiety of the detergent can be estimated from the theory of hydrophobic interactions.[31] By subtracting these values from the experimental ones, one should obtain a consistent set of thermodynamic parameters for the contributions of the EO chain, if additivity holds, and the simple concept of desolvation of EO chains with the establishment of additional hydrophobic contacts between the ethylene groups in the EO chains on the micelle is true. This, however, was not the case for the data reported here, and for those of Crook, *et al.*,[18] for OPE_n's with n = 1 to 10. In the latter data, the free energy increments per EO group, $\Delta(\Delta G^\circ)_n = \Delta G^\circ(n) - \Delta G^\circ(n-1)$, and the analogous $\Delta(\Delta H^\circ)_n$ and $\Delta(\Delta S^\circ)_n$ are positive at low temperatures. The increments become smaller for larger n's and at high temperatures, and even are negative in some cases. For the transfer of hydrogen-bonding groups from water to a nonpolar environment, all three thermodynamic parameters are positive, with magnitudes decreasing at higher temperatures.[31–33] Thus the increments calculated for the data of Crook, *et al.*,[18] and the data presented here can be interpreted by postulating that the EO groups are *partially* transferred from the fully aqueous to a less polar environment. An incomplete transfer is not unexpected since there must be a considerable extent of favorable interaction between water and the polyethoxy chain on the micelle, so that the latter is kept in solution. This conclusion is supported by the observation that the ratio $\Delta(\Delta H^\circ)/\Delta(\Delta S^\circ)$ for micellization is much smaller than the corresponding ratio for the transfer of alcohols from water to a hydrocarbon.[34]

Further, $\Delta(\Delta G^\circ)_n$ is nearly constant from n = 2 to 6 at all except the highest temperatures,[18] having a value of about 0.18 kcal/mol, for $t < 50°$. Above n = 6, the increment sharply drops to an average of about 0.04 kcal/mol, and is nearly constant up to n = 10. The latter value is comparable to the value, 0.035 kcal/mol, obtained by us from the difference in ΔG°'s for OPE_{9-10} and OPE_{30}. Similar but much less marked breaks occur[18] in the increments of ΔH° and ΔS° at n = 6. The marked difference between the behavior of the first six EO groups and subsequent ones can be explained, as stated earlier, if one assumes that the first EO groups, near the nonpolar core of the micelle, lose some of their water of hydration, presumably due to the need for close packing of the nonpolar tails. In longer chains, the EO groups beyond the sixth one are located sufficiently far from each other so that their local environment is changed very little compared to that for the monomer.

B. Micelle Formation in Ethylene Glycol–Water Mixtures. The cmc of all three detergents, OPE_{9-10}, OPE_{12-13}, and NPE_{30}, is raised considerably by the presence of ethylene glycol (Table II and Figure 1) and hence the free energy of micelle formation, ΔG°, becomes less negative (Table IV). While the effect is much smaller than that of strong protein denaturing agents such as urea or guanidinium salts,[20] the cmc is raised several-fold in the solutions studied here. The increase is larger than for ionic detergents.[35,36] This might appear surprising in view of the weakness of ethylene glycol as a protein denaturant,[2,3] since much higher concentrations are required to disrupt interactions in most proteins studied. This difference could arise because in the micelles considered here, the main role of ethylene glycol presumably consists of the increased solubilization of the nonpolar chains of the detergents, *i.e.*, a disruption of hydrophobic interactions in the micelle. From the discussion of chain length effects (section *A*), one may conclude that there is little change in the solvation state of the polyethoxy moiety in water, beyond the first six ethoxy groups, and even less change is expected in the mixed water–glycol solvent. In contrast, the unfolding of proteins requires the disruption of other noncovalent interactions as well, some of which may be more resistant to the influence of ethylene glycol.

(32) G. Némethy and H. A. Scheraga, *J. Chem. Phys.*, **36**, 3401 (1962).

(33) The transfer of polar compounds, *e.g.*, alcohols, from water to a nonpolar solvent involves both the transfer of nonpolar groups, which is a "hydrophobic effect," and the desolvation of the hydrogen-bonded polar group, resulting in a high positive enthalpy.[34]

(34) N. Laiken and G. Némethy, *J. Phys. Chem.*, **74**, 3501 (1970).

(35) M. F. Emerson, Ph.D. Dissertation, Washington University, St. Louis, Mo., 1966.

(36) A. Ray, unpublished data, 1966.

When ln (cmc) is plotted against the concentration of ethylene glycol of the solution, the slope $\partial \ln (\text{cmc})/\partial c_{EG}$ at 25° is seen to vary more strongly at low glycol concentrations (Figure 1). Above about 20% glycol, the slope is very similar for all three detergents studied and at all three temperatures. Apparently, the effect of high glycol concentrations is similar on the three detergents. This supports the contention just made, *viz.*, that the main effect of glycol is on the solubility behavior of the nonpolar part of the detergent.

The difference in the temperature dependence between water and solutions containing large amounts of glycol is striking (Figure 2). While micelle formation is endothermic in water, at least at low temperatures (*cf.* section *A*), the addition of ethylene glycol causes $\Delta H°$ to decrease and micelle formation becomes exothermic at glycol concentrations above about 5–16% (Table III). The glycol concentration corresponding to athermal formation of micelles obviously depends on the extent of endothermicity in pure water.

The entropy of micelle formation, $\Delta S°$, which has large positive values in water, becomes less and less positive as the ethylene glycol content is increased (Table IV). The net decrease in entropy, in going from pure water to about 50% ethylene glycol at 35°, is about the same (19–23 cal/deg mol) for the three detergents within the limits of the experimental error. Thus as the glycol concentration increases, aggregation of the nonpolar chains is increasingly governed by the energy difference between the interactions of hydrocarbon groups with each other in the micelle and with the solvent, respectively, instead of the entropy-directed hydrophobic interactions in water. The decrease of Δc_p in the mixed solvent as compared to that in water indicates the same thing.

The thermodynamic parameters were obtained by curve-fitting to measurements at only three temperatures, resulting in an uncertainty in $\Delta H°$ and $\Delta S°$ which is too large for an accurate analysis of the thermodynamics of interactions with ethylene glycol (Table III). Nevertheless, some trends are obvious, especially in the values for 35° (Table IV) for which the errors are much smaller. Both $\Delta H°$ and $\Delta S°$ change more rapidly with glycol content between 0 and 20–30% than at higher glycol concentrations. Such a change also was seen in the ln (cmc) curves, discussed above. This behavior can be explained in terms of differential solvation.[37] Since glycol–hydrocarbon interactions are more favorable than water–hydrocarbon interactions, it can be expected that, at relatively low glycol concentrations, the hydrocarbon chains of the detergent monomers are preferentially interacting with glycol, *i.e.*, the local concentrations of glycol molecules near the solute monomers exceed the average solvent composition. The local composition of the solvent, therefore, changes more rapidly than the stoichiometric composition. This causes a large change in the thermodynamic

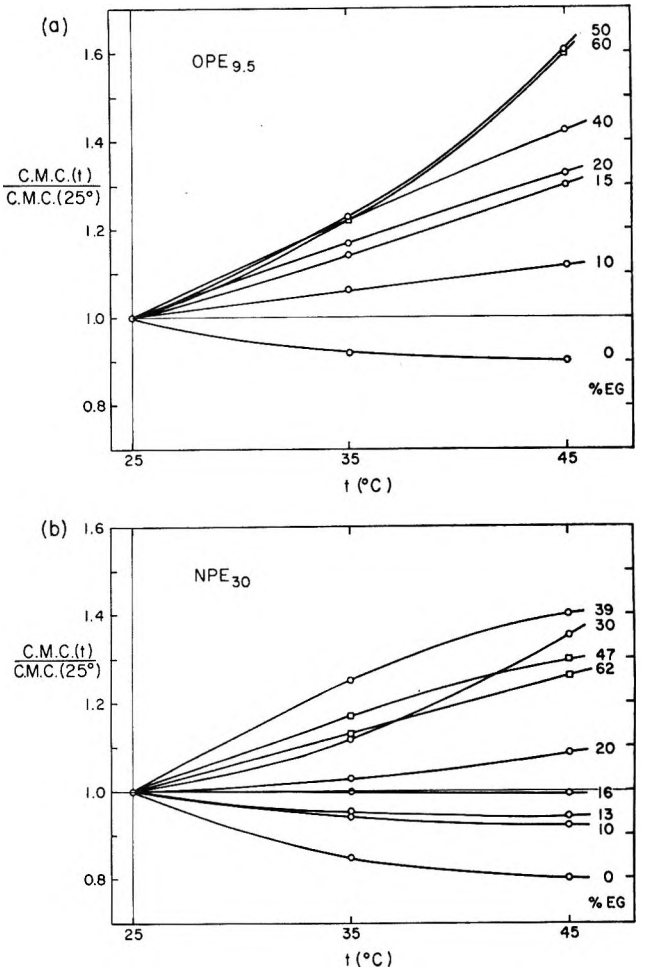

Figure 2. The variation of the relative cmc, cmc(t)/cmc(25°), with temperature (t) at different ethylene glycol concentrations (given as volume %) for (a) OPE_{9-10} and (b) NPE_{30}.

parameters of micelle formation with respect to glycol content. On the other hand, when the overall glycol content increases further, the extent of relative preferential solvation, *i.e.*, the difference between the bulk and the local composition, becomes smaller, and hence the thermodynamic parameters of micelle formation also change more slowly. Preferential solvation has also been invoked by Timasheff and Inoue[38] in protein–solvent interactions.

The interaction of the polyethoxy chain with the solvent may be complex. As is well known,[12] the ether oxygen atoms are involved in hydrogen bonding with water in aqueous solution. On the other hand, the

(37) As pointed out by a referee, nonuniform changes of the thermodynamic parameters with solvent composition could arise also from the existence of cooperative interactions between solvent molecules in the mixed solvent. Since one of the causes of preferential solvation may be the presence of cooperative solvent structural changes (in addition to the simple effect of the differences between solvent–solute interaction energies), the two explanations are not necessarily exclusive of each other. An unambiguous interpretation would require an understanding of the details of ethylene glycol–water interactions, which presumably involve strong structural changes of the solvent medium.

(38) S. N. Timasheff and H. Inoue, *Biochemistry*, 7, 2501 (1968).

ethylene groups, in analogy with other alkyl groups, may be expected to increase the structural order in the surrounding water. Studies of molecular models indicate that the formation of a hydrogen-bonded network of water molecules next to the ethylene groups may be compatible with hydrogen bonding to the ether oxygens. The geometry of the polyethoxy chain is also compatible with the existence of several favorable interactions with properly oriented ethylene glycol molecules, *viz.*, hydrogen bonds between the OH of the glycol and the ether oxygen of the detergent molecule and van der Waals interactions between the C_2H_4 groups can be formed simultaneously.

In a recent theoretical study of dilute solutions of monohydric alcohols in water,[34] based on a model of water structure,[32,39] it was shown that the transfer of the hydroxyl group of an alcohol from water to a nonpolar medium is accompanied by large changes of both enthalpy and entropy, with the former predominating. This indicates qualitatively the source of the relatively large changes in enthalpy and entropy of micellization when the composition of the water–ethylene glycol mixture is changed. An extension of the model to glycols should be possible.

Since the difference spectra observed[23] correspond to the shift of the absorption band accompanying the transfer of an aromatic group from aqueous to nonpolar medium, an analysis of the spectra and their changes may provide information both on the local structure of the micelle near the aromatic groups incorporated,[29] and, when phenol is used as an indicator, on the partition equilibrium of phenol between the micelles and the surrounding medium A systematic study of the uv spectra of phenol and other aromatic compounds in aqueous and nonaqueous solvent mixtures is now in progress.

Acknowledgment. We wish to thank Miss Hilda Malodeczky for her competent technical assistance.

(39) G. Némethy and H. A. Scheraga, *J. Chem. Phys.*, **36**, 3382 (1962).

Effects of the Urea–Guanidinium Class of Protein Denaturants on Water Structure: Heats of Solution and Proton Chemical Shift Studies

by S. Subramanian, T. S. Sarma, D. Balasubramanian, and J. C. Ahluwalia*

Department of Chemistry, Indian Institute of Technology, Kanpur, Kanpur, India *(Received June 22, 1970)*

Publication costs borne completely by The Journal of Physical Chemistry

The integral heats of solution of urea at 9 and 15° and of thiourea, guanidinium chloride, 1,3-dimethylurea, and tetramethylurea in water at 25 and 35° have been measured at concentrations close to infinite dilution and the excess heat capacities, ΔC_p°, of urea (at 12, 20, and 30°) and other reagents (at 30°) have been derived. The ΔC_p° values at 30° range from 52 cal deg^{-1} mol^{-1} for tetramethylurea to −18 cal deg^{-1} mol^{-1} for guanidinium chloride. These are explained in terms of changes induced in water structure. The conclusions drawn from the heat capacity studies are corroborated by nmr chemical shifts of water protons in solutions of these denaturants. The relevance of the changes in water structure brought about by these reagents to the mechanism of denaturation has been discussed.

Introduction

The importance of water structural changes in relation to protein conformation has been realized in recent years as is evident from an increasing amount of work done in this area. However, the exact mechanism of protein denaturation brought about by various reagents is still unclear. Whether there is a single mechanism for denaturation caused by a variety of external additives is also an open question. A group of workers believe that reagents of the urea–guanidinium class may have two principal effects, namely, a possible direct interaction of these compounds with amide and peptide groups and a hydrophobic effect on nonpolar groups.[1–6]

(1) J. A. Gordon and J. R. Warren, *J. Biol. Chem.*, **245**, 5663 (1968).
(2) J. A. Gordon and W. P. Jencks, *Biochemistry*, **2**, 47 (1963).
(3) W. P. Jencks, *Fed. Proc., Fed. Amer. Soc. Exp. Biol.*, **24**, S-50 (1965).

The alternative possibility of urea and other denaturants exerting its influence through changes in water structure has also been considered recently.[7,8] Most of the workers favor the view that urea acts as a net water structure breaker.[9-16] Abu-Hamidayyah,[17] on the other hand, concluded from the behavior of a few properties in aqueous solution that urea enhances water structure. This view has been severely criticized recently by Holtzer and Emerson[18] and other workers with some validity. The third possible view (based on thermochemical and nmr studies) that urea has essentially no net effect on water structure was reported by us recently.[19] It is clear that even though most of the workers believe that urea interacts with water so as to reduce the structuredness of water, the nature of urea–water interaction is not yet clearly established. Some studies which have been reported on the urea class of denaturants (thiourea, 1,3-dimethylurea (DMU), 1,1,3,3-tetramethylurea (TMU), and guanidinium chloride) with a view to find their effect on water structure are also not conclusive.[20-22] The study of excess partial molal heat capacities, ΔC_p^0, of solutes in water gives one of the most potent methods of determining structural changes in water induced by the solutes.[23,24] The structure-making solutes when dissolved in water increase the ice-like[25] nature of water, and the melting of such a structure requires greater energy with the result that such solutes give rise to positive excess partial molal heat capacities.[26] The reverse is true for structure-breaking solutes. We, therefore, undertook the study of heats of solution and excess partial molal heat capacities of these denaturants in water, as well as proton chemical shifts of water in aqueous solutions of these reagents, to find out whether the results obtained from these studies support our previous reported findings[19] that urea has no net effect on water structure or are consistent with the more popular view that urea tends to break water structure, and to look for any correlation between the effect of denaturants on water structure and their denaturing ability.

Experimental Section

The heats of solution, ΔH_s, of the denaturants in water were measured at millimolal concentrations in a submarine calorimeter described elsewhere.[23] The temperature control in the external bath for calorimeter studies was as good as ±0.002°. Deionized distilled water was used for these as well as magnetic resonance measurements. The proton chemical shifts of the water protons were measured at 23 ± 1° in a Varian A 60D spectrometer. Acetone was used as the internal standard, which at the low concentration (0.5 *m*) that we used in our studies does not alter the chemical shifts of water protons to any significant degree[19,27,28] ($\Delta\delta$ = 0.5 cps). Recently Gordon and Thorne, who have studied in great detail the effect of internal references on pmr chemical shifts in aqueous solutions, also recommended acetone for aqueous nonelectrolyte solutions.[29] The internal consistency of the chemical shifts was checked by measuring that of water in 4 *M* NaBr solutions. The shift in the chemical shifts of water protons in this solution was $\Delta\delta = 20 \pm 1$ cps which agreed with the value reported by Hartman.[30]

Urea was obtained from May and Baker (assay ≥99.5%), while 1,3-dimethylurea (DMU), tetramethylurea (TMU), and guanidinium chloride (GuCl) were procured from Sigma Chemical Co. Urea was recrystallized from water and was dried at 60° for 2 hr. Thiourea was recrystallized from ethanol, dimethylurea from isopropyl alcohol, and guanidinium chloride from water containing HCl at pH 4.6. Tetramethylurea was used as such, the glpc analysis of the sample carried out on a 5-ft 30% SE silicone rubber column showed the presence of ~1% low-boiling impurity.

Results

The integral heats of solution of urea in water at several concentrations in the range 1×10^{-3} to 8×10^{-3} *m* at 9 and 15° are given in Table I. The heats of

(4) D. R. Robinson and W. P. Jencks, *J. Amer. Chem. Soc.*, **87**, 2462 (1965).
(5) D. R. Robinson and W. P. Jencks, *J. Biol. Chem.*, **238**, PC 1558 (1963).
(6) D. E. Goldsack, *Biopolymers*, **6**, 164 (1968).
(7) I. M. Klotz and K. Shikama, *Arch. Biochem. Biophys.*, **123**, 551 (1968).
(8) G. G. Hammes and J. C. Swann, *Biochemistry*, **6**, 1591 (1967).
(9) H. S. Frank and F. Franks, *J. Chem. Phys.*, **48**, 4746 (1968).
(10) K. Arakawa and N. Takenaka, *Bull. Chem. Soc. Jap.*, **40**, 2739 (1967).
(11) W. A. Hargraves and G. C. Kresheck, *J. Phys. Chem.*, **73**, 3249 (1969).
(12) G. A. Vidulick, J. R. Andrade, P. P. Blanchette, and T. J. Gilligan, III, *ibid.*, **73**, 1621 (1969).
(13) J. H. Stern and J. D. Kulluck, *ibid.*, **73**, 2795 (1969).
(14) W.-Y. Wen and C. L. Chen, *ibid.*, **73**, 2895 (1969).
(15) F. Franks and D. L. Clarke, *ibid.*, **71**, 1155 (1967).
(16) G. G. Hammes and P. R. Schimmel, *J. Amer. Chem. Soc.*, **89**, 442 (1967).
(17) M. Abu-Hamidayyah, *J. Phys. Chem.*, **69**, 2720 (1965).
(18) A. Holtzer and M. F. Emerson, *ibid.*, **73**, 26 (1969).
(19) S. Subramanian, D. Balasubramanian, and J. C. Ahluwalia, *ibid.*, **73**, 266 (1969).
(20) C. A. Swenson, *Arch. Biochem. Biophys.*, **117**, 494 (1966).
(21) K. Sasaki and K. Arakawa, *Bull. Chem. Soc. Jap.*, **42**, 2485 (1969).
(22) J. A. Glasel, *J. Amer. Chem. Soc.*, **92**, 375 (1970).
(23) S. Subramanian and J. C. Ahluwalia, *J. Phys. Chem.*, **72**, 2525 (1968).
(24) T. S. Sarma, R. K. Mohanty, and J. C. Ahluwalia, *Trans. Faraday Soc.*, **65**, 2533 (1969).
(25) H. S. Frank and M. W. Evans, *J. Chem. Phys.*, **13**, 507 (1945).
(26) H. S. Frank and W.-Y. Wen, *Discussions Faraday Soc.*, **24**, 133 (1957).
(27) H. G. Hertz and W. Spalthoff, *Z. Elektrochem.*, **63**, 1096 (1959).
(28) R. A. Y. Jones, A. R. Katritzky, J. N. Murell, and N. Sheppard, *J. Chem. Soc.*, 2576 (1962).
(29) J. E. Gordon and R. L. Thorne, *J. Phys. Chem.*, **73**, 3643 (1969).
(30) K. A. Hartman, Jr., *ibid.*, **70**, 270 (1966).

solution of urea at 25 and 35° were reported earlier from our laboratory.[19] The heats of solution of thiourea, 1,3-dimethylurea, tetramethylurea, and guanidinium chloride in water at 25 and 35° at several concentrations are listed in Table II.

Table I: Integral Heats of Solution of Urea in Water at 9 and 15°

Temp, 9.0 ± 0.05°		Temp, 15.0 ± 0.05°	
$m \times 10^3$	ΔH_s	$m \times 10^3$	ΔH_s
1.98	3717	2.72	3694
2.15	3745	2.99	3672
2.31	3719	3.18	3718
2.48	3688	3.31	3654
2.62	3738	4.43	3687
4.42	3730	4.71	3708
4.57	3722	10.07	3657
6.65	3700		
7.80	3726		
ΔH_s° = 3720 ± 20 cal mol^{-1}		ΔH_s° = 3684 ± 25 cal mol^{-1}	

Since the measurements of heats of solution were made in very dilute solutions (1×10^{-3} to 1×10^{-2} *m*) and the uncertainty arising from any concentration dependence being within the experimental error, the heats of solution at infinite dilution, ΔH_s°, were taken to be the mean of a number of measurements. The uncertainty in ΔH_s° is expressed as standard deviation from the mean value. The values of ΔH_s° thus obtained are listed in Table III. For comparison and for deriving excess partial molal heat capacities the ΔH_s° values of urea in water at 25 and 35° which were reported previously[19] were reevaluated for consistency, and the revised values are given in Table III. The excess partial molal heat capacities of urea at 12, 20, and 30° and of other denaturants at 30° which were derived by the integral heat method[19,24,31,32] are also given in Table III.

The differences in the nmr chemical shifts of water in these solutions of the denaturants over that in pure water are presented in Figure 1. We define $\Delta\delta$ as equal to (δ of the water proton in the given solution) − (δ in pure water). A positive value of $\Delta\delta$ would indicate an increase in the hydrogen bonding of water in solution relative to pure water (*i.e.*, the solute is a structure maker) and a negative $\Delta\delta$ would mean that structure disruption in the solvent has occurred in the solution relative to pure water (*i.e.*, the solute is a structure breaker). It is worth pointing out here that while this correlation between resonance line shift and structure modification is conventionally used and is in general valid, the possibility exists that an external additive may promote water structure and yet shift the water proton resonance line to higher field. This would happen if the structure being promoted is not the usu-

Table II: Integral Heats of Solution of Some Protein Denaturants at 25 and 35°

Compound	Temp, 25.0 ± 0.03°		Temp, 35.0 ± 0.03°	
	$m \times 10^3$	ΔH_s, cal mol^{-1}	$m \times 10^3$	ΔH_s, cal mol^{-1}
Thiourea	1.08	5458	2.17	5443
	1.51	5467	2.61	5437
	2.42	5413	2.82	5417
	2.64	5449	3.56	5411
	3.34	5395	4.59	5448
	3.71	5428	5.59	5403
	4.63	5453	5.61	5392
			6.29	5409
			6.80	5454
			8.31	5421
			9.12	5404
			9.70	5421
	ΔH_s° = 5438 ± 26 cal mol^{-1}		ΔH_s° = 5422 ± 19 cal mol^{-1}	
Dimethylurea	3.43	192	2.20	573
	4.63	187	2.45	596
	5.58	193	2.72	604
	6.30	187	3.51	587
	6.90	192	4.64	586
	8.23	183	5.76	570
	9.27	177	6.16	573
	9.65	185	7.30	581
	10.66	186	8.97	561
			9.79	572
			10.53	555
	ΔH_s° = 137 ± 5 cal mol^{-1}		ΔH_s° = 578 ± 15 cal mol^{-1}	
Tetramethylurea	0.92	−5703	1.13	−5223
	1.25	−5732	1.24	−5189
	1.75	−5720	1.73	−5192
	2.16	−5763	2.40	−5210
	2.55	−5711	2.88	−5194
	2.90	−5735	3.11	−5226
	3.58	−5716	3.87	−5210
	3.82	−5703	4.23	−5217
	4.32	−5757	4.70	−5226
			5.16	−5210
	ΔH_s° = −5727 ± 22 cal mol^{-1}		ΔH_s° = −5210 ± 14 cal mol^{-1}	
Guanidinium chloride	1.10	4514	1.81	4355
	1.30	4523	2.25	4322
	1.76	4485	2.87	4320
	2.41	4509	3.99	4313
	2.80	4519	4.68	4309
	3.02	4509	5.45	4327
	3.33	4505	6.05	4318
	3.80	4512	6.64	4323
	4.30	4504	6.94	4336
	5.08	4513	7.45	4334
	5.51	4551	8.04	4310
	ΔH_s° = 4510 ± 10 cal mol^{-1}		ΔH_s° = 4325 ± 15 cal mol^{-1}	

(31) C. M. Criss and J. W. Cobble, *J. Amer. Chem. Soc.*, **83**, 3223 (1961).

(32) J. C. Ahluwalia and J. W. Cobble, *ibid.*, **86**, 5377 (1964).

Table III: Standard Heats of Solution and Excess Heat Capacities of the Denaturants in Water

Compound	$\Delta H_s°$, cal mol^{-1} 9°	15°	25°	35°	ΔC_p^0, cal mol^{-1} deg^{-1} 12°	20°	30°
Urea[a]	3720 ± 20[b]	3684 ± 25[b]	3686 ± 33[b]	3725 ± 38[b]	−6.0 ± 4	0 ± 5	3.9 ± 7
Thiourea			5438 ± 26	5422 ± 19			−1.6 ± 4
1,3-Dimethylurea			187 ± 5	578 ± 15			39 ± 2
Tetramethylurea			−5727 ± 22	−5210 ± 14			52 ± 3
Guanidinium chloride			4510 ± 15	4325 ± 15			−18.5 ± 3

[a] Values at 25 and 35° taken from ref 19 were reevaluated. [b] Standard deviation from the mean value.

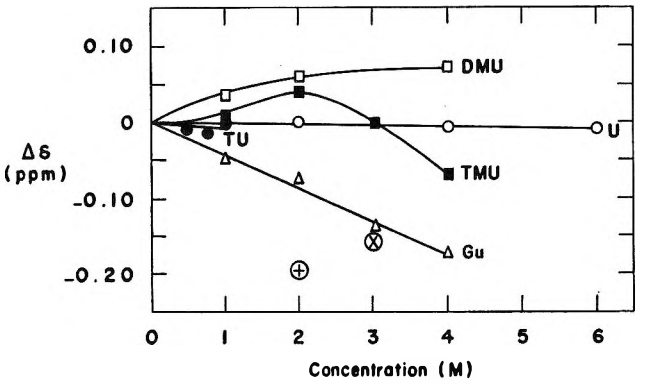

Figure 1. Proton chemical shifts of water in aqueous solutions of the denaturants. $\Delta\delta$ = (δ water in aqueous solution) − (δ in pure water). Measurements were made at 60 Mcps: ○, urea; ●, thiourea; □, dimethylurea; ■, 1,1,3,3-tetramethylurea; △, guanidine hydrochloride; ⊕, NaBr; ⊗, NaCl (from ref 30).

ally assumed linearly bonded "icelike" lattice, but one where the water molecules are more densely packed *via* nontetrahedral hydrogen bonds.[33] In this situation, the water protons are shielded by oxygens and would resonate at higher fields. Hence, one has to view the nmr results in conjunction with other experimental data on the system under investigation. It may be seen from Table III that limiting excess heat capacities ΔC_p^0 of urea decrease from a slightly positive value of 3.9 ± 7 cal mol^{-1} deg^{-1} at 30° to 0 ± 6 cal mol^{-1} deg^{-1} at 20° and to a negative value of −6.0 ± 5 cal mol^{-1} deg^{-1} at 12°, indicating that urea has little net structure-making or -breaking effect around 20°, but it appears to be the structure breaker at temperatures below 20°.

Thiourea (see Table III) like urea has a ΔC_p^0 value (−1.6 ± 4 cal mol^{-1} deg^{-1}) essentially close to zero at 30° suggesting that this compound has essentially no net structure-making or -breaking propensities at 30°. 1,3-Dimethylurea with a ΔC_p^0 = 39 ± 2 cal mol^{-1} deg^{-1} and tetramethylurea with ΔC_p^0 = 52 ± 3 cal mol^{-1} deg^{-1} have moderately large heat capacities in line with those of structure-promoting solutes. The methyl groups presumably account for positive excess heat capacities. Guanidinium chloride behaves like a uniunivalent electrolyte in that it has a negative heat capacity value of −18.5 ± 3 cal mol^{-1} deg^{-1}. This is understandable since the chloride ion is known to be a structure breaker,[30,34] and alkali metal chlorides are known to have negative excess heat capacities.[26]

The proton resonance chemical shift data, illustrated in Figure 1, indicate that the water proton signal does not change significantly in thiourea solutions as compared to pure water itself as was also found in the case of aqueous urea. This further substantiates the heat capacity observations. Guanidinium chloride sends the water signal upfield, the extent of the change varying almost linearly with the solute concentration. Structure-breaking electrolytes, *e.g.*, NaCl or NaBr, do likewise, and the shifts of the signal for these compounds at 2 and 3 *M* are included in Figure 1 for comparison. 1,3-Dimethylurea gives a small downfield shift of the nmr signal, an effect that does not change much with concentration. Tetramethylurea yields an initial downfield shift until a concentration of 2 *M* is reached, beyond which the $\Delta\delta$ passes through zero and then to negative values (upfield). This may signify a change in the TMU from an initial structure-making capacity to a structure-disrupting one at higher molarities. Repeated experiments with various changes in the concentration of the solute reproduce this behavior of tetramethylurea from an initial structure maker to a structure breaker at higher molarities.

Discussion

In an earlier communication[19] based on nmr and excess heat capacity studies of aqueous urea solutions at 30° we had suggested that the effect of addition of urea to water may be neither promotion nor destruction of the solvent structure. We had further suggested the possibility that urea molecules may simply be accommodated in the bulk water clusters *via* urea–water hydrogen bonds. The formation of such mixed sandwich clusters would lead to no significant heat capacity changes or shifts in the water proton resonances. However, it has been pointed out by Holtzer and Emerson[18] (in criticism of Abu-Hamidayyah's paper[17]) that the heat capacity of solid urea not being different from that in water solution at room tempera-

(33) E. Wicke, *Angew. Chem., Int. Ed. Engl.*, 5, 106 (1966).
(34) M. Kaminsky, *Discussions Faraday Soc.*, 24, 171 (1957).

ture may be fortuitous, *i.e.*, according to them it is possible that at lower temperatures this may not be so. In fact, the partial molal heat capacities of urea solution at infinite dilution from 2 to 40° which were obtained by Gucker and Ayres[35] by extrapolating apparent molal heat capacities ϕC_p as a function of $\sqrt{m}$ to infinite dilution indicate that $\bar{C}_{p_2}^0$ decreased as much as from 22.85 ± 7.8 cal mol^{-1} deg^{-1} at 40° to 8.64 ± 7.5 at 20°. The excess partial molal heat capacity, ΔC_p^0, obtained by subtracting the heat capacity C_{p_2} of pure solid urea from the partial molal heat capacity, $\bar{C}_{p_2}^0$, appears to be positive around room temperature but becomes negative at lower temperatures. Since apparent molal heat capacity, ϕC_p, of Gucker and Ayres[35] had large concentration dependence and the extrapolation of ϕC_p to infinite dilution was made from large concentration, we felt that the estimation of $\bar{C}_{p_2}^0$ and therefore ΔC_p^0 of urea in aqueous solution at lower temperature might be subject to uncertainty.

On the other hand, the limiting excess partial molal heat capacity ΔC_p^0, obtained directly from integral heats of solution measurements at very low concentration, neither involves any uncertainty in extrapolation nor requires the knowledge of accurate values of C_{p_2} of urea. We have therefore extended our previous measurements on integral heats of solution of urea in water at 25 and 35° to 15 and 9° to obtain accurate limiting excess heat capacities, ΔC_p^0, of urea at lower temperatures.

The ΔC_p^0 value of urea in water (see Table III) decreases from a positive value of 3.9 ± 7 cal mol^{-1} deg^{-1} at 30° to a negative value of −6.0 ± 5 cal mol^{-1} deg^{-1} at 12°. It is therefore no longer valid to say that urea enhances water structure as suggested by Abu-Hamidayyah[17] or does not have any net structure-making or -breaking effect as postulated by us earlier,[19] at all temperatures. Indeed at lower temperature the negative ΔC_p^0 values support the prevalent view obtained from other studies that urea breaks water structure. But the effect seems to be rather small and dependent on temperature. This behavior is supported by studies on the concentration dependence of apparent molal volumes of aqueous urea solutions as a function of temperature.[36] Whereas at temperatures higher than 25° ϕ_V does not exhibit significant changes with concentration, at 0° ϕ_V changes quite a bit with concentration and that too in a nonlinear fashion. Also the coefficient of thermal expansion of ϕ_V at 0° is abnormally large at lower temperatures and decreases toward a normal value as the temperature is raised.[36]

The results reported in this paper for the thiourea–water system; *i.e.*, negligible excess heat capacity and negligible changes in the water proton signal, seem to suggest that urea and thiourea act in a similar way toward water. Hence, whatever may be the nature of the urea–water system, a similar picture for thiourea can be envisaged. Unfortunately, studies on the thiourea system had to be restricted to 1.5 *M* concentrations because of the limited solubility of this reagent in water at the chosen temperature.

1,3-Dimethylurea and tetramethylurea are both structure makers, as is indicated by their positive ΔC_p^0 values. Substitution of hydrogens by methyl groups in urea enhances the heat capacity in solution since the thermal melting of the Frank–Evans "icebergs"[25,26] around methyl groups requires additional energy. The nonpolar groups enforce water structure around them and in that process lower the enthalpy and entropy and enhance the heat capacity.[26]

The proton chemical shifts of water in aqueous 1,3-dimethylurea are sent downfield when compared to pure water, indicative of structure making by this solute. For tetramethylurea, up to a solute concentration of 2 *M* there seems to be structure promotion, and beyond this we see a reversal of this trend. This nonuniform variation of $\Delta\delta$ for different molarities of tetramethylurea in water is surprising but not unique. Glew, *et al.*,[37] studying the *tert*-butyl alcohol–water system in the highly aqueous region, obtained a maximum in the downfield shift of the water proton signal around a solute concentration of 4 *M* at 0°. This is in agreement with thermodynamic properties of *tert*-butyl alcohol and other nonelectrolytes in water[38] which also exhibit extrema around this concentration. This initial downfield shift of the water signal has been explained by Glew[37] as due to solvent caging around the weakly interacting interstitial nonelectrolyte, which breaks down at higher molarities to give an upfield shift. In analogy, the behavior of tetramethylurea may well be an entropy driven hydrophobic interaction that reduces the structure-making propensities of the solute leading ultimately to the collapse of the solvent cagelike order, at higher concentrations of TMU.

The data reported for guanidinium chloride suggest that this reagent behaves as a structure breaker. The ΔC_p^0 value for this solute is negative, and here the water signal moves upfield. For uniunivalent chlorides, as mentioned earlier, the ΔC_p^0 is negative in aqueous solution, and the chloride ion being a structure breaker,[28,32] seems to us to be partly responsible for both the heat capacity and the proton resonance shift effects.

The correlation between the nmr and the calorimetric results is gratifying. According to the usual interpretation of nmr data, we see that DMU behaves as a structure maker and guanidinium chloride as a structure breaker over a wide range of concentration. The calorimetric observations, made at very low concentra-

(35) F. T. Gucker, Jr., and F. D. Ayres, *J. Amer. Chem. Soc.*, **59**, 2152 (1937).

(36) R. H. Stokes, *Aust. J. Chem.*, **20**, 2087 (1967).

(37) D. N. Glew, H. D. Mak, and N. S. Rath, *Chem. Commun.*, 254 (1968).

(38) F. Franks, "Physicochemical Processes in Mixed Aqueous Solvents," Heinemann, London, 1967, Chapter 3.

tions, support these. For TMU at low concentrations, nmr spectroscopy suggests a structure-making propensity and a reversal of this property at higher concentrations. Calorimetric studies at very low concentrations agree with the nmr results. For urea and thiourea the effect seems small both in nmr spectroscopy and in calorimetry.

It is interesting to compare the results of our study with the infrared studies of Swenson. Swenson[20] had concluded from his infrared studies that urea does not perceptibly alter water structure while 1,3-dimethylurea promotes more structure. However, his results on tetramethylurea and on guanidinium chloride are in discord with ours. The maximum that we obtained in the $\Delta\delta$ values for tetramethylurea is not reflected in the ir data where, for all concentrations of the solute the apparent tendency is to disrupt structure. Swenson[39] has suggested that the discrepancy between his ir studies and our results may be explicable on the basis of steric effects. The ir method is measuring something like the average hydrogen bond strength in the solution. The bond is primarily between the keto group of TMU and water molecules. This interaction may be weakened due to steric effects brought about by the structured water about the four methyl groups. In the light of these, it would be worthwhile to study other thermodynamic properties of the tetramethylurea–water system. The disagreement between Swenson's and our results in guanidinium chloride is more striking. While our results classify this compound as a structure breaker, infrared studies suggest that this may be a structure maker. The dilution volume decrement observed[40] on the addition of water to a concentrated solution of the denaturant is just the same for 8 *M* urea and for 4 *M* guanidinium chloride. Inasmuch as these two are good denaturants at the respective concentrations, they would be expected to behave much the same way in aqueous solution. Thiourea gives[40] a negligible volume decrement consistent with our view that it affects water structure very little.

The ultrasonic absorption studies of Hammes and Schimmel[16] and of Arakawa and Takenaka[10] indicate that urea breaks water structure. However, the interpretation by Arakawa and Takenaka[10] of their results is questionable. On examining carefully the data presented by them in the plot of α/f^2 (where α is the sound absorption coefficient) *vs.* concentration of urea, as compared to water component only, the more logical interpretation would seem to be that only at temperatures at or below 20° does urea break water structure and that possibly to a small extent, which is in agreement with our observation. Sasaki and Arakawa[21] have concluded from their ultrasonic studies on aqueous solutions of methylated ureas that the relative decreasing order of structure-making propensities is TMU > 1,3-DMU > urea. This is the same order as observed by us. However, their conclusion that 1,3-DMU is a structure breaker, and the structure-breaking ability being less than urea, appears to follow from their results only at low concentrations. The data[21] presented by them in the plot of α/f^2 (structure) *vs.* concentration at moderate concentrations of 1,3-DMU as compared to water component rather seem to indicate that 1,3-DMU is a weak structure maker.

The measure of water structure is something different for almost every technique, and one should be careful in generalizing the results from a limited number of studies. Nevertheless, there seems to be enough evidence from this work and from other studies to enable us to make some rational comments on the effect of some of the commonly used denaturants on water structure. Urea and thiourea do not seem to alter water structure appreciably. Urea may be at the most classified as a weak structure breaker at lower temperatures while equally good or rather better denaturant guanidinium chloride is a structure breaker and exhibits the behavior expected of normal salts. 1,3-DMU and TMU are both structure makers, the structure-making ability of TMU being larger than that of 1,3-DMU.

If one considers the observations that urea, being one of the good denaturants, does not alter water structure appreciably and that there does not exist any simple correlation between the effect of denaturants on water structure and their denaturating ability, it is quite likely then that changes in water structure induced by these reagents may have after all nothing to do with the effect of these reagents on protein denaturation. Glasel[22] has also made somewhat similar conclusion from his recent deuteron magnetic relaxation studies on aqueous solutions of some denaturants. He has found that urea affects the water structure least while dimethyl sulfoxide which is a denaturant under severe conditions results in greatest effect among the simpler molecules.

It is also possible that the effect of denaturants on water structure gets modified in the presence of proteins, and such structural changes in water may play an important role in the denaturation of proteins. In this respect it might be worthwhile to continue to look into the mechanism of weakening of hydrophobic forces by denaturants such as urea.

Acknowledgments. It is with pleasure that we gratefully acknowledge the generosity of Dr. Nitya Nand of Central Drug Research Institute, Lucknow, India, for the use of the nmr spectrometer. Grateful thanks are also due to Sigma Chemical Company for gift samples of methylated ureas.

(39) C. A. Swenson, personal communication.

(40) S. Katz, *Biochim. Biophys. Acta*, 154, 468 (1968).

Interactions of Gases in Ionic Liquids. I. The Solubility of Nonpolar Gases in Molten Sodium Nitrate[1a]

by Paul E. Field* and William J. Green[1b]

Virginia Polytechnic Institute and State University, Department of Chemistry, Blacksburg, Virginia 24061
(Received August 12, 1970)

Publication costs borne completely by The Journal of Physical Chemistry

A new method is described for determining the solubility of gases in molten salts at pressures ranging between 0.5 and 2.0 atm. Solubility results are reported for helium, argon, nitrogen, and carbon dioxide over the temperature range 315 to 402°. All four solute gases were found to obey Henry's law over the pressure range studied. The temperature dependence of the solubilities was fitted by means of a linear least-squares calculation to the equation $\log K_p = b + mT^{-1}$ (°K) where K_p has the units mol of gas/cc of melt atm. The values calculated for the four gases of b and m, respectively, are: He (−5.871, −703.6); Ar (−5.938, −769.1); N_2 (−5.710, −599.2); CO_2 (−7.898, +585.1). The heats of solution are found to be endothermic except for carbon dioxide. The present results are compared with previous work and discussed in light of the Uhlig cavity model.

Introduction

Approximately 23 papers have reported gas solubilities in molten salt solvents over the past 13 years. A review of the systems reported indicates an almost complete lack of systematic study. The simpler nonpolar gases such as helium, neon, argon, and perhaps nitrogen, oxygen, chlorine, and carbon dioxide have been most thoroughly studied in such complex melts as mixed alkali metal–alkaline earth metal–transition metal fluorides whereas the polar gases such as HF, DF, H_2O, BF_3, and NH_3 have either been studied in the complex melts or the simpler alkali halide or nitrate salts. Even in the case of simple gas–simple salt systems there exists the complicating factor that the majority of studies have been made in solvents containing mixed alkali metal cations. Experimental techniques reported can be categorized into three classes: (1) absorption, where the solubility is determined by means of observing the volumetric or manometric change in the solute or the gravimetric change in the solvent; (2) elution, where the solubility is determined from the quantity of gas stripped from a saturated solution; and (3) cryometric, where the solubility is determined from the freezing point depression of the solvent.

The purpose of this paper is to describe a simplified elution technique for the determination of gas solubilities in molten salts and to report our first results in a program to investigate systematically solute and solvent parameters in gas–molten salt systems. We report results for helium, argon, nitrogen, and carbon dioxide in molten sodium nitrate at saturation pressures around 1 atm over the temperature range of 315–400°.

Experimental Section

Materials. Reagent grade sodium nitrate obtained from Baker was used without further treatment. The gases were used directly from the cylinders. Airco helium, argon, and dry nitrogen and Matheson Bone Dry carbon dioxide were employed.

Apparatus. A diagram of the apparatus is shown in Figure 1. It consists of the following components connected in series and forming a closed loop: coaxial stainless steel tubing branched by means of a brass Swagelok heat exchanger tee consisting of an outer tube ($^5/_8$ in.), which was welded to the mouth of a 1-l. stainless steel vessel (Hoke gas sampling cylinder) and served as the gas return, and an inner tube ($^3/_8$ in.), which served as the gas supply and terminated about 1 in. above the bottom of the vessel. A 1-kg charge of salt was placed in the vessel prior to connecting it to the rest of the loop. With the additional exception of the diaphragm pump all other components were of Pyrex glass construction. Connection to the stainless steel tubing was made by means of Teflon ferrules on 6-mm glass tubing fitted into 0.25-in. brass Swagelok reducing unions on the brass tees. Stainless steel ferrules were used in connecting the brass tees to the stainless steel tubing. The gas supply and return lines were connected by means of stopcocks so that the furnace volume of the loop could be excluded and gas circulated through the glass portion only. The gas return line contained a condenser-type cooling coil connected through a small

(1) (a) Presented in part at the 155th National Meeting of the American Chemical Society, San Francisco, Calif., April, 1968; (b) from the Ph.D. Thesis of William J. Green, Virginia Polytechnic Institute and State University, Oct 1969.

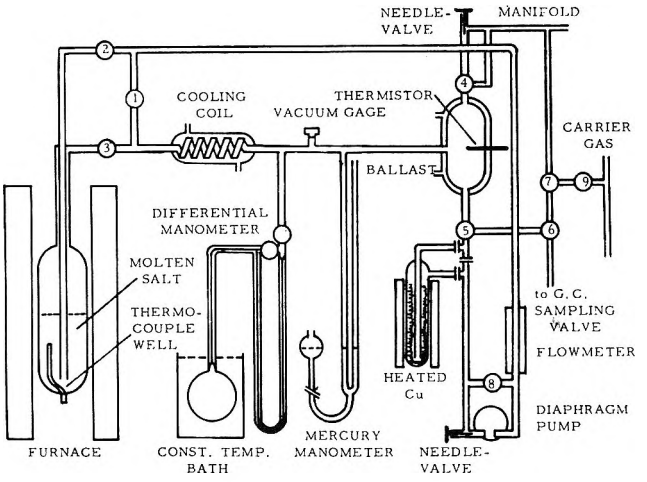

Figure 1. Gas solubility apparatus.

manifold to an 800-ml ballast, both of which were thermostated with water jackets through which water from a constant temperature bath was circulated. Side arms on the small manifold connected to a 0–1000 μ thermocouple vacuum guage (Hastings Model DV-6), a mercury manometer equipped with a leveling bulb, and a differential dibutyl phthalate manometer. The differential manometer had a 1-l. reservoir on the closed side which was immersed in the constant temperature bath. The ballast volume was connected by means of a needle valve and by-pass stopcock to a vacuum line manifold which was used for evacuating the loop and also for introducing the solute gas into the loop. A bead thermistor was inserted into the ballast in order to monitor temperature fluctuations. The ballast was connected to a series of three three-way stopcocks which served as part of the gas sampling system. The loop was completed with a Teflon needle valve in a series with a Model 4K Dynapump (Neptune) and a flowmeter located on the supply side of the pump. For the work with argon it was necessary to insert a copper mesh trap between the gas sampling stopcocks and the pump.

The salt vessel was located in a 5-in. i.d. furnace having an 18-in. zone (Hevi-Duty). The overall size of the vessel was about 11 in. long and 3.5 in. in diameter. The ends of the furnace were plugged with glass wool wads about 4 in. thick. The furnace was controlled by a proportioning temperature controller (Barber Colman Model 293C) which was activated by a chromel–alumel thermocouple. The temperature of the molten salt was measured with a second chromel–alumel thermocouple which was calibrated against NBS melting point standards of tin, lead, and zinc. The thermocouple well was an S-shaped length of $^1/_8$-in. stainless steel tubing welded to an opening in the bottom of the vessel. The tip of the thermocouple was located about midradius and midheight in the melt.

Procedure. The experimental operation consisted of three steps: (1) saturation, (2) elution, and (3) analysis. Saturation was achieved by initially bringing the salt to the desired temperature and evacuating the entire loop. The gas was introduced into the loop to the desired pressure through the needle valve on the manifold. The flow rate was adjusted to approximately 1–2 l./min with the pump needle valve. Saturation was carried out for a 6-hr period.

The uniqueness of the method rests in the step following saturation in which the loop is evacuated to a pressure of 100 μ. We had observed in earlier studies that during evacuation of the gas phase over a saturated molten salt solution contained in a Pyrex vessel the liquid is completely quiescent. As we shall point out in a later section the nonequilibrium step entails negligible degassing of the melt. Following evacuation of the gas phase, helium was introduced into the loop to approximately 1 atm of pressure. Circulation of the eluting gas was commenced and carried out for a 12-hr period.

The analysis of the resultant gas mixture of the solute gas and the eluting gas was made with an Aerograph Model 90-P gas chromatograph (Varian) fitted with a gas sampling valve having a 10-ml sampling volume connected to the loop. The sampling volume and connecting lines were evacuated prior to introducing the gas mixture into the sampling volume. Sampling was repeated at approximately 5-min intervals. Usually, the average of four samples was taken for the calculation of the solubility. Except when the solute gas was helium, helium was used as both the eluting gas and the carrier gas in the chromatograph. In this way only the presence of the solute gas was detected. The output of the chromatograph was recorded on a 10-in. strip chart recorder equipped with a Disc integrator. In order to detect components of the gas mixture other than the solute, packed columns were used in the chromatograph. Since oxygen was observed as a decomposition product of the nitrate melt, separation of the oxygen from the various solute gases was necessary. Two different columns were employed in this study. The separations for nitrogen and argon employed a 6-ft column packed with 30–60 mesh Molecular Sieve 5A (Wilkens) giving retention times (min) for oxygen (1.1), argon (1.3), and nitrogen (1.7). The separation of carbon dioxide from oxygen employed an 18-in. column packed with 60–200 mesh Davidson Silica Gel Grade 950 (Fisher) giving retention times (min) for oxygen and nitrogen (0.3) and carbon dioxide (1.6).

Because oxygen and argon are not readily separated by gas chromatography, it was necessary to remove the oxygen from the eluted gas mixture prior to analysis for argon. This was done following elution by by-passing the furnace portion of the loop and circulating the gas in the remainder of the loop with the copper mesh

trap in line. The trap was heated to approximately 400° and circulation was carried out for an additional period of 2 hr.

The procedure for the helium study employed argon as the eluting and carrier gas.

Calculations. The solubility at a given temperature, T_m, was calculated as $C_d = n_g/V_m$ where n_g is the number of moles of gas dissolved in the volume of molten salt, V_m, which was determined from the weight of salt used and its density at T_m based on the equation given by Janz.[2] The number of moles was calculated, assuming ideal gas behavior, as $n_g = P_g V_L/RT_g$ where V_L is the volume of the loop, R is the gas constant, and T_g is the temperature of the gas in the thermostated loop. The partial pressure of the eluted solute, P_g, was determined by $P_g = A_{GC}/k_{GC}$ where A_{GC} is the average area of the chromatograph peaks obtained in consecutive samples and k_{GC} is the chromatograph calibration constant for the solute gas. Peak areas were recorded as "counts" on the Disc integrator. The estimated accuracy of a solubility determination is ±5%. All partial pressures were corrected for the residual solute pressure following the evacuation step. In the earliest experiments the correction was based on measured evacuation times and the pumping speed of the system. After incorporation of the thermocouple vacuum gauge into the loop, corrections were based on the measured residual pressure.

Results

The equilibrium constant, K_p, related to Henry's law, is taken as

$$K_p = C_d/P_s \text{ (mol of gas)/(cc of melt)(atm)}$$

It should be noted that the conventional constant associated with Henry's law, K_H, is related to K_p as

$$K_p = 1/K_H\bar{V}_m$$

The distribution coefficient, K_c (of theoretical interest), is defined as the ratio of the concentration of the solute in solution to its concentration in the gas phase

$$K_c = C_d/C_g = K_pRT_m \qquad (1)$$

In keeping with common practice, the equilibrium process is defined in two steps as

$$X(P_s,g) \xrightarrow{I} X(P' = C_dRT_m,g) \xrightarrow{II} X(C_d,soln)$$

where I refers to the isothermal expansion of the ideal gas having $\Delta H_I = 0$ and $\Delta S_I = -R$ in P'/P_s. The second step, II, refers to the solution process at constant concentration of the solute. For the overall process, the standard enthalpy of solution, ΔH^s, is equal to ΔH_{II}, and the entropy of solution for step II, usually written as ΔS_c, is given by difference as

$$\Delta S_c = \Delta H^s/T_m + R \ln K_pRT_m \qquad (2)$$

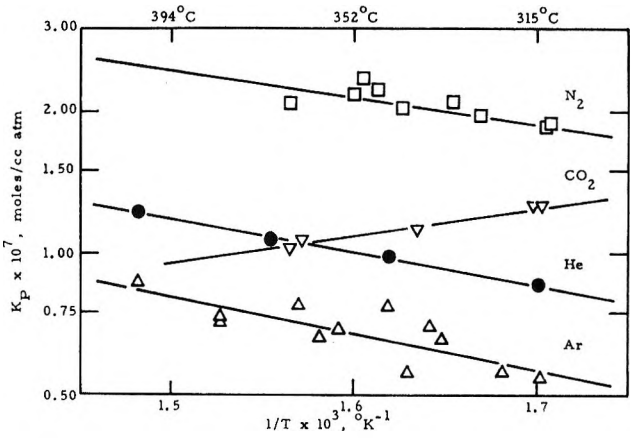

Figure 2. van't Hoff plot for gases in $NaNO_3$.

Henry's law is obeyed for the four gases helium, argon, nitrogen, and carbon dioxide in molten sodium nitrate over the pressure range studied. The temperature dependence of the Henry's law constant, K_p, was evaluated by means of the van't Hoff relation. These values are shown in Figure 2 as log K_p *vs.* $1/T$. The lines drawn through the data were computed by a linear least-squares fit. The thermodynamic quantities of solution for each solute were evaluated from the slope and intercept of the fitted curves as indicated by eq 2. These values are given in Table I for each gas along with the pressure and temperature ranges studied. The uncertainties listed are precision indices of one standard deviation. The temperature dependent quantities are reported at 10% above the melting point of the solvent.

The magnitude of the solubility for all four gases reported is within the range 0.5 to 2.5 × 10^{-7} mol/cc-atm over the temperature interval 315–400°. For helium, argon, and nitrogen, we find the endothermic heats of solution about 3 kcal/mol and entropies of solution around −5 cal/deg mol. Carbon dioxide differs in both quantities from the other solutes not only in the sign of its heat but in that its entropy of solution is significantly more negative by almost a factor of 3.

Discussion

Previous results for the solubility of helium, argon, and nitrogen in sodium nitrate have been reported by Copeland and coworkers[3] and Cleaver and Mather.[4] With the exception of Copeland and Zybko's[3a] helium solubility which was determined at one temperature only, both groups report Henry's law solubilities over

(2) G. J. Janz, "Molten Salts Handbook," Academic Press, New York, N. Y., 1967, p 42.

(3) (a) J. L. Copeland and W. C. Zybko, *J. Phys. Chem.*, **70**, 181 (1966); (b) J. L. Copeland and L. Seibles, *ibid.*, **70**, 1811 (1966); **72**, 603 (1968).

(4) B. Cleaver and D. E. Mather, *Trans. Faraday Soc.*, **66**, 2469 (1970).

Table I: Solubility Results in Sodium Nitrate[a]

	Helium	Argon	Nitrogen	Carbon dioxide
m	-703.60 ± 0.04	-769.15 ± 0.18	-599.15 ± 0.18	$+585.08 \pm 0.03$
b	-5.87 ± 0.06	-5.94 ± 0.28	-5.71 ± 0.30	-7.90 ± 0.04
$K_p \times 10^7$, mol/cc atm	1.06 ± 0.01	0.72 ± 0.02	2.24 ± 0.03	1.05 ± 0.01
	(2.16 ± 0.01)	(0.75 ± 0.07)	(0.58 ± 0.07)	
ΔH^s, kcal/mol	3.22 ± 0.18	3.52 ± 0.81	2.74 ± 0.83	-2.68 ± 0.12
	(3.28 ± 0.11)	(3.8 ± 1.7)	(3.96 ± 2.2)	
ΔS_c, eu	-5.3 ± 0.3	-5.6 ± 1.3	-4.5 ± 1.4	-14.6 ± 0.2
	(-3.8 ± 0.2)	(-5.0 ± 2.6)	(-5.3 ± 3.4)	
Pressure range, atm	1.25–1.29	0.96–1.34	0.94–1.24	0.92–1.20
Temperature range, °C	315–402	315–402	313–366	314–366

[a] Values calculated from the linear least-squares fit of $\log K_p = (m/T) + b$. The uncertainties listed are taken at one standard deviation. K_p and ΔS_c are given at $1.10T_{mp} = 637$°K. Values in parentheses were calculated from solubility data reported by Cleaver and Mather in ref 4.

approximately a 100° temperature interval at pressures up to about 500 atm. Our results are in reasonable accord with those found by Cleaver and Mather.

Cleaver and Mather's results for each solute are reported at three temperatures and include an uncertainty obtained from several pressure dependent determinations at each temperature. We have included these uncertainties in a recalculation by our least-squares program of the temperature dependence of their solubilities. The values for K_p and ΔS_c at 637°K and for ΔH^s are included in parentheses in Table I for comparison with our values. For all three gases, the agreement in the heat of solution is very good. For argon, we are in excellent agreement for the solubility over the entire temperature range. We differ in the solubility for both helium and nitrogen. In the former case Cleaver's value is twice ours, while in the latter case our value is over four times larger. Since the slopes are equivalent, the entropies, which are related to the intercepts, reflect the disparities in the solubilities. It is interesting to note that in both cases where the solubilities do not agree no systematic error is apparent.

We differ with Copeland and coworkers by at least an order of magnitude smaller in solubility and of opposite sign in the heat of solution. The major difference in technique between Copeland's studies and Cleaver's and our studies appears to lie not in the pressure ranges studied but in the means of analysis. Copeland, *et al.*, use a manometric absorption method, whereas Cleaver's and our methods involve an elution process. The reason for the differences between Copeland's results and ours is difficult to assess. Since both techniques involve considerable agitation of the melt during saturation, it does not appear likely that supersaturation provides a reasonable explanation. Cleaver and Mather have discussed Copeland and coworkers' results in comparison to their own results and suggest the difficulty of Copeland's values is a consequence of determining the solubility as the small difference of two quantities of similar magnitude. Based on our general agreement with Cleaver's results we feel justified in assuming reasonable accuracy for our results and consider it worthwhile to examine the thermodynamic properties found.

Blander, *et al.*,[5] introduced the Uhlig[6] model for the calculation of gas solubilities in molten salts based on the surface free energy of formation of the cavity created by the solute molecule. The expression is derived in terms of the distribution coefficient, $K_c = C_d/C_g$, as

$$-\ln K_c = A\gamma/kT \qquad (3)$$

where A is the surface area of the cavity taken equal to the surface area of the solute molecule and γ is the "microscopic" surface tension of the molten salt assumed equal to the "macroscopic" surface tension. The calculation of A for the gas molecules is based on their van der Waals radii and in the case of linear polyatomic molecules, such as N_2 and CO_2, on the radius obtained by the appropriate sum of their bond distances and the van der Waals radius of the terminal atom. In the latter case, two alternatives are possible. If the molecule is assumed to be freely rotating the cavity area is based on the spherical region swept out by the calculated radius. On the other hand, the cavity area of a nonrotating molecule would be based on a cylinder having hemispherical ends and cross-sectional diameter determined by the van der Waals radius of the terminal atoms and length of the right cylinder determined by the sum of the bond distances.

A summary of both the experimentally determined and the calculated values of the distribution coefficients for all four gases at 637°K is presented in Table II. We have included both the spherical and cylindrical cavity geometries for nitrogen and carbon dioxide.

(5) M. Blander, W. R. Grimes, N. V. Smith, and G. M. Watson, *J. Phys. Chem.*, **63**, 1164 (1959).

(6) H. H. Uhlig, *ibid.*, **41**, 1215 (1937).

Table II: Comparison of Calculated and Experimental Distribution Coefficients in Sodium Nitrate at 637°K[a]

	Solute						
	Helium		Argon,	Nitrogen		Carbon dioxide	
	Cavity						
	Sphere	Sphere	Sphere	Sphere	Cylinder	Sphere	Cylinder
r, Å	1.22[b]	1.79[c]	1.92[b,c]	2.05[b]	1.50[d]	2.56	1.40[d]
d, Å					1.10[e]		1.16[e]
A, Å^2	18.7	40.2	46.3	51.8	38.6	82.3	45.0
10^3K_c (calcd)	88.5	5.43	2.46	1.20	6.68	0.02	2.91
10^3K_c (exptl)	5.54	5.54	3.72	11.72	11.72	5.50	5.50
$\frac{K_c \text{ (exptl)}}{K_c \text{ (calcd)}}$	0.06	1.02	1.51	9.78	1.76	240	1.89

[a] Surface tension taken at 114.15 dynes cm^{-1} from ref 2, p 82. [b] Radii used by Blander, *et al.*,[5] Copeland *et al.*,[3] and Cleaver and Mather.[4] [c] van der Waals radii taken from ref 8 and 9. [d] van der Waals radii for nitrogen and oxygen from ref 7. [e] Bond lengths taken from ref 10.

The values listed in Table II for the radii, r, and the bond lengths, d, are taken directly from the literature[3-5,7-10] except for the spherical radii of nitrogen and carbon dioxide. These values are calculated from the values listed for the dimensions of the cylindrical cavities. The radius for helium of 1.22 Å, originally used by Blander and coworkers and subsequently by others, is not in accord with the more recently assigned value of 1.79 Å.[9] Calculations based on both values are included in Table II. The significant improvement in the agreement between the calculated and experimental values of the distribution coefficient of helium is obvious and serves as well to illustrate the sensitivity of the calculation to the choice of cavity dimensions.

The ratios of the experimental to calculated values of the distribution coefficients for helium, argon, and the cylindrical geometries of nitrogen and carbon dioxide all lie within a factor of 2. These values are even slightly better than those found by Blander, *et al.*, for the rare gases in molten fluoride melts. To the approximation that the solubility would exceed the calculated hard sphere solubility due to ion-induced dipole and ion-permanent quadrupole (N_2 and CO_2) interactions, the distribution coefficient ratio would be expected to be greater than 1.

The strict delineation between a freely rotating and nonrotating solute molecule cannot be made because of the inseparability of the partition function of the solute in solution. However, the Uhlig model would appear to serve as an adequate guide in interpreting the solution process. In comparing various solutes, it is reasonable to anticipate an increasing interaction energy to be correlated with increasingly hindered rotation. Since the cavity formation is an endothermic process and any form of ion–molecule interaction would be expected to be exothermic, the observed heat of solution will be the sum of the two processes. Comparison of the heats of solution presented in Table I shows this expected trend with an apparent limiting value of around 3.2 for helium and argon and becoming increasingly more exothermic for nitrogen and carbon dioxide, although the uncertainty in ΔH^s for nitrogen makes the distinction less clear.

A similar effect would be anticipated in the entropy of solution, ΔS_c. The assignment of a major fraction of the entropy of solution to the decrease in the rotational entropy of the gas was reported previously from isotope studies of HF and DF in a fluoride melt.[11] Again the situation is not clear for nitrogen. However, a calculation of the rotational contribution to gaseous CO_2 at 637°K yields 15.7 eu.[12] A detailed analysis of all the contributions to the entropy of solution is not warranted on the limited data available. However, a comparison of the solution entropies (Table I) between helium and argon which have no rotational entropy, on the one hand, and carbon dioxide, on the other, shows a difference of about 10 eu. Assignment of this difference to a decrease in the free rotation of CO_2 is consistent with the proposed cylindrical cavity.

Acknowledgment. The authors wish to thank the National Science Foundation for grants GP-5144 and GP-8576 in support of this work.

(7) L. Pauling, "The Nature of the Chemical Bond," 3rd ed, Cornell University Press, Ithaca, N. Y., 1960, p 260.

(8) G. A. Cook, Ed., "Argon, Helium and the Rare Gases," Vol. I, Interscience, New York, N. Y., 1961, p 13.

(9) J. E. Huheey, *J. Chem. Educ.*, 45, 791 (1968).

(10) E. A. Moelyn-Hughes, "Physical Chemistry," 2nd ed, Pergamon Press, New York, N. Y., 1964, p 519.

(11) P. E. Field and J. H. Shaffer, *J. Phys. Chem.*, 71, 3218 (1967).

(12) K. K. Kelley and E. G. King, *U. S. Bur. Mines Bull.*, 592 (1961).

Solute–Solvent Effects in the Ionization of Tris(hydroxymethyl)acetic Acid and Related Acids in Water and Aqueous Methanol[1]

by Saul Goldman,[2] Pavel Ságner,[3] and Roger G. Bates*

Department of Chemistry, University of Florida, Gainesville, Florida 32601 *(Received September 28, 1970)*

Publication costs assisted by the National Science Foundation

The equilibrium behavior and solvent effect in the ionization of tris(hydroxymethyl)acetic acid (TH of interest in view of the structural relationship of this acid to acetic acid and to protonated tris(methyl)aminomethane (THAM), for which similar data are already available. Emf measurement without liquid junction were used to obtain the pK of THAA from 5 to 50° in water and from 10 to 4 50 wt % methanol–water solvent mixture. The standard changes of Gibbs energy, enthalpy, entropy, capacity for the ionization of THAA in the two solvent media were calculated from pK and its temper efficient. The thermodynamic functions for the transfer of the ionization process from water to 50% were also obtained. The results are compared with those for other acids structurally related to THA monotonic decrease in the Gibbs energy of ionization and the decreasing negative value of the entrop in the order pivalic acid–propionic acid–acetic acid–THAA are attributed to the changing inducti of the substituent groups. The pK of THAA, like that of other acids of the same charge type, is l 50% methanol than in water. The solvent effect on $\Delta S°$ and $\Delta C_p°$, however, is small. It is sugges the labile structure of water is broken down by interaction with the hydrophilic acid molecule in a similar to its destruction by methanol. Examined in terms of estimates of electrostatic charging eff results lend support to the view that specific solute–solvent interactions are of primary importance in ing for the acid–base behavior of THAA and related proton donors.

Introduction

There is increasing recognition of the importance of specific solute–solvent interactions in accounting for the equilibrium and kinetic behavior of electrolytes in solution. The numerous factors influencing this behavior include the structures of the solute and solvent species, especially their hydrogen-bonding capabilities,[4] the ionic charges, and the dielectric properties of the solvent medium.[5]

The equilibrium constants or the rates of selected chemical reactions involving ions offer a means of identifying the several solute and solvent parameters concerned. Much useful information can be obtained, for example, by a study of the ionization constants of weak acids and bases of different structures and charge types as a function of the properties of the solvent.[6] The use of solvent mixtures permits a range of dielectric constants to be obtained, but this procedure introduces the added complication of preferential solvation of the species participating in the ionization process.

The substitution of hydrophilic groups into the acid molecule enhances the interaction with the aqueous solvent, and a determination of pK reveals the influence of this interaction on the degree of dissociation. Likewise, a comparison of the dissociation constant of the same acid in water and in a mixture of water and methanol over a range of temperatures aids in elucidating the influence of the lowered dielectric constant and water activity on the changes in Gibbs energy, entropy, and enthalpy for the dissociation process and sheds light on the nature of the solute–solvent interactions which are operative in these systems.

The dissociation constant of acetic acid in water[7] and in methanol–water[8] solvents is well known, and the entropy and enthalpy changes for the dissociation of this acid in water and in 50 wt % methanol have also been determined.[7,9] Tris(hydroxymethyl)acetic acid may be expected to be hydrophilic in contrast with acetic acid, the methyl group of which is hydrophobic. It is therefore of interest to study the effect of this increased interaction with water on the dissociation of the carboxyl group that is common to both acids and on the associated thermodynamic quantities for the dissocia-

(1) This work was supported in part by the National Science Foundation under Grant GP 14538.

(2) National Research Council of Canada Postdoctorate Fellow.

(3) On leave from the College of Chemical Technology, Pardubice, Czechoslovakia.

(4) B. W. Clare, D. Cook, E. C. F. Ko, Y. C. Mac, and A. J. Parker, *J. Amer. Chem. Soc.*, **88**, 1911 (1966).

(5) I. M. Kolthoff and S. Bruckenstein in "Treatise on Analytical Chemistry," I. M. Kolthoff and P. J. Elving, Ed., Interscience, New York, N. Y., 1959, Part I, Vol. 1, Chapter 13; H. Ohtaki, *Bull. Chem. Soc. Jap.*, **42**, 1573 (1969).

(6) R. G. Bates, *J. Electroanal. Chem. Interfacial Electrochem.*, **29**, 1 (1971).

(7) H. S. Harned and R. W. Ehlers, *J. Amer. Chem. Soc.*, **54**, 1350 (1932); *ibid.*, **55**, 652 (1933). See also R. A. Robinson and R. H. Stokes, "Electrolyte Solutions," 2nd ed. Butterworths, London, 1959, Appendix 12.1.

(8) T. Shedlovsky and R. L. Kay, *J. Phys. Chem.*, **60**, 151 (1956).

(9) M. Paabo, R. A. Robinson, and R. G. Bates, *J. Amer. Chem. Soc.*, **87**, 415 (1965).

tion process. Inasmuch as the thermodynamics of the dissociation of protonated tris(hydroxymethyl)-aminomethane have also been studied in water[10] and in 50 wt % methanol,[11] a comparison of the data for the two acids of different charge may be expected to reveal the effect of charge type under conditions of approximately equal hydrophilic character.

The dissociation constant of tris(hydroxymethyl)-acetic acid (THAA) was determined in water from 5 to 50° and in 50 wt % methanol from 10 to 40° by emf measurements of the cell

$$\mathrm{Pt;H_2\ (g,\ 1\ atm),\ THAA}\ (m_1),\ \mathrm{NaTHA}\ (m_2),\ \mathrm{NaCl}\ (m_3),\ \mathrm{AgCl;Ag}$$

where m represents molality and THA is the tris(hydroxymethyl)acetate ion. The method used was very similar to that employed by Harned and Ehlers[7] in their determination of the dissociation constant of acetic acid. The standard changes of Gibbs energy, entropy, enthalpy, and heat capacity were derived from the change of pK with temperature. The results have been compared with similar data for other acids structurally related to acetic acid. The comparison suggests that the labile structure of water is broken down by interaction with the hydrophilic acid molecule in much the same way that it is destroyed by methanol and by the hydration of ionic species.

Experimental Section

A commercial sample of tris(hydroxymethyl)acetic acid was purified by crystallization from isopropyl alcohol; it assayed 100.2% (standard deviation = 0.1) when titrated with a standard solution of sodium hydroxide to the phenolphthalein end point. The stock buffer solutions were prepared by weight methods from the THAA, the standard alkali solution, a twice-crystallized sample of sodium chloride, and spectrograde methanol. The cell solutions (12 in water and 6 in methanol–water) were made by dilution of the stock solutions with distilled water or with 50 wt % methanol–water. Dissolved air was removed by bubbling purified hydrogen before the cells were filled.

The cells have been described elsewhere,[12] as has the preparation of the hydrogen and silver–silver chloride electrodes.[13] The values of the emf were measured both with a digital voltmeter reading to 0.01 mV and with a precision potentiometer (Leeds and Northrup type K-3) standardized with a group of saturated Weston cells maintained at constant temperature. The measurements by the two methods agreed to 0.02 mV in all cases. The temperatures of the constant temperature bath were measured with a calibrated quartz thermometer and were known to 0.01°K.

Results

The measured values of the emf (E) were corrected in the usual way to 1 atm partial pressure of hydrogen. Two cells were prepared from each of 16 cell solutions and a single cell from each of the remaining two solutions. The duplicate measurements agreed to 0.05 mV on the average.

The pK was determined by extrapolating values of the function pK' to zero ionic strength; pK' is defined by

$$\mathrm{p}K' \equiv \mathrm{p}K - \log \frac{\gamma_{\mathrm{Cl}^-}\gamma_{\mathrm{THAA}}}{\gamma_{\mathrm{THA}^-}} = \frac{E - E^\circ}{(RT\ln 10)/F} + \log \frac{m_{\mathrm{Cl}^-}m_{\mathrm{THAA}}}{m_{\mathrm{THA}^-}} \quad (1)$$

Equation 1 is obtained by combining the Nernst equation for the emf of the cell with the mass law expression for the acidic dissociation of THAA. Inasmuch as the anion is only slightly hydrolyzed at the pH values of the buffer solutions, $m_{\mathrm{THAA}} = m_1 - m_{\mathrm{H}^+}$ and $m_{\mathrm{THA}^-} = m_2 + m_{\mathrm{H}^+}$. The molalities of hydrogen ion were estimated from the equation

$$-\log m_{\mathrm{H}^+} = \frac{E - E^\circ}{(RT\ln 10)/F} + \log m_3 - \frac{2A(Id_0)^{1/2}}{1 + 4B(Id_0)^{1/2}} \quad (2)$$

which is obtained from the Nernst equation for the cell by substituting the Debye–Hückel formula for log $(\gamma_{\mathrm{H}^+}\gamma_{\mathrm{Cl}^-})$. In eq 2, A and B are the Debye–Hückel constants for the appropriate temperature and solvent

Table I: pK of Tris(hydroxymethyl)acetic Acid in Water and in 50 Wt % Methanol–Water

	Water			50 wt % MeOH–H_2O		
t, °C	pK^a	Est uncertainty	pK (calcd)[b]	pK^a	Est uncertainty	pK (calcd)[c]
5	4.5588	0.0036	4.5581			
10	4.5286	0.0040	4.5290	5.5832	0.0066	5.5834
15	4.5026	0.0031	4.5030	5.5331	0.0072	5.5331
20	4.4792	0.0037	4.4800	5.4885	0.0056	5.4880
25	4.4595	0.0035	4.4598	5.4479	0.0053	5.4478
30	4.4433	0.0030	4.4422	5.4122	0.0066	5.4124
35	4.4275	0.0041	4.4272	5.3809	0.0068	5.3815
40	4.4147	0.0036	4.4146	5.3553	0.0062	5.3548
45	4.4044	0.0034	4.4043			
50	4.3957	0.0031	4.3962			

[a] Derived from the experimental data. [b] pK (calcd) = $(1412.7/T) - 3.8915 + 0.012119T$. [c] p$K$ (calcd) = $(2499.7/T) - 9.0701 + 0.020573T$.

(10) R. G. Bates and H. B. Hetzer, *J. Phys. Chem.*, **65**, 667 (1961). S. P. Datta, A. K. Grzybowski, and B. A. Weston, *J. Chem. Soc.*, 792 (1963).

(11) M. Woodhead, M. Paabo, R. A. Robinson, and R. G. Bates, *J. Res. Nat. Bur. Stand.*, **69A**, 263 (1965).

(12) R. G. Bates, Ed., *Nat. Bur. Stand. (U. S.) Tech. Note*, **271**, 28 (1965).

(13) R. G. Bates, "Determination of pH," Wiley, New York, N. Y., 1964, Chapter 9.

Table II: Thermodynamic Functions (Molal Scale) for the Dissociation of Tris(hydroxymethyl)acetic Acid in Water and in 50 Wt % Methanol–Water at 15, 25, and 35°

	Water			50 wt % MeOH–H_2O		
	15°	25°	35°	15°	25°	35°
$\Delta H°$, cal mol^{-1} [a]	1860	1535	1199	3622	3070	2499
$\Delta S°$, cal $°K^{-1}$ mol^{-1}	−14.2	−15.3	−16.4	−12.7	−14.6	−16.5
$\Delta C_p°$, cal $°K^{-1}$ mol^{-1}	−32.0	−33.1	−34.2	−54.3	−56.1	−58.0

[a] 1 cal = 4.184 J.

dielectric constant,[14] d_0 is the solvent density,[14] and I, the ionic strength, is given by $m_2 + m_3 + m_{H^+}$.

Values for the standard emf of the cell, $E°$, in water and in 50 wt % aqueous methanol are given in the literature.[15,16] These literature values for the aqueous medium were adjusted by the empirical method according to which the activity coefficient of hydrochloric acid is taken as a standard.[17] By means of emf measurements at 25° of aqueous hydrochloric acid solutions of molality 0.01, $E°$ at this temperature was found to be 0.22264 V, or higher by 0.3 mV than the values tabulated in the literature. This same correction was applied at each temperature to obtain $E°$ for the water system. The values of $E°$ for the water–methanol systems[16] were used without further correction.

The procedure for obtaining the values of pK was as follows. Equation 2 was successively iterated (m_{H^+} being initially taken to be zero in computing I) until convergent values of both m_{H^+} and I were obtained. These latter values were then used to perform a least-squares fit through the linear regression of pK' on I. The least-squares estimate of the intercept of this regression was pK. The values of pK obtained in this way are entered in columns 2 and 5 of Table I. The least-squares estimates for the standard deviations of pK are listed in columns 3 and 6 of the same table.

The values of pK so obtained were fitted, by the method of least squares, to an equation of the form selected by Harned and Robinson[18]

$$pK = \frac{A_1}{T} - A_2 + A_3T \qquad (3)$$

where T is the thermodynamic temperature in °K. It was necessary to use double precision arithmetic (16 digits) in order to obtain a satisfactory fit to the data. The values of A_1, A_2, and A_3 are given at the bottom of Table I, and pK calculated with eq 3 is entered in columns 4 and 7 of this table.

Thermodynamic Functions

The standard molar changes of enthalpy, entropy, and heat capacity on dissociation of THAA were evaluated from eq 3 together with the numerical values of A_1, A_2, and A_3. The values obtained at 15, 25, and 35° are entered in Table II. The standard deviations of these quantities were estimated by application of the method of propagation of errors. The estimates are as follows: $\Delta H°$ = 34 cal mol^{-1} in H_2O, 97 cal mol^{-1} in MeOH–H_2O; $\Delta S°$ = 0.11 cal $°K^{-1}$ mol^{-1} in H_2O, 0.33 cal $°K^{-1}$ mol^{-1} in MeOH–H_2O; $\Delta C_p°$ = 5.0 cal $°K^{-1}$ mol^{-1} in H_2O, 22 cal $°K^{-1}$ mol^{-1} in MeOH–H_2O.

The standard Gibbs energy, enthalpy, and entropy changes for the transfer reaction

$$THAA(s) + H^+(w) + THA^-(w) = THAA(w) + H^+(s) + THA^-(s) \qquad (4)$$

where w indicates the aqueous medium and s denotes the 50 wt % methanol–water solvent, were also calculated. The values of these quantities at 15, 25, and 35° are given in Table III.

Table III: Thermodynamic Functions (Molal Scale) for the Transfer Process THAA(s) + H^+(w) + THA^-(w) = THAA (w) + H^+(s) + THA^-(s) between Water (w) and 50 Wt % Methanol–Water (s)

	15°	25°	35°
$\Delta G_t°$(diss),[a] cal mol^{-1}	1359	1348	1344
$\Delta H_t°$(diss),[b] cal mol^{-1}	1762	1535	1301
$\Delta S_t°$(diss),[c] cal $°K^{-1}$ mol^{-1}	1.40	0.63	−0.15

[a] $\Delta G_t°(\text{diss}) = (RT \ln 10)(p_sK - p_wK)$; experimental values of pK. [b] $\Delta H_t°(\text{diss}) = \Delta H°(s) - \Delta H°(w)$. [c] $\Delta S_t°(\text{diss}) = \Delta S°(s) - \Delta S°(w)$.

Discussion

Gibbs Energy. The standard Gibbs free energies of ionization in water (column 2 of Table IV) decrease monotonically in the sequence pivalic acid (trimethyl-

(14) R. G. Bates and R. A. Robinson in "Chemical Physics of Ionic Solutions," B. E. Conway and R. G. Barradas, Ed., Wiley, New York, N. Y., 1966, Chapter 12.

(15) R. G. Bates and V. E. Bower, *J. Res. Nat. Bur. Stand.*, **53**, 283 (1954).

(16) M. Paabo, R. A. Robinson, and R. G. Bates, *J. Chem. Eng. Data*, **9**, 374 (1964).

(17) R. G. Bates, E. A. Guggenheim, H. S. Harned, D. J. G. Ives, G. J. Janz, C. B. Monk, J. E. Prue, R. A. Robinson, R. H. Stokes, and W. F. K. Wynne-Jones, *J. Chem. Phys.*, **25**, 361 (1956).

(18) H. S. Harned and R. A. Robinson, *Trans. Faraday Soc.*, **36**, 973 (1940).

Table IV: Thermodynamic Functions (Molal Scale) for the Dissociation of a Series of Structurally Related Carboxylic Acids at 25°

Acid	Water[a]				50 wt % MeOH–H_2O			
	$\Delta G°$	$\Delta H°$	$\Delta S°$	Ref	$\Delta G°$	$\Delta H°$	$\Delta S°$	Ref
$(CH_3)_3CCOOH$	6865	−724	−25.4	*a*				
CH_3CH_2COOH	6649	−200	−22.9	*a,b*				
CH_3COOH	6488	−94	−22.1	*c*	7722	−52	−26.1	*d*
$(CH_2OH)_3CCOOH$	6084	1535	−15.3	This work	7432	3070	−14.6	This work

[a] D. H. Everett, D. A. Landsman, and B. R. W. Pinsent, *Proc. Roy. Soc., Ser. A*, **215**, 403 (1952). [b] H. S. Harned and R. W. Ehlers, *J. Amer. Chem. Soc.*, **55**, 2379 (1933). [c] R. A. Robinson and R. H. Stokes, "Electrolyte Solutions," 2nd ed, Butterworths, London, 1959, Appendix 12.1. [d] M. Paabo, R. A. Robinson, and R. G. Bates, *J. Amer. Chem. Soc.*, **87**, 415 (1965).

acetic acid) > propionic acid > acetic acid > THAA, and this same trend holds for acetic acid and THAA in 50 wt % methanol–water (column 6). The decrease in free energy (increase in degree of dissociation) may be explained qualitatively by the differing inductive effects of the groups adjacent to the carboxylate site. Thus, the three methyl groups in pivalic acid will induce the greatest relative charge density on the carboxylate site, while, because of its three hydroxyl groups, THAA will have the smallest relative charge density at this point.[19] Furthermore, this inductive effect on the dissociation constant of the acid seems to override any other effects caused by the varying degrees of hydrophobic character of the acid molecules.

In changing the solvent from water to 50 wt % methanol–water, both acetic acid and THAA show an increase in standard free energy of dissociation. This observation is consistent with the effect of the lowered dielectric constant of the mixed solvent in increasing the electrostatic free energies of the ions produced in the dissociation process.

Entropy. The standard entropy of dissociation of a neutral acid in a polar solvent may be expected to be negative, since ions are more capable than neutral molecules of partially immobilizing and orienting solvent molecules about themselves. This expectation is borne out by the negative values entered in columns 4 and 8 of Table IV. It is seen from these values of $\Delta S°$ that the standard entropy changes become less negative in the following sequence: pivalic acid–propionic acid–acetic acid–THAA. This order may also be qualitatively explained by the differing inductive effects of the substituent groups in the acid molecules. As the charge density of the carboxylate site of the anion decreases, so too does the carboxylate site decrease in its capacity to orient the partially immobilized solvent molecules about itself.

It is interesting to note that the standard entropy of dissociation of acetic acid is more negative in the methanol–water solvent mixture than in water. This fact is consistent with the observation that the standard entropy of solution of the alkali halides in methanol–water mixtures becomes steadily more negative with increasing methanol content.[20] This trend has been explained as follows:[20,21] The methanol–water mixtures are less structured than pure water, and therefore these mixed solvents can be thought of as offering less resistance than pure water to solvent reorientation. For this reason, ions or centers of charge will orient solvent molecules more readily in methanol–water media than in water. The greater degree of orientation results in a more negative standard entropy of dissociation in the mixed solvent.

It is therefore surprising to note that the value of $\Delta S°$ for the ionization of THAA does not change substantially from the water solvent to the methanol–water medium. It may well be that the three hydrophilic hydroxyl groups in THAA cause a partial breakdown of the water structure to occur in the aqueous medium, in contrast with the initial enhancement of structure believed to result from the solution of some substances containing hydrophobic alkyl groups. The THA^- anion in pure water thus finds itself surrounded by a solvent medium whose degree of structure is comparable to, or even less than, that of the 50 wt % methanol–water mixture. If this is the case, the degree of reorientation and partial immobilization of the solvent molecules by the THA^- anion may not be greater in 50 wt % methanol than in pure water. As a consequence, the negative shift in the value of $\Delta S°$ observed for acetic acid in going from water to 50 wt % methanol need not necessarily occur with THAA.

Enthalpy. The standard changes in enthalpy of ionization of the acids vary monotonically with solute structure (columns 3 and 7 of Table IV). As the enthalpy change is the sum of the free energy and entropy contributions, this variation may be attributed to the fact that both $\Delta G°$ and $\Delta S°$ vary monotonically with solute structure.

Heat Capacity. The standard changes in heat capacity for the dissociation of THAA appear to be almost the same in water and in 50 wt % methanol–water

(19) C. K. Ingold, "Structure and Mechanism in Organic Chemistry," 2nd ed, Cornell University Press, Ithaca, N. Y., 1969.

(20) W. M. Latimer and C. M. Slansky, *J. Amer. Chem. Soc.*, **62**, 2019 (1940).

(21) D. D. Eley and D. C. Pepper, *Trans. Faraday Soc.*, **37**, 581 (1941).

(Table II). These values depend on an evaluation of the second derivative of emf with temperature and therefore involve relatively large experimental uncertainties; hence, no attempts at interpretation appear justified.

Transfer Energy. It is of interest to examine the transfer energy $\Delta G_t°$(diss) given in Table III. This quantity can be expressed in terms of the transfer energies of each of the three species participating in the dissociation of THAA as follows

$$\Delta G_t°(\text{diss}) = \Delta G_t°(H^+) + \Delta G_t°(THA^-) - \Delta G_t°(THAA) \quad (5)$$

where the Gibbs energy change in each case is for the transfer process

species i (stand. state in H_2O) = species i (stand. state in 50% MeOH)

The determination of these transfer energies individually is sometimes useful in assessing the relative importance of electrostatic charging effects and specific solute–solvent interactions on the sign and magnitude of the change in pK.[6] Unfortunately, the high solubility of THAA in water precludes a measurement of the transfer functions for the undissociated acid directly. Consequently, it is difficult at present to interpret the values in Tables I and II in terms of the interactions between solute and solvent species, as has been done for certain other acidic dissociation processes.[6,22,23]

Protonated tris(hydroxymethyl)aminomethane (THAM) is a positively charged acid very similar in structure to THAA. The standard thermodynamic quantities for the transfer process analogous to eq 4 have been calculated from the dissociation constant of protonated THAM in water and in 50 wt % methanol–water over a suitable range of temperatures.[10,11] The value of $\Delta G_t°$(diss) was found to be -337 cal mol^{-1} at 25°, as compared with 1348 cal mol^{-1} for THAA (see Table III).

It is virtually certain that the proton is highly solvated both in water and in 50% methanol. Very little is known, however, about the structure of the solvated proton, and the several estimates of the transfer energy of this ion are widely disparate.[24] Fortunately, an examination of the differences between the transfer energies for THAA and THAM·H$^+$ can be made without an estimate of the transfer energy of the proton. Thus, it is found that the standard Gibbs energy change for the process

$$HA(s) + A^-(w) + BH^+(w) + B(s) = HA(w) + A^-(s) + BH^+(s) + B(w) \quad (6)$$

where, for simplicity, HA and B are written for THAA and THAM, respectively, is 1685 cal mol^{-1} at 25°, on either the molality or mole fraction scales. Hence

$$\Delta[\Delta G_t°(\text{diss})] = [\Delta G_t°(BH^+) - \Delta G_t°(B)] + [\Delta G_t°(A^-) - \Delta G_t°(HA)] = 1685 \text{ cal mol}^{-1} \quad (7)$$

It is convenient to divide the transfer energies for a mole of ions BH$^+$ and A$^-$ from water to 50% methanol each into two terms[24,25]

$$\Delta G_t°(\text{i}) = \Delta G_t°(\text{el}) + \Delta G_t°(\text{nonel}) \quad (8)$$

The "electrostatic" term represents the difference in energy due to charging effects of the Born type[26] resulting from the different dielectric constants of the two media. All other effects, including the difference in work required to create a cavity for the ions in the two media, contribute to the second term.

Both THAA and THAM contain the bulky hydrophilic grouping $(CH_2OH)_3C-$, and it is not unreasonable, therefore, to assume that their approximately equal sizes and strong similar interactions with water molecules will assure that the standard energy changes produced on transfer of these uncharged species from water to 50% methanol will be nearly the same and will correspond closely with the nonelectrostatic part of the transfer energy for the ions THA$^-$ and THAM·H$^+$. The observed difference $\Delta[\Delta G_t°(\text{diss})]$ might thus be largely dependent on electrostatic charging effects

$$\Delta[\Delta G_t°(\text{diss})] \approx \Delta G_t°(\text{el, } BH^+) + \Delta G_t°(\text{el, } A^-) \quad (9)$$

The evaluation of charging effects in terms of coulomb forces is hampered by the irregular shapes of many ions of interest and by a lack of knowledge both of effective ionic radii and of the variation in dielectric constant with distance from the ionic surface. Nevertheless, there have been partially successful attempts to improve the Born treatment by allowing for dielectric saturation in the immediate vicinity of the ions.[27,28] In addition, allowance has been made for electrostatic interactions of a higher order.[25] In Figure 1, the sum of the electrostatic terms represented on the right side of eq 9, as calculated in three different ways, is plotted as a function of ionic radius. It is evident that the effective radii of the ions THAM·H$^+$ and THA$^-$ would have to be small to account for charging effects as large as the 1685 cal mol^{-1} found for $\Delta[\Delta G_t°(\text{diss})]$. In actuality, the radius of THAM·H$^+$ has been estimated[11] to be about 4 Å, on the basis of a spherical model.

(22) R. Gaboriaud, *Ann. Chim.*, 2, 201 (1967).
(23) P. Schindler, R. A. Robinson, and R. G. Bates, *J. Res. Nat. Bur. Stand.*, 72A, 141 (1968).
(24) O. Popovych, *Crit. Rev. Anal. Chem.*, 1, 73 (1970).
(25) M. Alfenaar and C. L. deLigny, *Recl. Trav. Chim. Pays-Bas*, 86, 929 (1967).
(26) M. Born, *Z. Phys.*, 1, 45, 221 (1920).
(27) L. G. Hepler, *Aust. J. Chem.*, 17, 587 (1964).
(28) R. H. Stokes, *J. Amer. Chem. Soc.*, 86, 979 (1964).

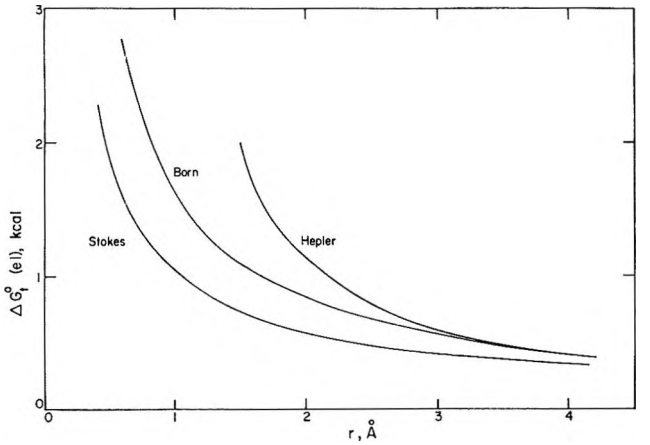

Figure 1. Calculated molar electrostatic energies for the transfer of the ions THAM·H$^+$ and THA$^-$ from water to 50% MeOH–H_2O, plotted as a function of spherical ionic radius.

The present results point once again to the inadequacy, emphasized elsewhere,[22,29] of attempts to explain the equilibrium properties of systems involving ions by Born charging effects alone. The most serious defect of the Born-type treatment remains its inability to account for the opposite signs of the energy changes for cations and anions on transfer from water to methanol–water solvents. It now seems well established by various nonthermodynamic approaches[24,25,30] that simple cations are stabilized by the 50 wt % methanol–water medium while anions of comparable size suffer an increase of free energy. Explanations for these differences must be sought in the details of the specific solute–solvent interaction, the importance of which appears to outweigh that of Born-type effects in accounting for the behavior of electrolytes in solution.

Acknowledgment. The authors are indebted to Professor R. A. Robinson for suggesting a comparison of the acid–base properties of THAA and THAM and for purifying a portion of the THAA used in this study.

(29) A. S. Quist and W. L. Marshall, *J. Phys. Chem.*, 72, 684 (1968).
(30) A. L. Andrews, H. P. Bennetto, D. Feakins, K. G. Lawrence, and R. P. T. Tomkins, *J. Chem. Soc. A*, 1486 (1968).

Estimation of Induction Energies Using Gas–Liquid Chromatography

by Edwin F. Meyer* and Richard A. Ross

Chemistry Department, DePaul University, Chicago, Illinois 60614 *(Received June 22, 1970)*

Publication costs borne completely by The Journal of Physical Chemistry

The ability of a polar solute to induce a dipole into a nonpolar solvent has been investigated using gas–liquid chromatography. The resulting energy of attraction (kcal/mol) has been estimated for acetone (1.3), chloropentane (1.1), and capronitrile (2.1) in Apiezon M. Thermodynamic properties of solution have been measured for these solutes as well as *n*-hexane and isobutylene in Apiezon M. The importance of eliminating the influence of the solid support on retention volumes (hence the derived thermodynamic properties) is very apparent.

There are three types of attractive energy which contribute to cohesion among neutral, nonhydrogen bonding, polar molecules: orientation (permanent dipole–permanent dipole), induction (permanent dipole–induced dipole), and dispersion (interaction of the instantaneous dipoles of the nucleus–electron arrangement). Of these, induction has generally been considered unimportant. Recently, however, evidence has been presented that this contribution may be quite significant in the interaction of polar organic liquids.[1–3]

The present paper describes an approach to quantitative estimation of induction energies between polar solutes and nonpolar solvents. The molecules studied provide values for comparison with those of Meyer, *et al.*,[3] obtained by a completely different approach involving pure liquid systems.

Theoretical Section

That the thermodynamics of solution may be profitably studied using gas–liquid chromatography is well established.[4] The free energy, enthalpy, and entropy

(1) R. F. Weimer and J. M. Prausnitz, *Hydrocarbon Process.*, **44**, 237 (1965).
(2) E. F. Meyer and R. E. Wagner, *J. Phys. Chem.*, **70**, 3162 (1966).
(3) E. F. Meyer, T. A. Renner, and K. S. Stec, *J. Phys. Chem.*, **75**, 642 (1971).
(4) See, *e.g.*, H. Purnell, "Gas Chromatography," Wiley, New York, N. Y., 1962.

of solution at infinite dilution of volatile solutes in nonvolatile solvents are readily obtained through studies of retention volumes as a function of temperature, sample size, and the amount of liquid phase in the column.

The quantities of primary interest in this study are the energies of solution at infinite dilution of a polar molecule and its nonpolar counterpart (*e.g.*, acetone and isobutylene) in a nonpolar solvent (*e.g.*, Apiezon M). These are readily obtained from the enthalpies of solution by assuming the vapors behave ideally and subtracting RT.

The energy of solution at infinite dilution for a polar solute will be the sum of dispersion and induction energies between it and the solvent. Orientation cannot contribute because there is but a single dipole in a sea of nonpolar material. Thus, a reliable estimate of the dispersion contribution to the energy of solution for the polar solute allows evaluation of its induction energy by difference.

The Slater–Kirkwood equation[5]

$$E_{\text{disp}} = \frac{\alpha_1\alpha_2}{r^6\left[\left(\frac{\alpha_1}{N_1}\right)^{1/2} + \left(\frac{\alpha_2}{N_2}\right)^{1/2}\right]}$$

where α is polarizability, N is the number of electrons in the outer shell, and r is the distance between interacting centers, has been shown to be fairly reliable for interactions in simple hydrocarbons.[6] Our use of it is as follows: Interacting molecules are considered to be made up of groups. For example, acetone contains two methyl groups and one carbonyl group; Apiezon M (AM) is comprised of molecules containing nine methylene groups per methyl group.[7] Dispersion energies are calculated for pairwise interacting groups and weighted sums are produced for each solute–solvent pair. For example, in the acetone–AM case, energies are calculated for the following pairs: CH_3–CH_3, CH_3–CH_2, CO–CH_3, and CO–CH_2. Since the empirical formula of the AM corresponds to $CH_3(CH_2)_{18}CH_3$, the weighting factors are $^4/_{60}$, $^{36}/_{60}$, $^2/_{60}$, and $^{18}/_{60}$, respectively, for one acetone molecule in a sea of Apiezon M molecules.

By assuming r is the same for all solute–solvent pairs at infinite dilution in the same temperature range, ratios of dispersion energies can be produced with no knowledge of the absolute distances between interacting centers. In this manner the following ratios were obtained: acetone–AM/isobutylene–AM = 0.883; chloropentane–AM/hexane–AM = 1.009; and capronitrile–AM/hexane–AM = 0.992. Multiplication of these ratios by the dispersion energy of isobutylene–AM in the first case and hexane–AM in the second and third cases produces the dispersion interaction of the corresponding polar molecule with the AM. But the dispersion energy for the nonpolar solutes is just the measured energy of solution at infinite dilution, since in the absence of a permanent dipole, there can be no orientation or induction contributions to the interaction. Subtraction of the dispersion contributions from the measured energies of solution of the polar solutes produces their induction energies.

Appropriate treatment of the retention volumes[4] for each solute molecule also provides its standard free energy and entropy of solution at infinite dilution.

Experimental Section

All compounds were research grade materials of 99% purity. Retention times were measured using an F&M Scientific Corp. dual column gas chromatograph, Model 720. Flow rates were measured using the soap bubble method, and corrections were made for the vapor pressure of the soap solution. A mercury manometer was used to measure the inlet pressure of the helium carrier gas. The compressibility correction factors of Stock and Rice[8] were applied to the retention volumes to compensate for the pressure gradient across the column.

Temperatures were measured with a thermocouple calibrated against an NBS certified thermometer. The oven containing the column was controlled to 0.2°.

Three 10-ft columns of $^1/_4$-in. copper tubing were made with 7.5, 15, and 30% Apiezon M on Chromosorb W, 50–60 mesh size, AW-DMCS treated solid support. Specific retention volumes, V_g, were obtained for each of these columns at a series of temperatures.

Attempts were made to correlate V_g with sample size and extrapolate to infinite dilution (zero sample size), but the variation in V_g was of the same order as the experimental error therein; 3-μl samples were therefore used in all cases, and the assumption made that solute interactions are negligible for this sample size.

In order to maximize precision in comparing retention volumes of polar and nonpolar counterparts, they were mixed before injection into the column. Acetone and isobutylene were injected simultaneously, as were hexane, chloropentane, and capronitrile.

Least-squares analyses of log V_g *vs.* $1/T$ data were made for each solute on each column, and enthalpies of solution were evaluated from the slopes. Plots of the enthalpies for each solute *vs.* the inverse of the percentage liquid phase on the column were extrapolated to 0.01 (100% liquid phase) to minimize any influence of the solid support on the solute. Similar plots were made for the log V_g's at one temperature for the evaluation of free energies and entropies of solution.

Results

Table I lists the constants for the log V_g *vs.* $1/T$ equations, the standard deviation in log V_g, and the

(5) H. Margenau, *Rev. Mod. Phys.*, 11, 1 (1939).

(6) K. S. Pitzer, *Advan. Chem. Phys.*, 2, 59 (1959), see p 75.

(7) Based on nmr analysis performed in our laboratory.

(8) R. Stock and C. B. F. Rice, "Chromatographic Methods," Chapman and Hall, 1968, p 30.

standard enthalpy of solution for each of the solutes on each of the columns. Table II lists the standard enthalpy, free energy, and entropy of solution for each solute at infinite dilution and 100% liquid phase. Table III lists the energies of solution, the dispersion contributions, and the induction energies for each solute. The values of Meyer, *et al.*,[3] are included for comparison.

Table I: Log $V_g = m(10^3/T) + b$

	% liquid	m	$-b$	Std dev	$-\Delta H°_{soln}$, kcal
Hexane	7.5	1.564	2.815	0.031	6.61
	15.0	1.466	2.643	0.009	6.16
	30.0	1.415	2.495	0.016	5.94
Chloropentane	7.5	1.804	2.976	0.025	7.70
	15.0	1.710	2.824	0.013	7.27
	30.0	1.667	2.695	0.015	7.09
Capronitrile	7.5	1.908	2.991	0.027	8.18
	15.0	1.883	3.069	0.008	8.07
	30.0	1.852	2.964	0.004	7.94
Isobutylene	7.5	1.186	2.257	0.021	4.93
	15.0	1.141	2.561	0.010	4.71
	30.0	1.078	2.389	0.013	4.43
Acetone	7.5	1.425	2.757	0.038	6.02
	15.0	1.317	2.901	0.009	5.52
	30.0	1.306	2.805	0.011	5.50

Table II:[a] Thermodynamic Properties of Solution in Apiezon M at Infinite Dilution and 100% Liquid Phase

	$-\Delta H°$, kcal	$-\Delta G°$, kcal	$-\Delta S°$, eu
Hexane	5.78	2.24	8.9
Chloropentane	6.93	3.06	9.8
Capronitrile	7.88	3.45	11.2
Isobutylene	4.32	1.06	9.1
Acetone	5.20	1.46	10.5

[a] $\Delta G°$ and $\Delta S°$ values refer to 400°K for the first three solutes; to 355°K for the last two.

Table III: Energies of Solution and Their Component Parts

	$-\Delta E°_{soln}$	E_{disp}	E_{ind}	E_{ind}[a]
Hexane	4.98	4.98	0	
Chloropentane	6.13	5.02	1.1	0.8
Capronitrile	7.08	4.94	2.1	2.0
Isobutylene	3.61	3.61	0	
Acetone	4.49	3.19	1.3	1.3

[a] See ref 3.

Discussion

Comparison of the results of this work with the earlier values for induction energies lends support to the validity of both methods, and for the importance of induction energies in intermolecular interactions in liquids.

The maximum standard deviation in log V_g corresponds to a variation of about 0.1 kcal in the enthalpy of solution values. This would lead to a possible variation of 0.2 kcal in induction energy, since the latter is obtained by difference from the enthalpy data. The earlier values may be off by 0.1 kcal, so the results of the two approaches agree within the maximum experimental error.

Agreement of the induction energies in this work with those obtained using pure liquid systems[3] is significant only insofar as the time average distances between interacting centers are the same. We can estimate the effect of distance on induction energy by considering the effect of temperature on the energy of vaporization of a nonpolar molecule such as hexane. The latter energy is all dispersion, which depends on distance in the same way as induction energy. We may therefore expect the percentage change in induction energy to approximate that of dispersion energy, which is under 2% for every 10° at the boiling point, and decreases as the temperature rises. Thus, even though the comparison of induction energies is made at different temperatures, the agreement is certainly significant.

Another point which should be raised is that we are comparing induction energies between polar molecules (ref 3) and those between the polar molecule and a nonpolar solvent molecule. In general, the polarizabilities of the groups comprising the polar molecule and the nonpolar solvent are quite similar (*i.e.*, they can accept an induced dipole to the same degree), making the comparison a valid one.

The standard states to which the thermodynamic properties refer are as follows: The solute in the gas phase is assumed ideal, at 1 atm and 0°. The solute in the solvent is at the same concentration as in the gaseous standard state and at 400°K for hexane, chloropentane, and capronitrile; at 355°K for acetone and isobutylene.

A search of the literature did not reveal any data to which direct comparisons of our results can be made. However, the thermodynamic properties of hexane in several hydrocarbon solvents have been measured by several authors.[9-11] A comparison of their results with ours is made in Table IV. The main reason for the discrepancy is the difference in temperature of the measurements. The present work involves a temperature about 60° higher than these references, so less negative values of enthalpy, free energy, and entropy are expected. The magnitudes of the differences are reasonable. For example, the enthalpy of vaporiza-

(9) A. B. Littlewood, *Anal. Chem.*, 36, 1441 (1964).

(10) A. Kwantes and G. W. A. Rijnders, "Gas Chromatography 1958," D. H. Desty, Ed., Butterworths, London, 1958, p 125.

(11) Y. B. Tewari, D. E. Martire, and J. P. Sheridan, *J. Phys. Chem.*, 74, 2345 (1970).

tion of hexane changes by about 0.1 kcal every 10°; if the same is true for its enthalpy of solution in hydrocarbon solvents, the value at 127° should be roughly 0.7 kcal lower than at 60°.

Table IV: Thermodynamic Properties of Solution of *n*-Hexane in Some Alkanes Using Glc

Solvent	*t*, °C	$-\Delta H°$	$-\Delta G°$	$-\Delta S°$
n-Hexadecane[a]	60	7.00	3.27	11.2
n-Hexadecane[b]	60	6.87	3.27	10.8
n-Tetracosane[b]	60	6.63	3.17	10.4
n-Tetracosane[c]	80	6.27	2.92	9.5
Apiezon M[d]	127	5.78	2.24	8.9

[a] See ref 9. [b] See ref 10. [c] See ref 11. [d] This work.

The entropy of solution values in Table II vary directly with the strength of the solute dipole. It seems reasonable that the entropy of solution in a nonpolar solvent should be greater for a molecule which can form what might be considered a "dipole–induced dipole complex" with the solvent than for one which cannot do so. Littlewood,[9] on the other hand, observed that the dipole moment of the solute has no marked effect on its entropy of solution. While his work is of greater precision, we have taken steps to eliminate the influence of the support on our results. At present it is not clear why our results differ.

The importance of taking into account the influence of the solid support has recently been given emphasis by Urone, *et al.*[12] They have measured sorption isotherms of several vapors in some common glc solvents, on some common glc supports, and on/in combinations of the two. They find that even DMCS treatment, while it severely deactivates the support, does not eliminate its influence on the sorption isotherm.

These authors have observed that the amount of sorbate adsorbed on the support itself is independent of the quantity (above 1%) of liquid phase on the support. Consequently, they suggest that the influence of the support on retention volumes may be allowed for by using several columns with different liquid loadings, plotting V_g *vs.* percentage liquid phase, and extrapolating to zero liquid phase. The corresponding value of V_g represents the constant contribution of the support and is to be subtracted from observed V_g's.

Our observation is that the variation of V_g with liquid loading *in the glc experiment* does not allow such treatment of the data. It is conceivable that complete equilibration of the solute with the underlying solid may not occur, at least at the flow rates we used (about 40 ml/min). (Urone, *et al.*,[12] state that equilibration took from 2 to 5 min in their experiments.) The retention volumes were highest for the 7.5% column, and those for the 15 and 30% columns were closer together than those for the 7.5 and 15% columns. The indication is that the influence of the support diminishes with increased liquid loading. In the light of this observation, the present approach to minimizing the influence of the support on V_g and the thermodynamic properties derived therefrom seems quite reasonable.

The choice of isobutylene as a nonpolar counterpart of acetone may be open to some question, since it has a dipole moment of 0.5 D. However, induction energies are related to the square of the dipole moment[3], and this quantity for isobutylene is but 3% of that of acetone. This is certainly within the experimental error of our induction energies.

In conclusion, it can be stated that induction energies in common polar liquids contribute in the order of kilocalories to the total energy of attraction. They are certainly not negligible, as has commonly been thought.

Acknowledgments. We thank Dr. T. J. Murphy for nmr analysis of the Apiezon M.

(12) P. Urone, Y. Takahashi, and G. H. Kennedy, *J. Phys. Chem.*, **74**, 2326 (1970).

NOTES

The Relative Rates of the Reactions of Hydrogen Atoms with Hydrogen Iodide and Hydrogen Bromide

by R. J. Letelier,[1] H. L. Sandoval, and R. D. Penzhorn*

Chemistry Department, Faculty of Physical and Mathematical Sciences, University of Chile, Santiago, Chile *(Received September 8, 1970)*

Publication costs borne completely by The Journal of Physical Chemistry

The photochemistry of hydrogen halides has been a subject of renewed interest in recent years,[2] mainly because they are a convenient source of thermal and 0–3 eV hot hydrogen atoms.[2f] Nevertheless, no direct measurements of the relative rates of the reactions of hydrogen atoms with hydrogen halides have been found in the literature.

We have investigated the photolysis of HI and HBr in the presence of ethylene, monofluoroethylene, tetrafluoroethylene, and iodine. Experimentally only the hydrogen quantum yield (Φ_{H_2}) was measured using an apparatus and technique described in a previous paper.[3] Φ_{H_2} was defined as the ratio of the rate of hydrogen produced from a olefin–hydrogen halide–CO_2 mixture over that of the same hydrogen halide–CO_2 mixture without the olefin. At low conversions and under thermal conditions (excess of CO_2 generally greater than 20 times the combined reagent pressures) only the reactions

$$H + HX \longrightarrow H_2 + X \quad (X = I \text{ or } Br) \quad (1)$$

$$H + X_2 \longrightarrow HX + X \quad (2)$$

$$H + C_2F_xH_y \longrightarrow C_2F_xH_{y+1} \quad (x + y = 4) \quad (3)$$

$$H + C_2F_xH_y \longrightarrow H_2 + C_2F_xH_{y-1} \quad (4)$$

are of interest. The Φ_{H_2} is related to the partial pressures of the various reactants by the following equation

$$\left(\frac{1}{\Phi_{H_2}} - 1\right)^{-1} = \frac{k_4}{k_3} + \frac{k_1HX}{k_3C_2F_xH_y}$$

or

$$= \frac{k_1HX}{k_2X_2}$$

The results have been plotted in Figures 1–3A, employing the least-squares method. As expected, a zero intercept was found for C_2H_4 and C_2F_4 regardless of the H atoms source employed, whereas with C_2FH_3 a small positive intercept, which has been attributed

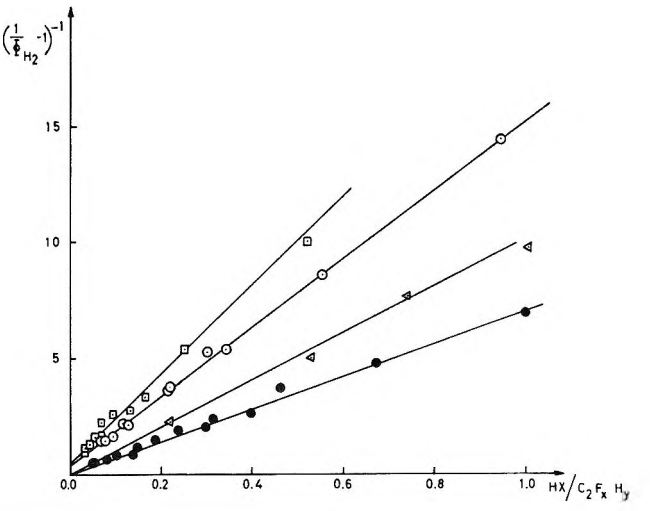

Figure 1. Photolysis of: △, C_2F_4–HI; ●, C_2F_4–HBr; ⊡, C_2FH_3–HI; and ⊙, C_2FH_3–HBr mixtures at room temperature.

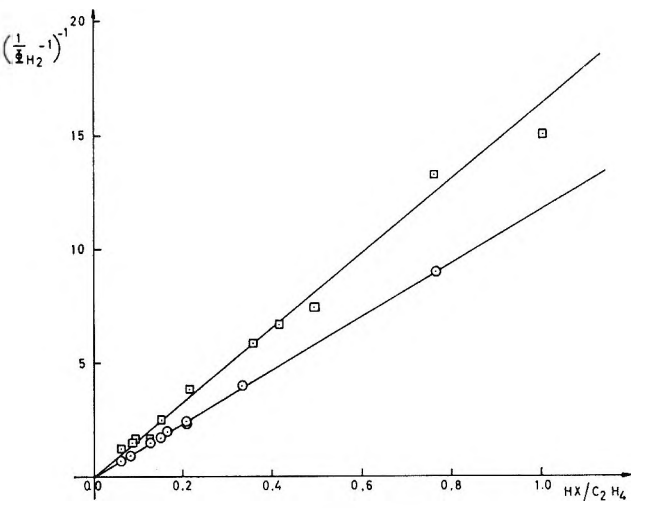

Figure 2. Photolysis of: ⊡, C_2H_4–HI; and ⊙, C_2H_4–HBr mixtures at room temperature.

* To whom correspondence should be addressed at the Department of Chemistry, Catholic University of America, Washington, D. C. 20017.

(1) Abstracted in part from a dissertation presented by R. J. L. in partial fulfillment for the degree of Doctor of Philosophy in Chemical Engineering of the University of Chile.

(2) (a) J. H. Sullivan, *J. Chem. Phys.*, **30**, 1293 (1959); **36**, 1925 (1962); (b) R. M. Martin and J. E. Willard, *ibid.*, **40**, 2994, 3007 (1964); (c) R. D. Penzhorn and B. de B. Darwent, *J. Phys. Chem.*, **72**, 1639 (1968); (d) R. A. Fass, *ibid.*, **74**, 984 (1970); (e) L. E. Compton and R. M. Martin, *ibid.*, **73**, 3474 (1969); (f) A. Kuppermann and J. M. White, *J. Chem. Phys.*, **44**, 4352 (1966).

(3) R. D. Penzhorn and H. L. Sandoval, *J. Phys. Chem.*, **74**, 2065 (1970).

Table I: Ratios of Moderated Rate Constants

Photolyzed sample	k_3/k_1	k_4/k_3	Photolyzed sample	k_3/k_1 or k_2/k_1
$HI-C_2H_4$	0.0593 ± 0.0074		$HI-C_2F_4$	0.106 ± 0.003
$HBr-C_2H_4$	0.0843 ± 0.0008		$HBr-C_2F_4$	0.143 ± 0.004
$HI-C_2FH_3$	0.0512 ± 0.0041	0.6 ± 0.1	$HI-I_2$	14.05 ± 0.92
$HBr-C_2FH_3$	0.0662 ± 0.0026	0.45 ± 0.27	$HBr-I_2$	19.05 ± 0.63

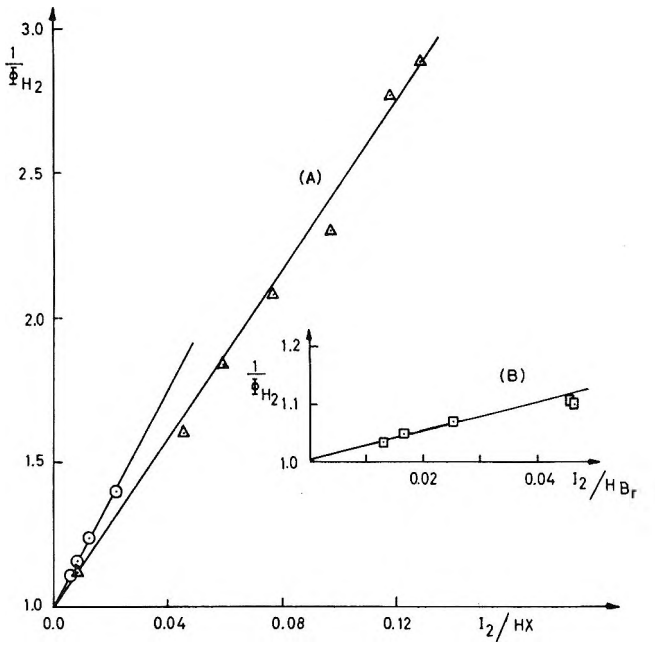

Figure 3. (A) Photolysis of: △, HI–I_2; and ⊙, HBr–I_2 mixtures at room temperature and in the presence of 250 Torr of CO_2. (B) Photolysis of: ⊡, HBr–I_2 mixtures at room temperature and in the absence of a moderator.

to an abstraction reaction,[3] was observed. The intercept was found slightly different with each of the two hydrogen halides. The ratios of the rate constants that can be calculated from the slopes and intercepts of the straight lines, obtained with our experimental data, are summarized in Table I. With proper weighting factors, these results can be combined to give for k_{HI}/K_{HBr} the value of 1.35 ± 0.03. For thermal hydrogen atoms, the k_4/k_3 ratio should not depend upon the H atom source. Within experimental error, this seems to be in agreement with our experimental data. Therefore, for the calculation of one of the k_{HI}/k_{HBr} ratios an average intercept of 0.53, common to both hydrogen halides, was employed together with the slopes obtained for the C_2FH_3 systems.

The similarity between the ratio of rate constants for hot reactions and the ratios for preexponential factors of the corresponding thermal processes have recently been indicated.[2c,d] Some data have been obtained (Figure 3B) in the present experiments which provide further information on that topic. When the total pressure is less than 4.3 Torr, as in all of the data given in Figure 3B, the reactions may be assumed to be those of hot H. The slope of the line in Figure 3B gives $k_{I_2}^*/k_{HBr}^* = 2.8$. Schwarz, *et al.*,[4] and Williams and Ogg[5] obtained a value of 4.0 for $k_{I_2}^*/k_{HI}^*$, hence $k_{HI}^*/k_{HBr}^* = 0.7$ at 2537 Å.

The ratio of the preexponential factors (A_{HI}/A_{HBr}) for thermal H, based purely on the kinetic theory diameters of 2.4, 3.7, and 4.1 Å for H, HBr, and HI, respectively, turns out to be 1.2. This provides additional support for the suggestion that the ratios of rate constants in hot reactions are closely equal to the ratios of the preexponential factors of the corresponding thermal processes. It is important to point out that the energy distribution of the hot H atoms produced from HI is different from that of HBr, and that, therefore, this is a very qualitative comparison, because the hot rate constants will be dependent upon the average relative velocity of the hot atoms and the reagent. This may explain the fact that our value for k_{HI}^*/k_{HBr}^* is lower than unity rather than equal to or slightly greater than unity as would appear to be more reasonable.

Furthermore, combination of the k_{HI}/k_{HBr} value with the preexponential factor ratio, calculated from collision theory, suggests that the activation energy difference $E_{HBr} - E_{HI}$ should be rather small, of the order of 0.0 ± 0.1 kcal/mol, assuming an arbitrary error of 20% for the preexponential factor ratio. Taking $E_{HI} = 0.6$ kcal/mol,[2c] a value of 0.6 ± 0.1 can be calculated for E_{HBr}. This activation energy is is in good agreement with the value of 0.7 kcal/mol calculated by Sato,[6] and 1 kcal/mol obtainable from Bodenstein's data;[7] but is less satisfactory when compared with the potential energies of activation of $V_{HI}^* = 1$ kcal/mol and $V_{HBr}^* = 2$ kcal/mol calculated with the BEBO method.[8]

Acknowledgements. The support of this work, through a research grant and a fellowship to one of us (R.J.L.) from the Comisión Nacional de Investigaciones Cientificas y Technologicas, is gratefully acknowledged.

(4) H. A. Schwarz, R. R. Williams, Jr., and W. H. Hamill, *J. Amer. Chem. Soc.*, **74**, 6007 (1952).

(5) R. A. Ogg, Jr., and R. R. Williams, *J. Chem. Phys.*, **13**, 586 (1945).

(6) S. Sato, *ibid.*, **23**, 2465 (1955).

(7) M. Bodenstein and H. Lutkemeyer, *Z. Phys. Chem.*, **114**, 208 (1924); M. Bodenstein and G. Jung, *ibid.*, **121**, 127 (1926).

(8) M. S. Johnston and C. Parr, *J. Amer. Chem. Soc.*, **85**, 2544 (1963).

Deactivation of Vibrationally Excited Ethane. A Comparison of Two Methods of Measuring the Pressure Dependence

by Frank R. Cala and Sidney Toby*

School of Chemistry, Rutgers University, New Brunswick, New Jersey 08903 *(Received September 21, 1970)*

Publication costs borne completly by The Journal of Physical Chemistry

The combination of methyl radicals together with its reverse reaction, the decomposition of ethane, is an important system for the study of vibrational energy transfer. A convenient parameter for the pressure dependence of this system is the median fall-off pressure $P_{1/2}$, at which the rate of stabilization of the complex equals its rate of decomposition. $P_{1/2}$ has been obtained by measuring the rate of methyl combination relative to abstraction (method I) and by pyrolysis of ethane (method II). Recently Grotewold, *et al.*,[1,2] measured $P_{1/2}$ by studying the cross-combination ratio of methyl radicals with ethyl or isopropyl radicals. This ingenious method (III) depends on the fact that at reduced pressures fall-off in the combination of methyl radicals will occur before fall-off for heavier pairs of radicals. Comparisons[1,2] of the three methods have yielded good agreement for methods I and II with $P_{1/2}$ showing a small temperature dependence in the range 25–800°. Values obtained by method III have disagreed sharply[1,2] with other experimental values and also with the predictions of RRKM theory,[3] and method III data have therefore been criticized.[4,5]

There has been no direct comparison of data obtained by method III with those obtained by another method for the same system. This note describes such a comparison with all data being obtained from the photolysis of acetone and of acetone-d_6 at 298°.

Experimental Section

The apparatus used has been described previously[6] and consisted of a conventional high-vacuum system with greaseless valves in the photolysis and product fractionation sections. The beam from an Osram 75-W high-pressure mercury arc was made parallel with a quartz lens and filled the quartz photolysis cell, volume 0.558 l. A Corning 7-54 filter with a Kimax plate limited the photolysis to the 3130-Å region. Spectroquality (Matheson Coleman and Bell) acetone and acetone-d_6 (Merck, Sharpe and Dohme) were dried over Drierite and distilled. Products were analyzed by gas chromatography as follows: carbon monoxide, methane, and ethane were separated with a silica gel column at 25°, methyl ethyl ketone (MEK) and 2,5-hexanedione (HXD) with a Porapak Q column at temperatures of 150–220°. Photolyses at temperatures below 298° and at low pressures gave no measurable HXD.

Results and Discussion

The photolysis of gaseous acetone (A) at 3130 Å and 298° is described by the following mechanism

$$A + h\nu \longrightarrow CH_3 + CH_3CO$$

$$CH_3CO\ (+A) \xrightarrow{1} CH_3 + CO\ (+A)$$

$$CH_3 + A \xrightarrow{2} CH_4 + CH_2COCH_3$$

$$CH_3 + CH_2COCH_3 \xrightarrow{3} C_2H_5COCH_3$$

$$2CH_3\ (+A) \xrightarrow{4} C_2H_6\ (+A)$$

$$2CH_2COCH_3 \xrightarrow{5} (CH_3COCH_2)_2$$

An additional source of methane, important at low pressures, has been shown[7] to originate from the reaction of CH_3 with adsorbed acetone

$$CH_3 + A_{ads} \xrightarrow{6} CH_4 + (CH_2COCH_3)_{ads}$$

It follows that

$$R_M/R_E^{1/2} = \{k_2[A] + k_6(S/V)\}/k_4^{1/2} \qquad (1)$$

where R_M and R_E are the rates of formation of methane and ethane, k_6 is a heterogeneous rate constant, and S/V is the surface to volume ratio of the photolysis cell.

Equation 1 may be rearranged to

$$\frac{R_E[A]^2}{R_M^2}\left\{\frac{k_2[A] + k_6(S/V)}{k_2[A]}\right\}^2 = \frac{k_4}{k_2^2} \qquad (2)$$

where the term in braces squared is the heterogeneous correction. This term was evaluated by using the value of k_2 given by Shaw and Toby[6] and taking k_6 from the data of Konstantatos and Quinn,[7] assuming that k_6 for quartz is the same as for Pyrex and that it is independent of pressure. A plot of the left-hand side of eq 2 against acetone pressure is given in the upper portion of Figure 1 and shows the pressure dependence of k_4. The heterogeneous correction is small (<10%) above 15 Torr and has a negligible effect on $P_{1/2}$. Also included in the plot are data of Sato, Takahashi, and Tsunashima.[8]

(1) J. Grotewold, E. A. Lissi, and M. G. Neumann, *J. Chem. Soc. A*, 375 (1968).

(2) F. Casas, C. Previtali, J. Grotewold, and E. A. Lissi, *ibid.*, 1001 (1970).

(3) B. S. Rabinovitch and D. W. Setser, *Advan. Photochem.*, **3**, 1 (1964).

(4) K. J. Hole and M. F. R. Mulcahy, *J. Phys. Chem.*, **73**, 177 (1969).

(5) A. N. Dunlop, R. J. Kominar, and S. J. W. Price, *Can. J. Chem.*, **48**, 1269 (1970).

(6) H. Shaw and S. Toby, *J. Phys. Chem.*, **72**, 2337 (1968).

(7) J. Konstantatos and C. P. Quinn, *Trans. Faraday Soc.*, **65**, 2693 (1969).

(8) S. Sato, C. Takahashi, and S. Tsunashima, *Bull. Chem. Soc. Jap.*, **43**, 1319 (1970).

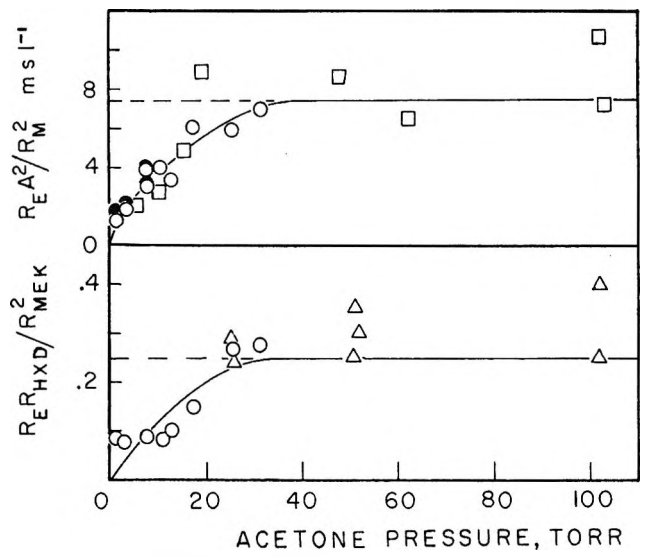

Figure 1. Plot of $R_E[A]^2/R_M^2$ (upper) and $R_E R_{HXD}/R_{MEK}^2$ (lower) against acetone pressure at 298°. Data: □, Sato, *et al.*;[8] △, Brinton;[10] ○, this work; ●, this work with heterogeneous correction.[7] $(k_4)_\infty/k_2^2$ taken from Shaw and Toby.[6]

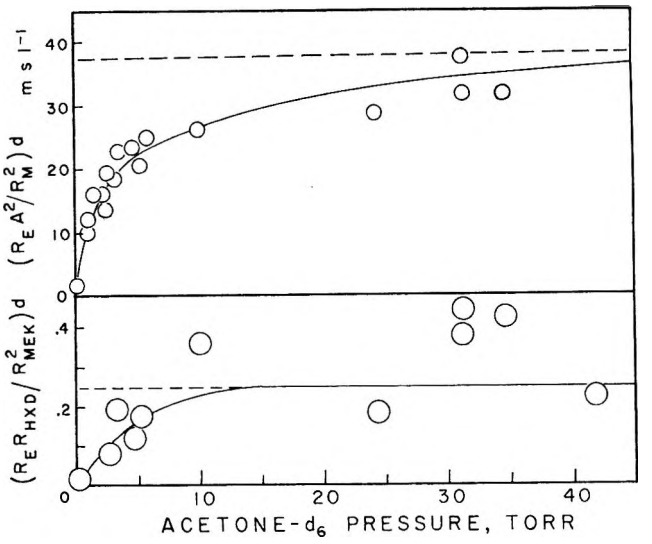

Figure 2. Plot of deuterated $R_E[A\text{-}d_6]^2/R_M^2$ (upper) and deuterated $R_E R_{HXD}/R_{MEK}^2$ (lower) against acetone-d_6 pressure at 298°. Deuterated $(k_4)_\infty/k_2^2$ taken from tabulation by G. O. Pritchard and M. J. Perona, *Int. J. Chem. Kinetics*, **1**, 509 (1969).

The cross-combination rule[9] yields the relation

$$R_E R_{HXD}/R_{MEK}^2 = 0.25 \qquad (3)$$

The left-hand side of eq 3 is plotted against acetone pressure in the lower portion of Figure 1 and includes some data of Brinton.[10] The corresponding plots for acetone-d_6 are shown in Figure 2.

There are large uncertainties in the values of $P_{1/2}$ measured by both methods. Method I is heavily dependent on the value taken[11] for $(k_4)_\infty/k_2^2$. Method III entails considerable experimental error because of the difficulty in measuring R_{HXD} in the presence of large amounts of acetone. Within these large uncertainties, however, both methods lead to the same results at 298°. Our best overall estimates are $P_{1/2}(C_2H_6^*) = 9.5 \pm 3$ Torr and $P_{1/2}(C_2D_6^*) = 3.5 \pm 1.5$ Torr in reasonable agreement with the compilation of data by Hole and Mulcahy.[4]

These values are too imprecise for detailed speculation to be warranted, but it is interesting to note that our results indicate a substantial isotope effect in the decomposition of chemically activated ethane, assuming equal deactivating efficiencies for acetone and acetone-d_6. This disagrees with the work of Kistiakowsky and Roberts,[12] who found no difference in the values of $P_{1/2}$ (evaluated from Lindemann plots) but is in line with the large isotope effects that have been found in the decomposition of comparable chemically activated species.[13]

Although this work shows that methods I and III give satisfactorily concordant values of $P_{1/2}$ at 298°, it does not explain the wide discrepancies obtained at temperatures below 150°.[2,4] This lack of agreement is important since it casts doubt on the well-established model of vibrationally excited ethane as a loose complex.[3] Grotewold, *et al.*,[2] have argued strongly for a more rigid complex with free rotation of methyls replaced by a low frequency bending. More work at the lower temperatures should resolve this point.

Acknowledgments. We are grateful to the National Science Foundation for the support of this work. Dr. G. O. Pritchard offered helpful criticism.

(9) J. A. Kerr and A. F. Trotman-Dickenson, *Progr. Reaction Kinetics*, **1**, 105 (1961).

(10) R. K. Brinton, *J. Amer. Chem. Soc.*, **83**, 1541 (1961).

(11) For example the value given by Shaw and Toby[6] of log $(k_2/(k_4^{1/2})_\infty) = 3.17 \pm 0.17 - (9440 \pm 350)/2.303RT$ corresponds to a range of $(k_4)_\infty/k_2^2$ from 6.5 to 11.0 mol sec l.$^{-1}$ at 298°.

(12) G. B. Kistiakowsky and E. K. Roberts, *J. Chem. Phys.*, **21**, 1637 (1953).

(13) See, for example, J. W. Simons, B. S. Rabinovitch, and R. F. Kubin, *ibid.*, **40**, 3343 (1964); K. Dees and D. W. Setser, *ibid.*, **49**, 1193 (1968); G. O. Pritchard and M. J. Perona, *Int. J. Chem. Kinetics*, **2**, 281 (1970).

Kinetics of the Oxidation of Hexacyanoferrate(II) by Chloramine-T

by M. C. Agrawal and S. P. Mushran*

Chemical Laboratories, University of Allahabad, Allahabad, India
(Received September 28, 1970)

Publication costs borne completely by The Journal of Physical Chemistry

The sodium salt of *N*-chloro-*p*-toluenesulfonamide, $CH_3C_6H_4SO_2N \cdot NaCl \cdot 3H_2O$, commonly known as chloramine-T acts as a strong oxidizing agent in both acidic

and alkaline media and has been widely used for the direct and indirect determination of several inorganic and organic substances.[1-3] Among a few kinetic investigations made with this oxidant, Coull and coworkers[4] studied the kinetics of the decomposition of hydrogen peroxide in presence of hydrochloric acid. Dell'erba and Spinelli[5] investigated the effect of alkalinity on rate constants of the reaction between alkyl sulfides and chloramine-T. Kinetics of the chlorination of *p*-cresol[6] and the oxidation of glycerol[7] by chloramine-T have also been studied. Recently, Prasad and Mushran[8] have investigated the mechanism of the osmium(VIII)-catalyzed oxidation of some α-hydroxy acids by chloramine-T.

Oxidation of hexacyanoferrate(II) by chloramine-T is a rapid reaction in an acidic medium. In 1 *N* HCl hexacyanoferrate(II) has been directly determined using potentiometric or amperometric[9] or visual titration[10,11] techniques. It has been observed that the oxidation does not take place in alkaline solutions and that within the pH range 6 to 7 it proceeds with a measurable velocity. In the present communication kinetics of the oxidation of hexacyanoferrate(II) by chloramine-T has been studied in feebly acidic media with a view to shed some light on the oxidation mechanism involving this oxidant.

Experimental Section

An aqueous solution of potassium hexacyanoferrate(II) was prepared fresh from AnalaR, B.D.H. sample. Chloramine-T solution was prepared from E. Merck, *pro analysi* sample and was standardized iodometrically. Several buffer solutions were prepared by mixing suitable amounts of 0.1 *M* solutions of mono- and disodium hydrogen orthophosphates (Analar grade). All other chemicals used were of analytical reagent grade. Doubly-distilled water was used throughout the course of investigations.

Kinetics were followed by estimating the hexacyanoferrate(III) formed, colorimetrically using a Klett-Summerson photoelectric colorimeter within the transmission range 400–450 mμ. pH measurements were made on a Leeds and Northrup direct reading pH meter.

Results

The kinetics of the oxidation of hexacyanoferrate(II) was investigated at several initial concentrations of the reactants (Table I). It was observed that the reaction is initially rapid but subsequently follows first-order dependence with respect to hexacyanoferrate(II). Pseudo-first-order constants, calculated from the straight-line portions of the log–time plot (Figure 1), show a linear increase with increase in initial concentration of chloramine-T. In equivalent amounts of hexacyanoferrate(II) and chloramine-T the reaction follows second-order kinetics after the initial rapid reaction (Figure 2). Increase in pH decreased the rate of reaction and a plot of log k_1 against pH showed a straight line with slope = −1 (Figure 3). It is concluded that the oxidation process follows first-order dependence with respect to hexacyanoferrate(II), chloramine-T, and H^+ ion concentrations.

Table I: Dependence of Rate Constants at 32°

Expt no.	$[Fe(CN)_6^{4-}] \times 10^4$, *M*	[Chloramine-T] $\times 10^3$, *M*	pH[a]	$k_1 \times 10^4$,[b] sec^{-1}	$10k_2$,[c] l. mol^{-1} sec^{-1}
1	2.8	2.0	6.95	2.70	1.35
2	3.2	2.0	6.95	3.15	1.57
3	3.6	2.0	6.95	3.00	1.50
4	4.0	2.0	6.95	3.07	1.53
5	4.4	2.0	6.95	3.30	1.65
6	3.2	1.6	6.95	2.60	1.62
7	3.2	2.8	6.95	3.04	1.38
8	3.2	4.0	6.95	5.20	1.30
9	3.2	6.0	6.95	7.50	1.25
10	3.2	2.0	5.95	26.9	13.5
11	3.2	2.0	6.20	15.3	7.65
12	3.2	2.0	6.55	6.22	3.11
13	3.2	2.0	6.75	3.84	1.92
14	3.2	2.0	7.10	2.04	1.02

[a] 40% of the phosphate buffer was used to maintain constant pH. [b] First-order rate constants in $[Fe(CN)_6^{4-}]$. [c] Second-order rate constants.

Influence of other factors such as ionic strength and temperature was also studied. A threefold increase in the ionic strength was made by using different amounts of buffer (20% to 60%) and it was observed that the rate of the reaction remains unchanged. Addition of perchlorate (total μ changed from 0.24 to 0.54) showed a very slight increasing effect on the reaction rate (k_1 changes from 3.15 to 3.84 × 10^{-4} sec^{-1}).

The rate of reaction was measured at 32, 37, 42, and 47°. The rate constants (k_1) were obtained as 3.15, 3.84, 4.61, and 5.20 × 10^{-4} sec^{-1}, respectively. The

(1) A. Berka, J. Vulterin, and J. Zyka, "Newer Redox Titrants," Pergamon Press, New York, N. Y., 1965.

(2) W. Smulek, *Wiad. Chem.*, **9**, 505 (1955).

(3) A. Berka, *Chemie (Prague)*, **10**, 121 (1958).

(4) J. Coull, H. B. Hope, and B. Gouguell, *J. Amer. Chem. Soc.*, **57**, 1489 (1935).

(5) C. Dell'erba and D. Spinelli, *Ric. Sci. Parte 2: Rend. Sez. A*, **7**, 456 (1964).

(6) T. Higuchi and A. Hussain, *J. Chem. Soc. B*, 549 (1967).

(7) K. Weber and F. Valic, *Z. Phys. Chem.*, **238**, 353 (1968).

(8) B. Prasad and S. P. Mushran, Doctoral Thesis, Allahabad University, 1970.

(9) V. A. Khadeev, A. K. Zhdanov, and L. G. Rechkina, *Uzb. Khim. Zh.*, **6**, 28 (1960).

(10) A. S. Komarovski, V. F. Filonova, and I. M. Korenman, *Zh. Prikl. Khim.*, **6**, 742 (1933).

(11) W. Poethke and F. Wolf, *Z. Anorg. Allg. Chem.*, **268**, 244 (1952).

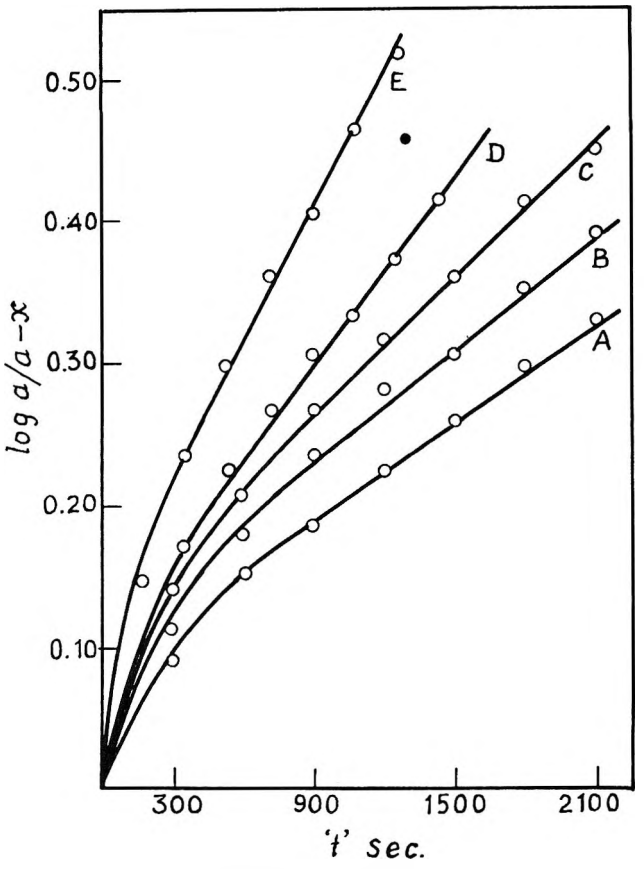

Figure 1. First-order rate plots in $Fe(CN)_6^{4-}$ at 32°: $[Fe(CN)_6^{4-}] = 3.2 \times 10^{-4}$ *M*, pH 6.95, and [chloramine-T] = 1.6, 2.0, 2.8, 4.0, and 6.0×10^{-3} *M* in A, B, C, D, and E, respectively.

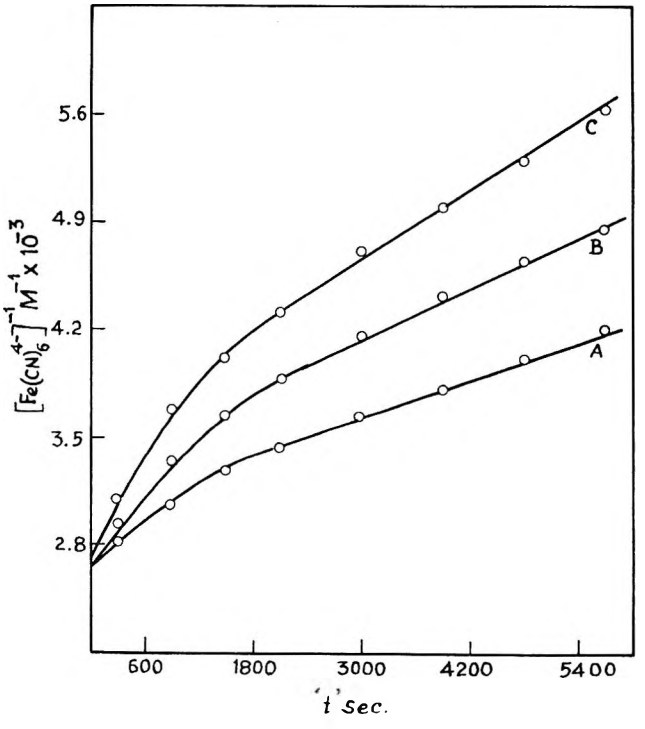

Figure 2. Second-order rate plots at 42°: $[Fe(CN)_6^{4-}] = 4 \times 10^{-4}$ *M*, [chloramine-T] = 2×10^{-4} *M*, and pH 5.90, 6.05, and 6.20 in A, B, and C, respectively.

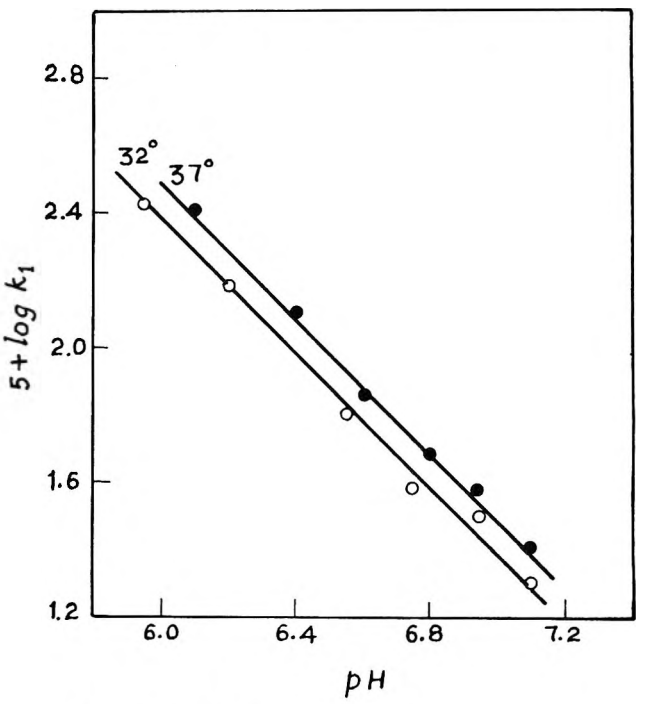

Figure 3. Plot of log k_1 against pH.

energy of activation of the oxidation process was found to be 4.60 kcal/mol.

Discussion

In aqueous solutions, chloramine-T hydrolyzes[12] to *p*-toluenesulfonamide and hypochlorite. However, under the conditions of this study (pH 6 to 7) the *N*-chloro-*p*-toluenesulfonamide is largely ionized and hypochlorous acid is only slightly dissociated; the hydrolysis process may be written as

$$CH_3C_6H_4SO_2NCl^- + H_2O + H^+ \rightleftharpoons CH_3C_6H_4SO_2NH_2 + HOCl \quad (1)$$

In an acidic medium, however, the following steps are reported[4]

$$CH_3C_6H_4SO_2NCl^- + H^+ \underset{k'_{-1}}{\overset{k'_1}{\rightleftharpoons}} CH_3C_6H_4SO_2NHCl \quad (2)$$

$$2CH_3C_6H_4SO_2NCl^- + 2H^+ \rightleftharpoons CH_3C_6H_4SO_2NCl_2 + CH_3C_6H_4SO_2NH_2 \quad (3)$$

The disproportionation of *N*-chloro-*p*-toluenesulfonamide into *p*-toluenesulfonamide and dichloramine-T, represented by step 3, has been studied in detail by Higuchi, Ikeda, and Hussain.[13] They have observed that *N*-chloro-*p*-toluenesulfonamide being a fairly strong acid ($pK_a = 4.55$[14]) is undisproportionated

(12) R. Dietzel and K. Taufel, *Apoth.-Ztg.*, **44**, 989 (1929).

(13) T. Higuchi, K. Ikeda, and A. Hussain, *J. Chem. Soc. B*, 546, (1967).

(14) J. C. Morris, J. A. Salazar, and M. A. Wineman, *J. Amer. Chem. Soc.*, **70**, 2038 (1948).

at higher pH and in alkaline solution dichloramine-T does not exist. It is, therefore, obvious that in feebly acidic media (pH 6 to 7) *N*-chloro-*p*-toluenesulfonamide is the predominant species of chloramine-T which reacts with hexacyanoferrate(II) in a slow and rate-determining step as follows

$$CH_3C_6H_4SO_2N\cdot HCl + Fe(CN)_6^{4-} \xrightarrow{k'_2} \text{reactive intermediate} \quad (4)$$

$$\text{intermediate} + H^+ + Fe(CN)_6^{4-} \xrightarrow{k'_3} CH_3C_6H_4SO_2NH_2 + 2Fe(CN)_6^{3-} \quad (5)$$

As a one-electron change is more likely in oxidation processes,[15] a reactive intermediate is formed in step 4 which immediately reacts with another molecule of hexacyanoferrate(II) to give the products *p*-toluenesulfonamide and hexacyanoferrate(III) (step 5).

Applying steady-state conditions with respect to all the intermediates and taking $k'_{-1} > k'_2[Fe(CN)_6^{4-}]$, the following rate equation is obtained

$$-\frac{d}{dt}[Fe(CN)_6^{4-}] = -\frac{1}{2}\frac{d}{dt}[\text{chloramine-T}] = k[Fe(CN)_6^{4-}][\text{chloramine-T}][H^+] \quad (6)$$

where

$$k = \frac{2k'_1k'_2}{k'_{-1}} = \frac{2k'_2}{K} = \frac{2k'_2}{2.82 \times 10^{-5}}$$ (K being 2.82×10^{-5} [14])

The value of the termolecular rate constant, k, has been experimentally obtained as 14×10^5 l.^{2} mol^{-2} sec^{-1} and therefore the rate constant for the rate determining step may be calculated as $k'_2 = 19.7$ l. mol^{-1} sec^{-1}. This is a fairly high value and therefore well accounts for the low energy of activation. The negative entropy of activation (−16.5 eu) and the ionic strength effects also support the interaction between an uncharged molecule and an ion in the rate-determining step.

The derived rate law (6) suggests the first-order dependence in hexacyanoferrate(II), chloramine-T, and H^+ as has been experimentally observed.

Further, the initial fast reaction may be partially attributed to the fact that in acidic media some *N*-chloro-*p*-toluenesulfonamide is converted to dichloramine-T (step 3) which is more reactive species than chloramine-T. From the work of Soper[16] and others[14] it has been possible to compute the equivalent concentrations of all the individual species as a function of pH and total concentration. Such computations have revealed that the disproportionation of *N*-chloro-*p*-toluenesulfonamide (step 3) is very little between pH 6 and 7. The "initial fast reaction" which under some conditions amounts to 30% of the total reaction cannot, therefore, be accounted for due to dichloramine-T only. It seems likely that the mechanism of the reaction is more complex than the one presented. It may be possible that the decreasing rate of reaction with time may be the result of inhibition by *p*-toluenesulfonamide leading to a repression of hydrolysis or disproportionation.

Acknowledgment. Thanks are due to CSIR, New Delhi for the financial assistance to M. C. A.

(15) W. C. E. Higginson and J. W. Marshall, *J. Chem. Soc.*, 447 (1957).

(16) F. G. Soper, *ibid.*, **125**, 1899 (1924).

Reactions of Fast Hydrogen Atoms with Ethane[1a]

by J. E. Nicholas, F. Bayrakceken, and R. D. Fink*[1b]

Department of Chemistry, Amherst College, Amherst, Massachusetts 01002 *(Received October 5, 1970)*

Publication costs assisted by the Division of General Medical Sciences, National Institutes of Health

Translationally excited atoms produced by photochemical techniques[2-8] are particularly useful for studying epithermal or so-called "hot" chemical reactions as their initial kinetic energies are well defined. We wish to report the results of our studies of the reactions of photochemically produced deuterium atoms with ethane in a system where the initial energy of the deuterium is 2.0 eV and an efficient radical scavenger, bromine, is present. In previous work with 2.8 eV deuterium atoms and ethane,[3] DBr was used as both the source of D atoms and as radical scavenger, and measurements were made of the ratio of D atoms undergoing all possible "hot" reactions with ethane to those D atoms which were collision-moderated to thermal energies. The primary photolytic step is

$$DBr + h\nu \longrightarrow D^* + Br$$

A straightforward mechanism that can be written for such a photochemical system is

(1) (a) This research was supported by National Institutes of Health Grant GM 13966. (b) Alfred P. Sloan Fellow.

(2) R. J. Carter, W. H. Hamill, and R. R. Williams, Jr., *J. Amer. Chem. Soc.*, **77**, 6457 (1955).

(3) R. M. Martin and J. E. Willard, *J. Chem. Phys.*, **40**, 3007 (1964).

(4) A. Kuppermann and J. M. White, *ibid.*, **44**, 4532 (1966).

(5) C. C. Chou and F. S. Rowland, *J. Amer. Chem. Soc.*, **88**, 2612 (1966).

(6) R. G. Gann and J. Dubrin, *J. Chem. Phys.*, **47**, 1867 (1967).

(7) R. G. Gann and J. Dubrin, *ibid.*, **50**, 535 (1969).

(8) C. C. Chou and F. S. Rowland, *ibid.*, **50**, 2763 (1969).

$$D^* + C_2H_6 \longrightarrow HD + C_2H_5 \quad (1)$$

$$D^* + C_2H_6 \longrightarrow C_2H_5D + H \quad (2)$$

$$D^* + DBr \longrightarrow D_2 + Br \quad (3)$$

$$D^* + DBr \longrightarrow D + DBr \quad (4)$$

$$D^* + C_2H_6 \longrightarrow D + C_2H_6 \quad (5)$$

The results of both the earlier work on ethane and this present work are interpretable on the basis of this mechanism. In the earlier work on the ethane system the substitution reaction 2 and the energy moderating reaction 4 do not seem to be explicitly considered in the kinetic derivation. Bromine atoms formed in the primary photochemical process and in subsequent reactions of DBr undergo termolecular recombination while the other radicals are scavenged by DBr. The radical products of reactions 1 and 2 yield C_2H_5D and HD, respectively, and consequently the abstraction and substitution products cannot be distinguished. Thermalized D atoms are scavenged by DBr to give D_2. This complete mechanism is consistent with results obtained in the DBr scavenged system for 2.8 eV deuterium atoms. It was the object of the present work to further test the reaction mechanism in the following respects: by changing the initial energy of the D atoms; by the addition of Br_2 to the system as a separate, more efficient radical scavenger, thus simplifying the reaction scheme leading to HD, D_2, and C_2H_5D products; and by deduction of the relative rates of some of the processes involved.

Deuterium atoms with an initial kinetic energy of 2.0 eV were produced from DBr which was mixed with hydrocarbon and, where appropriate, Br_2 (at average total reagent pressures of 300 mm with constant Br_2 pressure of 90 mm) in cylindrical quartz cells (2.5-cm i.d. and 25-cm length) by irradiation with 2138-Å light from a low-pressure Zn arc. Emission lines at 2025 and 2062 Å were removed by a *cis*-butene-2 filter (10 cm pressure, path length 3 cm). All reagents were purified by vacuum distillation before use. After irradiation, HD and D_2 products were separated by freezing out condensable reactants and products in liquid N_2. It was demonstrated as a separate series of experiments using known amounts of HD and D_2 that there were neither diffusion losses nor entrapment losses of these products using the separation scheme described above. The products were analyzed by mass spectrometry. The mass spectrometer was a quadrupole resonance type whose electron source was operated under controlled conditions eliminating background mass peaks at masses 4 and 3. It was carefully calibrated before, during, and after sample analysis by direct use of HD and D_2 mixtures for detection at the appropriate masses.

Mixtures of various DBr/ethane ratios were photolyzed at 296 ± 2°K and the product ratio D_2/HD was measured for both the DBr scavenged system and that to which Br_2 had also been added. Dark experiments, otherwise identical, were carried out to check background signals at each product mass. The percentage decomposition of DBr was kept below 1.0.

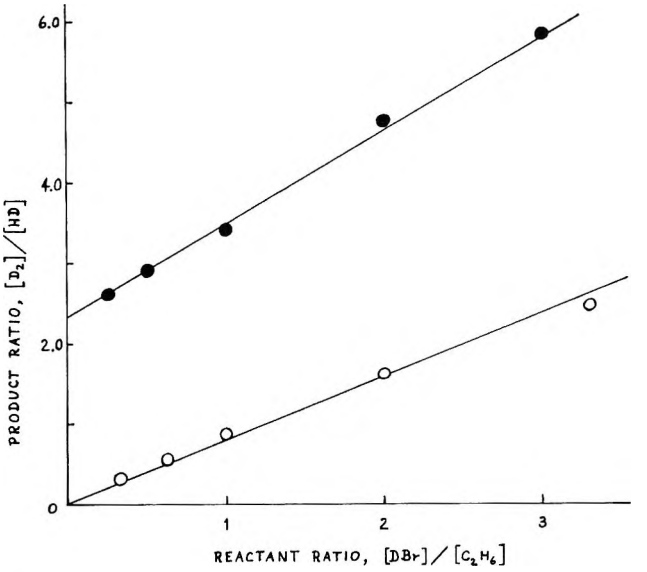

Figure 1. Product ratios as a function of reactant ratios for 2138 Å photolysis of DBr in C_2H_6. Closed circles: $[D_2]/[HD]$ for DBr scavenged system; open circles: $[D_2]/[HD]$ for Br_2 scavenged system. Points shown are averages of at least three individual runs.

For the DBr scavenged system the variation of the product ratio, D_2/HD, with reactant ratio, DBr/C_2H_6, can be straightforwardly derived from the reaction sequence suggested above. Thus, if s_i is the average interaction cross section for the ith process in the energy range from the initial energy with which D* is formed to threshold, one may write

$$(D_2)/(HD) = [(s_3 + s_4)/(s_1 + s_2)] \times [(DBr)/(C_2H_6)] + s_5/(s_1 + s_2)$$

The result of plotting this product ratio against the reactant ratio is shown in Figure 1. As with the results for 2.8 eV deuterium atoms[3] a straight line was obtained. The intercept corresponds to $s_5/(s_1 + s_2)$, that is the ratio of collisions with ethane that result in moderation to those that result in hot reaction. With 2 eV deuterium atoms the result is 2.35 ± 0.15 compared with 2.2 for 2.8 eV atoms. The slightly lower probability of hot reaction at the lower energy seems reasonable. $(s_1 + s_2)/(s_1 + s_2 + s_5)$ may also be calculated. This gives the fraction of atoms that react on collision with ethane or "integral reaction probability" as it has been termed.[6] The value obtained is 0.30 ± 0.02. The slope of the line corresponds to $(s_3 + s_4)/(s_1 + s_2)$ and so any variation with initial energy does not lead to such straightforward interpretation. It may be

expressed as the ratio of total probability of interaction of D* with DBr (hot reaction + moderation) to the probability of hot reaction with ethane. The result was 1.15 ± 0.10 for 2 eV atoms compared with 2.25 for 2.8 eV atoms. However, as described above $(s_1 + s_2 + s_5)/(s_1 + s_2)$ may be deduced, and knowing $(s_3 + s_4)/(s_1 + s_2)$, the ratio $(s_5 + s_1 + s_2)/(s_3 + s_4)$ may be calculated. This gives the relative *total* probabilities of interaction with ethane and DBr. The result at 2 eV is 2.9 ± 0.4 and at 2.8 eV from the earlier work[3] a result of 1.4 may be deduced. A possible interpretation of this result is that the cross sections for total interaction with ethane and DBr approach each other with increasing energy.

In the bromine scavenged system the relative rates of reaction of radical with Br_2 are approximately ten times faster[9] than with DBr. Having used a threefold higher pressure of Br_2 than DBr in all these samples, effectively all thermalized species react to form bromides which are undetected. One can write $(D_2)/(HD) = s_3(DBr)/s_1(C_2H_6)$ which predicts a straight line through the origin for a plot of D_2/HD *vs.* DBr/C_2H_6.

As shown in Figure 1, such a result was obtained. The slope is given by s_3/s_1, which corresponds to the relative probability of abstraction reaction of D* with DBr and ethane. The result obtained was 0.8 ± 0.05. At this energy, 2 eV, which is the only one for which this measurement has been performed, the relative *total* probability of interaction is $(C_2H_6/DBr) = (2.9/1)$ and for the abstraction reaction only is $(C_2H_6/DBr)/(s_1/s_3) = 1.25 \pm 0.08$. The only threshold energy for primary H abstraction measured for hydrocarbon is ~0.3 eV.[7] As regards DBr, its bond energy (3.9 eV) is lower than CH in ethane (4.2 eV), and the corresponding abstraction reaction has a lower activation energy[10] and presumable threshold energy. This might lead one to predict that the cross section for abstraction from DBr would be higher than that for abstraction from ethane at fairly low energies. However, competing with this postulated difference is the sterically enhanced probability of abstraction of H from ethane rather than the well shielded D from DBr.[11] The relative weighting of this factor in this specific system is unknown.

Acknowledgment. We wish to acknowledge the assistance of W. W. Phillips, C. H. Manstein, S. Topes, M. H. Nicholas, and C. Nicholas in completing this work. The correct isotopic analyses of A. Kropf were also most helpful.

(9) G. C. Fettis and J. H. Knox, *Progr. React. Kinet.*, **2**, 30 (1964).

(10) F. Bach, K. F. Bonhoeffer, and E. A. Moelwyn-Hughes, *Z. Phys. Chem.*, **27B**, 71 (1934).

(11) Detailed discussions of steric and bond energy effects are given by F. Schmidt-Bleeck and F. S. Rowland, *Angew. Chem.*, **3**, 769 (1964); R. L. Wolfgang, *Progr. React. Kinet.*, **5**, 97 (1965).

Solvated Electron or Not?

by T. R. Tuttle, Jr.,* and Philip Graceffa

Department of Chemistry, Brandeis University, Waltham, Massachusetts 02154 *(Received October 19, 1970)*

Publication costs borne completely by The Journal of Physical Chemistry

We have observed that sodium metal dissolves in a mixed solvent consisting of tetrahydrofuran-d_8 (THF-d_8) and naphthalene-d_8 to give a green solution which is paramagnetic. Dilute sodium solutions yield electron spin resonance (esr) spectra such as those shown in Figure 1. At relatively high temperatures the esr spectrum consists of four equally intense equally spaced hyperfine components which undoubtedly arise from the interaction of the unpaired electron with a single Na^{23} nucleus. Such a spectrum is shown in Figure 1 (a). As temperature is lowered the separation between the hyperfine components is reduced in a manner similar to that observed in the esr absorption spectra of alkali metals dissolved in amine solvents.[1-9] Also, as temperature is lowered a single line absorbance grows in at the center of the hyperfine pattern as is shown in Figure 1 (b). The analogous single line absorbance which has been observed in esr spectra of alkali metal solutions in amines has been assigned to the solvated electron.[1-9]

The similarity between the esr spectra of amine solutions of alkali metals on the one hand and our solution of sodium in the somewhat exotic mixed solvent described above is both clear and striking. For this reason, except for certain prejudices, it is tempting to offer a common explanation for the spectra of these different systems in terms of analogous sets of species. Unfortunately, we already have separate explanations for the spectra of metal solutions in amines on the one hand[1-9] and for sodium solutions in the THF-d_8–naphthalene-d_8 solvent on the other.[10] Nevertheless, we may profit by examining each explanation in turn as it is applied to the system for which it was not intended.

(1) K. D. Vos and J. L. Dye, *J. Chem. Phys.*, **38**, 2033 (1963).

(2) K. Bar-Eli and T. R. Tuttle, Jr., *ibid.*, **40**, 2508 (1964).

(3) K. Bar-Eli and T. R. Tuttle, Jr., *ibid.*, **44**, 114 (1966).

(4) J. L. Dye and L. R. Dalton, *J. Phys. Chem.*, **71**, 184 (1967).

(5) R. Catterall and M. C. R. Symons, *J. Chem. Soc.*, 6656 (1965).

(6) R. Catterall, M. C. R. Symons, and J. W. Tipping, *J. Chem. Soc. A*, 1529 (1966).

(7) L. R. Dalton, J. C. Rynbrandt, E. M. Hansen, and J. L. Dye, *J. Chem. Phys.*, **44**, 3969 (1966).

(8) R. Catterall, M. C. R. Symons, and J. W. Tipping, *J. Chem. Soc. A*, 1234 (1967).

(9) V. A. Nicely and J. L. Dye, *J. Chem. Phys.*, **53**, 119 (1970).

(10) N. M. Atherton and S. J. Weissman, *J. Amer. Chem. Soc.*, **83**, 1330 (1961).

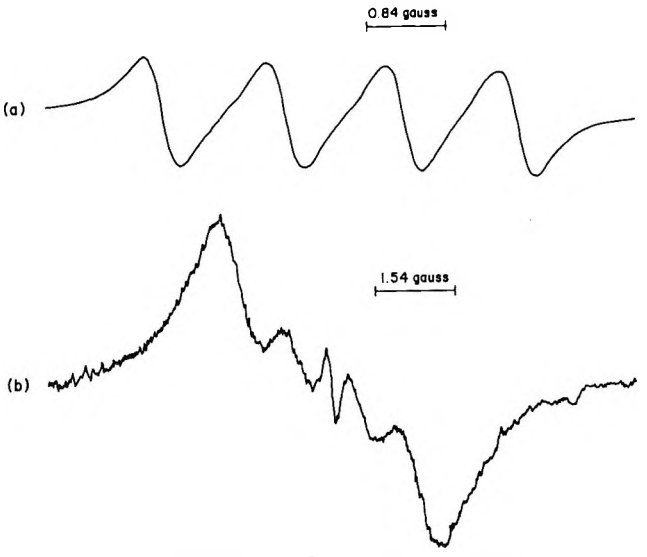

Figure 1. Electron spin resonance spectra of sodium dissolved in THF-d_8; naphthalene-d_8 solvent (solvent is a saturated solution of naphthalene-d_8 in THF-d_8 at room temperature). Plots are of dx''/dH *vs.* H with H decreasing from left to right: (a) 77°; (b) 35°.

Alkali metal solutions in amines are generally described in terms of two paramagnetic[7-9] species: (1) the metal monomer which accounts for the hyperfine components in the spectrum, and (2) the solvated electron which accounts for the single line. No substantial difficulty arises in applying this explanation to the spectra in Figure 1 even including embellishments designed to explain the temperature dependence of the hyperfine structure.[2-4,9] However, it is difficult to credit this explanation because it appears to conflict substantially with the model customarily invoked to explain esr spectra of sodium–ether–naphthalene systems.[10]

The green solution obtained by dissolving sodium in a THF–naphthalene mixture is usually described as consisting of naphthalenide ions and their ion pairs with sodium cations.[10] Under the conditions of our experiment the esr spectrum is accounted for by invoking exchange reactions which modulate the proton–electron hyperfine interactions[11-13] so that the naphthalenide ion gives only a single absorbance and the ion pair yields the four lines which result from the interaction between electron and ^{23}Na nucleus.[12,13] Application of this model to alkali metal solutions in amines leads us to identify the two paramagnetic species present as the solvent negative ion and its ion pair with the alkali metal cation. Actually, little difficulty arises in accounting for the esr spectra of alkali metal amine solutions on this basis except perhaps for the large magnitude of the electron–nuclear hyperfine coupling constant observed in some cases.[3,4,9] If we ignore this possible difficulty for the moment we are left with two different explanations for the same phenomena. The question is which explanation is to be preferred?

For the present we shall adopt the view that a unified explanation of the observations under discussion is to be preferred and so we shall examine the two possibilities outlined above to see which is the more firmly based on experimental fact. The identification of the single absorbance as being due to the solvated electron stems from analogy with metal solutions in ammonia. In these solutions the electron is supposed to be trapped in a cavity and solvated by the surrounding solvent molecules. The principal experimental basis for this structural model[14,15] is the volume expansion data for the solution. This model also receives support through theoretical considerations from the correlation of the position of the optical absorption with the size of the cavity.[16] However, the extension of this structural model of the solvated electron to systems related to the alkali metal ammonia solution only provides an explanation of the single esr absorption observed in these systems without at the same time giving additional support for the model itself. Furthermore, application of the cavity model to the Na–naphthalene-d_8–THF-d_8 system flatly contradicts the notion that the unpaired electron resides on a naphthalene molecule, a notion which is strongly supported by observation of proton (or deuteron) hyperfine structure in dilute solutions of naphthalene in THF reacted with sodium.[10,17,18] Conversely, the extension of the idea of a molecular negative ion as being responsible for the single line esr absorption observed in amine and ammonia solutions of the metals not only provides an explanation for this absorption line, but receives support from experimental data already available. If the solvent negative ion is to give rise to a single line in sodium–ammonia solutions the electron–nuclear hyperfine interactions must be averaged out by electron exchange as is the case in the Na–THF-d_8–naphthalene-d_8 system we have studied. Even if the isotropic hyperfine coupling is averaged out by electron exchange, the contact interactions between electrons and the magnetic nuclei, here ^{14}N and ^{1}H, should be detected in the form of shifts of the nuclear resonances. Such shifts in fact have been reported[19-22]

(11) R. Chang and C. S. Johnson, Jr., *J. Amer. Chem. Soc.*, **88**, 2338 (1966).
(12) J. C. Danner, Ph.D. Thesis, Brandeis University, 1966.
(13) F. C. Adam and S. I. Weissman, *J. Amer. Chem. Soc.*, **80**, 1518 (1958).
(14) N. N. Lipscomb, *J. Chem. Phys.*, **21**, 52 (1953).
(15) R. A. Stairs, *ibid.*, **27**, 1431 (1957).
(16) J. Jortner, S. A. Rice, and E. G. Wilson in "Metal Ammonia Solutions," G. Lepoutre and M. J. Sienko, Ed., W. A. Benjamin, New York, N. Y., 1963, p 222.
(17) R. L. Ward and S. I. Weissman, *J. Amer. Chem. Soc.*, **79**, 2086 (1957).
(18) T. R. Tuttle, Jr., R. L. Ward, and S. I. Weissman, *J. Chem. Phys.*, **25**, 189 (1956).
(19) H. M. McConnell and C. A. Holm, *ibid.*, **26**, 1517 (1957).
(20) J. V. Acrivos and K. S. Pitzer, *J. Phys. Chem.*, **66**, 1693 (1962).
(21) D. E. O'Reilly, *J. Chem. Phys.*, **41**, 3729 (1964).
(22) T. R. Hughes, Jr., *ibid.*, **38**, 202 (1963).

and correspond in the case of ^{14}N to a coupling constant of about 50 G[23] and in the case of the protons to a coupling constant of about 10 G.[24] Because of this large contact interaction between ^{14}N and the unpaired electron the structural model with the electron attached to a molecule seems more reasonable than the cavity model in which the electron resides in a spherical hole surrounded by ammonia molecules oriented so that the protons line the cavity surface and the nitrogens are more remote.

If this structural model is extended to the species which gives rise to the alkali metal nuclear hyperfine interaction in metal ammonia and metal amine solution the observations must be explained in terms of a metal cation–solvent anion ion pair. No difficulty arises except in the cases where the alkali metal splitting become a very large fraction of the splitting for the atom in the gas phase.[25] Then it is apparent that less of the electron is transferred from metal to solvent and the species is probably better described as a monomer, or solvated atomic complex. In this case also the cavity model is less suited to account for the experimental facts.

Acknowledgment. This work has been supported in part under a grant from the National Science Foundation.

(23) Calculated using the estimate of unpaired electron spin density at ^{14}N given by S. Golden, C. Guttman, and T. R. Tuttle, Jr., *ibid.*, **44**, 3791 (1966).

(24) Estimated using corrected susceptibility data given in ref 22.

(25) R. Catterall, M. C. R. Symons, and J. W. Tipping, *J. Chem. Soc. A*, 1529 (1966).

The Second Triplet Level of 1,5-Dichloroanthracene in Fluid Solutions[1]

by J. P. Roberts[2] and R. S. Dixon*

Atomic Energy of Canada Limited, Whiteshell Nuclear Research Establishment, Pinawa, Manitoba, Canada
(Received September 7, 1970)

Publication costs assisted by Atomic Energy of Canada Limited

Establishing the positions of triplet energy levels is of fundamental importance in studying the mechanism of intramolecular radiationless transitions in organic molecules. This is particularly true of triplet levels which are approximately degenerate with the first excited singlet state, S_1, since these levels are implicated in the mechanism of intersystem crossing between the singlet and triplet manifolds.[3] It has been suggested[4] that the widely varying quantum yields of fluorescence and phosphorescence in aromatic hydrocarbons are attributable to the relative positions of S_1 and T_2, but experimental evidence in support of this is sparse.

One method of determining higher triplet energy levels is by measurement of well resolved triplet–triplet absorption spectra. Spectra corresponding to $T_2 \leftarrow T_1$ transitions of some substituted anthracenes in a Lucite matrix have been reported,[5] but such spectra have not yet been observed in liquids. The observations in rigid media[4-7] show that the $T_2 \leftarrow T_1$ absorptions occur in the near-infrared region for anthracene and its derivatives. We have measured the triplet–triplet absorption spectrum of 1,5-dichloroanthracene in cyclohexane and perfluoromethylcyclohexane at room temperature by flash photolysis, and have placed its second triplet level below the first excited singlet state. The flash energies were 300–600 J with a flash duration of 5 μsec. Samples were degassed by a conventional freeze–pump–thaw technique. The apparatus for detection of transient absorptions is capable of routine measurement of spectra up to 1060 nm.[8]

Results and Discussion

Flash photolysis of a 10^{-4} *M* solution of 1,5-dichloroanthracene in cyclohexane produced a transient spectrum with absorption bands in both the visible and near-infrared regions (Figure 1). Hoffman and Porter[9] observed the triplet–triplet absorption of this compound under similar conditions and found λ_{max} at 425 nm. Figure 1a shows maxima at 420 and 442.5 nm, in close agreement with a recent observation of the 1,5-dichloroanthracene triplet produced by pulse radiolysis in cyclohexane.[10] Figure 1b shows maxima at 760, 850, and 955 nm in cyclohexane which all decayed at the same rate, indicating that they are characteristic of the same transient. For a given flash energy these five maxima in the visible and infrared regions all decayed at the same rate. Flash photolysis of an $\sim 5 \times 10^{-5}$ *M* solution of 1,5-dichloroanthracene in perfluoromethylcyclohexane gave a very similar spectrum to that obtained in cyclohexane (Figure 1) with the peaks shifted slightly to shorter wavelengths.

(1) Issued as AECL No. 3764.

(2) National Research Council of Canada Postdoctorate Fellow, 1968–1970.

(3) R. Pariser, *J. Chem. Phys.*, **24**, 250 (1956).

(4) R. E. Kellogg, *ibid.*, **44**, 411 (1966).

(5) R. G. Bennett and P. J. McCartin, *ibid.*, **44**, 1969 (1966).

(6) M. W. Windsor and J. R. Novak in "The Triplet State," A. B. Zahlan, Ed., Cambridge University Press, 1967, p 229.

(7) R. Astier and Y. H. Meyer, in "The Triplet State," A. B. Zahlan, Ed., Cambridge University Press, 1967, p 447.

(8) A. Singh, A. R. Scott, and F. Sopchyshyn, *J. Phys. Chem.*, **73**, 2633 (1969).

(9) M. Z. Hoffman and G. Porter, *Proc. Roy. Soc., Ser. A*, **268**, 46 (1962).

(10) T. J. Kemp and J. P. Roberts, *Trans. Faraday Soc.*, **65**, 725 (1969).

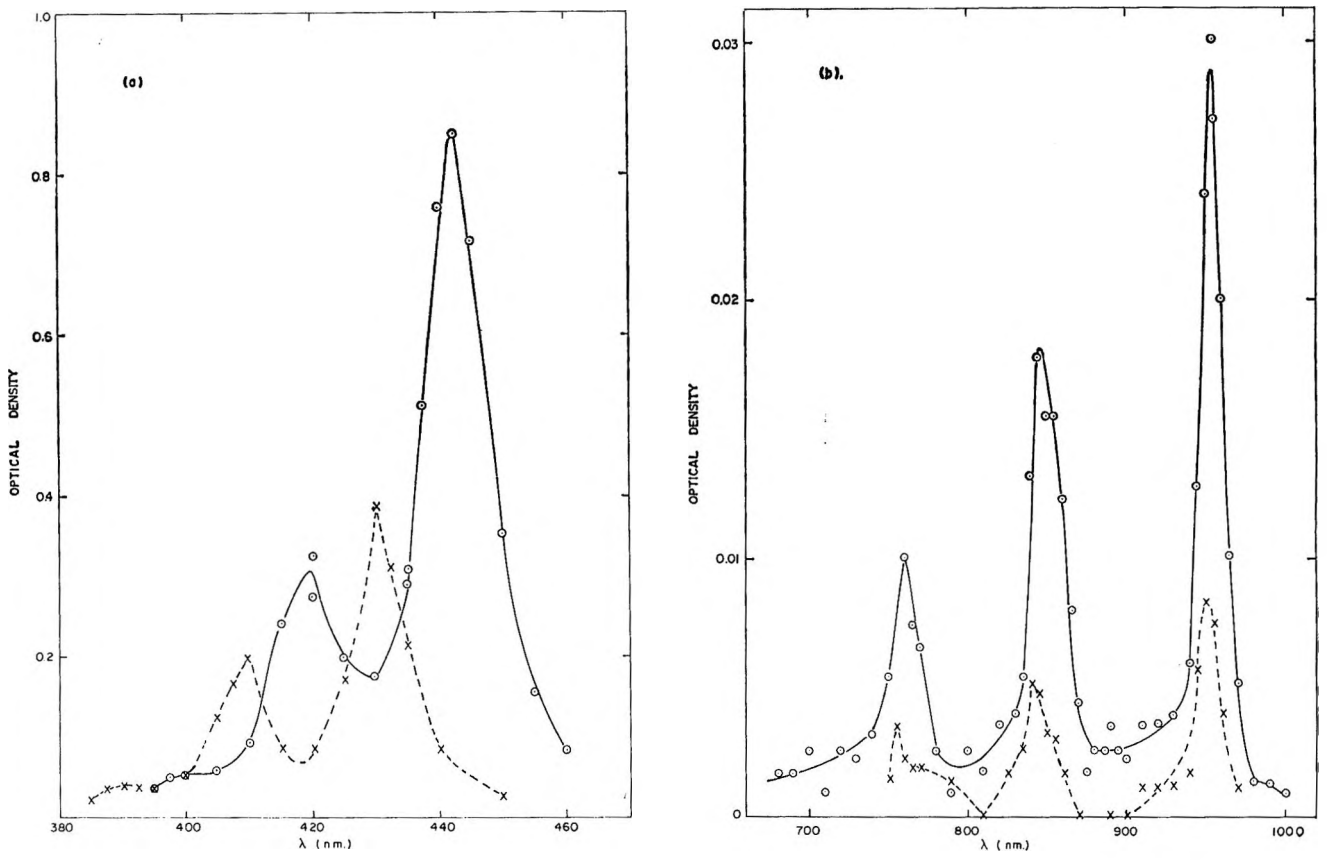

Figure 1. Triplet–triplet absorption spectrum of 1,5-dichloroanthracene (taken 10 μsec after peak of flash): ⊙, 10^{-4} M in cyclohexane; ×, ~5 × 10^{-5} M in perfluoromethylcyclohexane; (a) flash energy ~ 350 J; (b) flash energy ~ 550 J.

In cyclohexane the extinction coefficient at 955 nm was estimated by comparison of optical densities at 442.5 nm and 955 nm for a flash photolyzed 10^{-5} M solution of 1,5-dichloroanthracene, using the same flash conditions for both wavelengths. Using ϵ (442.5 nm) 64,300 M^{-1} cm^{-1},[10] ϵ (955 nm) 1000 M^{-1} cm^{-1}.

The similar decay rates of the visible and infrared absorption peaks indicate a common origin and our use of a fluid solvent enabled us to carry out quenching experiments to confirm this. Oxygen and ferric acetylacetonate were used as triplet energy quenchers. Neither had any effect on the positions of the absorption peaks; 10^{-4} M solutions of 1,5-dichloroanthracene in cyclohexane containing various amounts of oxygen were flashed. The lifetime of the transient absorption varied by a factor of 10 in these solutions but in all cases the extent of quenching was the same in the visible and near-infrared regions. However we were unable to measure oxygen concentrations with sufficient accuracy to allow determination of the rate constant for oxygen quenching. Porter and Windsor[11] previously observed that the triplet lifetime of anthracene, as measured by the decay of the visible absorption peak, varied over many flashes as oxygen was consumed. We also noted a variation in lifetime in oxygen-containing solutions but the decay rates of all the absorption peaks varied in the same way. More accurate quencher concentrations were obtained by using degassed samples of 10^{-4} M 1,5-dichloroanthracene in cyclohexane containing various amounts of ferric acetylacetonate. This chelate is an efficient triplet energy quencher[12] but our experiments indicated that it was consumed during the quenching process. Hence, all comparisons of decay rates were made on samples which had received only a few flashes. As with oxygen, the quenching of the absorption was the same for all the observed maxima in the visible and near-infrared.

For the solutions containing ferric acetylacetonate the decay of the lowest triplet state can be expressed by the equation

$$\frac{-\mathrm{d}[\mathrm{T}]}{\mathrm{d}t} = k_0[\mathrm{T}] + k_1[\mathrm{T}] + k_2[\mathrm{T}][\mathrm{Fe(AcAc)_3}] + \sum_Q k_Q[\mathrm{T}][\mathrm{Q}]$$

where k_0 is the rate of radiative decay (phosphorescence) and k_1 is the rate of radiationless crossing to the ground state. The summation term includes all quenching

(11) G. Porter and M. W. Windsor, *Proc. Roy. Soc., Ser. A*, **245**, 238 (1958).

(12) A. J. Fry, R. S. H. Liu, and G. S. Hammond, *J. Amer. Chem. Soc.*, **88**, 4781 (1966).

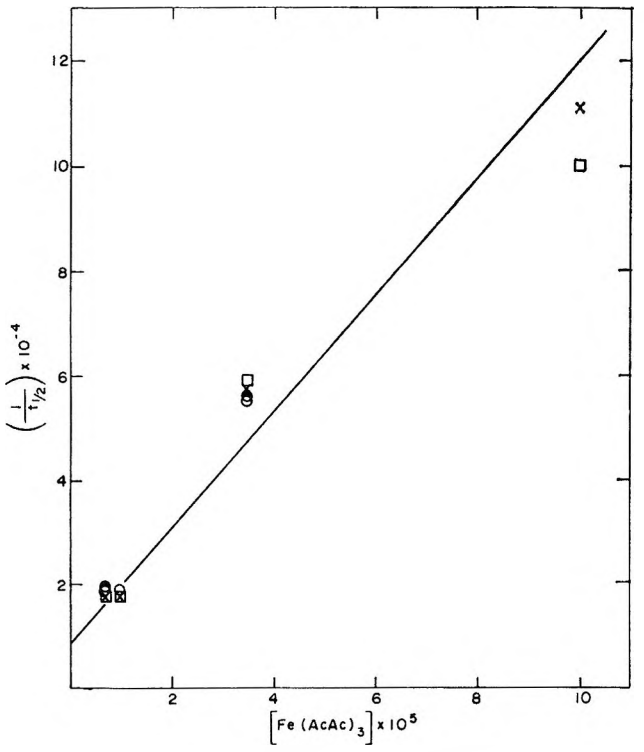

Figure 2. Triplet quenching by ferric acetylacetonate. Plot according to eq 1: ⊖, 420 nm; O, 760 nm; □, 850 nm; ×, 955 nm.

processes other than quenching by the chelate. The observed decays are close to first order so triplet–triplet annihilation is neglected. We can write

$$\frac{-d[T]}{dt} = k'[T] + k_2[T][Fe(AcAc)_3]$$

where

$$k' = k_0 + k_1 + \sum_Q k_Q[Q]$$

Since $[Fe(AcAc)_3]$ is approximately constant in our experiments we obtain an expression for the triplet lifetime

$$\frac{1}{t_{1/2}} = \frac{k'}{0.693} + \frac{k_2}{0.693}[Fe(AcAc)_3] \qquad (1)$$

Figure 2 is a plot of $(t_{1/2})^{-1}$ against concentration of ferric acetylacetonate, the half-lives being measured from the decays of absorption at 420, 760, 850, and 955 nm. The slope gives a value of $8 \pm 2 \times 10^8\ M^{-1}$ sec^{-1} for k_2, which is close to the quenching constant reported for the anthracene triplet.[12] The similar decay times for the visible and infrared absorption peaks are evident from Figure 2. The absorptions in cyclohexane at 420, 442.5, 760, 850, and 955 nm clearly originate from the common lower state T_1.

In order to account for the low quantum yield of fluorescence ($\Phi_f = 0.065$)[13] and high intersystem crossing efficiency of 1,5-dichloroanthracene in solution it has been postulated[5] that its second triplet state lies substantially below the first excited singlet state, S_1. Bennett and McCartin[5] flash photolyzed 1,5-dichloroanthracene in a Lucite matrix and observed the onset of infrared absorption at 895 nm with a single well defined peak at 855 nm, but did not observe the additional infrared peaks reported by us. Liu and Gale[14] have used the onset of absorption at 895 nm to place the second triplet level 72.5 kcal/mol above the ground state, S_0. This is slightly below S_1 which lies 73.4 kcal/mol above S_0. (If the absorption peak at 855 nm were the lowest energy $T_2 \leftarrow T_1$ transition this would have necessitated T_2 being above S_1.) Our results now indicate that the lowest energy $T_2 \leftarrow T_1$ transition of 1,5-dichloroanthracene in cyclohexane solution is at 955 nm, the bands at 850 and 760 nm being transitions from T_1 to higher vibrational levels of T_2. Data on the energy levels of 1,5-dichloroanthracene are summarized in Table I.

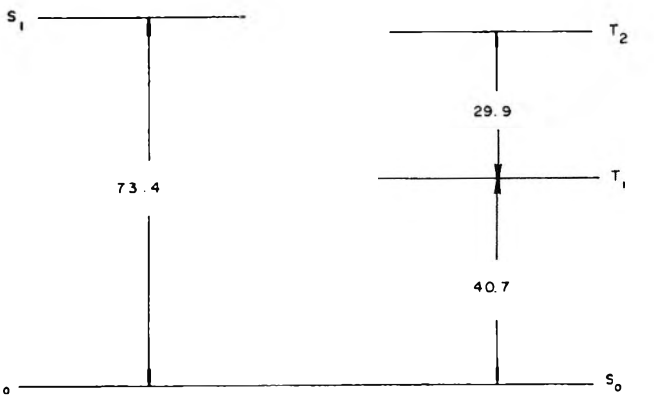

Figure 3. Energy level diagram for 1,5-dichloroanthracene; energies in kcal/mol.

Table I: Energy Levels and Vibrational Separations of 1,5-Dichloroanthracene

S_1[a]		T_1[b]	T_2[c]		T_n[c]	
E, cm^{-1}	ΔE, cm^{-1}	E, cm^{-1}	E, cm^{-1}	ΔE, cm^{-1}	E, cm^{-1}	ΔE, cm^{-1}
25,670		14,250	24,720		36,850	
(73.4)[d]		(40.7)[d]	(70.6)[d]		(105.4)[d]	
	1430			1290		1210
27,100			26,010		38,060	
	1390			1390		
28,490			27,400			
	1450					
29,940						
	1410					
31,350						

[a] Taken from the absorption spectrum in cyclohexane, measured on a Cary Model 14 spectrophotometer. [b] Reference 5. [c] All triplet levels ±50 cm^{-1}. [d] Kcal/mol.

(13) E. J. Bowen, *Trans. Faraday Soc.*, **50**, 97 (1954).

(14) R. S. H. Liu and D. M. Gale, *J. Amer. Chem. Soc.*, **90**, 1897 (1968).

The second triplet state is therefore located 70.6 kcal/mol above the ground state, *i.e.*, 2.8 kcal/mol below S_1 (Figure 3). This strongly supports the participation of the T_2 state in the intersystem crossing process for 1,5-dichloroanthracene and is in accord with the low fluorescence quantum yield.

Acknowledgments. We wish to thank Dr. A. Singh for the use of the flash photolysis apparatus, Miss M. Jonasson and Mr. F. Sopchyshyn for assistance in maintaining the equipment, and Dr. P. J. Dyne for his comments on the manuscript.

Dissociation Energies of Gaseous Gadolinium Dicarbide and Terbium Dicarbide

by E. E. Filby and L. L. Ames*

Chemistry Department, New Mexico State University, Las Cruces, New Mexico 88001 *(Received November 4, 1970)*

Publication costs assisted by the National Science Foundation

Relatively few investigations have been reported on the dicarbides of the rare earth metals gadolinium and terbium although Jackson, *et al.*,[1] and Hoenig, Stout, and Nordine[2] have published some thermodynamic data for GdC_2. A mass spectrometric investigation on the Langmuir vaporization of solid terbium dicarbide by Jackson, Bedford, and Barton[3] showed no gaseous TbC_2, whereas a later study by Haschke and Eick[4] indicated that it should be a significant vapor species. They have observed that the rare earth dicarbides of those metals with generally lower vapor pressure tend to vaporize to both the metal and the gaseous MC_2 molecules, and terbium metal has a relatively low vapor pressure.[5]

De Maria and coworkers[6,7] have discussed and used the hypothesis of Chupka, *et al.*,[8] that the C_2 group can act as a pseudooxide to correlate qualitatively the stabilities of various metal oxides and corresponding carbides. This correlation, coupled with the observation of gaseous TbO by Ames, Walsh, and White,[9] strengthened the possibility of finding a significant amount of gaseous TbC_2.

In contrast to these dicarbides, cerium dicarbide has been studied much more extensively[10-13] and therefore $D°_0(Ce–C_2)$ has been used as a reference in this investigation.[14]

All the previous thermodynamic data for these systems have been obtained from mass spectrometric investigations of the various solid–vapor equilibrium reactions. The study presented here uses instead isomolecular C_2-exchange reactions of the type

$$M_aC_2(g) + M_b(g) = M_a(g) + M_bC_2(g)$$

to determine mass spectrometrically the dissociation energies of GdC_2 and TbC_2. The advantages of this method, along with the development of the formulas used, have been discussed elsewhere.[14-16] Basically, the normal K_p in the equilibrium expression is replaced by a mass spectrometric K' in which P_i, the partial pressure of a species, is replaced by I_i, the measured intensity of the ith mass peak.

Experimental Section

The Bendix Time-of-Flight mass spectrometer used and the rest of the experimental setup have been described previously.[14] The cerium metal was obtained from D. F. Goldsmith Chemical and Metal Corp., the gadolinium metal from the Rare-Earth Division of the American Potash and Chemical Corp., and the terbium metal and carbon from Research Organic/Inorganic Chemical Co. The metals were reported by the suppliers to be of 99.9% purity while the carbon was 99.-999+% purity graphite.

Results

Isomolecular exchange reactions were established between cerium and gadolinium and between gadolinium and terbium. The Ce–Gd reaction consisted of four runs totaling 36 log K' *vs.* $1/T$ values, while a total of 49 points from four runs were obtained for the Gd–Tb reaction. Figure 1 shows the experimental data for the two reactions. No distinctions were made among the

(1) D. D. Jackson, G. W. Barton, Jr., O. H. Krikorian, and R. S. Newbury, "Thermodynamics of Nuclear Materials," IAEA, Vienna, 1962, p 529.

(2) C. L. Hoenig, N. D. Stout, and P. C. Nordine, *J. Amer. Ceram. Soc.*, **50**, 385 (1967).

(3) D. D. Jackson, R. G. Bedford, and G. W. Barton, University of California Radiation Laboratory Report, UCRL, 7362T (1963).

(4) J. M. Haschke and H. A. Eick, *J. Phys. Chem.*, **72**, 1697 (1968).

(5) C. E. Habermann and A. H. Daane, *J. Chem. Phys.*, **41**, 2818 (1964).

(6) G. Balducci, A. Capalbi, G. De Maria, and M. Guido, *ibid.*, **48**, 5275 (1968).

(7) G. De Maria, G. Balducci, A. Capalbi, and M. Guido, "High Temperature Mass Spectrometric Study of Neodymium-Carbon System," Meeting on Thermodynamics of Ceramic Systems, London, April 19, 1966.

(8) W. A. Chupka, J. Berkowitz, C. F. Giese, and M. G. Inghram, *J. Phys. Chem.*, **62**, 611 (1958).

(9) L. L. Ames, P. N. Walsh, and D. White, *ibid.*, **71**, 2707 (1967).

(10) G. Balducci, A. Capalbi, G. DeMaria, and M. Guido, *J. Chem. Phys.*, **43**, 2136 (1965).

(11) R. L. Faircloth, R. H. Flowers, and F. C. W. Pummery, *J. Inorg. Nucl. Chem.*, **30**, 499 (1968).

(12) P. Winchell and N. L. Baldwin, *J. Phys. Chem.*, **71**, 4476 (1967).

(13) G. Balducci, A. Capalbi, G. DeMaria, and M. Guido, *J. Chem. Phys.*, **50**, 1969 (1969).

(14) E. E. Filby and L. L. Ames, *High Temp. Sci.*, in press.

(15) D. L. Hildenbrand and E. Murad, *J. Chem. Phys.*, **43**, 1400 (1965).

(16) P. N. Walsh, D. Dever, and D. White, *J. Phys. Chem.*, **65**, 1410 (1961).

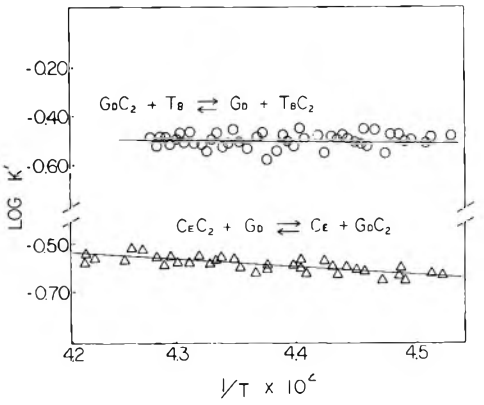

Figure 1. Variation of log K' with temperature for the Gd–Tb and Ce–Gd C_2-exchange reactions.

various runs for a given reaction because of the generally good agreement from run to run.

The second-law enthalpies, calculated by a weighted least-squares fit of the data, were reduced to 0°K using the heat contents for the gaseous metals given by Feber and Herrick[17] and those given in Table I for the gaseous dicarbides. These enthalpies, converted from $\Delta H°_{2289} = 12.5$ kcal/mol for the Ce–Gd reaction and $\Delta H°_{2279} = 0.82$ kcal/mol for the Gd–Tb reaction, are given in Table II.

Table I: Thermal Functions of Gaseous MC_2 Species

T, °K	$-(G°_T - H°_0)/T$, cal/deg mol			$(H°_T - H°_0)$, kcal/mole		
	CeC_2	GdC_2	TbC_2	CeC_2	GdC_2	TbC_2
2000	73.91	76.24	76.02	25.49	25.47	25.46
2100	74.54	76.87	76.65	26.94	26.92	26.92
2200	75.13	77.47	77.24	28.40	28.37	28.37
2300	75.71	78.04	77.82	29.86	29.83	29.83
2400	76.26	78.59	78.37	31.31	31.29	31.28

Table II: Reaction Enthalpies and Dissociation Energies (kcal/mol)

$$M_aC_2(g) + M_b(g) = M_a(g) + M_bC_2(g)$$

M_a	M_b	$\Delta H°_0$ (second law)	$\Delta H°_0$ (third law)	$D°_0$ (M_bC_2)
Ce	Gd	11.0 ± 2.0	11.8 ± 0.2	151 ± 3
Gd	Tb	0.9 ± 2.7	0.6 ± 0.3	150 ± 3

Table II also lists the third-law enthalpies at 0°K for the reactions calculated from the log K' values and the free energy functions given by Feber and Herrick and in Table I.

The thermal functions listed in Table I were calculated using the usual rigid-rotor harmonic-oscillator approximation assuming MC_2 to be a linear molecule.[7,13,14] The C–C bond length (1.24 Å) and the M–C bond lengths and stretching force constants were estimated by a previously used method.[14] They are 1.86 Å and 5.75 mdyn/Å for CeC_2, 1.79 Å and 5.96 mdyn/Å for GdC_2, and 1.78 Å and 5.97 mdyn/Å for TbC_2. The C–C stretching force constant was taken to be 13.1 mdyn/Å as has been reported for the C–C bond in sodium acetylide.[18] The bending force constants (k_δ/l_1l_2) were calculated using k_δ equal to 0.60 mdyn-Å/rad.[14] The calculated vibrational frequencies are 650 cm^{-1}, 458 cm^{-1} (d.d.), and 2040 cm^{-1} for CeC_2, 656 cm^{-1}, 464 cm^{-1} (d.d.), and 2044 cm^{-1} for GdC_2, and 655 cm^{-1}, 465 cm^{-1}, (d.d.), and 2044 cm^{-1} for TbC_2. The electronic multiplicities of the ground states were assumed to be equal to those for the corresponding monoxides[9] and no electronic excitations were considered.

Discussion

The dissociation energies of GdC_2 and TbC_2 were calculated from the enthalpies of the exchange reactions according to the equation

$$D°_0(M_bC_2) = D°_0(M_aC_2) - \Delta H°_0(M_aM_b)$$

starting with the value of 162 ± 2 kcal/mol given by Balducci, *et al.*,[13] for the dissociation energy for CeC_2. The dissociation energies obtained are also given in Table II.

The value for GdC_2 can be compared to the dissociation energy which is derivable from the results obtained by Jackson, *et al.*,[1] who measured $\Delta H°_{2150} = -37.9$ kcal/mol for

$$GdC_2(g) = Gd(g) + 2C(s)$$

Converting this enthalpy to 0°K using the heat contents from Table I, Feber and Herrick, and Stull and Sinke[19] (for graphite), and then combining the result with the heat of formation at 0°K of $C_2(g)$,[20] a value of 154 ± 5 kcal/mol is obtained. This quantity is in good agreement with the 151 ± 3 kcal/mol measured in this investigation.

There appear to be no data available for comparison with the 150 ± 3 kcal/mol determined here for the dissociation energy of TbC_2.

It is interesting to note that the differences between the dissociation energies for the dicarbides determined here and those for the corresponding monoxides[9] are 22.0 and 23.4 kcal/mol for Gd and Tb, respectively. These very similar differences are evidence in support of

(17) R. C. Feber and C. C. Herrick, "Ideal Gas Thermodynamic Functions of Lanthanide and Actinide Elements," Los Alamos Scientific Laboratory Report LA 3184 (1964).

(18) J. Goubeau and O. Beurer, *Z. Anorg. Allg. Chem.*, **310**, 110 (1961).

(19) D. R. Stull and G. C. Sinke, "Thermodynamic Properties of the Elements," *Advan. Chem. Ser.*, No. 18 (1956).

(20) "JANAF Thermochemical Tables," The Dow Chemical Co., Midland, Mich., 1963.

the pseudooxide character of the C_2 group. More extensive systematic investigations of the various successful qualitative correlations are needed to determine whether or not the hypothesis might have quantitative utility.

Acknowledgments. The National Science Foundation is gratefully acknowledged for its support of this research. The authors also wish to thank the New Mexico State University Computer Center for gratis use of computer time.

THEORY OF VISCOELASTICITY

An Introduction

by R. M. CHRISTENSEN, Shell Dev. Co., Emeryville, Calif.

Develops the continuum theory of viscoelasticity. It treats the linear theory extensively, including the thermochemical derivation of constitutive relations, and an examination of the techniques for solving boundary value problems. The book also presents an introductory study relative to the formulation of a nonlinear theory of viscoelasticity. Although the book emphasizes the general development of the theory, it also reviews matters of practical application. The chapter on mechanical properties determination provides a specific examination of such applications. *1970, 260 pp., $13.50*

IONIC INTERACTIONS

From Dilute Solutions To Fused Salts

A Volume in **Physical Chemistry**
Series Editor: **E. M. LOEBL**

edited by SERGIO PETRUCCI, Department of Chemistry, Polytechnic Institute of Brooklyn, Brooklyn, N. Y.

A comprehensive survey of ionic interactions in the entire range of concentrations from dilute solutions to fused salts. The chapters, which deal with the subject both theoretically and experimentally, are written by specialists in the fields of statistical mechanics, inorganic stereochemistry, chemical kinetics, and chemical structure. The first volume surveys the equilibrium and transport properties of dilute electrolytes and fused salts. Volume 2 contains two chapters on chemical kinetics and mechanism, one of which emphasizes the recently developed relaxation tools for the study of ionic association, and two chapters on the spectra and structure of electrolytes.

Volume 1: **Equilibrium and Mass Transport,** *1971, 421 pp., $19.50*
Volume 2: **Structure and Kinetics,** *1971, 292 pp., $16.50*

PHYSICAL CHEMISTRY

An Advanced Treatise

edited by HENRY EYRING, Department of Chemistry and Metallurgy, University of Utah, Salt Lake City, Utah, **DOUGLAS HENDERSON,** IBM Research Laboratories, San Jose, California, **and WILHELM JOST,** Institut fur Physikalische Chemie der Universitat Gottingen, Gottingen, Germany

Volume 1/**Thermodynamics**—edited by **WILHELM JOST**

CONTENTS: R. HAASE: Survey of Fundamental Laws. A. SANFELD: Thermodynamic Potentials. R. HAASE: Thermodynamic Properties of Gases, Liquids, and Solids. E. U. FRANCK: Gas-Liquid and Gas-Solid Equilibria at High Pressures, Critical Curves and Miscibility Gaps. H. STENSCHKE: Thermodynamics of Matter in Gravitational Fields and in Rotational Frames of Reference. J. WILKS: The Third Law of Thermodynamics. M. KLEIN: Practical Treatment of Coupled Gas Equilibria. H. KREMPL: Equilibira Systems at Very High Temperatures. R. H. WENTORF: High Pressure Phenomena. S. M. BLINDER: Caratheodory's Formulation of the Second Law. Author Index-Subject Index.

May 1971, about 625 pp., in preparation.

MOLECULAR BEAMS AND REACTION KINETICS

Course 44 of Italian Physical Society
Proceedings of the Interntl. School of Physics "Enrico Fermi"

edited by Ch. SCHLIER, Universitat Freiburg, West Germany.

Devoted to new information about the use of molecular beam techniques applied to problems of reaction kinetics. Topics discussed include: elastic and inelastic scattering, ionic reactions and electron reactions (excitation transfer), non-beam methods and the connections between beam and non-beam results, case studies of H^+- and H-transfer, computation of energy surfaces, and trajectory studies. *1970, 437 pp.,* $20.00.

SOLID ACIDS AND BASES

Their Catalytic Properties

by KOZO TANABE, Department of Chemistry, Faculty of Science, Hokkaido University, Sapporo, Japan

Reviews recent advances in the studies of acidic and basic properties of various metal oxides, sulfides, phosphates, carbonates, hydroxides and halides, mixed metal oxides, natural clay minerals, mounted acids, and active carbons. The structures of the acid and base centers, and the correlation between the acidic/basic properties and catalytic activity and selectivity, are reviewed systematically. The unity and special characteristics of heterogeneous acid and base catalysis are discussed in terms of integrated kinetic and structural studies. *1971, 175 pp., $11.50.*

CHEMICAL BONDS AND BOND ENERGY

A Volume in **Physical Chemistry**
Series Editor: **E. M. LOEBL**

by R. T. SANDERSON, Department of Chemistry, Arizona State University, Tempe, Ariz.

Presents a successful, original, semi-theoretical calculation of bond energies and heats of atomization. It describes a series of simple concepts and tabulates data on calculated bond energies of over 500 compounds. Included are calculations on almost every gas phase inorganic molecule for which data have been reported, plus 98 representative organic compounds and over 100 binary solids. The results provide the reader with important insights into the nature of chemical bonds and suggest explanations for many puzzling questions. *1970, 232 pp., $11.50.*

CRYSTAL CHEMISTRY AND SEMICONDUCTION IN TRANSITION METAL BINARY COMPOUNDS

by JACQUES P. SUCHET, Institut fur Anorganische Chemie, Stuttgart, Germany (on leave from Centre National de la Recherche Scientifique, Paris, France)

Provides the chemist and physicochemist with a detailed introduction to the problems of semiconduction in transition metals and rare earth compounds. The book provides the knowledge of crystal chemistry and crystal physics that is necessary for understanding past work on the mixed valency oxides and present investigations of the conduction process in crystals containing "magnetic" atoms—i.e. transition metal or rare earth atoms. About half of the book consists of a bibliographical digest that represents a thorough and specialized guide to the literature of the last twenty years. The book also includes useful theoretical bases on bonding and electrical conduction and discussions of actual problems and possible applications of magnetic semiconductor materials. *April 1971, 400 pp., $22.00.*

RYDBERG SERIES IN ATOMS AND MOLECULES

A Volume in **Physical Chemistry**
Series Editor: **E. M. LOEBL**

by A. B. F. DUNCAN, Department of Chemistry, The University of Rochester, River Campus Station, Rochester, N. Y. Rydberg states are an important class of excited electronic states of atomic and molecular systems. This book, specifically devoted to the subject, is a convenient source for both experimental data and information on current theories of Rydberg states. The author not only correlates Rydberg series of chemically similar systems, but also interprets these series in terms of electronic structures and orbital transitions. Theoretical principles necessary for understanding simple electronic systems are discussed in detail. *April 1971 119 pp., $7.50.*

ACADEMIC PRESS NEW YORK AND LONDON
111 FIFTH AVENUE, NEW YORK, N. Y 10003